

CRANFIELD UNIVERSITY

CHRISTOPHER STENNETT

THE IGNITION BEHAVIOUR OF ENERGETIC MATERIALS UNDER  
CONFINED COOKOFF

CRANFIELD DEFENCE AND SECURITY

PhD

Academic Year: 2018 - 2019

Supervisor: Prof JACKIE AKHAVAN

SEPTEMBER 2018

CRANFIELD UNIVERSITY

CRANFIELD DEFENCE AND SECURITY

PhD

Academic Year 2018 - 2019

CHRISTOPHER STENNETT

The Ignition Behaviour of Energetic Materials Under Confined Cookoff

Supervisor: Prof JACKIE AKHAVAN

SEPTEMBER 2018

© Cranfield University 2018. All rights reserved. No part of this publication may be reproduced without the written permission of the copyright owner.

## **ABSTRACT**

In a series of experiments and theoretical work, the process of ignition in confined energetic materials has been explored and understanding gained. Early work focused on the direct observation of the cook-off process but was hampered by the available technology. In more recent work, dynamic measurements of the deformation of the confinement have been explored, and refinements to the direct observation method have been made that make use of recent advances in camera technology. We have observed, for the first time, complex melting and development of gas spaces within which the early stages of ignition take place, and propose a new mechanism by which violent cook-off responses might develop in certain explosives.

## ACKNOWLEDGEMENTS

It is difficult to acknowledge everyone that has helped me to gain my current understanding, given that this has come about over the last 25 years or so, and forms the greater part of my adult (hah !) life. Furthermore, the work described in this thesis, while being by no means the only thread of research I have explored, has nevertheless been informed by workers in those other fields in less direct, but no less important ways. It would be best to approach this chronologically, and to try to remember the uncountable pleasant conversations and heated arguments that have helped me along the way.

For my initial work at FHD in 3D visualization techniques and computer model development, and for the later experimental studies of cook-off and shock initiation: Peter Haskins, Malcolm Cook, Phil Cheese, Justin Fellows, Richard Briggs, Andrew Wood, Phil Ottley, Steve Cowell.

For my early weeks at Shrivenham talking each other's ears off to Northumberland and back, and for the many long chats about instrumentation, electronic design and general wisdom, Keith Brook. For applying those methods out in the pouring rain, Trevor Lawrence, Daniel Flynn.

For my early days in the Dynamic Response group, rebuilding the capability, Gary Cooper and Paul Hazell; for the remainder of my six years there, during development of the PV gauge technique, Sue Sorber, Malcolm Burns, Peter "The Power" Taylor, James Ferguson, Andy Roberts.

For setting up the Hazard Test Lab, Matt Goldsmith; for keeping the Hazard Test Lab going, Scott Clews.

For asking questions that caused me to think, and hence helped me to understand: Jim Clements, Graeme Creighton, Mick Warden, Dave Harris, Paul Walker.

For constantly bugging me to get this done, for making space for me to do it, for supervision and support: Jackie Akhavan. Thanks, guv.

Throughout all this, for the insight into explosives processing, microstructure and materials science, and for giving me our son: Sally Gaulter. Who knew that being married to an explosives formulator is just as good as being one yourself ?

## TABLE OF CONTENTS

1	General Introduction.....	1
1.1	The Burning to Violent Reaction Problem	1
1.2	Outline of this Thesis	4
2	Experimental Considerations for Cook-off.....	6
2.1	Heating Regimes	6
2.1.1	Schematic Heating Profiles.....	6
2.1.2	Steady Temperature.....	6
2.1.3	Ramped Temperature .....	7
2.1.4	Complex Heating Profiles .....	10
2.2	Instrumentation	10
2.2.1	Internal Temperature Measurements.....	10
2.2.2	Pressure Measurement.....	12
2.2.3	Direct Observations.....	14
3	The Character of Thermal Damage .....	16
3.1	Introduction	16
3.2	Changes Occurring in the Early Stages of Heating	17
3.3	Observations of RDX and HMX	17
3.4	The Role of Melting	23
3.5	Concluding Remarks	25
4	The Role of Confinement.....	27
4.1	Introduction	27
4.2	Confinement Types	27
4.3	Classifications of Response Violence and $dE/dt$	28
4.3.1	Post-Experiment Evaluation .....	28
4.3.2	Asymmetry in Observed Damage to Confinement.....	29
4.4	Behaviour of the Confinement Prior to Gross Failure	30
4.5	Concluding Remarks	32

5	Computer Modelling of the Cook-off Process .....	33
5.1	Introduction .....	33
5.2	Arrhenius-Based Kinetics Models .....	34
5.2.1	Simple Heat Transfer.....	34
5.2.2	Cylindrically-Symmetric Example.....	34
5.3	Energetic Materials .....	37
5.3.1	Extension to Include Internal Heat Generation.....	37
5.3.2	Multi-step Decomposition Kinetics .....	40
6	A Hypothetical Mechanism for Violent Responses .....	42
6.1	Bulk Energy Release Rate in the Detonation Process .....	42
6.1.1	A Simple View of Detonation .....	42
6.2	Bulk Energy Release Rate During Burning .....	43
6.2.1	Burning Rates.....	43
6.3	Modes of Initiation .....	44
6.3.1	Initiation of Burning at a Single Site.....	44
6.3.2	Initiation of Burning at Multiple Sites Simultaneously.....	45
6.3.3	Concluding Remarks .....	49
7	General Conclusions.....	52
8	References.....	55
	Annex A: Supporting Publications.....	A-1
A.1	..... Direct Observations of Cook-off Events ...	A-2
A.2	..... Small-Scale Thermal Violence Experiments...	A-11
A.3	..... The Role of Binders...	A-23
A.4	..... Developments in a Small-Scale Test...	A-29
A.5	..... Hazard Characterization of Fox-7...	A-35
A.6	..... Development and Implementation of an Ignition ...	A-43
A.7	..... Cumulative Damage Hotspot Model...	A-55
A.8	..... Live Imaging and Heating of Confined RDX and HMX ...	A-63
A.9	..... One Dimensional Thermal Violence ...	A-71

A.10 ..... Development of a Dual-Windowed ... A-79

A.11 ..... Live Decomposition Imaging of HMX/HTPB ... A-86

Annex B: Presentations ..... B-1

B.1 ..... Direct Observation of the Onset of Ignition ... B-2

Annex C: ..... Co-Author Statements C-1





# 1 General Introduction

## 1.1 The Burning to Violent Reaction Problem

Burning to violent reaction (BVR) is a reasonably self-explanatory term to describe the behaviour of weapon systems under certain test conditions. Even a simple examination of tests, such as fragment or bullet impact, shows that, at its simplest level, the mechanism consists of the ignition of low-pressure burning in the energetic filling of the weapon, followed by gradual build-up of the intensity of the burn, and leading, in some circumstances, to violent mass reaction. An example of one aspect of the BVR phenomenon is shown in the still images taken from the video recording of such a test:

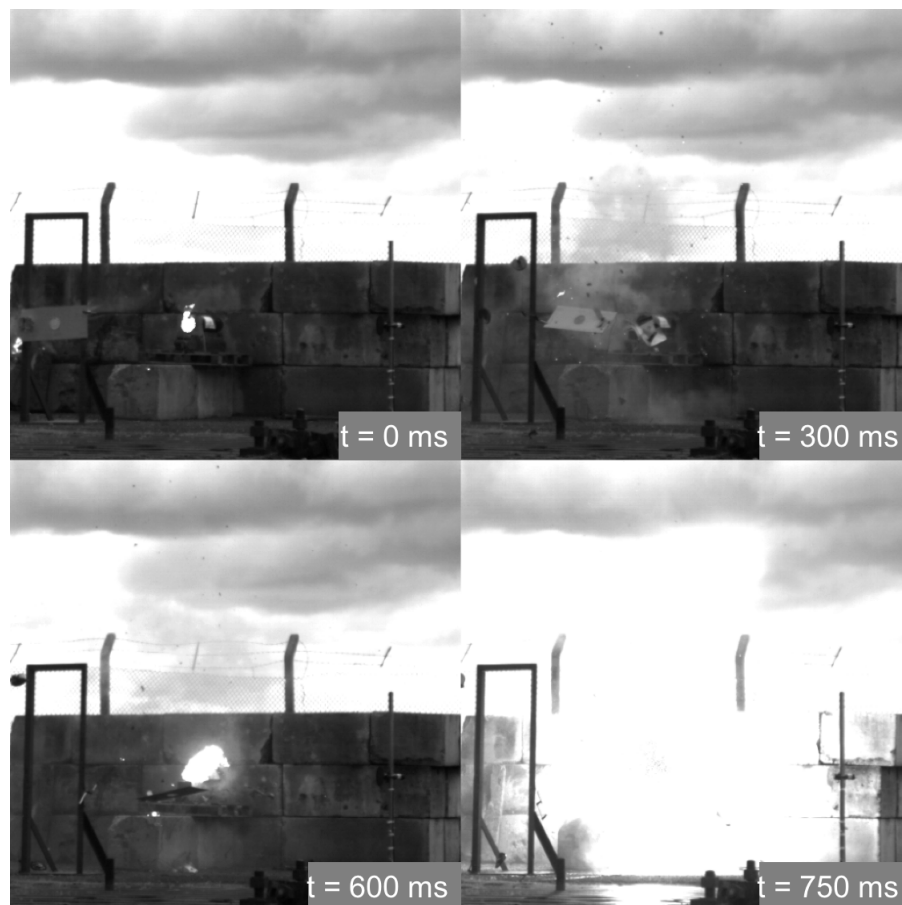


*Fig. 1: Bullet impact initiation of a propellant charge, showing delayed onset of first flame and eventual build-up of violent burn. Images taken at the instant of impact, and at 300, 600 and 750 ms after impact.*

In this test, a 0.5" AP bullet was fired at the test article at a velocity of  $850 \text{ ms}^{-1}$ , and it can be seen that there is a considerable delay from the impact, until the eventual mass burning of the propellant filling 750 ms after impact. A luminous flame can be seen at the moment of impact, and this quickly extinguishes before a second flame becomes visible 600 ms later. The initial flame is directly associated with the impact, but the subsequent behaviour seems to originate from a much slower process, and the burn takes 150 ms to reach peak intensity.

Similar behaviour has been noted in secondary explosives under medium strain-rate crushing and damage, for example in the Steven Test and the Susan Test, although in those configurations the delay between impact and mass burning was much shorter. In the Susan test, the explosive specimen is lightly confined and mounted at the front of a heavy projectile, and is impacted at relatively low speed ( $30$  to  $100 \text{ ms}^{-1}$ ) against a massive, rigid structure; in the Steven test, a lightly-confined specimen is mounted on a rigid structure and is impacted by a heavy, blunt projectile, again at speeds in the  $30$  to  $100 \text{ ms}^{-1}$  range. In both tests, close observation of the impact process shows clearly that the response occurs a considerable time after impact, after mass deformation of the energetic specimen, and not promptly within a few microseconds of the instant of impact, as is noted in shock-to-detonation transition (SDT) tests.

The long delay between the initial impact stimulus and the subsequent violent explosion arises because the initial stimulus causes localised burning, which then builds and develops away through the remainder of the energetic material. Whether this small initial burn can develop into a violence is governed by the properties of the material through which the burn propagates, which may have been chemically or mechanically altered by the impact stimulus, and which is unlikely to be spatially uniform in its properties.

The relatively simple UK EMTAP Tube Test [1] is designed to discriminate those energetic materials that may undergo BVR from those that cannot, with the aim that those materials that show violent responses would be rejected for use in weapon systems. In particular, the EMTAP Test 35 configuration – named “Internal Ignition” – deliberately ignites a specimen of the energetic material at ambient temperature in a confining capsule, and is a more formal and reproducible method to explore confined burning that is sometimes seen in impact tests.

Other test configurations, using the same geometry, provoke ignition in the energetic material by the application of external heating (via a fuel fire in the case of EMTAP Test 41, and via an electrical heater in the case of EMTAP Test 42), which leads the mechanism of chemical decomposition and thermal runaway and subsequent growth of reaction and final response. The thermally-driven response then forms a subset of the wider BVR problem, but shares broad features: heating provokes ignition at some relatively localised position within the system under consideration, and subsequently a reaction wave propagates away from there into the damaged surrounding material. Again, this initial reaction may eventually grow to consume all the available energetic material, releasing its stored chemical energy.

In the EMTAP Tube Tests, it is sometimes noted that the response of the energetic material differs within a series of ostensibly the same test. For example, a test report compiled by UK MoD [50] notes that of ten internal ignition tests on Octol, eight responded with a relatively mild “pressure burst”, whereas two responded with maximum violence, termed “detonation”. Similarly, in recent tube tests [1][3][4] for a composition of RDX/HyTemp (92/8 wt%), responses ranged from “pressure burst” to “detonation” across the full range of test configurations. Furthermore, only the EMTAP 41 (fast heating) configuration showed the most violent responses, whereas the internally-ignited and electrically-heated configurations showed either “pressure burst” or “deflagration”.

These observations raise important questions concerning the nature of the tube tests, and perhaps of standardised tests in general, and their ability to provide a reliable prediction of the BVR hazard posed by a particular energetic material in a particular weapon system. In particular:

- Is the variability in response prompted by some small variation between the tests as implemented, so that the test method is in some way defective; or is it a result of some feature intrinsic to the particular energetic material ?
- Is the response (variable or otherwise) observed in a test solely a result of the properties of the energetic material under test, or is the response due to a combination of the test configuration and the energetic material together ?
- If variability is intrinsic to the particular material, is this same feature present to a greater or lesser extent in other energetic materials, and is this feature the sole source of violent responses ? Could we determine the nature and

conditions in which this feature arises, and ‘design it out’ of new energetic materials, so that they can be guaranteed to not exhibit violent responses ?

- Are 10 tests sufficient to confidently assert that a consistent response of whatever level is the response that would always be observed for that test configuration ?
- Do the various different tests represent the ‘worst case’ stimulus ? That is, would some slightly different test configuration (for example, stronger or weaker confinement, different heating regimes) provoke a more violent response from those compositions that have shown a lesser response under the standard test configuration ?

The wider aim (towards which this thesis forms a small step) is continue to develop a deeper understanding of the mechanisms that control violence in cook-off. This improved mechanistic understanding will provide more realistic and predictive computer models to be built, and in turn these improved computer models can then be used to explore the parameter space for cook-off problems. Without computer modelling, experimental studies are limited by the lengthy process of experiments, particularly those at slow heating rates and with consequently long times to explosion.

## **1.2 Outline of this Thesis**

This thesis summarises the authors’ research into some aspects of the broader BVR problem, focusing mainly on the experimental methods and studies which have provided useful insights into some of the mechanisms that govern the growth of burning reactions. This body of work is related almost exclusively to thermally-driven initiation, which is known colloquially as ‘cook-off’, though throughout the last 25 years the author’s research has included the wider problems of deliberate or unintentional initiation by impact, shock propagation in non-explosive composites, and safety and hazard testing of explosives.

The thesis is not arranged chronologically, but rather first reviews research and experiments that began in the mid 1990s and remain active at the time of writing. Following this, I discuss some aspects of computer modelling of the cook-off process, and introduce ways in which the experimental work has informed that activity. Finally,

I introduce a new physical mechanism which potentially explains how violent explosive responses may arise under certain conditions.

## 2 Experimental Considerations for Cook-off

### 2.1 Heating Regimes

#### 2.1.1 Schematic Heating Profiles

The following figure shows schematic temperature/time profiles that have been used in prior studies of cook-off in the open literature. These represent temperatures applied to a confined charge, with the intent that ignition will be provoked; the only general temperature profile not shown is one where the temperature is elevated and then cooled back to ambient without ignition.

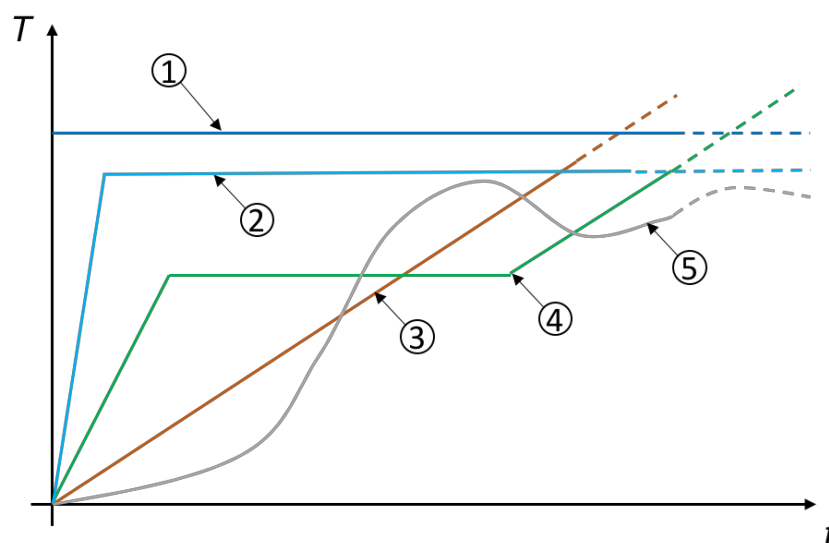


Fig. 2: Illustration of heating regimes: (1) steady high temperature; (2) ramp-and-hold; (3) steady ramp; (4) ramp-soak-ramp; (5) complex

#### 2.1.2 Steady Temperature

The simplest boundary profile to understand is illustrated by profile (1) in Fig. 2 where the test specimen begins at some high temperature, and is maintained there until a cook-off response is observed. The specimen bulk is initially assumed to be uniformly at the boundary temperature, so that this heating profile represents an idealised one, and it is obvious that it would be difficult or impossible to achieve this experimentally. Nevertheless, the steady high temperature heating regime is useful because it is the regime implied in experiments that determine the first-order reaction rate parameters [16][17].

The ODTX [14][15] experiment attempts to achieve the ideal steady temperature state (and hence to determine reaction rate constants) by heating the specimen to a given temperature in as short a time as possible. A spherical test specimen is quickly clamped between two pre-heated anvils each having an appropriate hemispherical cavity machined into one face. A hydraulic ram maintains a high clamping force, and a soft copper seal ensures that the specimen confinement remains gas-tight until the final cook-off response occurs. Active heaters around the exterior of the anvils maintain their temperature at the desired set-point throughout the experiment.

Despite this, the specimen in the ODTX experiment is initially cold, so that as it is introduced into the anvils and the experiment is closed, the external surface of the specimen heats and the inner surface of the specimen cavity cools. Following this, heat flows into the specimen (supplied by the external electrical heater) until thermal equilibrium is reached. Even though the test specimen in ODTX is small ( $\sim 2.0$  g), typically a few tens of seconds [10] are required for this equilibration to be achieved, so that for high-temperature, short-duration experiments, ignition can occur before thermal equilibrium is reached. Conversely, low-temperature experiments with very long ( $1000^3$ s seconds) times to ignition could be considered to have equilibrated to the nominal steady boundary temperature.

### **2.1.3 Ramped Temperature**

More usually, cook-off experiments begin with an initially cold specimen enclosed in a cold confining vehicle, and external heat is applied according to some prescribed regime. Ramped heating regimes are most commonly used, beginning at ambient temperature and increasing the applied temperature, measured at the surface of the test vehicle, at a constant rate of  $dT/dt$ , until a reaction occurs. Generally, closed-loop temperature controllers are used to achieve ramped heating profiles: a thermocouple is placed on the experiment and provides feedback to a PWM controller, which manipulates the electrical power to the heaters and aims to match the temperature on the feedback thermocouple to a pre-programmed profile.

From a practical standpoint very high heating rates (beyond  $30^\circ\text{C}$  per minute) are difficult to achieve without very strong heat sources, which introduce difficulty in temperature profile control: the various national Fuel Fire weapons tests are intended to achieve very

fast ramp to a high surface temperature heating rates, but with considerable short-term variations, as illustrated in Fig. 3.

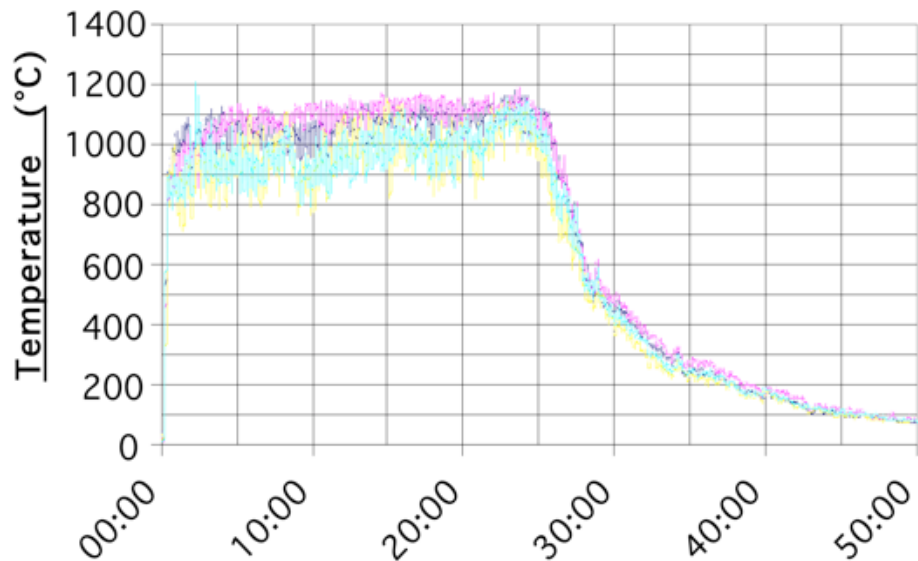


*Fig. 3: Fuel-fire test thermocouple history. Time is measured in minutes from first ignition of the fuel pool. This achieves the test specification of an ‘average temperature above 800°C within 30 seconds’ but measured temperatures vary by ~100°C on short timescales*

Clearly, however, the term ‘heating rate’ does not accurately capture the process of heat transfer in the particular experiment being conducted. As noted above, the rate is measured as an applied surface temperature, and when the rate is high the overall system response is dominated by heat transfer within the experimental vehicle, and in particular through the test specimen. Very fast heating produces a large temperature variation throughout the energetic, but even relatively slow heating regimes can result in a significant temperature variation if the specimen is physically large. For example, in the author’s work, presented in Annex A.3, we noted that the centre of a 50 x 50 mm cylindrical HMX/HTPB pellet was at 102°C at the point of ignition when the surface in contact with the confining vehicle was at 230°C. This was for a moderately fast applied heating rate of 10°C per minute; even at 0.5°C per minute, we noted the centre temperature to be 30 to 40°C cooler than the surface at the point of ignition. Other workers have also presented work showing that the internal temperature is non uniform: Wardell reported the STEX experiment [59] including an example plot for a slow cook-off experiment showing a variation of ~ 8°C in measured internal temperature after 48 hours of steady-rate heating.



This inevitable temperature variation has led to a common hypothesis that the violence of response of a given cook-off experiment can be related reasonably simply to the heating rate, by supposing that the event violence is governed by the volume of material that is above some threshold value. For faster heating rates, with a stronger spatial variation in temperature, a smaller volume will be above this threshold than for slower rates. The presumption generally follows that hot energetic materials are in some way more sensitive to initiation, though the detail of the mechanism for this increased sensitivity is not clearly explained [38][39]. This hypothesis generally fits with historical anecdotal observations, which tend to show that slow heating results in more violent cook-off than fast heating, but counterexamples are common. In a recent report of EMTAP Tube Tests [50] we noted several examples where the supposed trend is not present, and is sometimes reversed so that high heating-rate tests give more violent responses than low-rate ones.

Slow heating tests are generally intended to reduce the temperature variation across the test article to as little as possible, and often it is assumed that for the very slowest rate commonly used, the thermal equilibrium is reached. Historically UK and US standard slow-heating weapon qualification tests have specified a heating rate of 3.3 °C per hour, but this low rate is often criticised because accidental uncontrolled heating at such a low rate would be very unlikely to be encountered in any credible accident scenario. This rate was chosen based on the erroneous view that ‘slow heating provokes more violent responses’, and was therefore assumed to represent the ‘worst-case’ heating rate that would provoke the most violent response. The prevailing view was that if a given weapon system exhibited a non-violent response to this ‘worst-case’ stimulus, then it would exhibit non-violent responses at any faster (and more credible) heating rate.

An example of a truly thermally equilibrated experiment is Accelerating Rate Calorimetry (ARC) [9], in which a relatively small specimen of 2.0 g is used. The test is performed in two stages with the specimen contained in a sealed capsule and placed into a sophisticated oven. In the first stage the specimen is heated incrementally from ambient and at each increment, the temperature held steady for a short period to allow thermal equilibrium to be reached. During equilibration, the apparatus also determines whether the specimen has begun to generate heat, by comparison with an inert block placed at a thermally equivalent position to the specimen. Heating is incremented in small steps, allowing time for thermal equilibration between the inert block and the test

specimen after each increment. If, during the equilibration period heat generation is detected, then the apparatus switches to the second phase, where the temperature of the oven is dynamically controlled so that it tracks the temperature of the specimen as accurately as possible. The self-accelerating decomposition of the specimen then ‘drives’ the oven temperature. In the second phase the specimen cannot shed heat to the surroundings, at least while its temperature rises at a rate within the capacity of the apparatus to track. Eventually, the specimen explodes from its confinement, terminating the experiment. ARC therefore mimics the behaviour of an elementary cell of an energetic material embedded within a much larger bulk, and is valuable in defining safe processing parameters for large-scale melt-casting of explosives. The onset temperature of self-heating determined by ARC usually defines the absolute upper limit temperature that would be allowed in a given process.

#### **2.1.4 Complex Heating Profiles**

The introduction of electrical heating in small- and weapon-scale tests allows the experimenter free choice of the heating regime, even to the extent of using some kind of programmed controller to provide an arbitrary time-varying boundary temperature. This type of control is most often used in studies at very slow heating rates, which would otherwise be impractical to carry out within a reasonable time-scale. To improve efficiency in performing extreme low-rate tests it is often helpful to carry out initial heating to a moderate temperature at quite a fast rate, and after a period of steady applied temperature to allow thermal equilibration, to continue heating at the 3.3 °C per hour slow rate until ignition.

Ramp-soak-ramp heating (which is a relatively simple case of the more generally complex heating profile) however, introduces complexity and uncertainty into the such tests, mainly because the temperature across the system under examination is unlikely to be uniform except for those test articles with the smallest sizes, so that, at the beginning of the slow heating phase, the thermal profile will neither be uniform, nor, in general properly known.

## **2.2 Instrumentation**

### **2.2.1 Internal Temperature Measurements**

Knowledge of the internal temperature in the specimen in a cook-off experiment is essential both to assist in calibration and validation of computer models of cook-off, and

to provide insight into the onset of thermal runaway. For example, the SITI[55][53][51] experiment is used at Sandia to validate the XCHEM[52][54] computer model; ODTX data (for which the internal temperature is obtained as a consequence of the simply, symmetric geometry) have been used to obtain parameters[56] to calibrate the CHARM computer model[Annex A.6, A.7].

The main issue with obtaining internal temperature measurements is to do so while keeping control of the gas tightness of the confining body, and this is not a simple problem experimentally. In the author's early work [Annex A.1] this was accomplished using stainless-steel sheathed thermocouples, brazed through the wall of the confinement, but often a mechanical gland or thermocouple well can be used. Whichever mechanical method used, the presence of the embedded thermocouple introduces problems in filling the test specimen into the confinement to ensure good thermal contact between the thermocouple and the filling. Where castable compositions are studied (as in the authors work with RDX/TNT and HMX/HTPB [Annex A.1]) this is comparatively easily achieved, but for extruded or pressed materials it becomes necessary to prepare the specimen with channels to accommodate the thermocouples. In our later work [Annex A.2] pressed compositions were used, and suitable pockets were drilled into the specimen pellets to accommodate the thermocouples.

An additional issue with internal temperature measurement is illustrated in our experiments, where the thermocouples were of 1.6 and 3.0 mm diameter. The relatively high thermal mass of these devices resulted in quite long times to thermal equilibration with the surroundings, so that the ability to measure rapidly-changing temperature was limited. More recent work, for example by Smilowitz [21] and Kaneshige [55], has used butt-welded fine-wire thermocouples placed across the mid-plane of the experiment, and used test specimens composed of two identical pellets are placed around the thermocouple array. The thin gauge of the thermocouple wires ( $\sim 75 \mu\text{m}$  in the SITI test) means that the thermocouples equilibrate with the local specimen temperature quickly, and allows improved time resolution into the millisecond regime. Note, however, that there remains a limit to the speed at which a wire thermocouple can track the local temperature of the specimen, because it is necessary for the temperature of the sensing junction to reach equilibrium with its surroundings.

Non-contact measurement methods offer the potential for fast tracking of temperature, and Asay [22] has developed a method to calibrate and deploy infra-red emission

measurements to record temperature at timescales of a few  $10^3$ 's of microseconds. The infra-red technique, however, presents difficulties in deployment because the sensor system must have a light-path 'view' of the measurement point. Asay achieved this using quartz optical fibres, and was able to obtain measurements from within the bulk of the specimen. These were necessarily invasive in a similar way to embedded thermocouples, in the sense that the uniformity of the test specimen was disturbed by the presence of a foreign material of different thermal properties. In various separate conversations with other researchers, there is anecdotal evidence that invasive measurements may even influence the position at which thermal runaway eventually begins.

### **2.2.2 Pressure Measurement**

Internal pressure is another measurement that is very important in understanding the conditions at the onset of ignition and beyond. Various methods have been attempted, but all generally suffer from the same engineering considerations as for embedded thermocouples. It is challenging to route the electrical signals from within the confining body, and pressure measurements are most often made by placing the pressure sensor outside the confinement, connected via a tube soldered or mechanically fixed through the wall of the confinement [37]. This has the advantage that the sensor can be maintained at a steady temperature and calibration of the sensor as a function of temperature is simplified. In addition, if a sufficiently long connecting tube is used, then the sensor can be protected from the exploding confinement and re-used. However, this arrangement has several drawbacks.

Externally-mounted pressure gauges only provide accurate measurements when the internal pressure is relatively uniform, and equal throughout the interior of the confinement and along the connecting pipe. As the ignition begins develop into a growing reaction, this uniformity is lost: if the internal pressure changes more quickly than, for example, the time taken for a pressure wave to propagate along the connecting tube, then the sensor measurement will no longer accurately track these changes. Later during the growth of reaction, as fast burning develops and grows, the pressure varies even on small scales, locally within the specimen, and pressure measurement is impossible using a simple single-point pressure sensor.

External, tube-mounted sensors also influence the experimental method by increasing the free expansion volume within the confinement, by the addition of the internal volume of

the connecting tube to the overall confinement volume. To mitigate this influence, small-bore capillary tubes can be used, though there is a risk that these might become clogged by movement or damage to the specimen. Other tests, such as the NWC SSCB method [19][20] mount the pressure sensor directly into the wall of the confinement, and accept that it will be destroyed by the experiment, and also accept the increased complexity required to account for calibration variations as a function of temperature.

Other internal measurements have been considered, though these introduce different complexity in measurement. Piezo-resistive materials have been considered, so that sensors made from these materials could be embedded directly within the specimen pellet. However, there is no single ideal material from which a sensor could be made. The dependence of resistance on pressure is well-known for manganin, for example, but very high pressures (gigapascals) are required to produce an easily-measured resistance change. Urtiew [61] published results that showed that the calibration of manganin is insensitive to temperature up to 250°C, which is an advantage in pressure measurement accuracy. However commonly available foil gauges, as used in shock initiation experiments, require a pulsed constant-current power supply to avoid overheating and damage to the gauge, limiting the measurement time of this method to ~100 μs, and it is difficult to synchronise the ‘active time’ of the gauge to the moment of ignition with such precision. Carbon film gauges have also been used as pressure sensors, with a usefully large change in resistance as a function of pressure to allow measurement of low pressures, but these also show a very strong and variable temperature dependence on resistance, rendering them difficult to reliably deploy in cook-off type experiments. Piezo-electric materials, such as quartz or PVDF [63] have also been used to measure pressure in impact experiments but have not been applied to the cook-off problem, again because these materials exhibit strong temperature dependencies in their sensitivity [64]; in the case of PVDF, the pressure response is completely destroyed at even moderate temperatures of around 80 °C, again rendering them unsuitable for in-confinement pressure measurement.

In all types of electrical internal pressure sensing, of course, making the electrical connection through the confinement while maintaining a good pressure seal is, to say the least, problematic.

### 2.2.3 Direct Observations

In the author's early work [Annex A.1, Annex A.3] we began to investigate methods to directly observe the ignition process in confined cook-off by replacing part of the confinement with a transparent window. At that time, digital high-speed cameras were very much less mature, and high-speed observations required the use of a triggering signal to command the camera to begin recording, so that images were recorded only after the triggering signal was received. Such cameras, while offering good image quality and high framing rates, were therefore most generally used to observe experiments that were command-initiated, and used timing sequencers to synchronise the firing of the experiment with the operation of the camera. Their application to cook-off was therefore limited using some feature of the developing burn, such as increased light output or the increased strain measured on the casing of the confinement, to trigger image capture, and the behaviour prior to ignition was missed. Dickson [60] used this method to capture interesting images of the post-ignition burn, and also attempted to 'force' ignition using an electrically-activated embedded wire, with the signal to the initiation wire also being used to trigger image capture. Dickson was able to observe the initial stages of growth of reaction after initiation, and noted the propagation of luminous flames along newly-formed cracks spreading outwards from the initiation point. This led to the conclusion that the thermal explosion, in driving gases outwards from the initiation point, would open up new surfaces to support accelerating burning, and that this would be a plausible mechanism for high-rate energy release and hence violent cook-off.

Our early work [Annex A.1] used continuous low-rate video recording to observe the slow changes up to ignition and burning, and in the first experiments with relatively weak and non-gas-tight confinement we were able to observe the slow burning behaviour of a RDX/HTPB secondary explosive. In particular we saw a slowly-oscillating burn was set up, in which the developing flame caused the confinement to expand and allow gas to escape, following which the internal pressure in the confinement fell and the burning rate fell. This process repeated until the specimen was consumed. This qualitatively showed that the burning rate and confinement are co-dependent, and added support to the view that the type and gas-tightness of the confining structure was important in governing the burning behaviour.

That experiment was developed [Annex A.3] to improve the engineering design of the fitment of the observation window, allowing potential control over the degree of

confinement, and also to include features of the confining structure that, in post-firing examination, would be diagnostic of the violence of event. In these experiments we observed (at low framing rates) interesting melting and liquid flow migration prior to the emergence of the luminous flame and subsequent explosion, though again the low-rate video recording limited the details that were observable. In RDX/TNT we were unsurprised to observe melting of the composition, but noted that in all cases ignition was immediately preceded by obvious bubbling in the melted material, and that the ignition appeared to originate near the bubbled region, though the slow imaging rate from the camera prevented study of that ignition process in detail. In HMX/HTPB we noted an emergence of a liquid at the surface of the test specimen in the few seconds prior to ignition and explosion, but assumed that this was the DOS plasticiser migrating from the binder component.

More recently, with the development of digital high-speed cameras capable of continuous ring-buffer recording and post-trigger capture in 2000 to 2004, we have been able to develop the direct observation method further and record both the pre- and post-ignition behaviour at high framing rates [Annex A.8, Annex A.10, Annex A.11]. These observations have shown a much more complex behaviour in the specimens than had previously been closely observed, with significant changes in both pure nitramine explosives and explosive/binder systems, and these will be discussed in more detail in the next chapter.

### 3 The Character of Thermal Damage

#### 3.1 Introduction

The general view in cook-off studies has been that the confined energetic material remains relatively un-influenced by its temperature until the onset of ignition, and that thereafter the growth of reaction proceeds as an accelerating burning process, possibly resulting in the transition from deflagration to detonation. Studies of the changes during heating have placed a great deal of emphasis on the phase change from  $\beta$ -HMX to  $\delta$ -HMX and the conditions under which this can occur. For example, Dickson et al [60] view violent cook-off responses in HMX-based compositions as being the result of the weak pressure waves coupled with permeation of hot gases, which together emanate from the ignition point. The spread of reaction proceeds through the surrounding ‘thermally damaged’ and, in their view, violent response is caused by the increased sensitivity of  $\delta$ -HMX to initiation. In addition, in the region surrounding the ignition point, the surface area available for burning is considered to increase as a result of hot gases from the ignition being forced through this region, potentially between the binder and energetic particles.

Studies such as these are restricted to solid HMX-based PBXs, and there is an implied assumption that ignition is some instantaneous process which begins at a fixed and predictable location once the appropriate conditions are reached. Furthermore, the ‘instant of ignition’ is viewed as marking the end of purely slow-rate thermal change and the beginning of a purely burning process associated with the flames visible through the viewing window. Furthermore, there is another implied assumption that only relatively minor changes have occurred during the pre-ignition heating phase, so that the microstructure through which the hot gases permeate and create additional surface area largely resembles that of pristine, un-heated material.

Interesting behaviour has been noted recently in several experiments funded via the Weapons Science and Technology Centre (WSTC) to develop the Advanced Cookoff Experiment (ACE) vehicle, and has been reported as presented in Annex A.8 and B.1. These studies hoped to inform the earlier work with HMX-based PBX compositions, in which we saw that, just prior to ignition, liquid material was welled up across the visible surface of the pellets. At that time, we had assumed that this material was simply the DOS plasticiser component of the binder being forced out as it reached its boiling point.



In the ACE work presented, pure RDX and HMX powders, and HMX-based formulations were observed throughout the development of violent ignitions. More recent work, currently in publication has observed other pure materials, PBX mixtures and melt-cast compositions [68].

### **3.2 Changes Occurring in the Early Stages of Heating**

In early heating, where the temperature is below the critical temperature, thermal expansion is the most significant change in the heated specimen. Below the critical temperature, decomposition of the confined specimen is very low, though the empirical Arrhenius equation might suggest that reaction rates are non-zero for all temperatures above absolute zero.

Thermal expansion therefore would seem to be the primary change that occurs during early heating, before decomposition begins, and indeed this seemed to so for direct observations experiments such as those reported by the author and presented in Annexes [A.1, A.3]. In early glass-windowed experiments we had noted a gradual slow expansion of the HMX/HTPB pellets at temperatures below 150°C, which could not be attributed to the well-known  $\beta$ - $\delta$  transformation widely reported to lie in the range 159 to 165 °C. Rather, those experiments, showed temperature excursions recorded on the internal thermocouples in the 160 – 170°C temperature range accompanied by a more obvious and faster expansion, and these effects were attributed to the  $\beta$ - $\delta$  transformation.

The thermal expansion noted in those experiments was accommodated mainly by the intrinsic porosity of the specimen pellets, which were all in the range 94 to 96% T.M.D. In addition, the need to allow sufficient space to insert the test specimens into the confinement would introduce a small degree of ‘ullage’, which would again provide room for expansion. However, some expansion could potentially be accommodated by compression of the binder, given that HTPB in these compositions was cured to a hardness of 28 to 34 Shore A [67]. The elastic modulus of the binder, of course, depends strongly on the curing state and in general this varies widely even among compositions using HTPB as the binder; many explosive compositions do not even include a soft, accommodating binder component.

### **3.3 Observations of RDX and HMX**

In work reported in Annex A.8 and Annex B.1, pure RDX was observed to undergo melting and at moderate heating rates it was possible for complete melting to occur. The

specimens were initially low-density powders representing significant entrapped air, and upon melting this coalesced into a single bubble at the top of the specimen cavity, with molten material below. Bubbles were seen to develop within the liquid portion, rising and merging with the upper gas bubble, and the rate of bubble generation and overall vigour of gas production increased as the point of ignition neared. The period of melting, bubble development and slow convection-like circulation in RDX lasted tens of seconds; all traces of the original morphology and particulate nature of the specimen was eliminated.

Though relatively few experiments were conducted, in all of them a visible luminous flame was seen to commence from a point at the interface between the liquid and gas spaces. This was always preceded by increasingly vigorous bubbling at the eventual point of the onset of flame. Development of the flame occurred over hundreds of microseconds, propagating through the upper gas bubble at a speed of  $\sim 10 \text{ ms}^{-1}$ . As the luminous region grew, the liquid-dominated region was clearly compressed, with the compression accommodated mostly by decrease in size of the entrapped gas bubbles that had developed throughout the liquid. Compressive strain rates of  $2.5 \times 10^3 \text{ s}^{-1}$  were measured for the liquid portion taken as a whole, and some larger visible bubbles with diameters in the range 150 to 450  $\mu\text{m}$  were seen to uniformly compress to a  $V/V_0$  of  $\sim 0.1$ .

In each experiment with RDX the ignition process described above was terminated by the sudden de-confinement of the test vehicle, with shattering of the glass observation window and a relatively violent explosion.

By contrast, pure HMX powder underwent no mass-melting as had been observed for RDX. However, local melting was observed, occurring a few seconds before the onset of flame and subsequent ignition. The overall structure of HMX seemed to show the presence of solid powder, surrounded by a liquid-soaked powder region, and this all surrounded by semi-molten and bubbling material, indicating that gas generation at the same time as melting. The luminous flame began in the bubbling, gas-permeated region and propagated only through that region until the flame brightness overwhelmed the sensitivity of the camera and detail was lost, but the point of maximum brightness was followed within a few tens of microseconds by explosive de-confinement. As with RDX, the available gas spaces were seen to be compressed as the luminous flame grew in size, and luminosity was seen to begin in these compressed spaces before the arrival

of the main flame front, suggesting that gas compression driven by the developing flame could contribute to overall flame propagation.

Many more experiments were conducted than could be fully represented in the published work, so that some additional observations are presented here. Of interest is the experiment with a composition of HMX and un-plasticised Viton, and still images from the video record are shown in Fig. 4 during the last 4.0 seconds prior to ignition and explosion. These observations were noted at an applied temperature of  $\sim 240$  °C, substantially lower than the generally quoted ignition temperature of pure HMX.

These images clearly show the propagation and spread of a liquid layer across the surface of the specimen, and in the light of the pure HMX observations, we are more sure that this liquid is molten HMX. The presence of the Viton binder limits the spread of this liquid, and reduces the overall bubbling and irregularity in the specimen seen with the pure powdered HMX.

High-speed images taken later in this experiment are shown in Fig. 5, and show the development of the flame over 800 microseconds, beginning and spreading throughout the region where the molten HMX originated. There appears to be little or no propagation of the flame into the non-molten zone during the development of the burn, even up to  $\sim 1.3$  ms after first ignition where maximum flame brightness was seen, but the consequent pressure rise was sufficient to break the confinement non-violently.

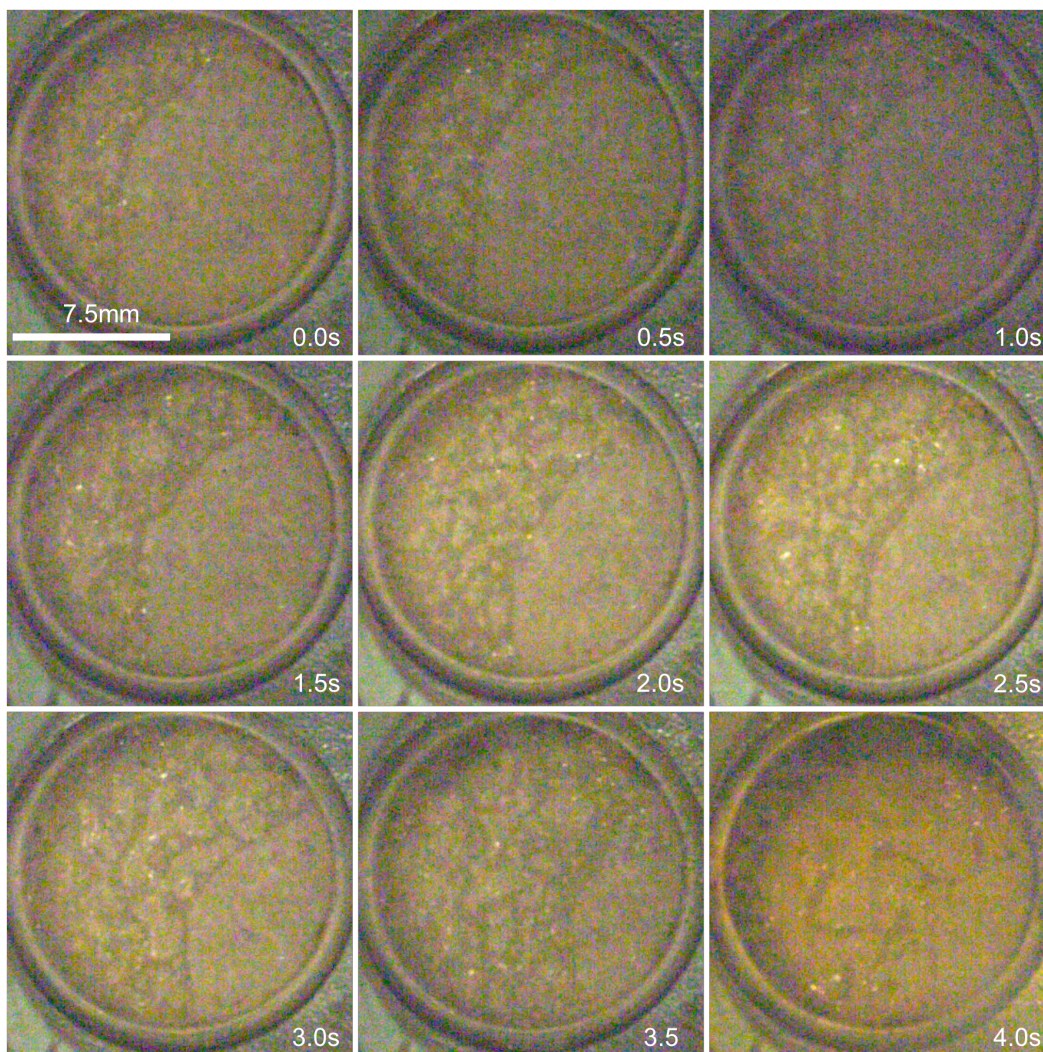


*Fig. 4: Melting and release of HMX from the binder matrix in a HMX/Viton 90/10wt% composition, over a period of ~4 sec. This behaviour occurs several seconds prior to the onset of luminous flame and associated explosion.*

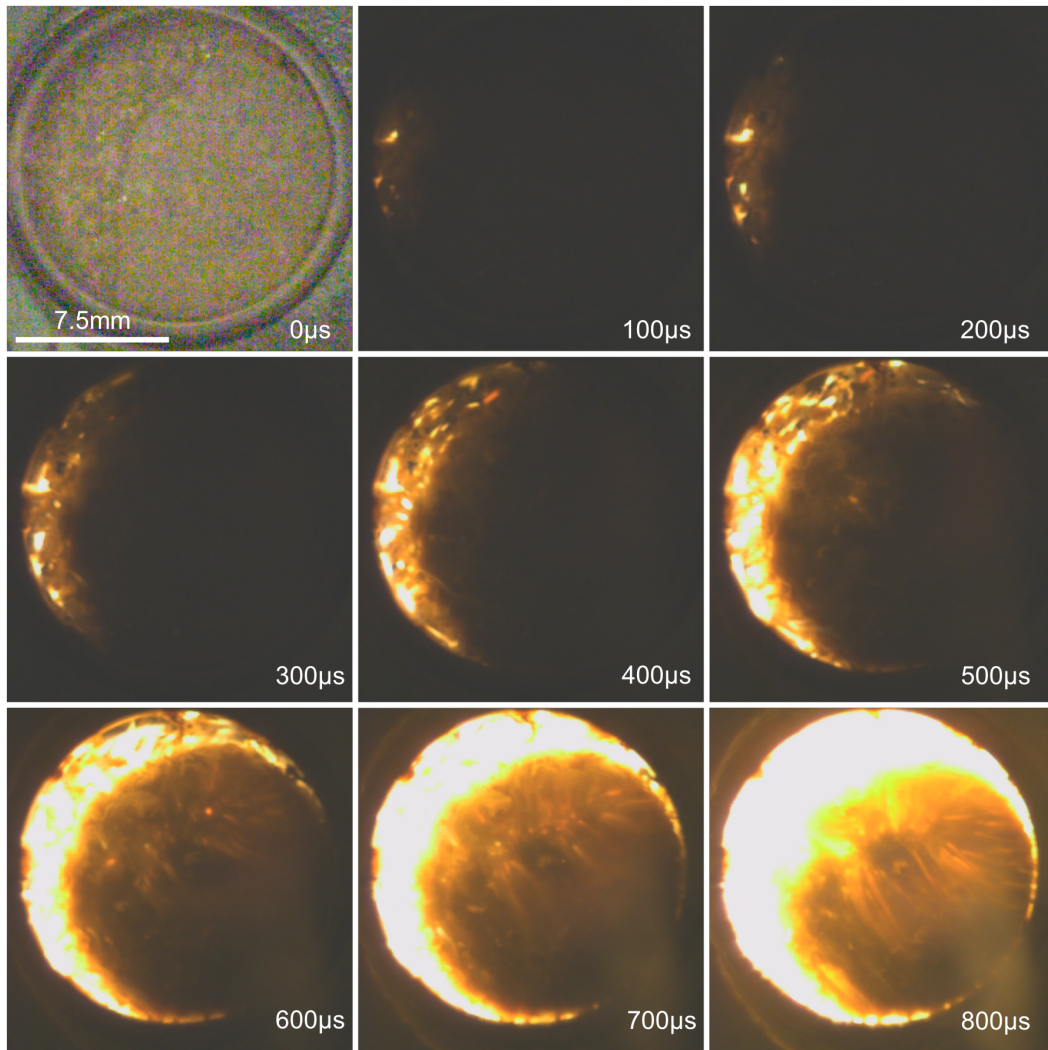


*Fig. 5: HMX/Viton 90/10wt% at ignition. The upper-left image indicates the reference geometry. Development of the flame reached maximum brightness at  $\sim 1300\mu\text{s}$  after onset, but confinement had leaked; burning continued for a further  $\sim 100\text{ ms}$*

Different behaviour was seen in compositions of HMX/Aluminium/Hytemp compositions, and one is shown in Fig. 6. In these experiments sudden and violent deconfinement occurred within a few tens of microseconds after the last recognisable camera image, around 400 to 500  $\mu\text{s}$  after the onset of flame. The roughly circular dark zone in these images is again attributed to the expulsion of liquid HMX, and the flame origin is at the centre of that zone.

Comparing these two HMX-based compositions, it should be noted that the temperature of the specimen would be expected to vary along radial lines, but would be relatively symmetrical around the circumference. For fast heating rates, it would be expected that the boundary temperature would be hottest, while for slow heating rates, self-heating of

the specimen would drive a higher temperature at the centre of the specimen, but in either case a circumferentially symmetric structure would be preserved. This circular structure can be seen in the HMX/Aluminium/Hytemp composition, with regions of solid and liquid material remaining in an approximately circular structure, and this leads to ignition at the centre of the specimen. By contrast this symmetrical structure is completely changed by the significant mobility of the liquid HMX, leading to ignition at some other location that is unrelated to the symmetry of the confinement or heating condition. This comparison suggests that the binder and microstructure of the composition influences the location at which ignition begins, and hence the growth of reaction away from the ignition point and into the surrounding material.

These observations also show that flame propagation into the solid or liquid material, if it occurs as proposed by other workers, must occur on fast time scales of the order of microseconds, and does so only after significant pressure has built up within the confinement. The initial stages of burning we have seen here all indicate that burning even up to a few tens of microseconds prior to de-confinement is restricted to the gas-permeated spaces.

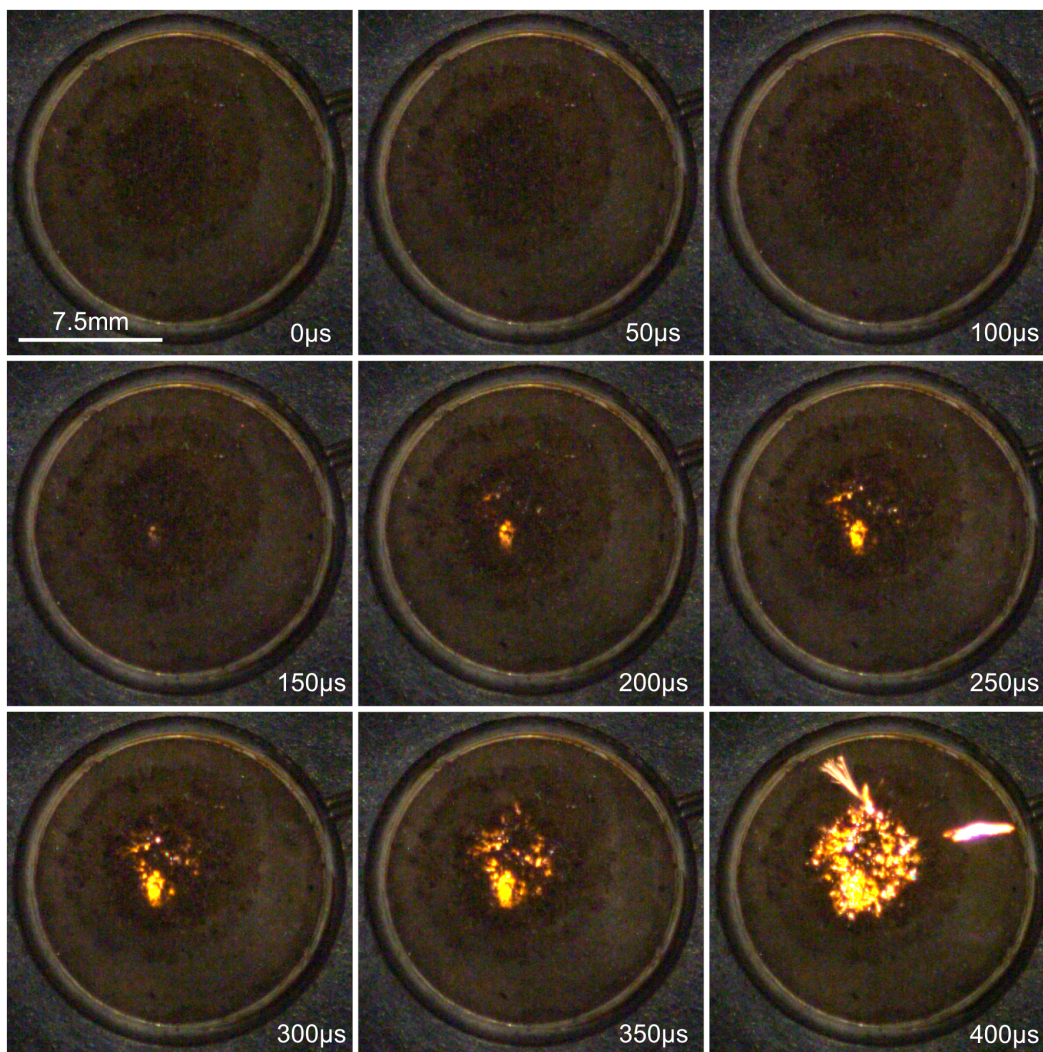


*Fig. 6: Ignition in HMX/HyTemp/Aluminium under slow heating. A violent explosion occurred at 450µs on the timescale of these images, completely de-confining the experiment and with total overexposure of the camera image*

### **3.4 The Role of Melting**

We have examined other materials to explore the influence that melting might have on the subsequent violence of response and propagation of reaction, and this was prompted by the observations of pure RDX.

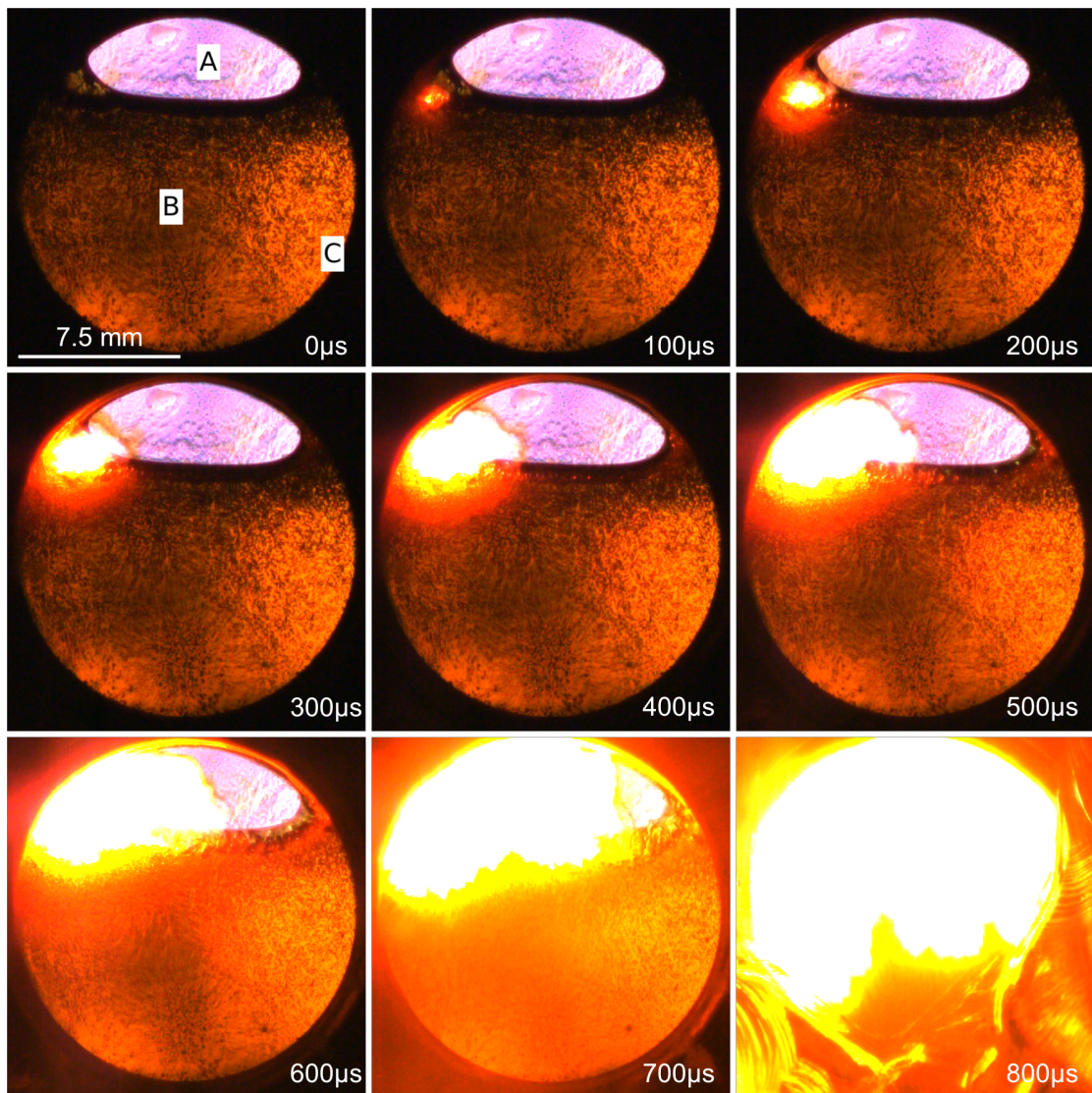


*Fig. 7: Ignition in RDX/TNT near ignition. A gas space (A) has developed above a pool of molten material (B), surrounded by a heated boundary (C). At low temperatures (90 to 210°C) most RDX remains solid, settling to the bottom of the specimen cavity. At higher temperatures (210 to 220°C) all RDX has melted and convection-like motion and of bubbles develops. Propagation of the flame and compression are similar to that seen in pure RDX.*

Where materials, like RDX/TNT or pure TNT melt, we consistently see the development of a fully liquid region that falls under gravity to the bottom section of the confinement, with one or a few large gas-filled regions rising to the top. Flame onset and propagation seems to be exclusively restricted to the gas-filled regions until a few tens of microseconds before final violent de-confinement, and again we observe no obvious propagation of flames into the liquid bulk in the early stages of flame development and pressure increase. This behaviour is similar for all those materials for which the melting temperature is significantly lower than the ignition temperature.



The molten zone is seen to be filled with gas bubbles, which develop within the liquid and are naturally buoyant and therefore rise. As with pure RDX, we see compression of the bubble-filled liquid, driven by the development of the luminous flame in the large gas spaces and the consequent increase in internal pressure.

### **3.5 Concluding Remarks**

Our experiments show that the microstructure of explosives under cook-off undergoes gross change as the ignition point nears, and that this is strongly influenced by the melting of the different components of the composition. For pure materials like RDX or TNT, where the melting point is significantly lower than the ignition temperature it is likely that complete melting will occur, except at the very fastest heating rates.

For materials encapsulated in inert binders, such as an RDX/HTPB composition, the existence of the melt pool is influenced by both the binder and to a lesser extent on the melting point of the energetic filler. For highly-loaded compositions it is possible that the binder does not form a continuous ‘web’ separating the explosive particles, so that under full melting the binder could separate and migrate leading to a large continuous melt pool and an associated continuous gas space similar to that seen in the pure materials. In low-loaded compositions, the binder could potentially form an open- or even a closed-cell foam structure, which would inhibit the formation of a large, continuous melt-pool and gas space. Instead, the molten energetic material would be confined to separate pockets, so that the flame igniting in one pocket would less easily propagate into adjacent pockets, limiting the overall rate of flame spread and associated gas production. In this way, the propagation of the flame immediately after ignition (and hence the early-time rate of pressurisation of the confinement) would be strongly influenced by the quantity of binder in the composition.

Even for materials like HMX, which do not completely melt before ignition, we can see that the binder influences the development and burning behaviour of large continuous gas spaces, and again, the presence of a greater proportion of binder would act to decrease the rate at which the initial flame can spread. This would, in turn lead to a lower rate of pressurisation of the confining capsule, potentially leading to a lower overall ‘violence’ of response. This, of course, is dependent strongly on the nature of the confinement, as will be discussed in the next section.



## 4 The Role of Confinement

### 4.1 Introduction

This section introduces the notion that the confinement in a cook-off event is more complex than simply ‘unconfined’ and ‘confined’, and explores the implications of this in the development of ignition and subsequent growth.

The behaviour of the confining structure has a strong influence on the response of the experimental specimen as the ignition process develops. Furthermore, the response of the confinement and the response of the specimen are co-dependent; the accelerating reaction in the specimen causes the confining structure to deform and begin to fail, and the failure of the confining structure (with its associated de-pressurisation) causes the reaction rate in the specimen to change.

### 4.2 Confinement Types

The authors experience and observation of different cook-off experiments has led to an informal classification for the types of confinement that are generally found, and these are presented in the table below.

Type	Designation	Description
Type I	Wholly unconfined	Gases able to freely escape from the confinement at all stages of the ignition process. Internal pressure during pre-ignition quickly equilibrates with atmospheric pressure
Type IIA	Leaking	Openings in the confinement are small, allowing gases to slowly escape. As the rate of gas generation within the confinement increases, internal pressure cannot remain in equilibrium with atmospheric pressure.
Type IIB	Dynamic de-confinement	Confinement is initially perfectly sealed, allowing no gases to escape. Internal pressure rises during ignition, but rising internal pressure can deform and open the confinement so that gases can then escape. Internal pressure increases, so does the leak rate.
Type III	Fully confined	Perfect sealing until the confinement grossly and completely breaks

The Koenen test [5] examines the response of an energetic material under variable confinement, and the test apparatus includes an orifice plate which allows gases to escape from the specimen during ignition. Successive tests are performed with orifices of different diameters, to restrict gas escape, thereby modifying the internal pressure and burning rate. Where large orifices are used, this is an example of a Type I confinement.

The Koenen test with very small orifices, or the EMTAP Tube Tests, represent a Type IIA confinement. Whether by design or accident, small leak pathways allow gases to escape, but as decomposition of the specimen progresses, self-pressurisation can occur as the rate of gas production exceeds the ability of the leak pathways to vent. This is similar to, but distinct from the Type IIB confinement, which is initially gas tight but where leaks can develop as the internal pressure deforms the confinement and opens leak pathways. Type III confinements represent those experiments in which the gas tightness is maintained throughout heating until the final, violent disruption of the confining structure.

The ability of the confinement to withstand internal pressure is another important aspect of the experimental design. Colloquially, experiments are classed according to confinement 'strength', with 'high' confinements being those which are expected to retain the initial experiment geometry to a high internal pressure, in contrast to 'low' confinements. Examples of Type III High Confinement experiments, offering gas tightness to very internal high pressures, would be ODTX (150MPa burst pressure) or SSVT (300-400 MPa burst pressure). VCCT [18] (burst pressure 8 to 80 MPa), or the glass windowed WSTC ACE experiment (burst pressure < 10 MPa) would be broadly classed as a Type III Low Confinement experiment, where ultimate failure occurs at a relatively low pressure.

### **4.3 Classifications of Response Violence and $dE/dt$**

#### **4.3.1 Post-Experiment Evaluation**

In considering the violence of cook-off response, at the most simplistic level it is straightforward to classify responses as 'violent' or 'non-violent', and this classification is generally obvious from the collateral damage that can be examined after the cook-off event has occurred. For example, if a munition is heated to ignition and an explosion results in the formation of a crater and the munition casing is reduced to small fragments, then this is clearly a more 'violent' response than if, on examination of the scene, the munition casing is recovered largely intact.

It is immediately clear that classification of the response into 'violent' and 'non-violent' categories is not adequate and offers little useful information, and various classification schemes have been proposed which distinguish the degree of response in a more formal and reproducible way. In particular the UK EMTAP Tube Test and the NWC SCB Test

[28], both of which have a scale of responses which aim to add fidelity to the test outcome. For example, the SCB test designates responses as:

<b>Response Designation</b>	<b>Number of sleeve fragments</b>	<b>Condition of retaining bolts</b>	<b>Condition of end plates</b>
Burn	<2	All intact	No deformation
Pressure rupture	<3	No more than two sheared	No deformation
Deflagration	<3	Two or more sheared	Deformation of one or both
Explosion	Many small fragments	All sheared	Deformation of one or both
Partial detonation	Many small fragments	All sheared	Perforation of one end plate
Detonation	Many small fragments	All sheared	Perforation of both end plates

Note that these designations include a brief description of the damage experienced by the confining structure, though these are somewhat subjective and not explicitly quantified.

The UK EMTAP Tube Test quantifies the energetic response in terms of the number of fragments into which the tube has been broken, with greater fragment counts indicating more violent responses.

#### **4.3.2 Asymmetry in Observed Damage to Confinement**

The SCB test classifications are of interest, particularly the distinction between ‘Partial Detonation’ and ‘Detonation’: partial detonation is evidenced by perforation of only one of the end plates, and the plate at the opposite end is deformed but not perforated. In these ‘partial detonation’ responses, this asymmetry in damage suggests two general processes that might have occurred. In the first, thermal explosion begins near one end of the tube and propagates into a detonation, which then perforates the plate at the opposite end of the experiment. In the second, a thermal explosion beginning near one end plate is alone sufficient to perforate the plate, and propagation towards the other end plate does not develop into detonation.

In the author’s work [24, Annex A.6] we carried out pipe-bomb experiments where the specimen l/d was 8, and deliberately restricted heating to one half of the tube. For RDX/TNT specimens we noted asymmetric damage in all experiments, generally with

fragmentation of the tube occurring locally to the heated area that indicated a moderately violent explosion there, and with much less damage to the un-heated end. This type of damage indicates a relatively rapid rate of pressurisation centred at the heated zone, and furthermore that the pressure within the confinement was not uniform at the point of confinement failure.

In one experiment with RDX/TNT we noted a very violent response, where the tube at the unheated end had been reduced to a large number of very small fragments. The fragments recovered from the heated zone were similar in size and character to those recovered from the other experiments on that material. This observation suggested that, in RDX/TNT, the mechanism of thermal explosion developing into a ‘detonative’ process was at work.

In all the RDX/TNT experiments, internal temperature measurements showed that most of the filling had exceeded the melting temperature, there remained a temperature gradient of approximately 70°C between the heated and un-heated ends at the time of ignition.

In similarly heated experiments with a RDX/HTPB filling, however, the responses were uniformly mild, with failure of the confinement occurring by an axial splitting of the confinement. This hoop failure mode indicates a relatively slow rate of pressurisation, and it is likely that the pressure within the confinement was approximately uniform at the point of confinement failure.

#### **4.4 Behaviour of the Confinement Prior to Gross Failure**

Williams and Matei [35][36] used the ODTX experiment to explore measurement of the violence of explosion in a more refined fashion than simply by counting the fragments produced by the confinement. In their work both the plastic deformation of the anvils, and the early motion of the anvils showed relationships to the expected behaviour of increasing violence of explosion with decreasing temperature, and even led to a means to estimate the internal pressure, and therefore diagnose detonation during and after ignition.

In the author’s work using an early direct-observation confinement [Annex A.3] we used the deformation of flat steel rear face of the confinement as an indicator of explosion violence, by simple post-test measurement. In this work a range of PBX compositions of increasing solids loading were used, with HMX contents in the range 88 to 95 wt%.

We noted increasing deformation with increasing solids loading, and furthermore there was a distinct change in slope at 90 to 92 wt% HMX that suggested that, beyond these solids loadings, a different growth mechanism might be at work.

More recent work has made detailed observations of the confinement during the early stages of ignition, using a variety of non-contact diagnostics. Wardell and Maienschein [59] presented an experiment in 2002 which incorporated radar measurement of the expansion of the confining cylinder, and used this to derive a metric of violence that compared the expansion velocity resulting from cook-off to the expansion velocity resulting from detonation within the same geometry. This method followed the well-known Gurney analysis, for which a large body of detonation-driven expansion data is published.

In the authors work, in 2010 and 2011 [Annex A.2][ Annex A.4] we published results from a small-scale cook-off test in which the cylindrical test specimen was confined in a thick-walled cylinder, and heated at one end. The other end of the confinement was machined with a pre-formed fragment, and instrumented with a particle Doppler velocimeter (PDV) to measure the acceleration of the fragment during and after de-confinement. In those works, test specimens were of a range of compositions, including HMX/NC, several HMX/fluoropolymer variants, TATB, TATB/Viton, RDX/TATB, and Tetryl. Geometries ranged from 10 mm right cylinders, to cylinders 40 mm long by 10 mm in diameter.

The acceleration of the pre-formed fragment was found to be not simple in all experiments. Pure TATB showed the simplest profile with a smooth acceleration of the fragment from rest, typically reaching  $100 \text{ ms}^{-1}$  within  $\sim 150 \mu\text{s}$  of the first onset of detectable motion. HMX/polymer compositions with 8% binder showed a similarly smooth acceleration, but reaching  $150 \text{ ms}^{-1}$  within 40-80  $\mu\text{s}$  of first motion. HMX/NC compositions, however, were more complex: ultimate velocities of  $\sim 200 \text{ ms}^{-1}$  were reached within 40 $\mu\text{s}$  of first motion, but the velocity history generally showed distinct changes in acceleration during this time.

The author's most recent work has again used the PDV method to observe the early-time motion of other test geometries, including the ODTV experiment [Annex A.9] and the WSTC ACE experiment [Annex A.10, Annex B.1]. In both these methods, we have applied both Williams' and Maienschien's reasoning to characterise the violence of

response in terms of the expansion velocity achieved at a prescribed extent of expansion. By choosing an extent of expansion at which the confinement had not yet opened, and hence the reacting gases were completely contained, we have found similar trends of this measure of violence as functions of both ignition temperature and energetic solids loading. Care must be taken, however, that the experimental geometry allows sufficient space, and offers sufficient confining capacity to allow the full development of the violent reaction to take place. For weak confinements, once the confinement opens and gases can escape, the internal pressure will fall and the incipient reaction will potentially be quenched.

#### **4.5 Concluding Remarks**

The confinement plays an important role in the cook-off process. The type of confinement (gas-tight, leaking, weak, strong) influences both the rate at which burning can develop and the ultimate extent of the burning reaction that can be achieved. Strong, sealed Type III confinements would generally be expected to provoke the most violent responses, but we have also noted violent responses in confinements of Type IIA and IIB.

The current understanding of metrics of violence in cook-off is generally not well established, though other workers are making progress in linking the rate of energy release during and after ignition to the behaviour of the confining structure as it begins to fail. This is an important link: most historic studies have used the post-firing debris as an indicator of violence. The authors' recent studies, particularly in the use of the heterodyne velocimeter to observe the early-time motion of the confinement, have strengthened this link, while also providing useful dynamic motion data that can be used to develop and validate coupled thermo-mechanical computer models of the cook-off process.



## 5 Computer Modelling of the Cook-off Process

### 5.1 Introduction

Early studies in cook-off have focused on two main topics of interest: the time taken for a particular specimen of an energetic material to ‘explode’ when heated; and what has been loosely termed the ‘violence of event’.

Much progress has been made on the former topic, to the extent that computer models now exist that can give quite good predictions of time-to-event. These models require the geometry of the system under consideration to be specified with good detail, and that the heating regime or environment be well-known, and also include a description of the decomposition chemistry of the particular explosive under study. The first part of this chapter discusses the principle of operation of time-to-explosion modelling.

Predictive models for violence of event are much less well-developed, and there are several reasons for this, but the main challenge is to accommodate physical processes happening on time scales that vary by orders of magnitude. During early decomposition, the model must only track changes occurring over minutes or even hours, and there is little appreciable mass motion in the system being simulated, except perhaps slow-rate thermal expansion. This phase can be accurately modelled without the need to explicitly track pressure changes. Conversely, after ignition, pressure becomes increasingly important and if the cook-off reaction can transition to detonation, then eventually pressure can dominate to the point that reaction propagation can be considered as a nearly adiabatic process. In the author’s recent work, we have seen that physical changes occur on millisecond or microsecond time-scale immediately prior to ignition. Though quite sophisticated computer models of the detonation process have been implemented (for example the implementation of the Jones-Wilkins-Lee equation of state in AutoDyn) these do not consider temperature as a key parameter at all, and temperature has no influence on the propagation of detonation waves in these models. This is evident from the formulation of the JWL equation of state:

$$P = A \left( 1 - \frac{\omega}{R_1 V} \right) e^{-R_1 V} + B \left( 1 - \frac{\omega}{R_2 V} \right) e^{-R_2 V} + \frac{\omega e_0}{V}$$

and it can be seen that only pressure and volume are used.

The key problem, therefore, is to reconcile the differing orders of magnitude and the different physical processes during the transition from purely thermal behaviour to purely pressure-dependent behaviour. We have seen that the transition from thermally-dominated to mechanically-dominated processes is a gradual process, and not one where different physical mechanisms simply ‘switch on’ when some conditions are reached. This indicates that coupled thermo-mechanical models are required to properly simulate the ignition and growth process. Our work in implementing a temperature-based initiation and detonation model [Annex A.6, A.7] was an attempt to begin the development of a so-called ‘global kinetics’ model, in the hope that a single description of the chemical decomposition kinetics could describe both cook-off and detonation processes.

## **5.2 Arrhenius-Based Kinetics Models**

### **5.2.1 Simple Heat Transfer**

The decomposition kinetics approach to modelling of cook-off is most easily illustrated with a simple 1D single-step model, of the type that can be implemented in applications such as Matlab in a straightforward manner. In this type of model, the spatial geometry of a given problem is discretised into a set of elementary cells of generally uniform shape, so that simple (and solvable) equations for the heat transfer within each cell can be calculated. The simple calculation, performed, over the set of cells then allows the global heat transfer in space to be computed, and complex problem geometries can be represented by a suitably-chosen set of elementary cells. Time integration is generally achieved by performing the spatial iteration to compute the heat transfer occurring over a short time-step,  $dt$ . By repeatedly calculating the heat flow in short time steps, the time-dependent behaviour of a complex geometry can be simulated.

### **5.2.2 Cylindrically-Symmetric Example**

To illustrate the implementation of decomposition chemistry in a thermal problem, a simple system is described. The simple model consists of a cylindrical geometry in which the temperature is prescribed as a function of time along the axis, and heat flows radially away from the axis into the cooler solid material of the cylinder body. The outer surface of the cylinder is assumed to be able to freely dissipate heat into an infinite heat sink. The problem, illustrated in Fig. 8, can be easily implemented in one dimension if the cylinder is assumed to be infinitely long and no axial heat transfer occurs.

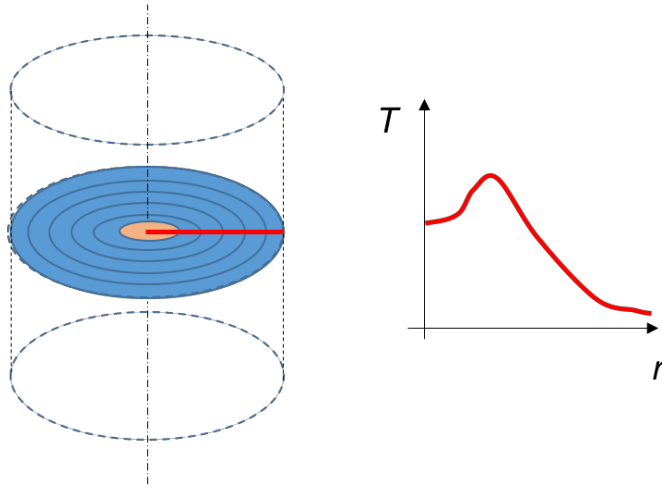


Fig. 8: 1D Cylindrically-symmetric example. The yellow region of at the centre of the cylinder represents a heat source whose temperature is manipulated as an input to the model. The blue region surrounding represents a solid material, through which heat transfers by conduction, and the outer edge of the cylinder is an infinite heat sink.

The diagram in Fig. 9 illustrates the basic meshing scheme, with simple examples of Fourier conductive heat transfer for the boundaries and internal conduction shown. Heat transfers into the left-hand edge of the mesh, following a time-varying temperature,  $T_{bound}$ . Conduction occurs across the interface between each element of the mesh, whose interface area is denoted by  $A$ , and whose spacing is denoted by  $l$ . The thermal conductivity,  $k$ , of the material influences the rate of heat transfer,  $Q$ . Temperatures throughout are denoted by  $T_n$ . Note that the ability of the model to represent reality is partly defined by the choice of these equations; for convective and radiative heat transfer, different formulae might be used and this is discussed later.

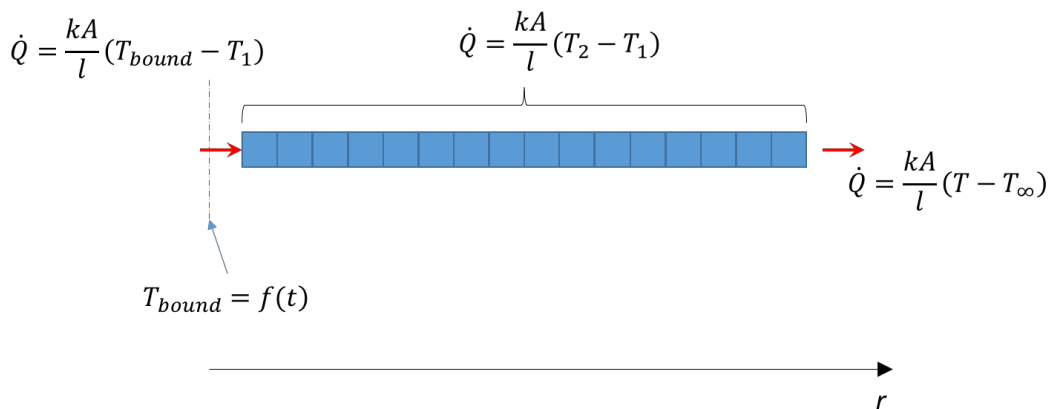


Fig. 9. Spatial discretisation of the cylindrical example, with temperature at the left-hand end of the mesh being specified by the time-varying parameter  $T_{bound}$ , and heat loss at the right dissipating into an infinite heat sink at temperature  $T_{\infty}$ .

The problem geometry (planar, cylindrical or spherical) is defined by the mass,  $m$ , of each element and, for the Fourier equations above, the inter-cell area,  $A$ . This is achieved by allowing these parameters to vary as a function of the radial distance of the cell from the axis. For a given cell whose left-hand and right-hand boundaries are at radial distances  $r_l$  and  $r_r$ , the mass,  $m$ , of the cell of material density  $\rho$ , are given in Fig. 10. Similarly, the interface areas at the left- and right-hand faces of the cell,  $A_l$  and  $A_r$  are shown.

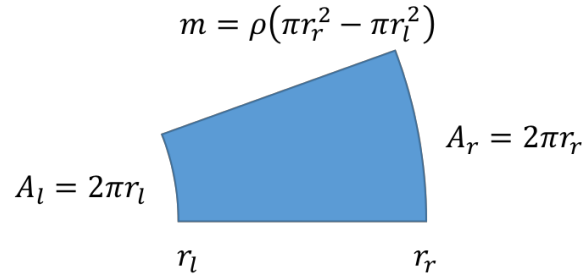


Fig. 10: Cell parameters to define the geometry of the problem, in this case cylindrical

For simple heat transfer without chemical reaction, a single time-step of the model operates in the following general way:

- Calculate the internal energy,  $Q_n$ , as the integral of the specific heat capacity curve
- Compute the change in energy,  $Q_c$ , resulting from heat conduction, occurring over a short time,  $dt$
- Calculate the new internal energy  $Q_{n+1}$  as  $Q_n + Q_c$
- Calculate the new cell temperatures from the updated internal energy
- Update the simulated time  $t \rightarrow t + dt$

This time-step calculation is repeated until a suitable ending condition for the simulation is met, which may be after some prescribed simulated time has been reached. More usually, however, the simulation is ended when the maximum rate of temperature rise exceeds some prescribed value in an attempt to specify that ‘ignition’ has occurred.

## 5.3 Energetic Materials

### 5.3.1 Extension to Include Internal Heat Generation

The above simple model scheme is easy to extend to include energetic materials, that is those which can release energy as a result of their temperature or other environmental conditions. For a given energy release,  $Q_e$ , resulting from chemical decomposition is included in the model at the stage where the new cell internal energy is calculated, and the energy update becomes:

$$Q_{n+1} = Q_n + Q_c + Q_e$$

For temperature-based decomposition, a simple way to include energetic materials is to use the Arrhenius relationship, which straightforwardly relates the rate of reaction of a material to its temperature:

$$k_A = A e^{-\frac{E_a}{RT}}$$

The two parameters  $E_a$  and  $A$  are constants that are specific to the particular chemical reaction under consideration, and must be obtained to fully ‘parameterise’ the reaction.  $E_a$  represents the activation energy of the reaction,  $A$  represents the collision frequency,  $R$  is the universal gas constant, and  $T$  is the temperature, resulting in the rate of reaction,  $k_A$ . The above equation, though empirically-based, is well supported by experimental observation, and techniques that measure chemical reaction rates as functions of temperature are commonly available to determine the reaction rate constants.

The dimensionless reaction rate,  $k_A$ , then allows calculation the mass fraction of material in a cell of mass,  $m$ , that is reacting in a short time,  $dt$ :

$$\dot{m} = k_A m dt$$

The specific energy,  $Q_x$ , of the energetic material then allows the energy contribution from the ongoing chemical reaction to be obtained:

$$\dot{Q}_c = \dot{m} Q_x$$

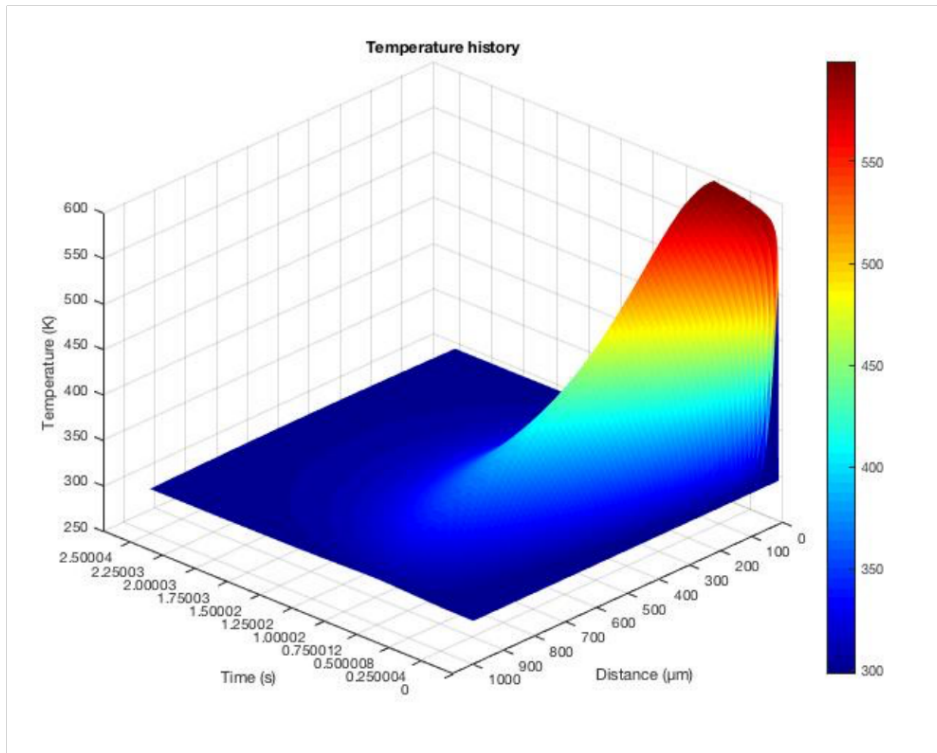
This simplified description illustrates the main components and approach of the modelling scheme, but, to aid clarity, omits many implementation details that are

necessary to ensure rigorous energy conservation and numerical stability. Of more interest is that this simple scheme forms the basis upon which additional physical mechanisms for decomposition can begin to be included. First, however, the things that this simple scheme can do will be discussed.

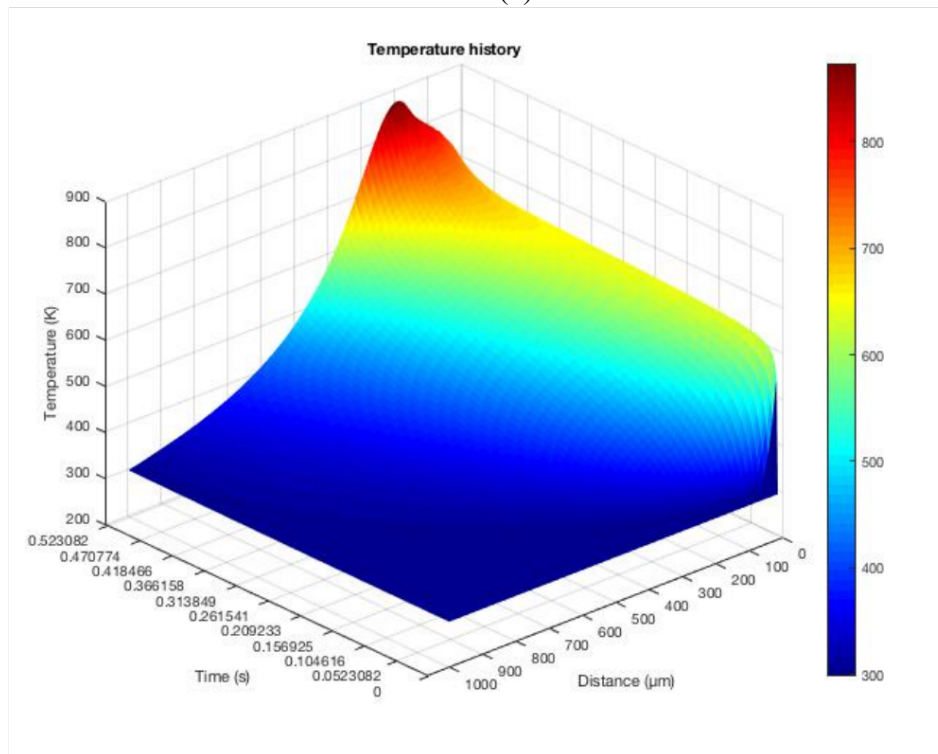
The plots in Fig. 11 shows the output from simulation runs of an implementation of the above scheme by the author[33]. In these simulations, the temperature boundary was specified as a rectangular pulse of 1 second duration, at different temperatures of 598 K (Fig. 11a) and 648 K (Fig. 11b). The vertical axis shows temperature, and the surface is coloured according to the scale bar to the right of the plot. The distance from the heated boundary progresses upwards and to the right; the simulated time advances upwards and to the left. The simulation was programmed to terminate at 2.5 seconds of simulated time, or when the temperature of any cell in the simulation exceeded 900 K.

The utility of the ongoing decomposition scheme is apparent from these simple runs: the lower-temperature pulse simulation shows essentially inert behaviour in the simulated material, and once the applied heat is removed the system cools to ambient temperature; the higher-temperature simulation shows thermal runaway and ‘ignition’ at a time of 0.52 seconds. Furthermore, the ignition location is a short distance away from the heated boundary. The location and time of ignition arose naturally from the ongoing decomposition, and were not prescribed in any way.

This type of model runs very rapidly and can be used to quickly explore more complex physical effects. For example, the plot shows the relationship between time-to-ignition and boundary temperature and between location of ignition and boundary temperature, where the boundary is held at a high temperature until ignition is detected. The relationship is clear, and is analogous in some ways to the  $P^2t$ -type relationships reported by Walker and Wasley [69] and more recently by James [34] in impact experiments.



(a)



(b)

Fig. 11: Temperature history plots for 1D cylindrically-symmetric energetic decomposition model runs with 1-second duration input pulses. (a) Simulation with a pulse temperature of 548 K, and coloured fringes of temperature between 273 and 550 K; (b) input pulse temperature of 648 K and coloured fringes between 273 and 900 K

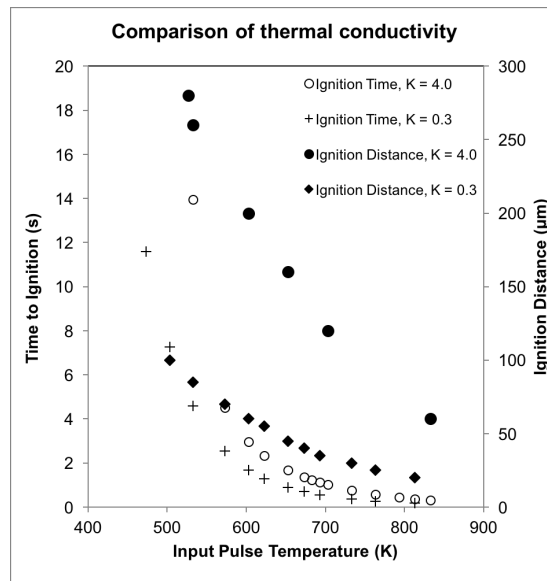


Fig. 12: Ensemble of runs with 1 second pulse durations at different pulse temperatures, for materials with two different thermal conductivities

### 5.3.2 Multi-step Decomposition Kinetics

The work reported by Catalano [14] clearly shows that the simple example of single-step decomposition kinetics scheme presented in the above model is inadequate to properly reproduce experimental data for one-dimensional time to explosion tests on secondary explosives. That work showed linear relationships between time to explosion and reciprocal temperature, whereas Frank-Kamenetskii [16], Zinn [7] and others have shown that a single-step kinetics scheme must produce curved relationships on such plots. More recently, Melius [31] explored the decomposition of nitromethane, a relatively simple nitramine, considering 48 component species linked by 312 elementary reactions. The simple example above, however, illustrates how single-step kinetics can be implemented, and shows how the McGuire-Tarver extension into multiple decomposition reactions can be implemented.

McGuire and Tarver therefore proposed a more complex, multi-step decomposition scheme to model the decomposition process. In the single-step scheme, each elementary cell is considered to be composed of two materials: the un-reacted initial energetic material; and decomposition gases. The model maintains a mass fraction for each cell that indicates the proportions of these two materials. The reaction rate for decomposition of the un-reacted material into gaseous products is then governed by an Arrhenius-type process, as discussed above.



McGuire and Tarver's extension was to consider the cell to be composed of multiple materials (simply designated A, B, C, ...) and maintains a mass fraction for each one. Furthermore, the overall decomposition from un-reacted material into gaseous products is split into decomposition in stages. For example, HMX and RDX, in their model, decompose in a linear chain from the un-reacted material, A, into an intermediate material, B, then into a second intermediate, C, before finally emerging as gaseous products, D. Arrhenius-type kinetics govern the decomposition between these four separate species, so that each stage of the chain can be programmed to decompose at a different rate.

Separate rate constants ( $E_a$  and  $A$  and specific energy,  $Q$ ) for each must be supplied to fully describe a given energetic material. Parameters are typically obtained by a trial-fitting process where candidate parameters are iteratively adjusted and modelled for a simple experimental geometry, such as the One-Dimensional Time-to-Explosion (ODTX) test [14][32].

This is partly because the TOPAZ code[70] is an implicit one that tracks only heat flow through the modelled geometry, and does not consider mechanical influences such as mass transport, or pressure wave propagation. In addition, the sub-model does not contain a formulation to describe the gas generation and flow that arise from a combustion process, but instead simply deposits the energy release by the chemical reaction back in to the elementary cells of the model as internal energy. This energy deposition is then manifest as a change in temperature by the integral of the heat capacity curve, and so allows temperature to rise without limit. By contrast, the real combustion is limited by the rate at which heat generated in the burn front can be deposited into the unburnt surface and raise its temperature.

## 6 A Hypothetical Mechanism for Violent Responses

### 6.1 Bulk Energy Release Rate in the Detonation Process

#### 6.1.1 A Simple View of Detonation

Consider a cylindrical pellet of length  $l$ , detonating with a velocity,  $D$ , when initiated from one end. The duration of the detonation will be:

$$t_d = \frac{l}{D}$$

and during this process the full chemical energy of the pellet will be released. During and after the detonation, the chemical energy will begin to become available to perform work on the surrounding media, for example some confining cylinder. The total chemical energy released during the detonation is the bulk energy release rate.

Taking a specific example of a TNT charge contained within an EMTAP burning tube, where detonation is initiated at one end. The EMTAP experiment consists of a pipe bomb with screw-on end caps, of internal diameter 31.4 mm and length 250 mm. For TNT, the detonation velocity is given as  $6.93 \text{ km s}^{-1}$ , and the geometry of the EMTAP burning tube is 31.4 mm diameter and 250 mm long. Assuming detonation is started at the mid-point of the tube and propagates simultaneously towards either end, the duration of detonation would be  $18.04 \mu\text{s}$ .

The energy released during this process is a simple function of the mass of the pellet and its specific energy. For a pellet of radius,  $r = 15.7 \text{ mm}$ , and a length,  $l = 250 \text{ mm}$ :

$$V = \pi r^2 h = 193.6 \text{ cc}$$

and for TNT the density,  $\rho$ , is given as 1.5 to 1.6  $\text{g cc}^{-1}$ , and the specific energy,  $q$ , is given as  $4.56 \text{ MJ g}^{-1}$ , so that the total energy,  $E$ , released during the detonation is:

$$E = \rho V q = 1368 \text{ kJ}$$

Considering the whole detonation, the process therefore releases energy at an overall bulk rate of:

$$\frac{dE}{dt} = \frac{E}{t_d} = 75.9 \text{ kJ } \mu\text{s}^{-1}$$

Note that the above argument ignores details such as the non-ideality of detonation in TNT, and features of detonation wave curvature and critical diameter. For example complete chemical reaction in the pellet would in reality occur a short time after emergence of the detonation front from the end of the pellet. Furthermore, in a real experiment that is initiated from a point at one end, this argument neglects the shock initiation process. Both these would result in a slightly longer figure for the duration,  $t_d$ , so that the energy release rate would be slightly lower than the figure quoted.

It is also important to note that the bulk energy release rate depends on the charge geometry: with larger charge diameters having a correspondingly larger bulk energy release rate. This is because the detonation wave spans the entire charge diameter in the plane perpendicular to its direction, so that at each instant the energy released is in the full diameter of the charge. For example, the time taken to complete detonation would be different in two charges of the same mass, one of which was in the form of a long cylinder and the other in the form of a thin flat disk, in which detonation was initiated across the entire flat end of each cylinder. Care must be taken to consider similar geometries when comparing the bulk energy release rates that might arise from different modes of burning and decomposition.

## **6.2 Bulk Energy Release Rate During Burning**

### **6.2.1 Burning Rates**

In low-pressure convective burning, for example in a pellet maintained at constant pressure, burn rates are orders of magnitude slower than the corresponding rate of consumption in the detonation process. This is supported by several sources in open literature. Maienschein and Chandler [46] conducted experiments using a 70 cc closed bomb apparatus, in which pellets of the test composition were ignited and allowed to burn, and instrumentation was provided by a pressure gauge to determine the bomb pressure and by wires embedded within the specimen to measure the surface regression rate as the burn progressed. Burn rates are presented as curves of surface regression rate as a function of pressure as the specimen generates gas and pressurises the low-volume bomb, with increasing burn rates observed at higher pressures. For example, steady burning of LX-04 (HMX/Viton 85/15 wt%) shows a relationship of:

$$u = 3.4 \times 10^{-3} + 9.5 \times 10^{-4}P$$

for pressure,  $P$ , in MPa and a burn rate,  $u$ , in  $\text{m s}^{-1}$ .

Son et al [47] conducted similar experiments using a constant-pressure apparatus with the capability to use high-speed video recording and embedded wires to measure the burning rates of a selection of explosives. These experiments were carried out at pressures in the 0.2 MPa to 100 MPa range, and show good agreement with Maienschein for LX-04 and other HMX, and HMX-based PBXs. Burning rates from 0.1 to 10  $\text{cm s}^{-1}$  were observed with a linear relationship with pressure in this lower regime, extending Maienschein's work.

Both Son and Maienschein noted erratic burning in some experiments with burning rates up to 100  $\text{ms}^{-1}$  reported by Maienschein. These were attributed to breakage of the pellets, leading to increase burn surface area and a consequent increase in total burn rate. The authors were careful to note that experiments showing this unsteady behaviour did not contribute to the smooth and practically burn rate dependence given above; that expression represents experiments in which the burning was 'planar'.

Glascoc et al [48] reported more recent experiments in burning rate measurements for HMX-based explosives at both elevated pressure and temperature. In particular, compositions of HMX/Viton (95/5 wt%) and HMX/DOA/HYTEMP (92.8/5.3/1.9 wt%) both showed an order of magnitude increase in burning rate at 180°C, compared with the burn rates at ambient temperature noted by Maienschein and Son. Burning rates in the range 1  $\text{ms}^{-1}$  to 20  $\text{ms}^{-1}$  were noted at this higher temperature, over the pressure range 2 MPa to 200 MPa.

## 6.3 Modes of Initiation

### 6.3.1 Initiation of Burning at a Single Site

The behaviour after ignition as a result of simple burning is now discussed. Consider the same EMTAP geometry tube as above, of 31.4 mm diameter and 250 mm length, filled with TNT, in which burning is initiated from a point on the axis of the filling and halfway along the tube. The burn front will progress outwards spherically from this point, consuming the specimen, generating gas and hence increasing the local pressure. For the first stage of this discussion, however, the pressurisation will be neglected.

At a reasonable low-pressure burning rate of 0.1  $\text{m s}^{-1}$ , and in the absence of burn acceleration due to local pressurisation, the burn front would propagate steadily from the centre to each end of the specimen (and hence completely consume the specimen) in a

time of 1.25 s. Even at the faster erratic burn rate of  $100 \text{ ms}^{-1}$ , corresponding to the erratic burning described by Maienschein, complete consumption of the specimen would occur in a time of  $1250 \text{ }\mu\text{s}$ .

Taking the properties of TNT above, the EMTAP tube filling would have a mass of 300.0 g, and an initial total chemical energy of 1368.3 kJ. The bulk energy release rate in this process would therefore be  $0.00109 \text{ kJ }\mu\text{s}^{-1}$  for a burn rate of  $0.1 \text{ ms}^{-1}$  (corresponding to a pressure of 10 MPa according to Maienschien and Son). Even for the faster erratic burning rate, the energy release rate would be only  $1.09 \text{ kJ }\mu\text{s}^{-1}$ . These figures are very much lower than that obtained for the detonation process in a similar geometry.

### **6.3.2 Initiation of Burning at Multiple Sites Simultaneously**

An extension of the above mechanism is as follows. Consider the simple case of two locations within a bulk of an energetic material, separated by a distance,  $d$ , and from which burning is initiated. As the burning propagates outwards, the burn fronts meet in the space between the two initiation sites, and do so after they have travelled half the initial separation. Shortly after this time, the energetic material between the two initiation sites is completely consumed. The corresponding time taken for the burn fronts to meet is then:

$$t_d = \frac{d}{2u}$$

for a burning rate,  $u$ .

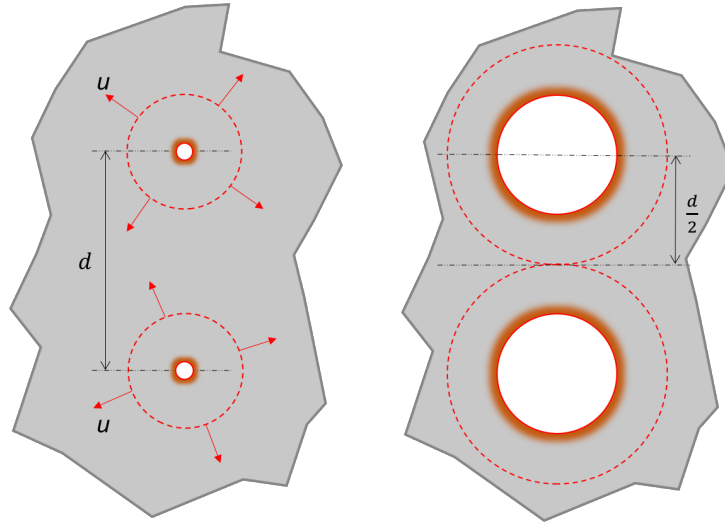


*Fig. 13: Simultaneous initiation of burning at two sites. The burning fronts from each initiation site meet after burning a distance  $d/2$*

The above argument is relevant to a mass of an energetic material which contains a number of identical initiation sites, evenly distributed and with an average spacing,  $d$ . In this case, when the burn fronts propagating at a constant speed,  $u$ , from each of the numerous sites eventually meet, the entire energetic mass will have been consumed, and this will occur in a relatively short time compared to the time taken for a single-point-initiated burn.

In an ideal 2D geometry, the packing arrangement which gives the closest spacing for a given number of initiation sites occurs on an equilateral triangular grid. This yields a time taken for the burn fronts to meet and completely consume the energetic bulk of:

$$t_d = \frac{d}{\sqrt{3}u}$$

For the 3D geometry, the ideal grid of points spaced evenly throughout the bulk would be most closely packed on a tetrahedral grid, again for a given number of initiation sites and assuming a constant burn speed,  $u$ , on an evenly spaced grid of separation,  $d$ . In this arrangement the time taken for the burn fronts to meet and completely consume the bulk is:

$$t_d = \frac{\sqrt{3}d}{2\sqrt{2}u}$$

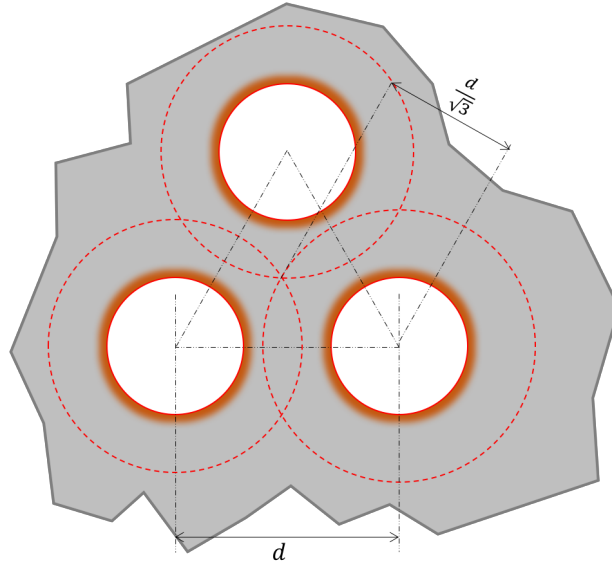


*Fig. 14: Burning from simultaneous initiation at multiple evenly distributed sites across a 2D slab of an energetic material, completely consuming all of the material when the burning fronts intersect*

In all these idealised geometries, for initiation sites uniformly spaced throughout the bulk, and for constant burn speed, the time taken to completely consume the bulk material is inversely proportional to the number of initiation sites, again assuming simultaneous initiation at each site. As the number of sites increases, then for an evenly-spaced grid the distance between sites decreases, and hence the time taken for complete consumption decreases.

The bulk energy release rate for a mass of energetic material, using the multiple-initiation-site model, can be calculated using the expressions above for the time taken for the burn fronts to meet, in a similar fashion to that outlined in the detonation argument at the beginning of this section. For this, again use the EMTAP burning tube geometry used above, with a TNT filling of density,  $\rho = 1.55 \text{ g cc}^{-1}$ , and of specific energy,  $q = 4.56 \text{ MJ kg}^{-1}$ . Furthermore, assume that within the bulk of the filing are a number of regularly-spaced initiation sites arranged on a tetrahedral lattice, with initial separation,  $d = 0.25 \text{ mm}$ . At each initiation site, burning commences and propagates spherically outwards at a fairly modest speed,  $u = 0.5 \text{ ms}^{-1}$ . Then, the total burn time until the burn fronts meet and the pellet is completely consumed is:

$$t_d = \frac{\sqrt{3}d}{2\sqrt{2}u} = 306.2 \mu\text{s}$$

The total energy contained within the pellet is given in by:

$$E = \rho V q = 1368.3 \text{ kJ}$$

Hence, the bulk energy release rate, under these assumptions, is:

$$\frac{dE}{dt} = \frac{E}{t_d} = 4.46 \text{ kJ } \mu\text{s}^{-1}$$

This figure remains very much lower than that for the purely detonative process obtained above, but is nevertheless a very rapid energy release and is within an order of magnitude of that found in detonation, and is within an order of magnitude of the detonative energy release rate. Note, also, that the simplistic derivation of  $dE/dt$  neglects any pressure-dependent burning rate effects: as burning progresses gases are release and these increase the local pressure near the burn front. This pressure increase would increase the burning rate, with a consequent increase in energy release rate.

Furthermore, the energy release rate depends upon the initial spacing of the initiation sites. The plot in Fig. 15 shows the overall energy release rate as a function of initiation site separation, for the range of steady burning rates noted in the literature. Note that perfectly simultaneous initiation of burning at all sites is assumed, so that these curves represent theoretical maximum energy release rates.



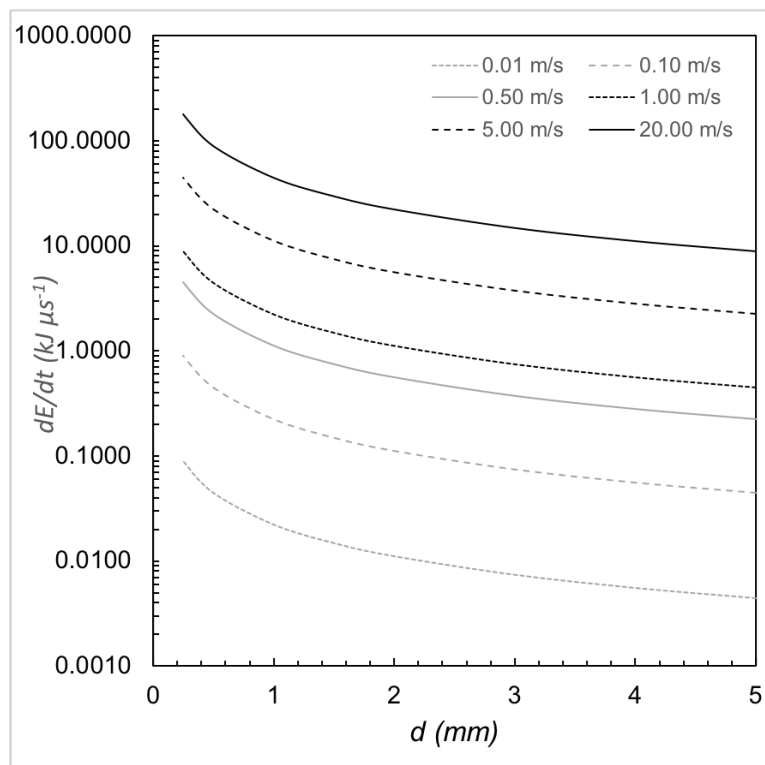


Fig. 15: Energy release rate as a function of initial separation of initiation sites, for steady burning rates, and assuming simultaneous initiation

The increase in overall bulk energy release rate according to the proposed mechanism arises from the large number of nearly simultaneous ignition sites, rather than as a function of the change in surface area that arises as burning spreads. In this hypothetical model of mass burning it is important to emphasise that the process is not classical detonation: these do not represent a supersonic, directional shock wave propagating through the material, and the high overall energy release rate arises as a result of burning processes only.

### 6.3.3 Concluding Remarks

The theoretical observations of the energy release rates achievable by mass burning presented here therefore suggest a hypothetical mechanism that might explain the violent responses observed in energetic materials that can undergo melting. The potential exists for energy release rates to be comparable to those obtained in detonation, but without the need to allow directional, supersonic shock waves to form. We have seen experimentally that melting is accompanied by evolution of gas bubbles, and, certainly in the case of pure RDX and in RDX/TNT, that the early stages of burning compress the bubble-laden material. It is reasonable at this stage to suppose that polymer-bound compositions

would likewise include molten material containing bubbles, though in those materials the presence of the binder would influence the distribution and nature of the molten material. The proposed mechanism, then, is that the first stage of burning raises the internal pressure in the confinement, and could then compress the bubble-filled regions. Adiabatic compression of the bubbles would then raise their temperature, provoking ignition at multiple sites across the compressed region, and that these ignitions occur closely spaced in time, leading to mass ignition and rapid energy release less than but comparable with that attained in full detonation.

Implementation of the pore collapse model into a dynamic hydrocode has shown that the temperature achieved by a given gas bubble depends on its size and the rate at which it is compressed, so that not all bubbles reach ignition temperature at the same time for a randomly distributed population of pores that we have examined in the pure nitramine experiments[Annex A.6, Annex A.7]. That work showed that very rapid compression is necessary to attain the high temperatures required to produce very fast rates of chemical decomposition that are consistent with the detonation process, but the hypothesis here is that these extreme reaction rates are not required in order to produce the slower burning reaction, so that the speed and extent of compression are more consistent with observed  $V/V_0$ . However, more theoretical work is needed to examine whether the expected temperature attained in the compressed gas spaces is consistent with the requirements for bulk burning.

The role of the binder in the composition seems to be consistent with this suggested mechanism. For binder-rich materials, where the energetic crystals are discretised and encapsulated by the binder, each crystal pocket would be expected to act as a potential ignition site, provided that the crystal inside the pocket had undergone melting and had allowed a gas bubble to form. Burning from these isolated pockets would be inhibited by the surrounding binder, slowing the rate of increase in pressure in the early stages of ignition, and limiting the rate of compression of other gas pockets nearby. The particle size of the energetic crystals would define the nature and distribution of the developing gas pockets, and this in turn would modify the time period over which compression-induced ignition in these pockets would occur as initial burning commences. For compositions with low quantities of binder, or for materials which were not thoroughly and intimately mixed, we would expect to find larger regions of melted and bubble-filled liquid. It may be that these larger regions are responsible for the generally more violent

responses, as a consequence of the compression of entrapped gas bubbles directly in contact with the surrounding melted energetic material, as seen in the pure RDX experiment.

The propose bubble-compression mechanism is at this stage hypothetical, and there is clearly a good deal of theoretical work to be done to support or refute it.

## 7 General Conclusions

The early stages of ignition are governed by the development of gas spaces within which the initial flame can propagate. Systems with significant ullage, and containing components which can undergo melting to a large degree can develop large spaces for the initial flame to propagate. RDX is an example of this, where the melting temperature is well below the ‘ignition’ temperature.

The opening of bulk cracks and consequent increase in burn surface area seems to be a separate mechanism from observations here. In the generally-understood cracking mechanism, it is implied that burning occurs at newly-exposed surfaces in the cracks, and as burning and pressure progresses, the rate of burning is directly related to the surface area of the cracked material. The work presented here, however, indicates that flames are initially restricted to the gas-filled volumes within the confinement, and that in the early stages of ignition the character, size and configuration of the gas spaces govern the initial behaviour. The early and middle stages of heating ‘set up’ the conditions for initial burning by allowing or inhibiting the development of these gas spaces. Ullage, for example, combined with materials that can undergo significant melting before ignition, can allow large contiguous gas spaces to coalesce; materials like HMX and NTO, where the melting temperature is close to the ignition temperature, there is simply less time for large melt spaces to develop before ignition occurs. Gas pockets are smaller and discrete.

There is an implicit assumption in this discussion that temperature is steadily increasing, and the reader might question whether this is also true for steady heating profiles such as in ODTX. However, the internal self-heating of the energetic material as decomposition gradually accelerates towards ignition ensures that, whatever heating profile is chosen, the temperature will vary across the experimental specimen and will be increasing.

The presence of binders and other additives both influence this: persistent binders such as HTPB or HyTemp which decompose at high temperature retain some structure which separates pockets of gas. In this state, flames beginning to burn in small, isolated regions will individually contribute less to the overall rate of pressurisation; isolated pockets will also act to limit the spread of the overall flame throughout the bulk of the specimen. Furthermore, the adhesion of persistent binders to the filler particles plays an important part, with weakly-attached binders allowing melting and gas production; strongly

attached binders will inhibit this. It would be interesting to attempt to correlate the mechanical properties of explosive compositions to the speed at which the initial flame can spread.

As the gas-space flames develop and intensify, and pressure increases, then burning into the liquid and remaining solid particles can begin to occur, but the presence of gas-filled spaces is required for the initial flames to develop. The evidence presented here sheds little light into the conditions under which the bulk-burning process arises: our visual observations are obscured by the intense light of the explosion, and the imaging rates of the camera limit temporal resolution of observations. Nevertheless, it is clear that, once gas-space burning (occurring at millisecond timescales) accelerates sufficiently, then the process that follows occurs on timescales in the region of a few tens of microseconds.

De-confinement therefore is likely also to be a factor – an initially tightly confined energetic with little ullage space has only a small volume in which gas spaces can develop, but partial de-confinement allows more free volume for these spaces to grow and fill with melt vapour, allowing more rapid propagation of the initial flame. De-confinement can also quench the incipient reaction, however, and we have observed this happening in some experiments with imperfect confinement sealing where the initially gas-tight capsule begins to leak.

The different stages of ignition can be related to the confinement types proposed earlier, focusing particularly on Type IIB (dynamically de-confining). In early heating, we have seen experiments that cause confinement to fail and leak before the onset of visible flames, and this is likely a result of the high vapour pressure of the molten specimens at increasing temperature. Materials of this type include DNAN, PETN, and sometimes TNT, all of which have a very low melting point compared with the stated ignition temperature. In these materials, leakage generally precludes an explosion, though the residual material within the confinement sometimes ignites and burns steadily at essentially constant atmospheric pressure.

As the gas-space flame develops, we have seen evidence for (but have not yet measured) a corresponding pressure rise which is capable of compressing the specimen. This pressure rise alone might be capable of causing the confinement to begin to leak (i.e. to become Type IIA) or might even be sufficient to cause gross failure and migration to Type I. Strong Type IIB and Type III confinements may withstand the initial

pressurisation from gas-space burning, but will ultimately fail at the onset of bulk burning. The type of confinement, its confining capability and the stage of ignition at which it fails is thus very important in understanding the ignition mechanism, and in the development of a predictive capability for cook-off.

The bulk compression of large melt-pools containing small bubbles is a potential mechanism to explain the violent responses generally observed in the cook-off of melt-cast materials, primarily RDX/TNT. This mechanism seems, however, to be plausible only for materials which become, or are already, highly porous. Compression in, for example, HMX and NTO seems to be limited to the regions in which melting and bubbling has occurred, and was not noted in material that seemed to have remained solid or wholly liquid.

## 8 References

- [1] Turner, N; “Energetic Materials Testing and Assessment Policy Committee Manual of Tests”, Defence Ordnance Safety Group, UK MoD, 2007
- [2] Stennett, C; “Test Report ES140506A - EMTAP Test No. 35: Internal Ignition DPX-1”, Energetics Hazard Test House, Cranfield University, 2014
- [3] Stennett, C; “Test Report ES140515B - EMTAP Test No. 41: Mini Fuel-Fire DPX-1”, Energetics Hazard Test House, Cranfield University, 2014
- [4] Stennett, C; “Test Report ES140506C - EMTAP Test No. 32: Electrically Heated DPX-1”, Energetics Hazard Test House, Cranfield University, 2014
- [5] Koenen, H., Ide, K. H. “Neuere Pruefmethoden fuer Explosive Stoffe”, Communications presentees au XXXIe Congres International de Chimie Industrielle dans la section Poudres et Explosifs, Liege, 1958, pp. 61–70.
- [6] D A Frank-Kamenetskii, “Diffusion and heat exchange in chemical kinetics”, Princeton University Press, ISBN 9781400877195
- [7] Zinn, J., Mader, C.L., *J. Appl. Phys.* **31**, 323 (1960)
- [8] Townsend, D L; Tou, J C; “Thermal hazard evaluation by an accelerating rate calorimeter”, *Thermochimica Acta*, **37** (1980) 1-30
- [9] Mores, F; Nolan, P S; O’Brien, G; “Determination of the self-accelerating decomposition temperature (SADT) from thermal stability data generated using accelerating rate calorimetry”, *I Chem E Symposium Series No. 134*, 1994, [www.icheme.org](http://www.icheme.org)
- [10] Cook, M D; Stennett, C; Haskins, P J; Briggs, R I; Wood, A D; Cheese, P J; “The role of binders in controlling the cook-off violence of HMX/HTPB compositions”, *Shock Compression of Condensed Matter AIP 0-7354-0341-4/06*, 2005, p 952
- [11] Dodd, A.B., Kaneshige, M.J., “Cook-off model development and analysis of energetic materials using Sandia Instrumented Thermal Ignition (SITI) Experimental Data”, *Proc 13<sup>th</sup> International Detonation Symposium*, 2006, p.516

- [12] Behrens, R., Thermal Decomposition of HMX: Morphological and Chemical Changes Induced at Slow Decomposition Rates”, *Proc. 12<sup>th</sup> International Detonation Symposium*, 2002, p.519
- [13] IDS 12.0384
- [14] Catalano, E; McGuire, R; Lee, E; Wrenn, E; Ornellas, D; Walton, J; “The Thermal Decomposition and Reaction of Confined Explosives”, *Proc. 6<sup>th</sup> Symposium (International) on Detonation*, NSWC ACR-221, 1976, p. 219
- [15] Stennett, C; “One-Dimensional Time-to-Explosion (ODTX) Testing of QRX-2xx Compositions”, Report No. DMAS/CS/1268/07, Cranfield University, 2008
- [16] Frank-Kamanetskii, D A; *Acta Physiochem. USSR*, 10, 363 (1939)
- [17] Merzhanov, A G; Averson, A E; *Combust. Flame*, **1971**, 16, 89
- [18] Alexander, K; Gibson, K; Baudler, B; “Development of the Variable Confinement Cookoff Test”, Report no. IHTR 1840, NSWC Indian Head, 1996, ADB214796
- [19] Pakulak, J; “Calibration of a super-small-scale Cookoff Bomb (SSCB) for predicting the severity of the cookoff reaction”, Naval Weapons Center Technical Publication 6414, 1983
- [20] Pakulak, J., Anderson, C.M.; “NWC Standard Methods for Determination of Thermal Properties of Propellants and Explosives”, Naval Weapons Center Technical Publication 6118, 1980
- [21] Smilowitz, L; Henson, B F; Sandstrom, M M; Asay, B W; Romero, J J; “The Evolution of Thermal Explosion – Spatial and Temperature Profiles Internal to a PBX9501 Thermal Explosion”, *Proc. 13<sup>th</sup> International Detonation Symposium*, 2006, p. 1026
- [22] Asay, B W; Son, S; Dickson, P M; Smilowitz, L B; Henson, B F; “An Investigation of the Dynamic Response of Thermocouples in Inert and Reacting Condensed Phase Energetic Materials”, *Propellants, Explosives, Pyrotechnics*, 2005, **30**(3): p. 199



- [23] Smilowitz, L; Henson, B F; Asay, B W; Romero, J J; Grim, G P; Saunders, A; Merrill, F; Morris, C L; McNeil, W; Marr-Lyon, M; Rightly, P; “Sub-sonic Thermal Explosions Investigated by Radiography”, *Proc. 14<sup>th</sup> International Detonation Symposium*, 2010, p. 898
- [24] Sorber, S., Stennett, C., Goldsmith, M., “Developments in a Small Scale Test of Violence”, *Shock Compression of Condensed Matter – 2011*, AIP Conf. Proc. 1426, 563-566 (2012) doi: 10.1063/1.3686341
- [25] Bauer, C.L., Rae, P.J., Stennett, C., Flower, H.M., “Small-scale Thermal Violence Experiments for Combined Insensitive High Explosive and Booster Materials”, *Proc. 14th International Detonation Symposium*, ONR 351-10-185, 2014
- [26] Stennett, C., Cook, M.D., “Direct Observations of the Onset of Ignition in Explosives When Heated to Elevated Temperatures”, MSIAC Science of Cookoff Workshop, 2015
- [27] Stennett, C., Cook, M.D., Briggs, R.I., Haskins, P.J., Fellows, J., “Direct Observation of Cook-off Events Using a Novel Glass-windowed Vehicle and Pipe Bombs”, *Proc. 12<sup>th</sup> International Detonation Symposium*, 2002, p.871
- [28] ST/SG/AC.10.11/Rev 5, “Recommendations on the Transport of Dangerous Goods”, United Nations, New York and Geneva, 2009
- [29] ST/SG/AC.10.11/Rev 5, “Recommendations on the Transport of Dangerous Goods”, United Nations, New York and Geneva, 2009, p 134
- [30] ST/SG/AC.10.11/Rev 5, “Recommendations on the Transport of Dangerous Goods”, United Nations, New York and Geneva, 2009, p 46
- [31] C. Melius. Thermochemistry and Reaction Mechanisms of Nitromethane Ignition. *Journal de Physique IV Colloque*, 1995, 05 (C4), pp.C4-535-C4-548. <10.1051/jp4:1995443>.<jpa-00253749>
- [32] Tarver, C.M.; McGuire, R.R.; Lee, E.L.; Wrenn, E.W.; Brein, K.R.; “The Thermal Decomposition of Explosives with Full Containment in One-Dimensional Geometries”, *Proc. Symposium (International) on Combustion*, vol 17, 1979

- [33] Stennett, C., “Nightdog: Thermomechanical Modelling and NDT”, Report No. CDC/CS/1875/17, 2016
- [34] James, H.R., “The Response of Homogeneous Explosives to Projectile Attack”, *Proc. 11<sup>th</sup> Symposium (International) on Detonation*, 1992, p. 581
- [35] Williams, M.R., Matei, M.V., “The Decomposition of Some RDX and HMX Based Materials in the One-Dimensional Time to Explosion Apparatus. Part 1. Time to Explosion and Apparent Activation Energy”, *Propellants, Explosives, Pyrotechnics* 31, No. 6 (2006), doi: 10.1002/prop.200600058
- [36] Williams, M.R., Matei, M.V., “The Decomposition of Some RDX and HMX Based Materials in the One-Dimensional Time to Explosion Apparatus. Part 2. Estimating the Violence of the Cook-off Event”, *Propellants, Explosives, Pyrotechnics* 32, No.1 (2007), doi: 10.1002/prop.200700001
- [37] Ho, S.Y., “Thermomechanical Properties of Rocket Propellants and Correlation with Cookoff Behaviour”, *Propellants, Explosives, Pyrotechnics*, 20, 206-214 (1995)
- [38] Victor, A.C., “Simple Calculation Methods for Munitions Cookoff Times and Temperatures”, *Propellants, Explosives, Pyrotechnics*, 20, 252-259 (1995)
- [39] Victor, A.C., “Equations for Predicting Cookoff Ignition Temperatures, Heating Times, and Violence”, *Propellants, Explosives, Pyrotechnics*, 22, 59-64 (1997)
- [40] Fuster, D., Hauke, G., Dopazo, C., “Parametric Analysis for a Single Collapsing Bubble”, *Flow Turbulence Combust.*, 2008, doi: 10.1007/s10494-008-9169-8
- [41] Long, G.T., Vyazovkin, S., Brems, B.A., Wight, C.A., “Competitive Vaporization and Decomposition of Liquid RDX”, *J. Phys. Chem. B* **2000**, 104, 2570-2574
- [42] Committee of Experts on the Transport of Dangerous Goods and on the Globally Harmonised System of Classification and Labelling of Chemicals, “Comments on the Koenen Test”, 2011, United Nations UN/SCETDG/39/INF.53, Geneva
- [43] Dobratz, B.M., “LLNL Explosives Handbook – Properties of Chemical Explosives and Explosive Simulants”, LLNL TR UCRL-51319, March 1981

- [44] Gibbs, T.R., Popolato, A., "LASL Explosives Property Data", University of California Press, Berkeley, 1980
- [45] Walker, F.E., Wasley, R.J., *Explosivstoffe* 17 (1), 9 (1969)
- [46] Maienschein, J L; Chander, J B; "Burn rates of pristine and degraded explosives at elevated temperatures and pressures", *Proc. 11<sup>th</sup> International Detonation Symposium*, 1998, p.
- [47] Son, S F; Berghout, C A; Bolme, D E; Chavez, D E; Naud, D; Hiskey, M A; "Burn Rate Measurements of HMX, TATB, DHT, DAAF and BTATz", *Proc. Combust. Inst.* **28** (2000) 919-924
- [48] Glascoe, E A; Springer, H K; Tringe, J W; Maienschein, J L; "A Comparison of Deflagration Rates at Elevated Pressures and Temperatures with Thermal Explosion Results", *American Institute of Physics* **1426**, 555 (2012) <http://dx.doi.org/10.1063/1.3686339>
- [49] Matei, M.V., "A study of cook-off in the One-Dimensional Time to Explosion Test", PhD Thesis, Cranfield University, 2001
- [50] Cheese, P., White, N., Rowlands, T., Stennett, C., "Cook-off Testing of Pressed PBXs", IMEMTS, Rome, May 2015
- [51] Kaneshige, M.J., Renlund, A.M., "Sandia Instrumented Thermal Ignition (SITI) Experiment for Cook-off Model Development and Validation", JANNAF 40<sup>th</sup> CR, 28<sup>th</sup> APS, 22<sup>nd</sup> PSHS and 4<sup>th</sup> MSS Joint Meeting, Charleston, SC, June 2005
- [52] Hobbs, M.L., Kaneshige, M.J., "Modeling HMX Ignition Using an Enthalpy Formulation", *Proc. 13<sup>th</sup> International Detonation Symposium*, 2006, p507
- [53] Dodd, A.B., Kaneshige, M.J., "Cook-off Model Development and Analysis of Energetic Materials using Sandia Instrumented Thermal Ignition (SITI) Experimental Data", *Proc. 13<sup>th</sup> International Detonation Symposium*, 2006, p507
- [54] Gross, R. J., Baer, M. R., and Hobbs, M. L., "XCHEM-1D A Heat Transfer/Chemical Kinetics Computer Program for Multilayered Reactive Materials," SAND93-1603 UC-741, Sandia National Laboratories, Albuquerque, NM 1993.

- [55] Kaneshige, M.J., Renlund, A.M., Schmitt, R.G., Erikson, W.W., “Cook-off Experiments for Model Validation at Sandial National Laboratories”, *Proc. 12<sup>th</sup> International Detonation Symposium*, 2002, p821
- [56] Cook, M.D., Haskins, P.J., Wood, A.D., “Parameterisation of the CHARM Reactive Flow Model using Kinetic Parameters Derived from Cook-off Experiments”, *Proc. 13<sup>th</sup> International Detonation Symposium*, 2006, p.638
- [57] Smilowitz, L., Henson, B.F., Sandstrom, M.M., Asay, B.W., Romero, J.J., “The Evolution of Thermal Explosion – Spatial and Temperature Profiles Internal to A PBX9501 Thermal Explosion”, *Proc. 13<sup>th</sup> International Detonation Symposium*, 2006, p.1026
- [58] Wood, A.D., “Advanced Cook-off Experiments – Testing of Neat Crystals of Energetic Materials”, Technical Report SYNACO/WSTC/ACE04/2017
- [59] Wardell, J.F., Maienschein, J.L.; “The Scaled Thermal Explosion Experiment”, *Proc. 12<sup>th</sup> International Detonation Symposium*, 2002, p. 384
- [60] Dickson, P.M., Asay, B.W., Henson, B.F., Smilowitz, L.B., “Thermal Cook-off Response of Confined PBX 9501”, *Proc. R. Soc. Lond. A* (2004) **460**, 3447-3455
- [61] Urtiew, P.A., Forbes, J.W., Tarver, C.M., Garcia, F., “Calibration of Manganis Pressure Gauges at 250°C”, *Shock Compression of Condensed Matter – 1999*, 2000, p.1019
- [62] Garcia, F., Forbes, J.W., Tarver, C.M., Urtiew. P.A., Greenwood, D.W., Vandersall, K.S., “Pressure Wave Measurements from Thermal Cook-off of an HMX-Based High Explosive PBX 9501”, *Shock Compression of Condensed Matter – 2001*, 2002, p.882
- [63] Obara, T., Bourne, N.K., Mebar, Y., “The Construction and Calibration of an Inexpensive PVDF Stress Gauge for Fast Pressure Measurements”, *Meas. Sci. Technol.* (1995) **6** 345
- [64] Jain, A., Prashanth, K.J., Sharma, K. A., Jain, A., Rashmi, P.N., “Dielectric and PiezoElectric Properties of PVDF/PZT Compositions: A Review”, *Polymer Science and Engineering* (2015) 1598

- [65] “Guide to Using Poled PVDF”, Precision Acoustics Ltd, <https://www.acoustics.co.uk/pal/wp-content/uploads/2015/11/Properties-of-poled-PVDF.pdf>
- [66] Whitworth, N.J., Maw, J.R., “Modelling ‘Hot-Spot’ Initiation in Heterogenous Solid Explosives”, *Shock Compression of Condensed Matter – 1999, 2000*, p. 887
- [67] Haska, S.B., Bayramli, E., Pekel, F., Ozkar, S., “Mechanical Properties of HTPB-IPDI-based elastomers”, *J. Applied Polymer Science* 64(12): 2347-2354, 1997
- [68] Stennett, C., Wood, A.D., Cook, M.D., “Direct Observation of Thin Layers of Pure Energetic Materials When Heated to Elevated Temperatures Under Confinement”, *International Detonation Symposium 2018*, in print
- [69] Walker, F.E., Wasley, R.J., “Critical Energy for Shock Initiation of Explosives”, *Explosivestoffe*, Vol. 17, No. 1, 1969, p.9
- [70] Shapiro, A.B., Edwards, A.L., “TOPAZ2D Heat Transfer Code Users Manual and Thermap Property Database”, UCRL-ID-104558, May 1990

# **Annex A: Supporting Publications**

## **A.1 Direct Observations of Cook-off Events ...**

---

Authors:	Stennett, C; Cook, M D; Briggs, R I; Haskins, P J; Fellows, J		
Title:	Direct Observation of Cook-off Events Using A Novel Glass-Windowed Vehicle and Pipe Bombs		
Publication Type:	International Conference	Venue:	12 <sup>th</sup> International Detonation Symposium
Date:	1998		

---

# DIRECT OBSERVATION OF COOK-OFF EVENTS USING A NOVEL GLASS-WINDOWED VEHICLE AND PIPE BOMBS

C. Stennett, M. D. Cook, R. I. Briggs, P. J. Haskins and J. Fellows  
QinetiQ, MoD Fort Halstead,  
Sevenoaks, Kent TN14 7BP, UK

Experiments were performed to examine the cook-off responses of two secondary explosive formulations, RDX/TNT 60:40 and RDX/HTPB 85:15, studied at different heating rates. The experiments were performed using two types of test vehicle, one a closed pipe-bomb sealed by screw-on end-caps, and the other a novel vehicle incorporating a thick glass window through which the filling could be observed. The pipe bomb experiments were further subdivided into two categories: heat was either applied to the entire surface of the vehicle, or to only a portion of the vehicle. Thermocouples were used to record the external temperature, and the temperature within the filling. In all experiments RDX/TNT 60:40 gave responses that were more violent than those displayed by RDX/HTPB 85:15. In one partially heated pipe bomb experiment there is strong evidence that a detonation occurred. The tests on RDX/TNT 60:40 using the glass-windowed vehicles showed melting and bubbling in the explosive just prior to ignition. These results are discussed.

## INTRODUCTION

In order to understand the Cook-Off behaviour of energetic materials charge-scale tests have been developed to examine the response of explosive compositions to both fast and slow heating rates<sup>1</sup>. In the UK, a mild steel pipe 300mm in length, with an internal diameter of 31mm and a 6mm wall thickness, is used as a test vehicle. At typical explosive densities this vehicle has a capacity of approximately 350g. Strong screw-on end-caps are used to close the vessel and provide sealing against internal pressure. The vehicle has been designed to fail in the centre of the tube rather than at the end-caps. In the early days of Cook-Off test development, such tubes were placed on a tray over a small liquid fuel fire. This test became known as the 'Mini Fuel Fire', and the tubes were referred to as 'Burning Tubes' (see Figure 1). However, in a typical run of ten tests variable results were often obtained. For example, anomalies have been observed in Cook-Off experiments on RDX/TNT 60:40; in the mini

fuel fire tests eight out of ten stores give mild pressure bursts while two detonated. Similar variable results have been found in all-up weapon trials. To date these results are not properly understood, yet it is vital to try to understand the reason for this variability. More recently, an electrical heating method has been developed. This has given increased control over the heating rate, and also how and where the tube is heated. These factors can play a crucial role in the outcome of the test.

Current knowledge suggests that, in most cases, when a weapon is heated a point is reached when a thermal explosion occurs. This thermal explosion usually occurs near the outer edge of the energetic material for all but the smallest weapons. This is often the case even for Slow Cook-Off where the heating rate can be as low as 3.3°C/hr. There is a fundamental need to identify the location and nature of the reactions leading to a thermal explosion in order to get a better understanding of the Cook-Off process as a whole. The objective of the work reported in this paper is to help achieve this goal.



## EXPERIMENTAL

Three types of experiment were performed on two types of formulations, RDX/TNT 60:40 a conventional melt-cast material, and a cast PBX consisting of 85% RDX and 15% HTPB.

A total of 32 firings were performed to cover the combinations of experiment type, heating rate and filling composition. The sixteen firings performed for each of the two test compositions were subdivided into groups depending on the experiment type: six firings were carried out using a fully heated Burning Tube, six using a glass windowed vehicle, and four using a partially heated Burning Tube.

For the fully heated and glass windowed vehicles, three different heating rates of  $20^{\circ}\text{Cmin}^{-1}$ ,  $8^{\circ}\text{Cmin}^{-1}$  and  $3^{\circ}\text{Cmin}^{-1}$  were chosen. The partially heated tubes were heated at  $20^{\circ}\text{Cmin}^{-1}$  and  $3^{\circ}\text{Cmin}^{-1}$ . Two firings were performed at each heating rate for the same test vehicle and composition configuration. The heating rates quoted were controlled using the temperature reading on the thermocouple farthest from the axis of the tube, just inside the tube wall.

The vehicles were heated using a nickel-chrome tape of  $\sim 4\Omega\text{m}^{-1}$  resistance connected to the 240V AC mains supply through a manually controlled variable transformer. This transformer allowed the applied voltage, hence the applied current and heating effect, to be adjusted. For the fully heated tubes a total length of 3m of heating tape was used; the partially heated and glass windowed vehicles required a shorter length of heating tape. It was necessary to exercise caution when controlling the applied current to avoid melting the heating tape. Connection to the mains supply was made using a ceramic connector block of suitable current rating.

Since bare nickel-chrome tape was used, it was necessary to prepare the heated surfaces of the vehicles to prevent short circuits. The vehicles were cleaned and degreased and then coated with a heat-resistant paint. Once this had dried, a layer of glass-fibre tape was wound over the surface of the vehicle, followed by a layer of self-adhesive Mylar tape that completed the electrical insulation. Figure 1 shows an example of a prepared vehicle.

The PBX (RDX/HTPB 85:15) was cast under vacuum to eliminate void formation, while the RDX/TNT 60:40 was cast using the conventional method. In each case the vehicles were over-filled and machined flat to minimise ullage. Other workers have shown that the presence of voids in the filling can have a dramatic effect on the time to explosion and its violence<sup>2,3</sup>.

After filling and final assembly the vehicles were taken to the firing facility. Prior to heating, the ambient air temperature in the firing cell was recorded.

In the case of the small glass-windowed vehicles, a mirror was placed at  $45^{\circ}$  to normal over the top centre of

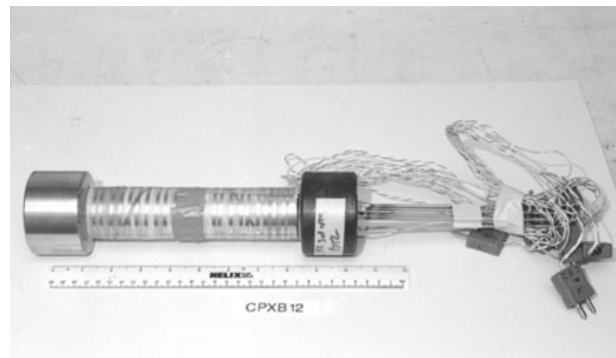


FIGURE 1. Prepared burning tube.

the charge in order that a close up video record could be made of each firing. An electric fan was used to remove smoke from burning material, that might obscure the view of the vehicle.

## EXPERIMENTAL VARIATIONS

In the first set of firings a conventional Burning Tube was heated electrically over its entire cylindrical surface. Six thermocouples were inserted into the vehicle through one of the end-caps, and were silver soldered in place to provide sealing against internal pressure. The thermocouples were positioned at different distances from the central axis of the tube, and were arranged in a spiral pattern to maximise the distance between each probe. The active ends of the probes were positioned at the centre of the tube. A seventh thermocouple was placed on the outside of the vehicle to monitor surface temperature. A sketch of the vehicle is shown in Figure 2.

A second set of firings were carried out using the same vehicle design, but in this instance only half the tube length was wrapped in heating tape. Again six thermocouples were silver soldered through one end-cap, but in these experiments three probes were positioned with their tips at the centre of the heated portion of the tube, and the other three with their tips in the unheated portion

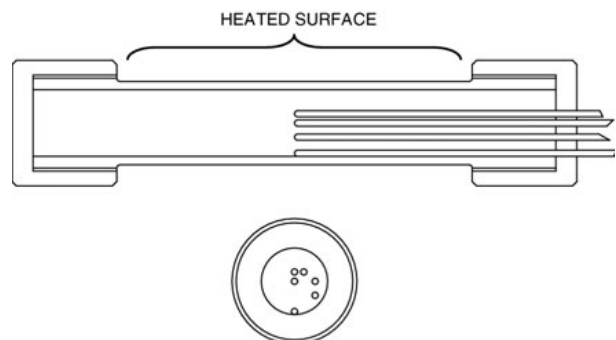
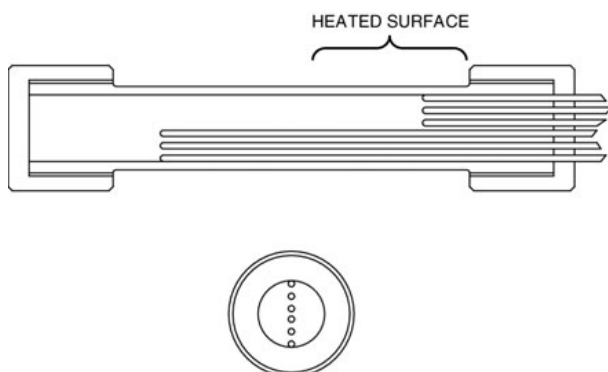


FIGURE 2. Sketch of fully heated burning tube showing thermocouple arrangement.

of the tube. Two further thermocouples were placed on the surface of the vehicle to monitor the temperature at the heated and non-heated zones of the vehicle. A sketch of this type of experiment is shown in Figure 3.



**FIGURE 3. Sketch of partially heated burning tube showing thermocouple arrangement.**

In the third set of experiments a new type of test vehicle was used. This consisted of a section of steel tube of 3.5mm wall thickness containing the filling. A 19mm thick glass window was placed on top, and the assembly was clamped between two flat steel plates of 10mm thickness. The end plates were clamped together with four tie bars to complete the confinement of the test sample. The upper plate was drilled with a large diameter hole through which the glass window and filling were visible. The steel tube section containing the test sample was 41mm in diameter and 55mm long, and had a capacity of approximately 100g of filling at typical explosive densities. Figure 4 shows a sketch of the vehicle configuration, whilst Figure 5 shows a photograph of a fully assembled vehicle ready to fire. This work was inspired by previous workers who have demonstrated the value of direct visual observation of cook-off experiments<sup>4</sup>.

Six thermocouples were fitted to the lower plate to record the temperature profile within the filling during the experiment. The thermocouples were soldered in place at different distances from the central axis, and were inserted so that their tips were positioned halfway along the tube. A grid of coloured lines was marked on the surface of the explosive, to emphasise any movement of the upper layer during heating. It should be noted that in none of the experiments were the vehicles lagged.

## INSTRUMENTATION

The temperatures were recorded using 'K' type mineral insulated thermocouples connected in parallel to two types of data logging devices. In the case of the Burning Tube experiments the thermocouples were commercially available 3mm diameter, 500mm long devices. In

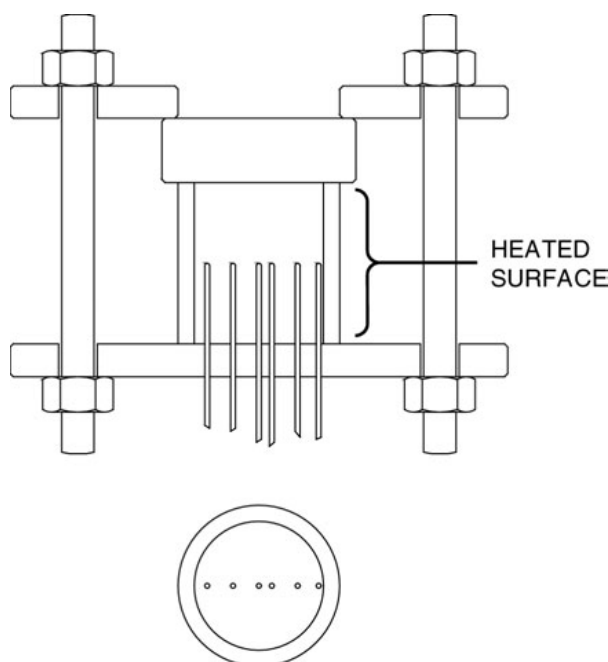


**FIGURE 4. Sketch of novel glass-windowed vehicle.**

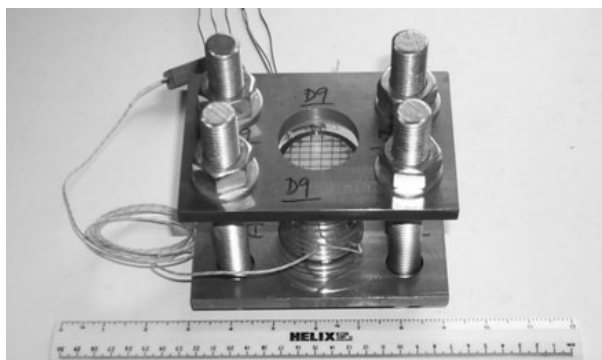


**FIGURE 5. Photograph of glass-windowed vehicle.**

the glass windowed vehicle experiments, the thermocouples were of 1.5mm diameter. The fully heated and glass-windowed vehicles were additionally instrumented with a single welded-tip thermocouple on the outside surface of the tube; the partially heated vehicles had a further two welded tip thermocouples on the outer surface.

The main data-logging device used was a Nicolet Odyssey transient recorder sampling at 10Hz; this was the prime method of recording the time-temperature profile for the experiment. A second data logging device was attached to a lap top PC, and was used to monitor the heating rate at the explosive/vehicle inner interface and to provide backup data capture. The secondary device sampled at 1Hz. Stills photographs were taken using both film and digital stills cameras.

In addition, individual video frames have been captured and used as illustrations. The video camera

resolution was standard 625-line PAL format, so that each pixel of the image of the glass-windowed vehicles covered approximately 0.25 sq. mm.

### RESULTS OF RDX/TNT 60:40 FILLED CONVENTIONAL BURNING TUBES

All experiments carried out on RDX/TNT 60:40 charges gave very violent events compared with the PBX (RDX/HTPB 85:15) charges. Typically the events (thermal explosions) took the form of pressure bursts. The cylinders were usually split into three, but sometimes into many more pieces, indicating a relatively rapid and violent pressurisation of the vehicle. In each case the vehicle failed in the centre of the tubular section, most often on the uppermost part of the tube. In one experiment the vehicle suffered considerable damage and was broken into approximately 40 small and medium-sized fragments.

In four of the six tests beads of RDX/TNT were found in the test arena, indicating ejection of molten material from the vehicles. In those experiments where the temperature profiles indicates solid material in the vehicle at the point of ignition, solid material was often recovered in the test arena. This material showed signs of local melting, but otherwise appeared to be in good condition. Figure 6 shows an example of recovered RDX/TNT material.

In four of the six experiments, the temperature-time plots showed anomalies in the temperature profiles. These took the form of a rapid and simultaneous reduction in the measured temperature on all six thermocouples in the experiment. These were labelled 'endotherms'. In each case the endotherm occurred as the core temperature of the vehicles reached 85–90°C. The endotherms were only observed on slow and medium heating rate experiments. In one experiment two endotherms were observed, the second occurring as the core temperature probe recorded 120°C. The cause of

the endotherms is unclear, but may possibly be due to mass melting of the filling, manifested on the temperature probes as absorption of latent heat. A second possibility may be that the seals on the vehicle failed, resulting in a fall in pressure and an associated drop in temperature. Further tests with additional instrumentation are required to understand this process.

### RESULTS OF RDX/HTPB FILLED CONVENTIONAL BURNING TUBES

All six experiments with the PBX (RDX/HTPB 85:15) filled charges gave relatively mild events, regardless of heating rate. The tubes all failed at the very centre portion and always on the upper face. In five of the experiments, the tube split along the axis producing an opening through which the enclosed gas and filling were ejected. In the sixth experiment, a small section of the tube became separated at the site of the ignition. This was the only instance of fragmentation in any of the six experiments.

In three of the six experiments, the contents of the vehicle burnt away completely in the minutes following the explosion. The residue from the burning was in the form of a low-density porous black ash. In the remaining three experiments, substantial proportions of the original filling were recovered from the test arena. These observations indicate that only a small amount of the filling took part in the reaction that caused failure of the vehicle.

One point of interest was that the explosive residue recovered showed marked discolouration in areas where it had been in contact with the hot inner surface of the test vehicle tube. Figure 7 shows an example of the material recovered from these experiments. This phenomenon was also noted where the explosive had been in contact with the thermocouples. By contrast, the appearance of the freshly broken surfaces of the material was pristine.

The temperature/time plots showed no evidence of the endotherm anomalies that were seen in the RDX/



FIGURE 6. RDX/TNT residue.



FIGURE 7. RDX/HTPB residue.

TNT experiments. Of the six experiments, two showed an unusually low ignition temperature, these occurring in the fast heating rate tests. There is evidence from the temperature recordings that an external fire occurred, resulting from the ignition of the electrical insulation on the tube. This undoubtedly led to localised and intense heating of the vehicle.

In one of the slow heating experiments there is clear evidence of thermal runaway in the period just prior to ignition. This was the only instance of thermal runaway observed in any of the experiments.

### RESULTS OF HALF-HEATED BURNING TUBE EXPERIMENTS WITH RDX/TNT

Of the four experiments with RDX/TNT in a partially heated vehicle, three resulted in a violent pressure burst centred within the heated portion of the tube. In these three experiments, the non-heated end of the tube showed less damage than the heated end, indicating a localised reaction of the filling. The fourth experiment in this set showed an interesting and very violent response. In this case the vehicle was completely destroyed, and more than 100 small fragments of casing were recovered. Figure 8 shows the recovered fragments of the vehicle.

It was interesting to note that the unheated end of the vehicle contributed most of the small fragments, whilst the damage to the heated end was similar in extent to that observed in the other three experiments.

In all four experiments there was evidence of beads of filling in the test arena, indicating ejection of molten material from the tube. The quantity of solid material recovered from the experiments was very small, even in those experiments whose temperature/time recordings indicate that a considerable proportion of the filling was solid at the point of ignition.

In two of the four experiments, endotherms similar to those observed in the fully heated tests were observed.



FIGURE 8. Vehicle remains from partially-heated RDX/TNT experiment.

Again these were only observed in the slow heating rate tests. Figure 9 shows the temperature history plot for the slow heating test on RDX/TNT. An 'endotherm' is clearly visible at 3200s.

### RESULTS OF PARTIALLY HEATED BURNING TUBE EXPERIMENTS WITH RDX/HTPB

The PBX (RDX/HTPB 85:15) gave relatively mild pressure bursts, again on the upper surface at the centre of the heated zone. In each experiment the vehicle split open with a crack aligned with the tube axis. The entire vehicle remained in one piece.

In all four experiments the material inside the vehicle burned in the period immediately following the event. In three of the experiments a significant proportion of the filling, in addition to that which had burned, was ejected from the vehicle and was recovered. The material inside the vehicle that had undergone burning remained in the form of a porous black ash. It is likely that this ash results from the binder component of the filling.

### OBSERVATIONS FROM RDX/TNT FILLED GLASS-WINDOWED VEHICLES

In all but one firing of the melt cast RDX/TNT 60:40 filled vehicles the glass window was shattered, the steel cylinder was broken into several pieces, and the end plates and tie bars were deformed. Figure 10 shows the extent of damage typical of this type of reaction. In the remaining experiment the glass window was broken and the filling burned in the open vehicle.

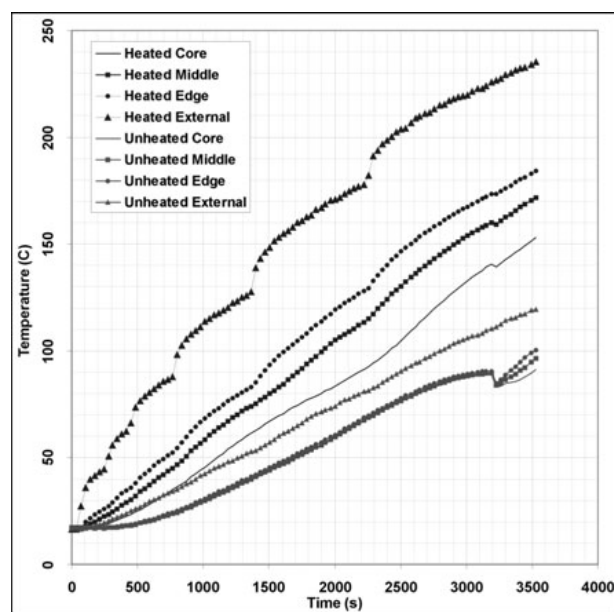
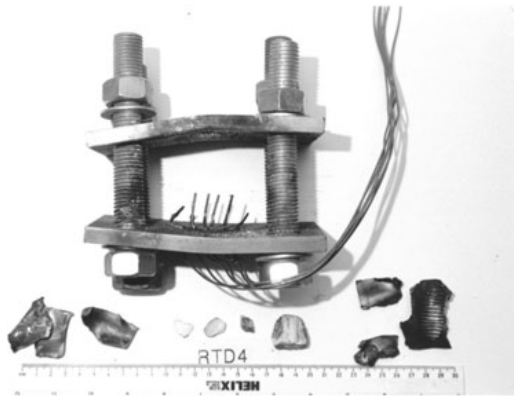


FIGURE 9. Temperature history of partially heated RDX/TNT experiment.



**FIGURE 10. Typical remains from RDX/TNT experiment.**

In the two fast heating rate experiments, approximately 40% of the filling was recovered after the event. This was in the form of relatively large pieces of material whose outer surface was melted, but whose freshly broken surfaces showed little evidence of degradation. Figure 11 shows an example of the material recovered from these experiments.

It should be noted that in both these experiments the ignition temperature was unexpectedly low: the outer thermocouples registered a temperature of approximately 100°C in each case. Furthermore, in both these experiments the electrical insulation was seen to ignite and burn for a short period just prior to ignition, so that locally the temperature experienced by the filling could have been much higher than that recorded on the thermocouples.

Observations through the glass window showed a darkening of the sample surface as the heating progressed. This started at the edge and worked evenly towards the centre. The colour change was coincident with the temperature achieving 88°C, and appears to be due to melting of the TNT component of the explosive. Once

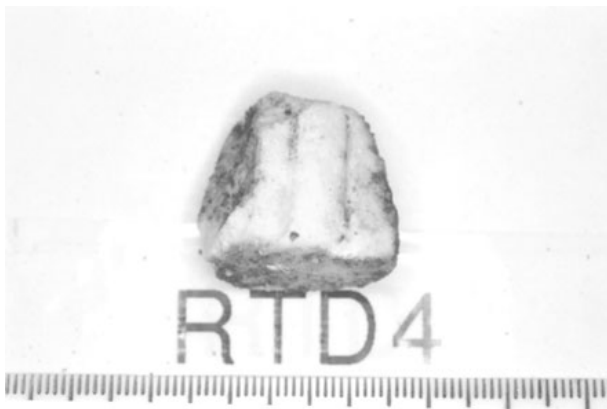


**FIGURE 11. RDX/TNT recovered from glass-windowed experiment.**

the whole surface area had darkened, and just prior to the explosion, some of the liquid component of the filling leaked from the vehicle and ignited. Bubbling was seen just under the glass in the liquid phase. The bubbling was indicative of an imminent explosive event.

### **OBSERVATIONS FROM RDX/HTPB FILLED GLASS-WINDOWED VEHICLES**

At the point of ignition in the experiments with RDX/HTPB 85:15, three of the six firings resulted in an explosion while the remainder showed burning of the filling within the vehicle. The explosions typically resulted in destruction of the glass window along with the viewing mirror sited directly above it. The steel components of the vehicle remained largely intact. There was only slight deformation of the tube body and the end plates.

In the two slow heating rate experiments, both of which displayed a small thermal explosion, almost all of the filling was recovered after the test. Examination of the filling showed that there was discolouration of the surfaces that had been in contact with the heated vehicle, while freshly broken surfaces appeared pristine. The third vehicle, which displayed an explosion, ignited and the contents burned away. In the remaining three experiments, which displayed an ignition and slow burning reaction, the contents of the vehicle burned away completely and were not recovered.

Three of the firings resulted in concentric burnings from the outer edges of the explosive inwards. In these firings the material ignited at ~160°C, began to burn inwards, and then quenched. The material re-ignited and quenched in a repeating process of increasing frequency, until the filling had been completely consumed. Figure 12 shows the burning reaction in the filling, and Figure 13, taken a few seconds later, shows that the reaction has quenched. In Figure 13, the grid marked on the surface of the unburned explosive is visible. Figure 14 shows the contents of the recovered vehicle.

Another feature of the majority of RDX/HTPB 85:15 firings was that at 120°C there was evidence of explosive oozing out under the glass window at the interface with the steel cylinder top. This material would sometimes catch light, and then extinguish after a short time. No discolouration of the surface of the filling was observed.

### **DISCUSSION**

The experimental results reported here give a comprehensive insight into the Cook-Off behaviour of two different classes of secondary explosives when heated.

All the RDX/TNT experiments which, at the point of ignition, were known to contain solid material, show low-order reactions. However, it should be noted that these were all more violent than any of those observed

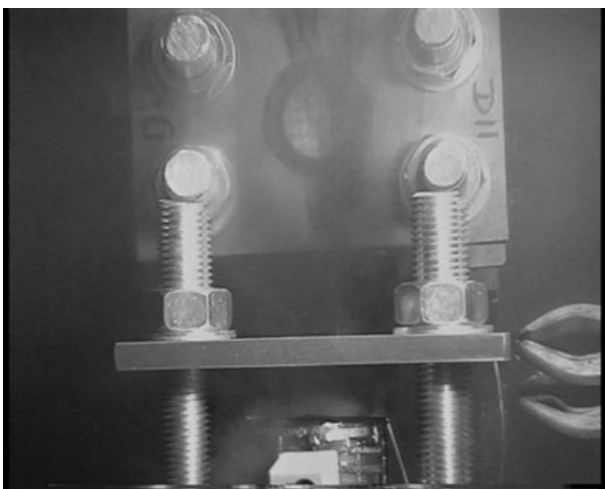


**FIGURE 12.** Video frame showing burning in RDX/HTPB 85:15.

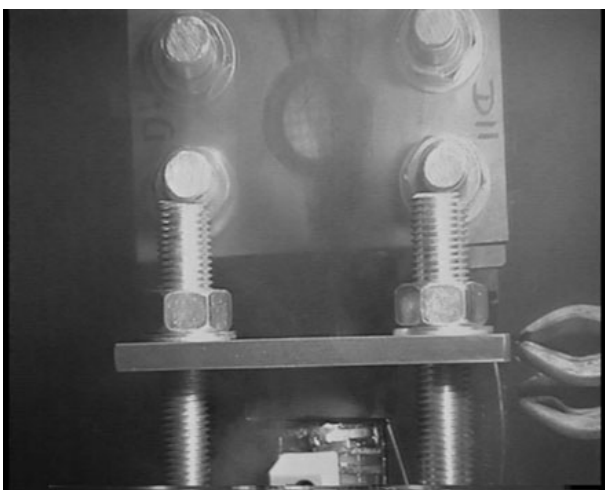


**FIGURE 13.** Video frame taken approx 5s after Figure 12.

with the RDX/HTPB composition. The only high-order reactions observed were in those experiments where the thermocouple recordings indicated that the filling was largely molten.

Of those glass-windowed vehicle tests on RDX/TNT which resulted in explosions, the explosions were immediately preceded by bubbling in the filling. This is perhaps to be expected because the glass-windowed vehicles were not well sealed, and hence the internal pressure was near atmospheric. All the events in the glass-windowed vehicles were relatively violent, resulting in fragmentation of the vehicle.

The 'endotherms' observed in the Burning Tube experiments with RDX/TNT are most likely associated with melting, probably combined with the failure of the seals on the vehicle as the hydrostatic pressure from the molten contents increased. Sealing failure would lead to

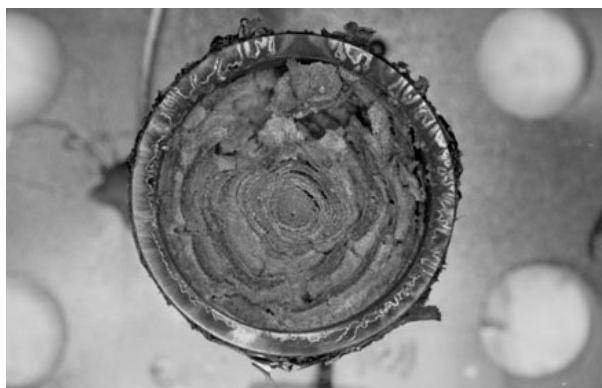


**FIGURE 14.** Residue from 'Cigar Burn' of RDX/HTPB 85:15 in glass-windowed vehicle.

a drop in pressure, and hence a simultaneous and rapid drop in temperature across the entire filling. This corresponds to the behaviour observed in the Burning Tube tests.

The two Burning Tube experiments that showed the most violent responses also showed 'endotherms' in their temperature records. It is therefore likely that the internal pressure in these experiments at the point of ignition was low, and that under these conditions, bubbling of the filling would be possible. The results therefore appear to indicate that the violent events observed in RDX/TNT correspond with bubbling.

These results seem to support the hypothesis that violent responses result from the increased shock sensitivity of hot, bubbling material. The ramped pressure wave from the thermal explosion is presumed capable of initiating a detonation in the liquid phase under these conditions. From this work it may be suggested that the propensity of RDX/TNT to produce violent responses depends on the strength of the pressure wave produced by the thermal explosion, and the state of the surrounding material. Similar conclusions have been reached by Kondrikov<sup>5</sup>.

There were no instances of violent responses in any of the RDX/HTPB experiments. In each case the failure of the vehicle was consistent with a pressure burst. In the partially heated tests, the failure of the vehicle was centred on the heated portion of the vehicle. This indicates that the ignition, although producing a relatively slow pressurisation of the vehicle, proceeds sufficiently quickly to cause localised damage.

The nature of the ash remaining after burning of the RDX/HTPB filling indicates that this is composed of binder material. This is notable when the high flame temperature evident from the melting of the glass window is considered. It would appear, then, that this type of binder may be capable of resisting or reducing the propagation of flames in the early stages of the growth of the reaction.

In all the glass-windowed experiments there is no evidence of large-scale damage to the filling during heating. No visible cracks were observed, although the smallest feature visible was approximately 0.25 mm sq., and therefore features smaller than this may have been missed.

Comparison of the RDX/TNT and RDX/HTPB experiments suggests that the molten phase of the filling is important in its propensity to produce violent responses to cook-off. Most modern PBXs would not be expected to have a molten phase on heating, and this may explain their mild behaviour when heated. However it should be noted that some PBXs having a low volume of binder (less than 10%) are known to respond violently to cook-off. This may be the result of their greater shock sensitivity and/or ease with which they are damaged.

## REFERENCES

1. Cheese, P., Briggs, R. I., Fellows, J., Haskins, P. J., Cook, M. D., "Cook-Off Tests on Secondary Explosives", 11th International Detonation Symposium, ONR 33300-5, 1998, pp. 272–278.
2. Chidester, S., Tarver, C., Green, L., Urtiew, P., "On the Violence of Thermal Explosion in Solid Explosives", *Combustion and Flame* **110**: 264–280 (1997).
3. Catalano, E., McGuire, R., Lee, E., Wrenn, E., Ornellas, D., Walton, J., "The Thermal Decomposition and Reaction of Confined Explosives", 6th Symposium (International) on Detonation, ACR-221 (1976).
4. Dickson, P. M., Asay, B. W., Henson, B. F., Fugard, C. S., "Observation of the Behaviour of Confined PBX 9501 Following a Simulated Cook-Off Ignition", 11th International Detonation Symposium, Snowmass, CO, 1998, pp. 606–611.
5. Kondrikov, B. N., "Investigation of Cook-Off-Type Test Methods", 11th International Detonation Symposium, ONR 33300-5, 1998, pp. 135–142.

## A.2 Small-Scale Thermal Violence Experiments...

---

Authors:	Bauer C L; Rae P J; Stennett C; Flower M		
Title:	Small-scale Thermal Violence Experiments for Combined Insensitive High Explosive and Booster Materials		
Publication Type:	International Conference	Venue:	International Detonation Symposium
Date:	2010		

---



## Small Scale Thermal Violence Experiments for Combined Insensitive High Explosive and Booster Materials

Clare L. Bauer<sup>†</sup>, Philip J. Rae<sup>‡</sup>, Chris Stennett\*, and Helen M. Flower<sup>†</sup>

<sup>†</sup>AWE, Aldermaston, Reading, RG7 4PR, UK

<sup>‡</sup>MST-8, LANL, Los Alamos, NM 87455

\*Explosives Science Group, DCMT Shrivenham, SN6 8LA, UK

**Abstract.** A small scale cook-off experiment has been designed to provide a violence metric for both booster and IHE materials, singly and in combination. The experiment has a simple, axisymmetric geometry provided by a 10 mm internal diameter cylindrical steel confinement up to 80 mm in length. Heating is applied from one end of the sample length creating pseudo 1-D heating profile and a thermal gradient across the sample(s). At the opposite end of the confinement to the heating block, a machined groove provides a point of rupture that generates a cylindrical fragment. The displacement of the external face of the fragment is detected by Heterodyne Velocimetry. Proof of concept experiments are reported focusing on HMX and TATB formulations, and are described in relation to confinement, ullage and heating profile. The development of a violence metric, based upon fragment velocity records is discussed.

---

### Introduction

For improved safety during development and scale-up of new and modified explosive formulations data are required on the response of the materials to credible handling and storage scenarios including cook-off<sup>1</sup>.

Interest in cook-off behaviour endures throughout the final article lifetime, with experiments and modeling being fielded in pursuit of a predictive response capability. Standard studies include sentencing tests such as burning tube and fuel fire which are qualitative and present results as numerical response levels<sup>2</sup>. Other experiments can be used to generate validation data and a predictive capability for models, such as STEX<sup>3</sup> and SITI<sup>4</sup>. However, the explosive masses required for these experiments and their general

complexity makes them difficult to field on new explosive formulations where typically only few hundred grams are manufactured.

Regulatory drivers require the selection of adequately performing materials with the lowest sensitiveness, explosiveness and mass. One difficulty is defining explosiveness or violence for small-scale reactions. The approach taken here is to quantify metal pushing ability. The challenge was therefore to develop a small scale cook-off experiment where violence of response, from a benign confinement rupture through deflagration to detonation is measured quantitatively and reproducibly.

Scoping experiments were conducted using a LANL thermal cook-off gun assembly using TATB and other formulations. The experiment had previously been optimised to study the cook-off response

of PBX9501 under varying inertial (projectile) and static (burst disk) confinement<sup>5, 6</sup>.

Since candidate materials included TATB, a material known to pressure burst confinements prior to DDT, it was decided that a strongly sealed system was required to retain reactive intermediates for exothermic gas phase reactions<sup>7</sup>. A variable point of weakness, or rupture disc, was designed to be accelerated by the reaction products and act as a quantitative metric of violence.

Previous work on deflagration to detonation transition (DDT) in granular HMX gives a good indication of the strong confinement and porosity required to achieve a short run distance to detonation<sup>8, 9</sup>. Extensive damage from thermal conditioning is necessary to reduce the run distances to the scale of this experiment. Work on granular HMX with approximately 30% porosity achieved run distances of 19 mm for heavily confined experiments and recent work at LANL shows that with relatively low porosities run distances of 50-100 mm are observed<sup>10</sup>.

In order to achieve maximum extent of reaction and still use the minimum sample masses, it was necessary to investigate a range of sample cavity lengths and temperature soak profiles.

## Experimental

A small scale cook-off experiment, figure 1, was designed to provide a high fidelity violence metric for both IHE and booster materials, singly and in combination. The experiment has an integral burst disk to allow thermal conditioning of formulations for extended periods without breaching of the confinement.

An axisymmetric geometry with a 10 mm internal diameter cylindrical 070M20 mild steel (1018 US Grade) confinement up to 80 mm in length was designed. Confinement is maintained up to several GPa by an internal pressure inconel c-seal. Heating is applied from one end of the sample length via two/three 150W cartridge heaters in a copper or brass heating block. Temperature control is provided by a thermocouple in the heating block. Additional thermocouples were inserted into the steel confinement. At the opposite end, a machined groove provides a point of rupture that generates a cylindrical fragment. The displacement of the exter-

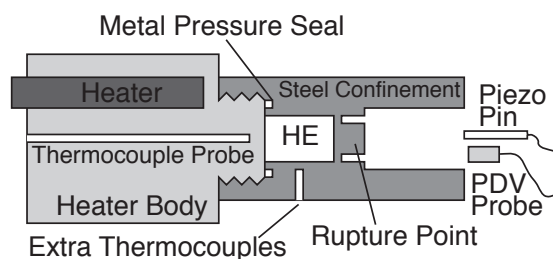


Fig. 1. A schematic of the experimental assembly.

Table 1. Formulations & PBXs used in cook-off experiments

Label	Composition data	Pellet length (mm)
L	Isostatically pressed 91:8 HMX/NC	4
M	Isostatically pressed TATB/Fluoropolymer	4
N	Die-pressed 92:8 HMX/HTPB shear mixed	8 & 10
P	Die-pressed 92:8 HMX/HTPB	8 & 10
Q	Die-pressed Tetryl	10
R	Die-pressed 91:8 HMX/NC	10

nal face of the fragment is detected by heterodyne velocimetry and is triggered by a piezoelectric pin.

Integration of the velocity vs. time history allows the fragment displacement to be found. Thus, the movement of the disc while still blocking the passage of reaction gasses to the atmosphere can be distinguished from free fragment flight. Once in free flight, rapid expansion of the product gases will occur by escaping around the sides of the fragment.

Calculations using the Sandia Hydrocode CTH were undertaken during the confinement design stage to verify that under both deflagration and full detonation, the rupture plug was correctly sheared from the body and would strike the piezo trigger pin.

For the experiments, the samples were subjected to a pseudo 1-D heating profile at rates of  $1^{\circ}\text{C min}^{-1}$  and  $10^{\circ}\text{C min}^{-1}$ . Extended thermal soaking at  $170^{\circ}\text{C}$  or  $180^{\circ}\text{C}$  was performed on HMX

Table 2. Relationship of the groove depth to shear area and rupture pressure.

Groove depth / mm	Shear area / mm <sup>2</sup>	Rupture Pressure / MPa (kpsi)
5	25.1	134 (19.4)
4	50.2	316 (45.8)
3	75.2	> 400 (58)

based samples in ramp-soak type experiments and at 250°C for TATB based samples. Materials studied are listed in table 1 with conditions for 10mm cook-off experiments in table 3 and for longer samples in table 4.

Upon rupture, a projectile would be generated. The velocity of which was dependent on the violence of reaction of the HE. Velocity was recorded by a Tektronix TDS 6804B 8GHz oscilloscope and Doppler velocimetry (Het-V), using a 4mW, 1550 nm diode laser <sup>11, 12</sup>. The data generated by the Het-V system were processed using a Fast Fourier Transform (FFT) method in an Igor Pro routine.

## Results

### Static pressure rupture testing

Several prototype confinement vehicles were manufactured with differing burst disk configurations. The designed point of weakness relies on a machined groove on the outside of the body. The depth of this groove determines how much steel the growing reaction must fracture in order to release the pellet. Thus a 5 mm groove leaves less material and offers less confinement than a 4 mm groove, etc. The area of material to be sheared is shown in table 2 together with the measured quasi-static burst pressure for the three groove depths.

### Cook-off: 10 mm length sample confinements

Cook-off experiments were undertaken using pellets of composition L as a source of well characterized material from which reactions of appreciable violence in confined cook-off could be expected. Pellet length was fixed at 4 mm as the samples were legacy machined material. Two pellets were used in

Table 3. The conditions for 10mm cook-off experiments. The ramp rate was set at 10°C min<sup>-1</sup> for both ramp-to-failure and 1.5 hr soak experiments. \* 5 hour soak, \*\* soak at 190°C.

Expt.	Steel groove (mm)	Profile	Expt.	Steel groove (mm)	Profile
L1	5	soak	Q2	4	rtf
L2	4	soak	LM1	5	rtf
L3	4	soak*	LM2	4	rtf
L4	4	soak**	P1	4	soak
L5	4	rtf	P2	4	soak
L6	3	rtf	N1	4	soak
L7	3	soak	N2	4	soak
M1	4	rtf	Q1	4	rtf

each experiment leaving a 2 mm long void space at the burst disc end of the sample volume equivalent to 19% ullage. Originally it was thought that the 10 mm long body would allow sufficient extent of reaction to distinguish between material responses without transitioning to detonation.

From figure 2 it may be seen that the experiment differentiated well between HMX based composition L samples subject to different soak times but under the same confinement. These data suggest that there is an optimum extent of degradation which gives the greatest reaction violence. This result is intuitive, as a violent reaction is expected to require significant porosity to support ignition but also enough material remaining for the reaction to propagate.

However, the 3 mm groove depth confinement has the effect of reducing the pellet velocity compared to a 4 mm vehicle under the same conditions. It is most likely that this results from the 3 mm confinement requiring more of the available energy to promote fracture and therefore results in a lower velocity.

For comparison, the results from a TATB based composition M cook-off suggest a slow, ductile failure in the manner of a pseudo-static pressure burst.

Experiments with a single pellet of composition L against the heater block followed by a pellet of composition M are shown in figure 3 (HMX:TATB). A 2 mm ullage space was left (20%) and a 4 mm groove depth confinement was used.

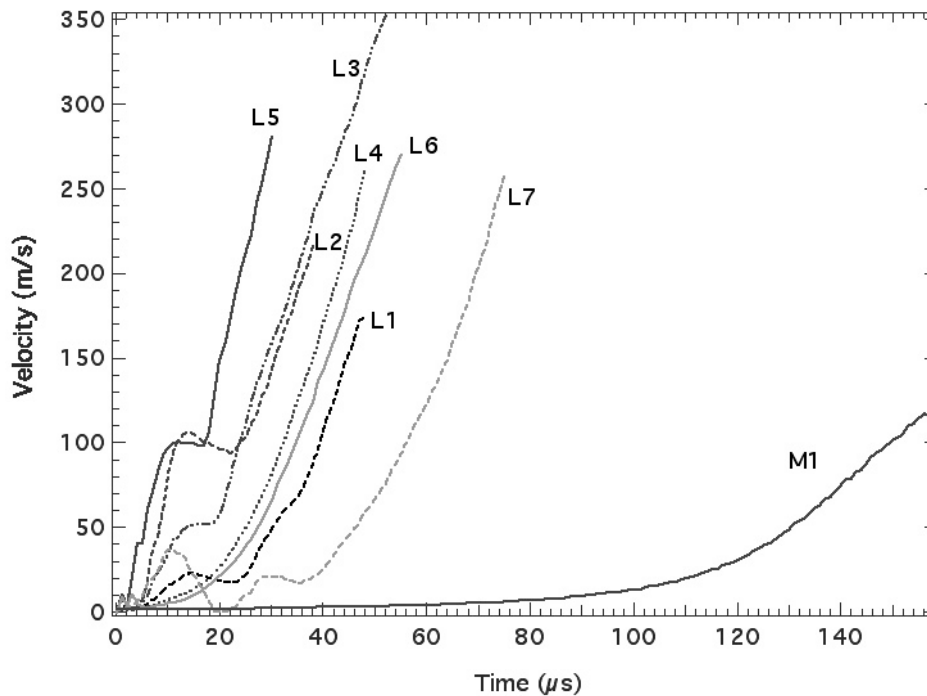


Fig. 2. Velocity/time profiles for HMX based composition L cook-offs in which confinement, soak duration and soak temperature were varied. A TATB based composition (M) cook-off is included for comparison.

Experiments LM1 and LM2 follow the trend of the composition L data for similar confinement and conditions, despite having half the mass of HMX present. There appears to have been little contribution from composition M (TATB) with unburnt material scattered around after rupture. In both cases the fragment velocity is influenced by the mass of HMX present.

Fragments from some of the 10 mm cook-off experiments were examined for evidence of shear localization during fracture. It has previously been shown that in 1018 steel, shear localization is suppressed unless the material had been shock pre-strained<sup>13</sup>. This prior finding was confirmed for the experiments presented here where optical microscopy of the rupture surfaces showed no evidence of adiabatic localization. Additionally, it was observed that the more violent cook-offs produced cleaner fracture surfaces with less sign of plastic deformation of surrounding material.

**Cook-off:** The effect of ullage in 10mm sample length confinements

In an effort to determine the influence of ullage on the violence of response in these particular experiments, the HMX/HTPB compositions N and P were tested with and essentially without ullage.

In response to the applied thermal profile a volume change of approximately 7%<sup>14</sup> resulting from the  $\beta - \delta$  phase change of HMX crystals would be expected<sup>15</sup>. Additionally there would be a small volume change due to thermal expansion of all constituents<sup>a</sup>. The configuration of the experiment delivers a thermal gradient across the sample such that the additional thermocouples show a temperature difference of 20°C across the sample confinement. This means that, assuming a linear gradient, the sample volume heated to the threshold for  $\beta - \delta$  phase change will only be of the order of 3.5 mm<sup>3</sup> or 0.45% of the total. Also, since HMX does not begin appreciable degradation until approximately 170°C, the gas generation of these samples during

<sup>a</sup>This excluded any compressible porosity that may also be generated.

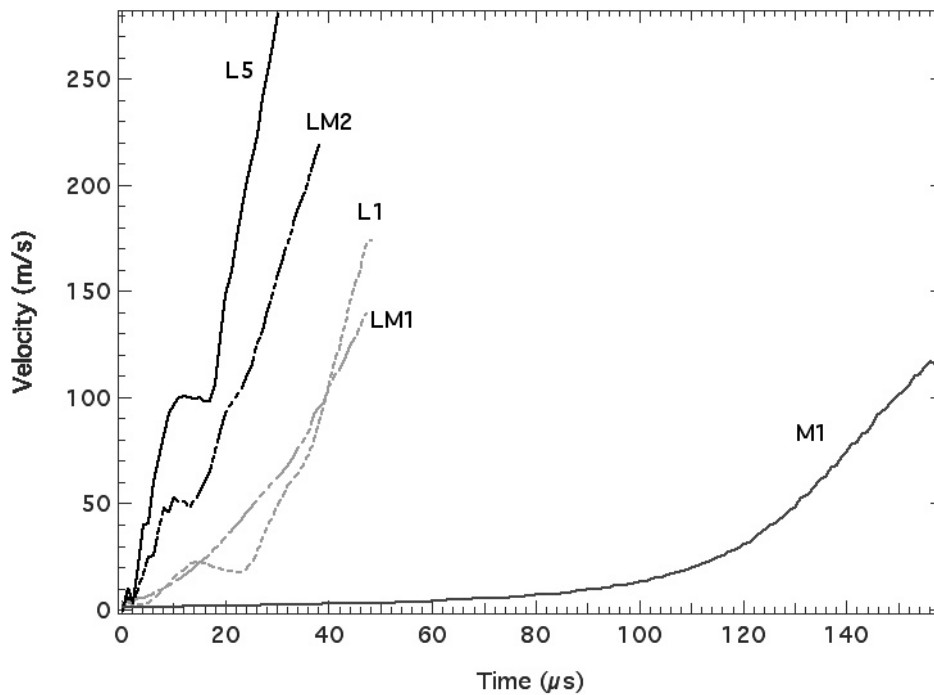


Fig. 3. Velocity/time profiles for composition L & M mixed cook-offs in comparison with separate cook-off of composition L and composition M

soak will be low. Thus, the reduction in the ullage after heating is from approximately 20% to 19% and relatively little gas will be generated from the HMX to expand internal voids and pores within the thermally damaged HMX. In this way, the applied thermal profile is effective in raising the bulk temperature of the material without excessive material damage, gas pressure increase prior to burning or HMX mass loss.

Results of the HMX/HTPB based experiments are shown in figure 4. The trend for lower projectile velocities in experiments with no void space is followed by all samples. All of the experiments show relatively low projectile velocities which is attributed to incomplete burn of the sample.

The inclusion of Tetryl in the data set illustrates the issue of the sample length used in the experiment influencing the violence of response. Tetryl will run to detonation from cook-off in a distance of 70mm<sup>16</sup>. Sample lengths are restricted to 10mm in these experiments and similarly low velocities have been observed for both Tetryl and HMX/HTPB formulations. This implies that, like Tetryl, the HMX/HTPB formulations may show a greater re-

sponse, and possibly distinction between formulations, with longer sample lengths.

#### Cook-off: 40mm to 80mm HE sample confinements

A table of cook-off experiments with fast and slow heating profiles that were performed on HMX based composition R pellets is shown in table 4. The groove depth in all cases was 4 mm. The body was insulated using glass fiber tape. In some experiments the insulation only extended half way along the body while in others the whole body was insulated. This lagging changed the thermal gradient along the explosive run length. The profile was recorded using up to four equispaced thermocouples.

It was determined that in order to obtain the best possible coupling of explosive response to projectile velocity, an alteration of the brass heater was necessary. It had been observed in some experiments that the brass heater had become prematurely detached from the confinement body despite the rupture of the fragment. The brass heater was altered to allow a short brass projection (2 mm long) to enter

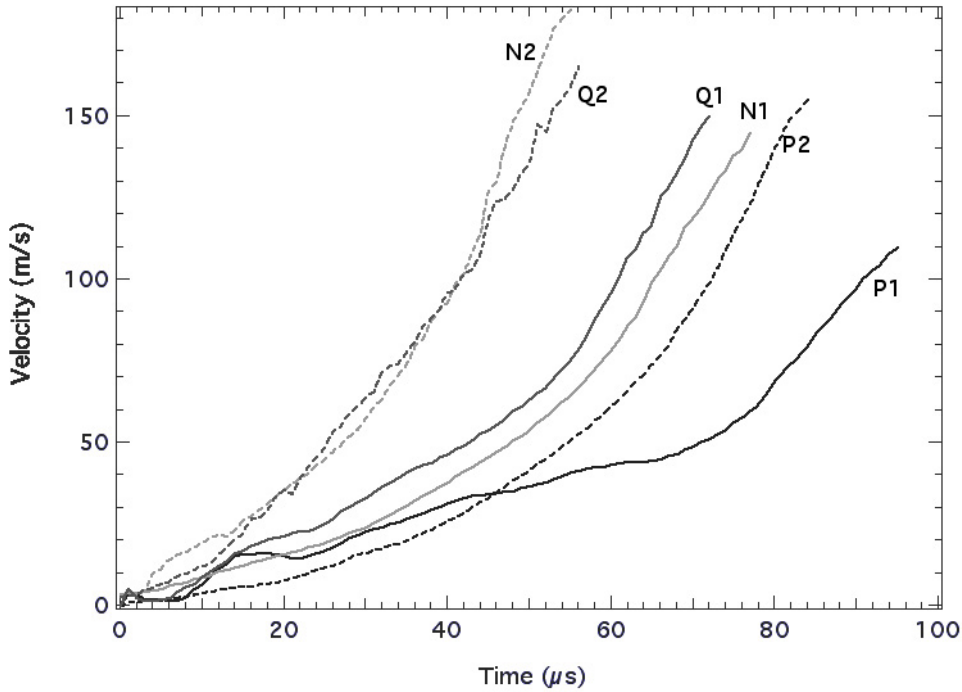


Fig. 4. Velocity/time profiles for HMX/HTPB and Tetryl.

the sample containing tube. This was done in an effort to reduce the dynamic force experienced by the sealing face and the threads by swelling of the brass projection under high pressure. The modification was successful in delaying separation of the heater from the body until such time as the rupture disc was in free-flight.

All confinement bodies had sample cavities 40 mm in length except experiment R8 which had a sample cavity of 80 mm. Experiments in italics in table 4 represent those conducted with the altered brass heating block. With the 2 mm intrusion into the confinement the full complement of  $4 \times 10$  mm pellets could not be accommodated. Therefore  $3 \times 10$  mm pellets were used leaving an 8 mm long void space at the burst disk end. All other experiments had no ullage.

Referring to figure 5, it can be seen that experiments with the same thermal profile exhibit velocity profiles which are similar after the heater modification. At early times in the velocity profile, before the fragment is in free-flight, the curves almost overlap. Further, the data indicates that the length of the insulation (lagging) on the experiment is negligible in comparison to the influence of ullage and

Table 4. A table of 40 mm and 80 mm experiments with and the associated thermal profile applied. RTF is continuous temperature ramp-to-failure. The profile for the 1.5 hr soak at 180°C was ramped to hold  $10^\circ\text{C min}^{-1}$  followed by  $10^\circ\text{C min}^{-1}$  to reaction.

Ramp	Half body lagging	Full body lagging
RTF $10^\circ\text{C min}^{-1}$	R2 <i>R4</i> <i>R5</i>	
RTF $1^\circ\text{C min}^{-1}$		<i>R7</i> <i>R8 (80 mm)</i>
180°C 1.5 hr + RTF $10^\circ\text{C min}^{-1}$		R1 <i>R3</i> <i>R6</i>

thermal profile.

In the overlapping trace cases, the curves indicate the intrinsic response of the HE under the given conditions. This intrinsic response may then be used to derive a violence metric based on the gradient of the early velocity record. While the fragment is still blocking the flow of most reaction gases to the atmosphere, the motion will be heavily influenced by the mechanical strength of the steel which depends entirely on the strain rate induced by the hot gases generated in the confinement and temperature. Essentially, this is the rate and extent of reaction of the explosive.

Once the fragment is in free flight, the motion will be a complex mix of acceleration from gases coming from a now pressure relieved reaction, air drag and residual velocity from the fracture process. This part of the data set is therefore less useful. As previously described, the timing of separation of the heater block from the confinement was variable, but always occurred after the projectile had entered free flight after the modification.

Experiment R7 shows the highest projectile velocity. However, early time data for velocity profiles R4, R5 and R7 almost overlaps. Some other traces (R1 & R2) show lower velocities, however, in these cases the heater modification was not used. Some experiments were repeated (R4 & R5 and R3 & R6) and show good reproducibility.

One of the aims of the experiments was to obtain a quantitative measure of violence with respect to metal-pushing ability. The gradients of the velocity/time profiles up to free flight offer the best basis for such a metric. It must be determined if other formulations converge on a single intrinsic velocity profile per confinement vehicle as HMX based composition R does.

#### Cook-off: Confinement expansion

The sectioned confinement vehicles from experiments with differing velocity records were examined.

The R7 vehicle in figure 6 shows evidence of an ignition(1) and growing reaction running in the direction of the burst disk up to a maximum (2). The deformation near the burst disk end appears to reach a steady velocity (3) but measurement of the vehicle show that this point corresponds to the end of the

explosive pellet and the region of ullage. The position of the inside face of the burst disk is shown by (4) and the position of the bottom of the machined groove by (5). There is no evidence to suggest that DDT was reached.

In order to provide a comparison with a true detonation, an experiment was undertaken with a sample of C4 and an L1A1 detonator. A velocity profile was recorded and the fragments of the vehicle were collected. A photograph of the pieces is presented in figure 7. The fragmentation was extensive with the greatest damage at the heater end where the detonator was located. None of the cook-off experiments undertaken show any confinement fragmentation approaching that of the detonated confinement. The velocity record for the detonative test, S1 in figure 5 shows that the velocity profiles for the series of composition R exhibit much lower gradients.

A different pattern of deformation was found in the confinement vehicles of experiments where relatively low velocities were observed, an example (R2) is shown in figure 8. Here consideration of the deformation in relation to a thick-walled cylinder leads to the conclusion that a pressure build-up over several 100  $\mu$ s is necessary in order to achieve the plastic work observed. It is likely that the confinement ballooned in the middle as the ends were reinforced by the heater block and the burst disk. The most likely point of ignition of this slow burn is shown by (1) and the maximum deformation by (2). As before, the position of the inside face of the burst disk is shown by (4) and the position of the bottom of the machined groove by (5).

#### Steel Hardness Testing

There is a well known reversible  $\alpha - \epsilon$  phase transition in iron and iron based alloys at  $\approx 13$  GPa<sup>13</sup>. Upon shock release back to 1 bar, residual microstructural changes remain that increase the hardness of the material. It was wondered if this harness 'signature' might be useful in detecting localized, and ambiguous, regions of detonation in steel confinements such as those used in this research.

Vickers hardness (HV) tests were undertaken on as-received confinement steel and the average was found to be  $195 \pm 5$  HV. The heated confinements in which deflagration had occurred had undergone

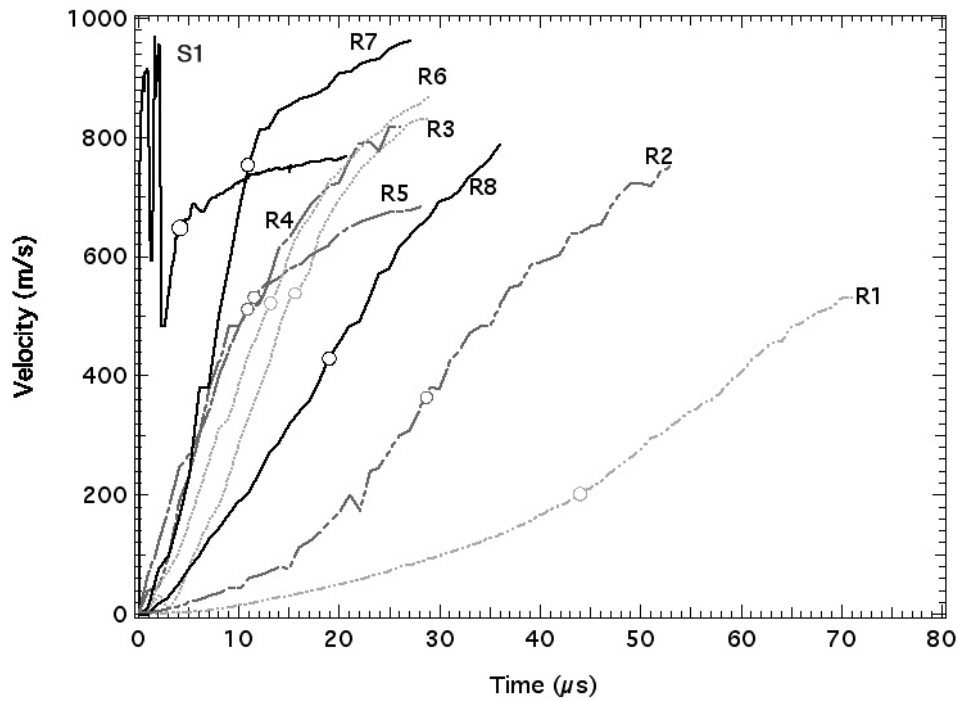


Fig. 5. Velocity / time data for the 40 mm and 80 mm experiments. Circles indicate the time at which the projectile has moved 3 mm from the starting position, after which it is considered to be in free flight. A detonative test (S1) is added for comparison.

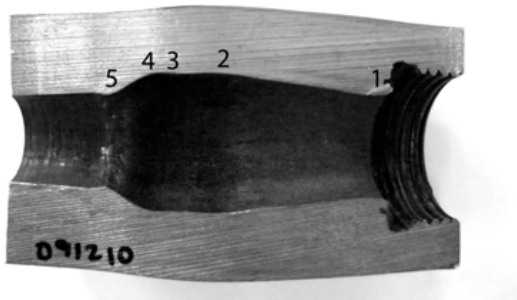


Fig. 6. The R7 confinement vehicle in section

considerable plastic deformation at pressures significantly below the  $\alpha - \epsilon$  phase change. The measured hardness from inside to outside the cylinder wall dropped from  $\approx 260$  to  $\approx 240$  HV. Considerable scatter in the values ( $\pm 10$  HV) was seen owing to the dirty nature of this steel but measurements were made in three confinements at a total of nine locations. Similar measurements were undertaken on a recovered fragment from the detonation experiment where the confinement was cold prior to ignition. The measured hardness was approximately



Fig. 7. Fragments of the vehicle in the detonative test.

the same across the wall thickness and had a value of  $220 \pm 10$  HV. The detonated fragment showed less overall plastic deformation than the deflagration confinements.

From this it is clear that the hardening associated with plastic deformation of the confinement is greater than that from the shock hardening process. Therefore, measurements of steel hardness are not a suitable method of deciding if local detonation has



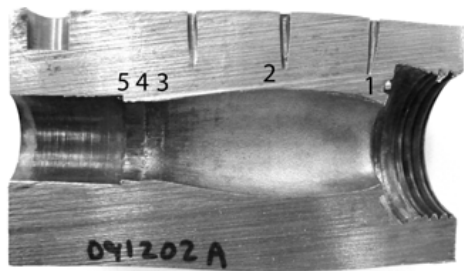


Fig. 8. The R2 confinement vehicle in section

occurred in low carbon steel confinements.

## Conclusions

The data presented here demonstrates the difficulty of generating DDT events in small masses of high density secondary explosives even held under extremely strong confinement and heated using aggressive thermal profiles. It has been shown that run lengths of less than 10mm are not capable of fully exploring the response of the material. Although the results do show differences between materials, these differences in the velocity profiles are not significant enough to draw firm conclusions regarding the relative violence of reaction of the materials. This demonstrates that under the reported level of confinement pressure, burst occurs before the materials have fully reacted.

Further, it has been shown that ullage influences the extent of reaction and thus the velocity profile observed. The presence of ullage allows greater expansion and cracking of the sample, particularly when HE crystalline phase transitions are encountered, this increases the surface area available to the initial burn part of the DDT process and gives space for product gases to expand into. These factors allow the reaction to progress to a greater degree resulting in a more violent rupture. Additionally, there is greater PV energy stored in the pressurized gas within the chamber also increasing the velocity.

The 40 mm sample lengths have been shown to be adequate to explore the full extent of reaction possible in HMX with this level of confinement. Additionally, it has been shown that even with significant lagging and a slow heating rate allowing a greater

degradation of the sample, 80 mm was not sufficient to induce a detonation owing to the high density of the undamaged starting explosive.

The data from the 40 mm experiments appears to show the maximum possible reaction of the material under these experimental conditions. From these data the early part of the velocity profile shows the greatest potential to be developed into a violence metric. The gradient of the velocity profile prior to free flight of the projectile is a function of the extent and rate of reaction of the explosive and the work done on the confinement vehicle to generate the projectile. Thus the gradient is the best indicator of the violence of reaction of the material and its ability to do work on a metal.

Data on the cook-off of different formulations is required to verify the suitability of this metric.

## Acknowledgments

The authors would like to acknowledge the work of G. Cooper at DCMT Shrivenham and discussions with G. Parker at LANL

## References

1. Asay, B., *Shock Wave Science and Technology Reference Library, Vol. 5: Non-Shock Initiation of Explosives*, Springer, 1 edition, 2010.
2. (DOSG), "EMTAP 35,41 and 42," in "Energetic materials testing and assessment policy committee, Manual of tests Edn. 3," pp. 1-1124, Defence Ordnance Safety Group (DOSG), Abbey Wood, UK, 2007.
3. Wardell, J. and Maienschein, J., "The scaled thermal explosion experiment," in "12th International Detonation Symposium," pp. 384-394, Office of Naval Research (ONR), San Diego, CA, USA, 2002.
4. Kaneshige, M. J., Renlund, A. M., Schmitt, R. G. and Erikson, W. W., "Cook-off experiments for model validation at Sandia National Laboratories," in "12th International Detonation Symposium," pp. 821-831, Office of Naval Research (ONR), San Diego, CA, USA, 2002.
5. Perry, W. L., Dickson, P. M. and Parker, G. R., "Quantification of reaction violence and com-

- bustion enthalpy of PBX 9501 under strong confinement,” *J. Applied Phys.*, Vol. 97, p. 023528, 2005.
6. Perry, W. L., Zucker, J. M., Dickson, P. M., Parker, G. R. and Asay, B., “Interplay of explosive thermal reaction dynamics and structural confinement,” *J. Applied Phys.*, Vol. 101, p. 074901, 2007.
  7. Belmas, R., Le-Gallic, C. and Lambert, P., “Pre-heating sensitization of a TATB composition part 1: chemical evolution,” *Propellants, Pyrotechnics and Explosives*, Vol. 29, p. 282, 2004.
  8. McAfee, J. M., Asay, B., Campbell, A. W. and Ramsay, J. B., “Deflagration to detonation in granular HMX,” in “9th International Detonation Symposium,” pp. 265–278, Portland, Oregon, USA, 1989.
  9. McAfee, J. M., Asay, B. and Bdzil, J. B., “Deflagration to detonation in granular HMX: ignition, kinetics and shock formation,” in “10th International Detonation Symposium,” pp. 716–723, Boston, MA, USA, 1993.
  10. Parker, G. R., Dickson, P. M., Asay, B. W. and McAfee, J. M., “DDT of hot, thermally damaged PBX 9501 in heavy confinement,” in “14th International Detonation Symposium,” Office of Naval Research (ONR), Couer d’Elene, ID, USA, 2010.
  11. Strand, O. T., Goosman, D. R., Matrinez, C. and Whitworth, T. L., “Compact system for high-speed velocimetry using heterodyne techniques,” *Rev. Sci. Instruments*, Vol. 77, p. 083108, 2006.
  12. Jensen, B. J., Holtkamp, D. B., Rigg, P. A. and Dolan, D. H., “Accuracy limits and window corrections for photon Doppler velocimetry,” *J. Applied Phys.*, Vol. 101, p. 013523, 2007.
  13. Dougherty, L. M., Cerreta, E. K., Pfeif, E. A., Trujillo, C. and Gray III, G. T., “The impact of peak shock stress on the microstructure and shear behavior of 1018 steel,” *Acta Materialia*, Vol. 55, pp. 6356–6364, 2007.
  14. Parker, G. R., Peterson, P. D., Asay, B. W., Dickson, P. M., Perry, W. L., Henson, B. F., Smilowitz, L. and Oldenborg, M. R., “Examination of morphological changes that affect gas permeation through thermally damaged explosive,” *Propellants, Explosives, Pyrotechnics*, Vol. 29, pp. 6356–6364, 2004.
  15. Smilowitz, L., Henson, B. F., Asay, B. W. and Dickson, P. M., “A model of the  $\beta$  -  $\delta$  phase transition in PBX 9501,” in “12th International Detonation Symposium,” pp. 103–111, Office of Naval Research (ONR), San Diego, CA, USA, 2002.
  16. Price, D. and Bernecker, R. R., “DDT behaviour of ground tetryl and picric acid,” in “Report NSWC/WOL TR 77-175,” pp. 1–62, Naval Surface Weapons Center, White Oak, Maryland 20910, Dahlgren, VA USA, 1978

### Discussion

Russ Maines, AFRL

Any plans to scale up, such that this information can be used for system-level design?

### Reply by Clare Bauer

Although the geometry of the experiment is simple enough to scale up there are no plans to do so at present. This series of experiments was designed to produce data to be applied to the selection of suitable formulations at an early stage in their development at small batch quantities. More cook-off data on different formulations singly and in combination is required to confirm and develop the violence metric. These experiments are the focus of onward work.

In future this experiment could certainly be scaled to accommodate samples in the order of a few times the mass of those currently used. However, the experiment relies on the material properties of the confinement, made from 1018 steel, and so cannot offer data specific to system materials and confinement. The level of confinement in this experiment will be in considerable excess of that offered by a system configuration.



### A.3 The Role of Binders...

---

Authors:	Cook M D; Stennett C; Haskins P J; Brigg R I; Wood A D; Cheese P J		
Title:	The Role of Binders in Controlling the Cook-off Violence of HMX/HTPB Compositions		
Publication Type:	International Conference	Venue:	Shock Compression of Condensed Matter
Ref:	AIP Conf. Proc.	845,	952 (2006); <a href="http://doi.org/10.1063/1.2263479">http://doi.org/10.1063/1.2263479</a>

---

# THE ROLE OF BINDERS IN CONTROLLING THE COOK-OFF VIOLENCE OF HMX/HTPB COMPOSITIONS

M. D. Cook<sup>1</sup>, C. Stennett<sup>2</sup>, P. J. Haskins<sup>1</sup>, R. I. Briggs<sup>1</sup>, A. D. Wood<sup>1</sup>  
and P. J. Cheese<sup>3</sup>

<sup>1</sup>*QinetiQ, Fort Halstead, Sevenoaks, Kent TN14 7BP, UK*

<sup>2</sup>*RMCS, Shrivenham, Swindon, SN6 8LA, UK*

<sup>3</sup>*Defence Ordnance Safety Group, Walnut 2c #67, MoD Abbey Wood, Bristol, BS34 8JH, UK*

**Abstract.** There is a clear difference in cook-off vulnerability between highly-loaded pressed compositions such as LX-14 (pressed 95.5% HMX/4.5% binder), which yield violent responses, and cast compositions with low loadings, such as CPX 301 (85% RDX/15% HTPB), which yield relatively mild responses. These two classes of composition differ primarily in the quantity of binder, and in the manufacturing method used in production. An experimental study was conducted in an attempt to determine the filling proportion beyond which violent responses are observed. Here we describe a series of small-scale cook-off experiments which studied pressed compositions of 88%, 91%, 95% and 96% HMX, mixed with cured, cross-linked HTPB. The experiments used a novel glass-windowed test vehicle, instrumented internally with thermocouples. A trend of increasing event violence with increasing proportion of HMX was found, although in none of the experiments was mass reaction recorded. The results from these experiments are discussed.

**Keywords:** HMX, explosive, Cook-Off, violence

**PACS:** 47.70.Fw, 66.30Xj

## INTRODUCTION

Historical evidence has shown that certain pressed PBXs with high HMX content, e.g. LX-10 (95% HMX/5% Viton) and LX-14 (95.5% HMX/4.5% estane) respond violently to thermal stimuli. With this type of explosive, cook-off tests often result in deflagration and sometimes even detonation. By contrast, work on cast PBXs containing a relatively large proportion of a flexible binder, e.g. CPX 301 (85% RDX/15% HTPB), respond much less violently to thermal stimuli. These observations have led us to the question: what is the minimum binder proportion required to ensure low-violence cook-off responses?

To address this question we have carried out a series of cook-off experiments on a range of pressed HMX/HTPB compositions in which the HMX content has varied from 88% to 96%.

## EXPERIMENTAL PROCEDURE

The Small-Scale Glass Windowed Cook-Off (SSGWCO) test vehicle used in this study is a development of that reported previously [1]. This earlier work clearly showed that the capability to observe activity within the vehicle during heating was particularly useful. The new vehicle design includes improved pressure sealing capacity, to

~100 bar static pressure, and a more flexible instrumentation capability.

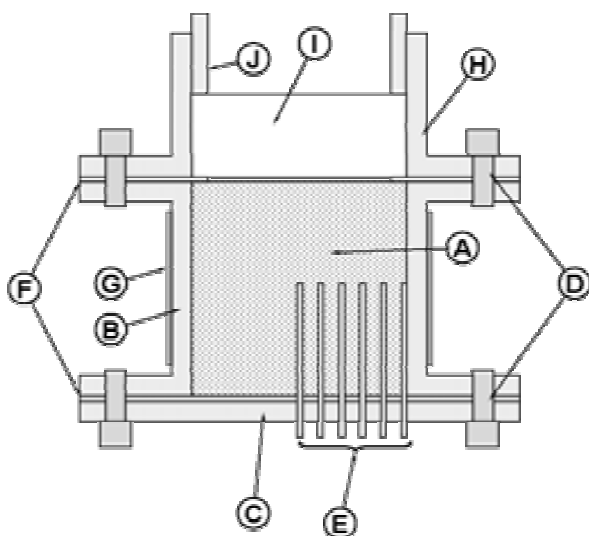


**FIGURE 1.** SSGWCO test vehicle cross-section

Fig. 1 shows a cross-sectional diagram of the SSGWCO test vehicle. The filling, A, is contained within a flanged mild steel tube, B, of internal dimensions 50mm x 50mm. The wall thickness is 5mm. A base plate, C, of 5mm thickness closes the lower end of the vehicle, and is clamped to the tube flange by six retaining bolts, D. Six K-type 1.5mm thermocouples, E, are fitted through the base plate so that their ends lie at the mid-point of the filling. The thermocouples are distributed evenly across the vehicle.

PTFE gaskets, F, are placed between the vehicle body and the end assemblies to provide gas sealing. The heating element, G, consisting of 1m of nickel-chrome heating tape, is wrapped around the tube body. The upper closure assembly, H, is clamped to the top flange of the tube with six retaining bolts. A glass window, I, is clamped to the top flange gasket using the window retaining ring, J.

The electrically heated Cook-off method has been described previously [1,2]. In this method, heating is achieved by a heating element wrapped around the outer surface of the test vehicle. The heating element consists of a 1m length of nickel-chrome heating tape, of 3.2mm width and 0.1mm thickness, and whose resistance is approximately 3Ω. The heating element is connected to the

electrical supply through a variable transformer which allows control of the current applied, and hence control of the heating effect. In these experiments the current was controlled manually.

## HEATING PROFILES

Two heating rates were chosen for the experiments, namely: 30°C/hour and 600°C/hour. Heating was carried out at these approximate rates, to maintain a constant temperature profile across the filling, as measured on the 6 thermocouples. In the faster rate experiments the aim was to achieve 120°C variation in temperature from centre to edge at the time of ignition. For the slower rate experiments, the aim was to achieve 30°C temperature variation across the sample at the time of ignition.

## COMPOSITIONS

Five formulations were chosen for this study, all consisting of HMX and cross-linked HTPB in different proportions. These are shown in Table 1.

The HMX was type B, having a bimodal particle size distribution of 35% (vol.) in the size range 45-150µm, and 65% (vol.) of a size smaller than 45µm. The density of the crystals was 1.84 g/cc.

**TABLE 1.** Formulations used. Two pellets of each composition were made; the filling density for each is shown. ‘V’ suffix indicates pressing under vacuum to improve filling density; all other compositions were pressed at atmospheric pressure

HMX	HTPB	% TMDs Pellet 1, Pellet2
88%	12%	94.0%, 96.9%
91%	9%	94.7%, 94.7%
95%	5%	94.8%, 94.5%
96%	4%	91.4%, 91.4%
96% (V)	4% (V)	94.7%, 98.6%

The binder system in all the formulations consisted of HTPB, DOS and a mixture of MDI/IPDI isocyanate curing agent. After 24 hours

partial curing the mixture was single-end pressed to a load of 127MPa at ambient temperature. The pellets were then inserted into the test vehicles, and cured for four days at ambient pressure and 60°C.

The filling densities, as shown in Table 1, are rather lower than would be expected for service use. This is probably a result of single-end pressing; isostatic pressing at elevated temperatures routinely yields filling densities >99% TMD.

The manufacture of the 88/12 compositions proved to be particularly difficult as this mix ratio is typically cast, rather than pressed, and remains semi-liquid even at room temperature. Partial curing of the pressing mixture gave a more workable material for pressing, but yielded finished pellets with variable filling density.

## RESULTS

A marked expansion of the filling was observed during the slow heating tests as the internal temperature reached 160-170°C. This coincided with a clear endotherm visible on the temperature recordings. This was attributed to the  $\beta$ - $\delta$  phase change in HMX [3].  $\delta$ -HMX occupies a greater volume than  $\beta$ -HMX, and therefore expansion of the material occurs at the transformation point. This expansion, beginning at a temperature of 165°C, was clearly visible in the slow heating rate experiments, but not so marked in those heated at the faster rate. At faster heating rates, much of the material remains at a temperature lower than that required for the  $\beta$ - $\delta$  transformation.

Table 2 summarises the experimental results. The violence of response is categorised into three divisions: A, B and C. Response A is characterised by a mild pressure failure of the vehicle, ejection of the sealing gaskets and bulging of the instrumentation plate to no more than 3mm. Response B is characterised by a medium pressure failure, with snapping of one or more retaining bolts, and with bulging of the instrumentation plate to approximately 6mm. Response C is the most violent, and is characterised by snapping of the retaining bolts, separation of one or both end closure assemblies, and bulging of the instrumentation plate to approximately 10mm. A graphical summary of the results is given in Fig. 2, which is a plot of average dent depth of the

SSGWCO vehicle base-plate and the percentage of binder.

**TABLE 2.** Experimental results summary.  $T_{ign}$  is recorded at the surface of the explosive;  $\Delta T$  is the temperature difference from centre to edge.

Shot ID	HR	Fill	Response type	$T_{ign}$	$\Delta T$
				°C	°C
1	Fast	88/12	A +burn	230	128
2	Fast	91/9	A +burn	234	132
3	Fast	95/5	A +burn	239	111
4	Fast	96/4	B	229	106
5	Fast	96/4	B	227	112
6	Slow	88/12	B + burn	213	35
7	Slow	91/9	B	214	37
8	Slow	95/5	B	214	30
9	Slow	96/4	C	208	22
10	Slow	96/4	C +burn	216	42

There was no evidence of mass reaction of the filling in any of the experiments. In all cases, it was clear that, immediately after the pressure burst, a considerable portion of unreacted filling was present. In five experiments, this unreacted material was found both inside the test vehicle and scattered around the test chamber; in the other five, the remaining material burned away in a steady fashion following the pressure burst.

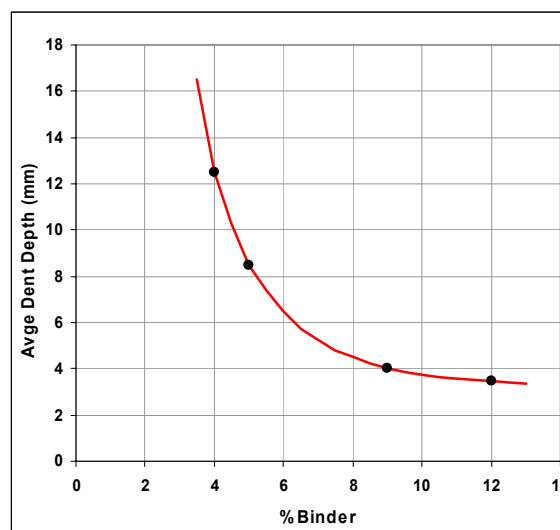


**FIGURE 2.** Plot of average dent of vehicle base-plate versus percentage binder.

## DISCUSSION

Although none of the events observed in these tests were particularly violent there is a clear trend of increasing violence with increase in HMX loading. Mass reaction could not however be ruled out under higher confinement than that afforded by the SSGWCO test vehicle. The simple criterion illustrated in Fig. 2 would suggest that there is a significant increase in reaction violence when the binder content is reduced from 8% to 6%. This may indicate the binder concentration limit beyond which non-violent cook-off responses cannot be guaranteed.

The behaviour at ignition is interesting. It is clear that, at the point of ignition, only a small proportion of the filling undergoes reaction. The remainder is ejected from the failed vehicle, or burns away in a steady fashion over a relatively long period. Previous experiments with RDX/TNT resulted in a similar ejection of unreacted material after the pressure burst [1], although in these cases post-event burning was not observed. Examination of the recovered PBX shows that no more than approximately 15g of PBX was consumed by the initial ignition.

The low filling density of all the compositions (~ 95% TMD) indicates that these compositions contained a number of small voids. It is well known that these should increase the sensitivity of the composition to initiation by mechanical means [4]. However, it is possible that by the time the ignition occurs any voids will have been closed either by simple thermal expansion or as a result of the  $\beta$ - $\delta$  phase transformation in HMX. Indeed, our results show no obvious sensitisation to the initial thermal explosion as we recovered damaged but unreacted pieces of PBX.

## CONCLUSIONS

The experiments reported here clearly show a general trend of increasing event violence with increasing HMX proportion. Although we have not been able to demonstrate a transition to violent mass reaction our results suggest that a binder concentration of 6-8% may be required to ensure benign cook-off responses.

We can interpret our results on the basis of the hypothesis that there are generally two possible stages in the cook-off reaction process. The first stage consists of the ignition of a small volume of the filling, driven purely by the external thermal stimulus. The size of this volume depends upon the temperature profile across the filling, and is therefore largely governed by the heating rate. At slower heating rates a greater volume of material ignites, and a more violent response is therefore generally observed.

Under certain conditions the initial ignition can give rise to propagation of reaction throughout the bulk material. The existence, or otherwise, of this second stage will depend on the mechanical-thermal stimuli produced by the ignition, and the sensitivity of the remaining bulk material. It appears that in our experiments the system does not undergo this secondary stage, quite possibly as a result of early failure of the confinement.

## REFERENCES

1. Stennett, C., Cook, M. D., Briggs, R. I., Haskins, P. J., Fellows, J., "Direct Observation of Cook-off Events Using a Novel Glass-Windowed Vehicle and Pipe Bombs", in *12th International Detonation Symposium*, San Diego, CA, 2002.
2. Cheese, P., Briggs, R. I., Fellows, J., Haskins, P. J., Cook, M. D., "Cook-off Tests on Secondary Explosives", in *10th International Detonation Symposium*, ONR 33300-5, 1998, pp 272-278.
3. Menikoff, R., Sewell, T. D., *Combust. Theory Modelling* **6**, 103-125 (2002).
4. Bowden, F. P., Yoffe, Y. D., *Initiation and Growth of Explosion in Liquids and Solids*, Cambridge University Press, 1952.





#### A.4      **Developments in a Small-Scale Test...**

---

Authors:	Sorber S; Stennett C; Goldsmith M		
Title:	Developments in a Small-Scale Test of Violence		
Publication Type:	International Conference	Venue:	Shock Compression of Condensed Matter
Ref:	AIP Conf Proc. <b>1426</b> , 563-566 (2012); <a href="http://doi.org/10.1063/1.3686341">http://doi.org/10.1063/1.3686341</a>		

---

# DEVELOPMENTS IN A SMALL SCALE TEST OF VIOLENCE

S. Sorber<sup>1</sup>, C Stennet<sup>2</sup>, M Goldsmith<sup>2</sup>

<sup>1</sup>*AWE Plc, Aldermaston, Reading, Berkshire, RG7 4PR, UK*

<sup>2</sup>*University of Cranfield, Shrivenham, Swindon, SN6 8LA*

**Abstract.** Utilising recent advances in diagnostic technologies, a test is under development to obtain a numerical value for the violence of response to thermal stimuli on a small explosive sample. The assembly is designed to accept pressed explosive pellets which enables the test to be conducted at the small-scale development stage and thus is anticipated to be of use in the screening of new materials.

Building on previously published work describing the test development, twenty-three new cook-off experiments have been conducted. Eleven explosive compositions were subjected to the same slow heat input profile. As a sample rapidly decomposed, part of the steel confinement was designed to rupture, producing a pellet whose velocity was measured using a Heterodyne Velocimeter (Het-V). Temperatures of the confinement unit were also recorded.

A development aim is to interpret this data to provide useful information on the violence of decomposition. This is discussed in the paper and leads to the data from these experiments being presented in order of increasing violence of response.

**Keywords:** Explosive, Thermal, Small-Scale, Violence

**PACS:** 47.40.Rs, 67.70 pj.

## INTRODUCTION

When formulating new explosives in today's regulatory and economical climate, an important goal is to characterise the formulation's scale of response to thermal insults as early as possible. Therefore, data such as the response to thermal insults, in the early stages of development supports a cost-effective and safe development.

Established tests provide qualitative indications of violence of response from thermal stimuli through dent/fragment analysis of heater anvils and visual observations. However, this paper presents data gathered using a small-scale test in development, whose aim is to quantitatively differentiate between explosive materials based on thermal explosiveness and sensitiveness using the same thermal input profile on a large number of compositions.

Previous work on this experimental geometry has shown that the test configuration is successful and the data captured can be used to obtain a measurement termed a 'violence metric' [1].

## EXPERIMENTAL GEOMETRY

Figure 1 shows the Small-Scale Velocity Test (SSVT) experimental geometry. It consists of two main components; a copper heater block and a steel confinement unit in which the sample explosives are housed. The steel confinement accommodates four 10 mm long by 10 mm diameter right cylindrical pellets.

The heater block (heated via two 150 W cartridge heaters) is screwed into one end of the steel confinement unit until it is in contact with the explosive, thereby sealing in the explosives. The

heater block thermal input profile was regulated by a Watlow Heater Controller which required two input temperatures for an accurate thermal profile; the heater block and confinement-unit temperatures. Also the temperature of the confinement unit at the time of decomposition needed to be recorded. K-type thermocouples were used for all these measurements.

At the right-hand end of the steel confinement unit in Figure 1, was a machined circular groove. When heated, the explosive samples started to decompose and generate gases, thus increasing the pressure in the cavity. When the cavity pressure was sufficient to overcome the manufactured thinner confinement at this grooved circle, a moving small steel pellet was formed. The velocity of the front face of this moving pellet was tracked for 30 mm via a 1550 nm Heterodyne Velocimeter [2, 3]. This was the main diagnostic for measuring the ‘violence’ of decomposition.

Copper was used where possible for consistency with previous work. [1], however in two experiments, the thread on the copper heater-block failed. The repeated experiment used either brass

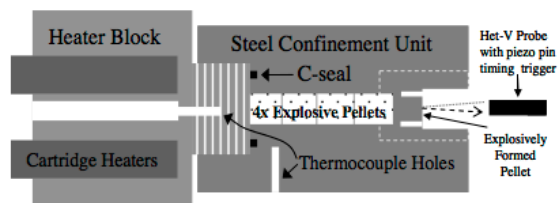


**Figure 1.** Schematic of the SSVT experimental assembly for Het-V measurements.

or steel for strength at higher temperatures.

Table 1 details the eleven explosive formulations tested. The explosives are arranged in (predicted) decreasing order of explosive thermal sensitivity from HMX through to TATB. The input profile selected was designed to instigate a reasonably violent response for the predicted more thermally sensitive explosives. The final thermal input profile chosen was as follows:

1. Soak, 20 mins, 30 °C
2. Ramp, 5 °C/min to 170 °C, soak 80 mins
3. Ramp to failure (RTF), 2 °C/min

## RESULTS AND ANALYSIS

One of the thermocouples used recorded the temperature of the confinement unit at the time of rupture. The data from these thermocouples show that temperatures between two experiments of the same compositions are generally repeatable.

Figures 2 to 4 show example Het-V results from three explosives chosen to highlight the key features observed across all eleven explosives tested. Each figure plots the data from two experiments on the same explosive. The velocity at 3 mm displacement pellet front face is taken as the furthest point at which the pellet can travel and still maintain full confinement of the product gases [1].

For every explosive, it was seen that the pellet velocity profile up to 3 mm displacement had two distinct parts. The first part, the ‘initial movement’

**TABLE 1.** Explosive formulations tested. \*Using binder density from pycnometry measurement.

Formulation	TMD (g/cc)	Composition (by weight)	
A	1.897	85 / 15	HMX type B /fluoropolymer
B	1.806	95 / 5	HMX type B/HTPB-IPDI
C	1.754	92 / 8	HMX type B /HTPB-IPDI
D	1.735*	92 / 4.8 / 3.2	HMX type B / HTPB-IPDI 1:1.1/ IDP
E	1.788	92 / 5.6 / 2.4	HMX type B /Hytemp 4454/DIDP
F	1.788	92 / 8	HMX type B / silastic 9050-50P
G	1.919	35 / 60 / 5	HMX type B/TATB type B /fluoropolymer
H	1.889	35 / 60 / 5	RDX / TATB /fluoropolymer
I	1.913	59 / 34.5 / 6.5	TATB type B /FOX-7 NSF 110 /fluoropolymer
J	1.883	95 / 5	FOX-7 NSF 110 /fluoropolymer
K	1.937	100	TATB type C

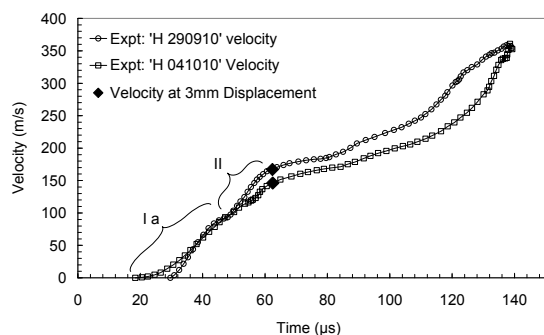


**Figure 2.** Formulation ‘H’ Het-V results for pellet motion. This is an example of a sharp acceleration in pellet velocity for the initial movement.

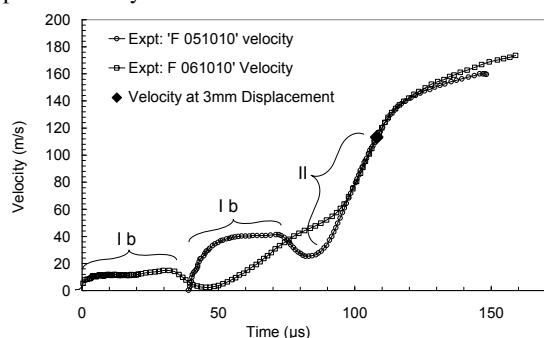


**Figure 3.** Formulation ‘F’ Het-V results for pellet motion. This is an example of a sharp acceleration with a pull-back in velocity for the initial movement.

is denoted as ‘I’. Each explosive formed a pellet whose velocity exhibited one of three different shapes in this ‘initial movement’. These three shapes are denoted ‘Ia’, ‘Ib’ and ‘Ic’ to represent sharp acceleration, sharp acceleration with pull-back and quiescent acceleration respectively.

The second part of the velocity profile is called the ‘late movement’, and denoted ‘II’ in Figures 2 to 4. The late movement part of the pellets’ velocity profile is a steady period of acceleration up to 3 mm displacement starting from a change in gradient following the initial movement. The late movement is observed to be similar for all the explosives.

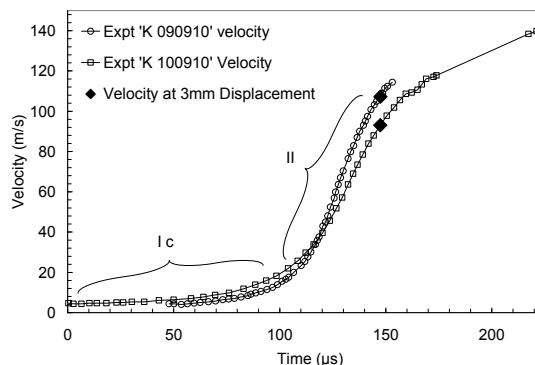


**Figure 4.** Formulation ‘K’ Het-V results for pellet motion. This is an example of a constant or quiescent acceleration in the initial movement.

**TABLE 2.** Gradients of velocity-time pellet motion near 3 mm displacement, termed the “violence”. The test samples are arranged according to their composition, starting with HMX and ending with TATB.

Expt ID (formulation & date)	Measurement of “Violence” (mm/μs <sup>2</sup> )	Standard Dev (mm/μs <sup>2</sup> )	Expt ID (formulation & date)	Measurement of “Violence” (mm/μs <sup>2</sup> )	Standard Dev (mm/μs <sup>2</sup> )
A 13&140910	2.67	0.05	G 170910	3.94	0.17
A 140910	3.66	0.22	G 220910	3.85	0.20
B 070910	3.13	0.15	H 290910	4.74	0.38
B 080910	3.31	0.13	H 041010	3.60	0.07
C 160910 a	3.65	0.14	I 240910 a	1.77	0.02
C 160910 b	3.41	0.21	I 240910 b	1.83	0.10
D 041010	6.44	1.04	J 230910 a	5.52	0.75
D 051010	3.22	0.16	J 230910 b	4.93	0.35
E 150910 a	2.71	0.13	K 080910 b	Thread Failure	
E 150910 b	Thread Failure		K 090910	2.35	0.05
F 051010	4.39	0.02	K 100910	2.00	0.09
F 061010	4.21	0.14			

## MEASUREMENT OF 'VIOLENCE'

In previous work [1], Bauer proposes a method to obtain a value for the violence of reaction from the pellet velocity histories. Namely, that "the gradient of the velocity profile prior to free flight of the projectile" is measured as this "is a function of the extent and rate of reaction of the explosive and the work done on the confinement vehicle to generate the projectile."

In order to maintain consistency, the same approach has been employed for the data in this paper in an effort to determine a measure of "violence". The results are presented in Table 2.

An average of three measurements were taken of the gradient just prior to the 3 mm displacement point. The standard deviation is also given as an indication of the error in this average and is larger for some experiments due to a larger scatter in the data points.

When assessing the data in Table 2, it should be borne in mind that, in this test geometry, the properties of the steel and the explosive are likely to contribute across *all* features of the Het-V data. Currently, the geometry and post-analysis method can not extract the contribution from only the explosives.

## CONCLUSIONS

Twenty-three experiments were conducted on eleven materials to record and assess the response of a range of explosive materials when subjected to a pre-defined thermal input profile.

Velocity data were captured for a dynamically formed pellet. In addition, the temperature of the confinement vehicle at the time of the event was also recorded. The analysis method chosen for the velocity data was in line with previous work [1].

After analysing the data, three different categories of response were observed in the velocity-time profiles of the explosively formed pellets. The potential mechanisms that contribute to the shape of the pellet velocity profile are assumed to originate from both the explosive and the steel properties. As yet, it is not clear which material (explosive or steel) dominates in the initial and late portions of the velocity profile and further exploratory work is required. For this reason, and

until further work can be done, the data presented in Table 2 are to be considered more as a broad grading of response rather than absolute measurements of "violence".

For example, out of the eleven compositions that were tested and ranked in order of violence, formulation J demonstrated more 'violence' than formulation I or K (see Table 2).

Not all the data collected has been presented here due to space constraints. Therefore, for the full data set, please contact the first author.

## FUTURE WORK

More experiments are planned on a twelfth composition which will enable more comparisons to be made between the materials already tested.

This is work in progress, and further effort is required to isolate the explosive contribution to the velocity records in this test geometry. In addition, tests exploring the spectroscopy of the decomposition products, a review of the geometry, and tests to match the pressure to the pellet velocities already recorded would be beneficial.

## ACKNOWLEDGEMENTS

The author would like to thank the staff of the Explosive Science Group at Shrivenham, Cranfield University for carrying out the experiments and the Formulations Team at AWE for providing the samples and funding.

## REFERENCES

1. Bauer, C. L., Rae, P. J., Stennett, C., Flower, H. M., "Small Scale Thermal Violence Experiments for Combined Insensitive High Explosive and Booster Materials", 14<sup>th</sup> International Detonation Symposium, Idaho, USA, p.974, 2010.
2. Strand, Oliver T., et al., "Velocimetry using heterodyne techniques," 26th Int. Conf. on High-speed Photography and Photonics, Alexandria, VA September 19-24, 2004, Proc. of SPIE 5580 (2005) 593.
3. Strand, O. T., et al., "Compact system for high-speed Velocimetry using heterodyne techniques," Rev. Sci. Instr. 77 (2006) 083108.



## A.5 Hazard Characterization of Fox-7...

---

Authors:	Flower, H., Stennett, C., Wortley, S.		
Title:	Hazard Characterization of Fox-7 Compositions with Varying Particle Size		
Publication Type:	Conference Paper	Venue:	14 <sup>th</sup> International Detonation Symposium
Date:	2010		

---



## Hazard Characterization of Fox-7 Compositions with Varying Particle Sizes

Helen Flower\*, Chris Stennett<sup>f</sup>, and Steve Wortley\*

\*AWE

Aldermaston, Reading, Berkshire, UK

<sup>f</sup>Cranfield University

Shrivenham, Swindon, UK

**Abstract.** Fox7 (1,1-diamino – 2,2 dinitroethene) remains a reduced sensitivity high explosive of great interest. Its relative stability to shock and thermal stimuli make it attractive to the explosives safety community whilst its detonation velocity and pressure make it a potentially viable prospect for those interested in performance. Fox7 with a range of particle sizes has been mixed with Viton and pressed into pellets for use in the UK one-dimensional time to explosion (ODTX) test. The data from these tests has been used to generate parameters for single-step decomposition kinetics. In addition, these experiments provide important data for the understanding of compositions' response to thermal environments.

There is little evidence of a trend in explosion time with initial Fox7 particle size; this is probably due to the mixing and pressing process.

---

### Introduction

Fox7 (1,1diamino – 2,2 dinitroethene) remains a reduced sensitivity high explosive of great interest. Its relative stability to shock and thermal stimuli make it attractive to the explosives safety community whilst its detonation velocity and pressure make it a potentially viable prospect for those interested in performance.

The thermal properties of Fox7 have been extensively studied using powder methods such as DSC<sup>1,2</sup>. This has helped to identify phase changes within the material but tells little about the kinetics at work during reaction.

It is well known that the hazard properties of different explosive compositions can be dramatically different, for apparently minor

changes in the formulation.

Fox7 with a range of particle sizes has been used in a selection of secondary explosive compositions, using Viton as the binder. The moulding powders have been pressed into hemispherical samples for use in the UK one dimensional time to explosion (ODTX) test.

The data from these tests can be used directly to generate parameters for single-step decomposition kinetics. In addition, these experiments provide important data for the understanding of compositions' response to thermal environments. Variation in particle size is well known to affect the DDT properties of explosive compositions and has also given measurable differences when tested using ODTX.

**Fox-7 characterisation**

The as-received Fox-7 powders were analysed using laser diffraction methods on a Malvern Instruments Mastersizer S. The relative distributions of the particles calculated using this method are shown in Table 1 and Figure 1.

**Table 1:** Particle size distributions of the Fox-7

<b>Fox-7 grade</b>	<b>D10</b>	<b>D50</b>	<b>D90</b>	<b>D4,3</b>
NSF 110	19.7	42.1	46.1	45.2
NSF 120	67.7	108.3	161.08	111.21
NSF 130	100	165.5	246.8	169.6

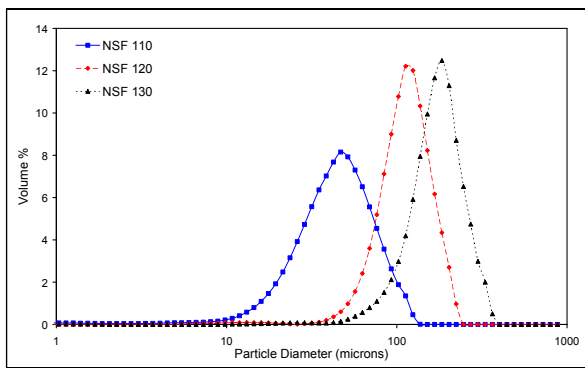


**Figure 1:** Particle size distributions of the Fox-7 powders

These distributions were deemed to be suitably distinct so that differences in the resulting formulations could be significant.

The results of the Malvern analysis were confirmed using optical and scanning electron microscopy. The SEM images from these analyses are shown in Figure 2- Figure 4.

Following analysis of the as-received powders they were then formulated into compositions for testing in the ODTX test.

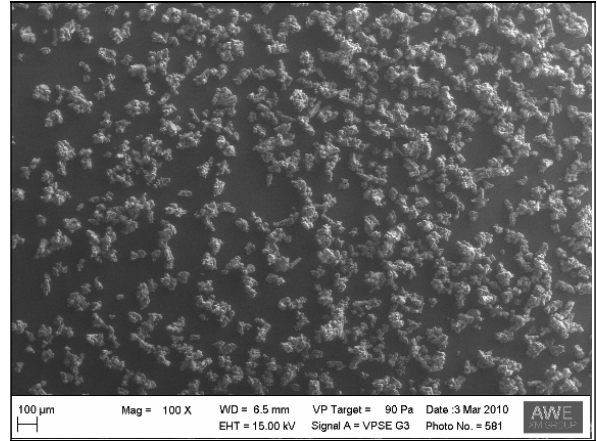


**Figure 2:** SEM image of NSF 110 (100X magnification, scale bar 100µm)

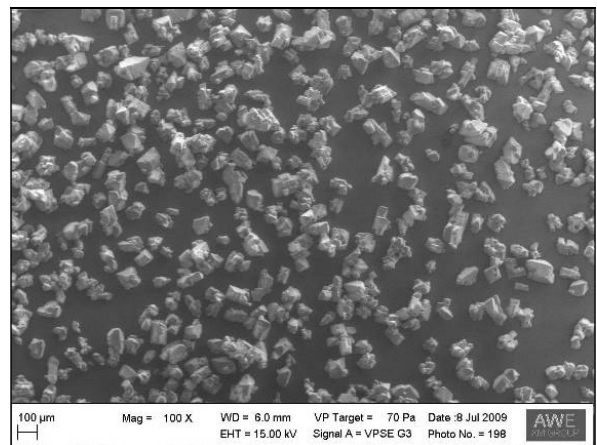


**Figure 3:** SEM image of NSF 120 (100X magnification, scale bar 100µm)

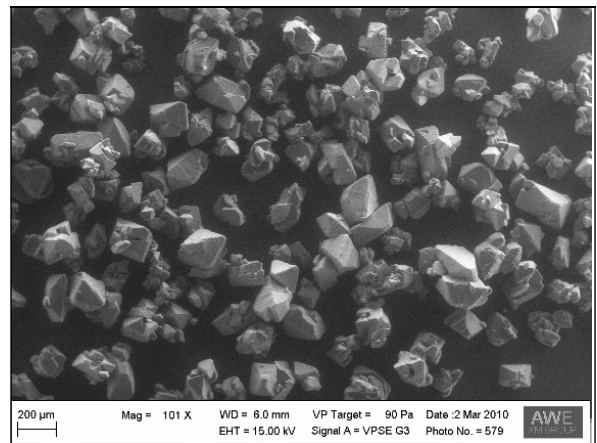


**Figure 4:** SEM image of NSF 130 (101X magnification, scale bar 200µm)

**Formulation of the Fox-7**

The Fox-7 was formulated with a binder to better simulate potential applications for the explosive. This also improved the pressing characteristics.

Viton, a fluoro-elastomer, was chosen as the binder because of its low volatility. The formulations were all made as 95:5 mixes of the relevant Fox-7 grade with Viton. The compositions produced are shown in Table 2.

**Table 2:** Compositions produced

Eurenco Fox-7 grade	Composition designation
NSF 110	FV/1
NSF 120	FV/2
NSF 130	FV/3

After formulation the resulting powders were subjected to the standard suite of UK small-scale powder hazard tests. These tests are specified by the Energetic Material Test and Assessment Policy committee (EMTAP)<sup>3</sup>.

The tests are designed to cover all the credible ignition stimuli resulting in accident scenarios.

They are used at an early stage in formulation to ensure suitability for scale-up.

The results of the tests are shown in Table 3. Of particular interest in this work is the temperature of ignition test results. This exposes 200mg samples of the explosives to an indirect heating rate of 5°C per minute.

The simplistic and very small scale thermal test used at this stage of formulation is unable to discern any significant variation in the temperature of ignition of the formulations.

Following the acceptable results achieved in these small-scale hazard tests the compositions could be pressed into suitable pellets for analysis. Pellets for the ODTX test and discs suitable for thermal conductivity measurements were pressed.

It is accepted that the particle size distribution after pressing will not be the same as that measured on the as-received Fox-7 powders. An optical examination of the surface of the thermal conductivity pellets was made to assess the variation in particle size after pressing.

Images from these optical assessments are shown in Figure 5 - Figure 7. It can be seen that the relative particle sizes of FV/1 and the other two compositions is distinctly different.

**Table 3:** Small-scale hazard data for the Fox-7 compositions

	FV/1	FV/2	FV/3
F of I	101	90	91
Electric spark	Ignitions at 4.5J not at 0.45J	Ignitions at 4.5J not at 0.45J	Ignitions at 4.5J not at 0.45J
Temperature of ignition /°C	226.5	226.1	225
Train	Ignites and supports train steadily throughout	Ignites and supports train steadily throughout	Ignites and supports train steadily throughout
Mallet friction	No reaction on any combination	No reaction on any combination	No reaction on any combination

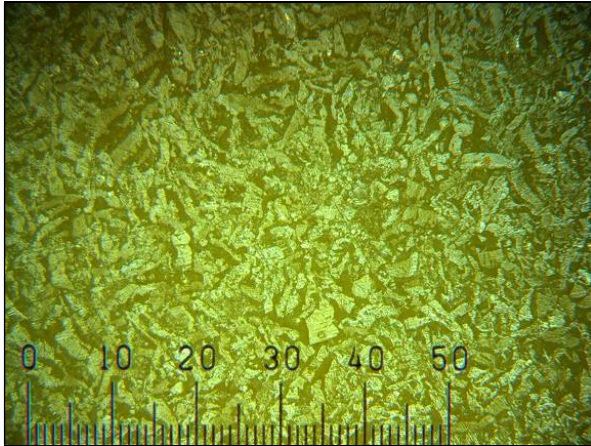


**Figure 5:** 20x optical micrograph of composition FV/1 pellet surface, scale in 10 x microns

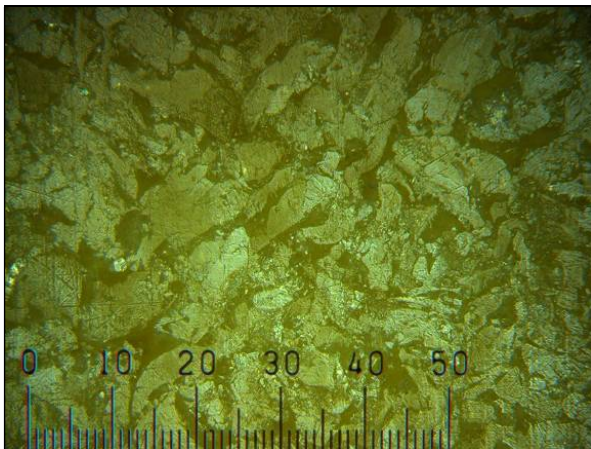


**Figure 6:** 20x optical micrograph of composition FV/2 pellet surface, scale in 10 x microns

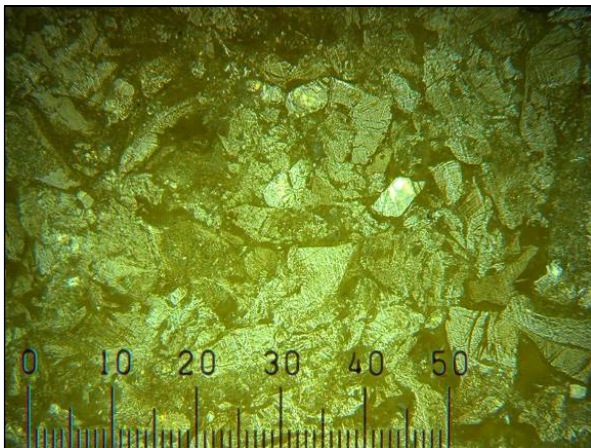


**Figure 7:** 20x optical micrograph of composition FV/3 pellet surface, scale in 10 x microns

## ODTX evaluation of formulations

The one dimensional time to explosion test was first developed at Lawrence Livermore National Laboratory and reported by Catalano et al.<sup>4</sup>.

The test is performed using an automated apparatus, shown in Figure 8.

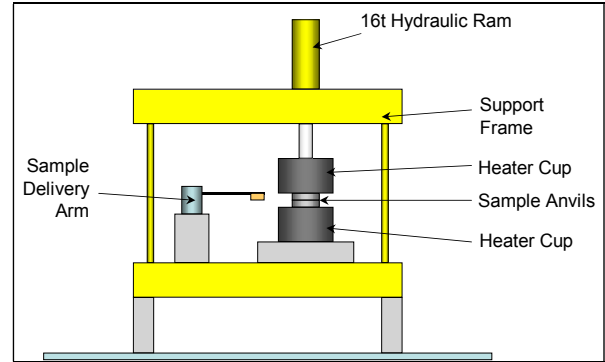


**Figure 8:** Schematic of the ODTX apparatus

During the test the sample is located between two aluminium anvils, each containing a hemispherical cavity. A sealing ring made from soft copper fits into a special groove in the mating face of each anvil to ensure that the cavity is completely sealed. A thermocouple is placed inside the lower anvil to accurately record the temperature at a point just below the sample cavity.

The two anvils are located within two heater cups made from steel, 100mm in external diameter and 75mm deep. The external cylindrical surface of each heater cup is covered with an electrical heating element, so that the cup, along with the anvil it contains, may be heated. A control thermocouple is attached to each heater cup, and is connected to a closed-loop temperature controller on the control panel. Sufficient time must be allowed for the anvils to equilibrate to the desired test temperature before the sample is inserted.

The upper heater cup is attached to the piston of a hydraulic ram so that the two heater cups can be compressed together with considerable force. The size of the anvils is such that a clamping pressure of 3000 psi is achievable. When the hydraulic ram is retracted, the two aluminium anvils are separated by a

space of approximately 40mm. This allows the sample to be inserted.

The sample delivery mechanism consists of an arm attached to an actuator driven by compressed air. The delivery arm is hollow and terminates in the sample cup; a vacuum pump is connected to the arm. When the vacuum pump is turned on, the spherical sample of the material under test can be attached to the arm; turning off the pump releases the sample. When the experiment is started, the delivery arm swings into the space between the anvils, and releases the vacuum holding the test sample to the vacuum cup. The test sample drops into the cavity in the lower anvil, and the sample delivery arm retracts. The hydraulic ram then clamps the upper aluminium anvil onto the lower anvil, and an automatic timer is started.

After a period of time (characteristic of the test sample and the initial temperature of the anvils) the test sample explodes; a microphone detects the explosion and stops the timer.

The spherical cavity in each anvil was measured by liquid displacement before and after testing, to assess the extent of plastic deformation in the anvil as a result of the reaction of the specimen. The post-reaction cavities were measured by taking the difference in weight in a water-filled burette before and

after filling both halves of the damaged anvils. Weighing was carried out using a two-figure balance, and the density of water was taken to be 1.0g/cc. A small quantity (<1%) surfactant was added to the water to reduce its surface tension and minimize the effect of the meniscus.

## Results

All of the formulations were tested in the ODTX at a range of temperatures from 200 to 260°C.

The results are plotted as a graph of the time to explosion versus the temperature for all the compositions, Figure 9.

Single step Arrhenius kinetics can be approximated for these compositions by use of the equation below:

$$\ln(t) = \left( \frac{E_a}{R} \right) \left( \frac{1}{T} \right) + \ln(A) \quad [1]$$

Where  $t$  is time,  $T$  temperature,  $R$  the molar gas constant,  $E_a$  the activation energy of the reaction and  $A$  the pre-exponential factor.

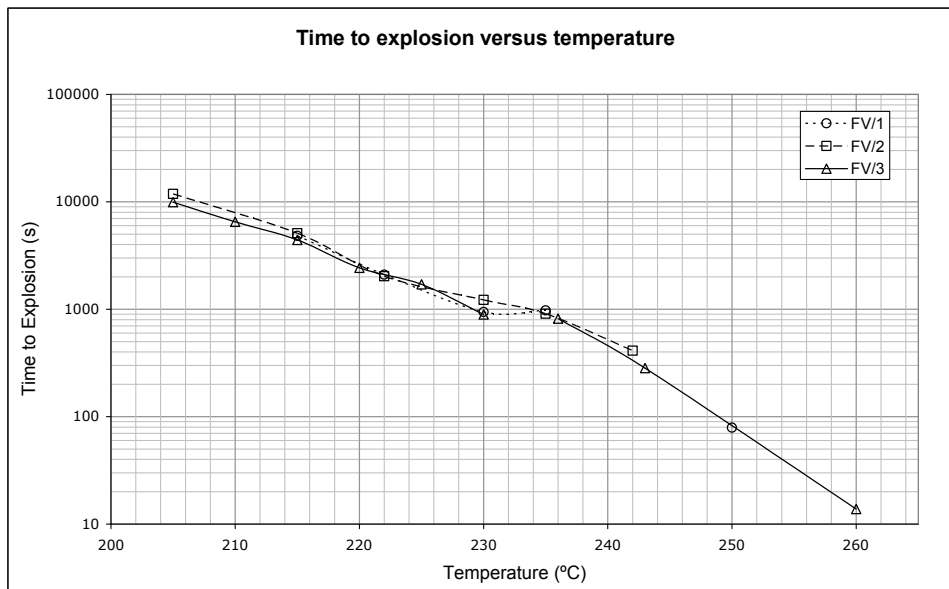
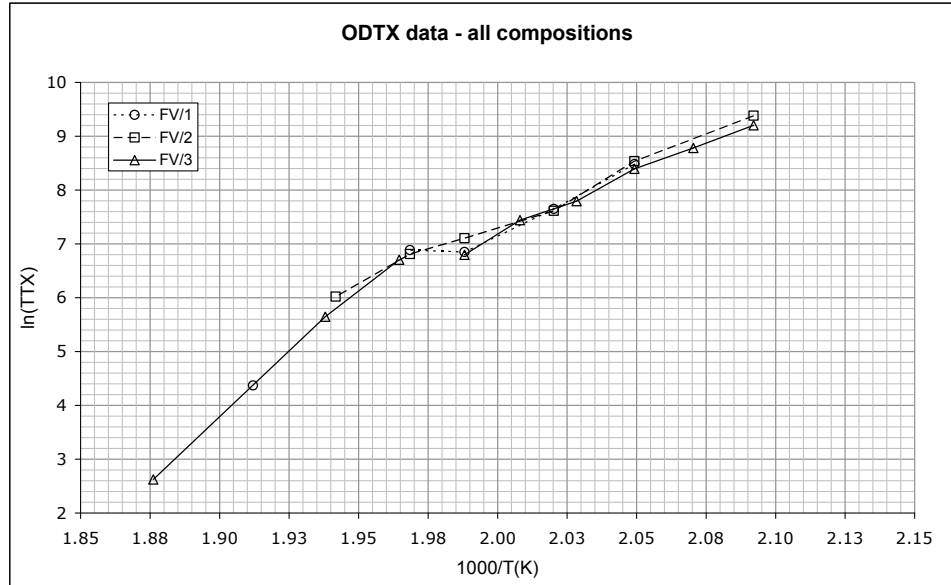


Figure 9: Time to explosion versus temperature for the compositions



**Figure 10:** Arrhenius-like plot of the ODTX data for all compositions

Plots of this form have been generated for each of the compositions and are shown in Figure 10. It is clear that the dependence of time to explosion on temperature is not linear when plotted in this manner. This suggests that the decomposition kinetics will not be properly described by a simple single-step scheme, as has been done for other compositions. However, linear fits have been made that indicate an approximate single-step kinetics scheme<sup>5</sup>.

This leads to the single-step kinetics parameters given in Table 4. All three compositions show similar kinetics schemes. In impact response it is generally considered that the larger particles will dominate the ignition and the smaller particles the growth of reaction. In other words the larger particles have the greatest affect on sensitiveness whilst the smaller particles dictate the explosiveness. This does not appear to be the case in this instance.

**Table 4:** Kinetics parameters for the compositions

Composition	Activation Energy /kJ mol <sup>-1</sup>	Pre-exponential factor
FV/1	87.5	34.5
FV/2	93.6	36.5
FV/3	91.9	37.5

In all firings it was noted that some plastic deformation of the aluminium anvils occurred. The mean relative expansions are given in Table 5.

**Table 5:** Assessment of reaction violence by measurement of relative expansion of spherical cavity

Composition	Mean Cavity Expansion (%)	$\sigma$ (%)
FV/1	8	5
FV/2	12	4
FV/3	36	21

It can be seen that, on average, the greatest expansion occurs with the composition having the largest nominal particle size. However, it should be noted that the standard deviation over all the firings is large, and this indicates that there is considerable variation in the extent of reaction from shot to shot. Given that the ODTX apparatus offers a reproducible thermal boundary and confinement, it would appear that specimen-to-specimen differences in composition are responsible for the variation in extent of reaction. Given further that all the specimens were produced from the same batch of FOX-7, and from the same mixed batch of final composition, it would appear that microstructural variations are responsible for reaction extent variability.

## Conclusions

Three grades of commercially available Fox-7 have been analysed using laser diffraction, SEM and optical microscopy.

These have been formulated with Viton and tested using the standard suite of UK small-scale hazard tests.

Pellets have been pressed and the impact of the mixing and pressing process on the particle size distributions assessed.

The formulations have been subjected to the UK ODTX test over a range of temperatures and single-step Arrhenius parameters have been obtained.

It would appear that there is little difference, at least from the point of view of ODTX, between the three compositions. This is perhaps unsurprising given that they were designed to be identical with the exception of the particle size of the energetic filler. If, as this work suggests, the particle size has little impact on cook-off response, then this would be of considerable benefit to formulators, because it would not be necessary to make sacrifices in processability to achieve the best hazard response.

The results indicate that these Fox-7 compositions have lower activation energies for thermal ignition than some RDX compositions and a similar thermal response to LX-04, an HMX:Viton composition<sup>6</sup>.

## Future Work

The kinetics developed here will be used in modeling of other experiments<sup>7</sup> to target the regimes of interest.

Techniques are under development to dissolve out the binder in compositions and accurately measure the precise particle size distribution after mixing and pressing. This will allow the results to be re-evaluated. This technique will be used in conjunction with narrower and bi-modal particle distributions to further investigate formulation variables.

This work will be extended to use Heterodyne Velocimetry as a means of measuring the violence of the reaction. This form of laser interferometry can be used to measure the speed with which the anvils come apart

## Acknowledgements

The authors would like to acknowledge the assistance of Adam Hazelwood on particle characterization and of Sally Gaulter and Mike Willcox on formulation development.

## References

- <sup>1</sup> Garmasheva NV et al., *Research of thermal decomposition of diaminodinitroethylene*, Proceedings of the 36th International Conference of ICT, 87-94, 2005
- <sup>2</sup> Östmark H et al., *Fox-7 – A new explosive with low sensitivity and high performance*, Proceedings of the 11th international Detonation Symposium, 807 – 812, 1998
- <sup>3</sup> Defence Ordnance Safety Group, *Energetic Materials Testing and Assessment Policy Committee manual of tests*, Volume 1(4), 2007
- <sup>4</sup> Catalano E et al., *The thermal decomposition and reaction of confined explosives*, Proceedings of the 6th international Detonation Symposium, 214 – 222, 1976
- <sup>5</sup> Merzhanov AG & Averson AE, *The present state of the thermal ignition theory: an invited review*, Combustion and Flame, **16**, 89-124, 1971
- <sup>6</sup> Dobratz BM & Crawford PC, *LLNL Explosives Handbook*, 6-84, 1985
- <sup>7</sup> Bauer C et al., *Small Scale Thermal Violence experiments for combined Insensitive High Explosive and Booster Materials*, Paper in these proceedings

© British Crown Owned Copyright 2010.MoD

## **A.6      Development and Implementation of an Ignition ...**

---

Authors:	Cook, M D; Haskins, P J; Stennett, C		
Title:	Development and Implementation of an Ignition and Growth Model for Homogeneous and Heterogeneous Explosives		
Publication Type:	International Conference	Venue:	11 <sup>th</sup> International Detonation Symposium
Date:	1998		

---



# DEVELOPMENT AND IMPLEMENTATION OF AN IGNITION AND GROWTH MODEL FOR HOMOGENEOUS AND HETEROGENEOUS EXPLOSIVES

M. D. Cook, P. J. Haskins and C. Stennett  
Defence Evaluation and Research Agency, Fort Halstead,  
Sevenoaks, Kent TN14 7BP, England

This paper describes the development and implementation of a new ignition and growth model for shock initiation of explosives in the DYNA2D hydrocode. The basic homogeneous model uses equations of state for both the reactants and product gases, along with temperature dependent Arrhenius chemical kinetics, to describe the bulk heating and subsequent reaction of the explosive when shocked. Heterogeneous effects are modelled using a hot spot model based on the notion of gas-filled pore collapse. As these gas-filled pores collapse their temperature rises rapidly. Explicit heat transfer calculations allow the energy stored in these pores to be transferred to a thin shell of surrounding explosive which can subsequently burn out into the bulk explosive. The necessary heat and mass transfer are all carried out by the burn routine. Using this model it has been possible to match experimentally derived fragment impact data. The use of the burn routine to model shock desensitisation is also described.

## INTRODUCTION

Over the years there have been a number of incidences where accidental initiation of weapons has led to a catastrophic outcome with resulting loss of life and equipment. In order to assess the safety of energetic materials when subjected to various accidental stimuli, a variety of tests are routinely conducted. These tests cover both powdered material and charge-scale experiments. By this means, a relative ranking of compositions to various stimuli can be obtained.

In recent years, the high cost of accidents and of all-up weapon testing has inspired a new thrust towards high performance insensitive munitions. As part of this drive there has been a significant quantity of research aimed at understanding the mechanisms of initiation and growth of reaction in energetic materials subjected to a variety of stimuli such as heat, mechanical deformation and electrical spark discharge. More recently, there has been the recognition that all-up weapons test are becoming

prohibitively expensive and a more focused testing programme is required. This has led to a greater interest in developing models to provide both an understanding and predictive capability.

Developing realistic models to describe the complex behaviour of energetic materials is a large undertaking. In the past, models attempting to describe the initiation, growth of reaction and detonation processes in explosives have been based on simple engineering fits. Whilst these approaches have undoubtedly had success, they are very limited in their real usefulness. In order to build a more realistic predictive capability it is apparent that a model based on fundamental principles of physics and chemistry provides the only real way forward. Such a model should be based on the important physical and chemical processes that control the initiation and propagation reactions in energetic materials. An advantage of developing such fundamentally based models is that a deeper insight into understanding the important physical and chemical processes controlling energetic material

behaviour can be obtained. This information can then be used to develop the next generation of energetic materials.

It is widely recognised that there are two types of explosive: homogeneous materials and heterogeneous materials. These two types of material are generally treated separately since they exhibit different initiation and growth of reaction properties. However, it is quite clear that homogenous and heterogeneous behaviour merely represent the two ends of a continuous spectrum. Homogeneous characteristics exist in all materials, but in heterogeneous materials it is possible for the effects of the heterogeneities to dominate under certain circumstances. Any model should therefore be constructed in such a way as to address the basic homogeneous nature first. It should be noted that it is widely recognised that heterogeneous explosives differ from their homogeneous counterparts by the fact that under certain conditions, such as when subject to a shock, they can concentrate energy into hot regions or ‘hotspots’<sup>1-8</sup>. If sufficient energy is produced in these ‘hotspots’ then they can burn outwards into the surrounding material leading to a possible growth of reaction and even detonation.

In this paper we give details of a new ignition and growth model for shock initiation of explosives which has been implemented in the DYNA2D hydrocode<sup>9</sup>. The model is based on temperature dependent Arrhenius chemical kinetics. This allows homogeneous explosives to be modelled through a bulk heating process. In addition, a pore collapse model has been developed to provide additional localised heating.

## GENERAL DESCRIPTION

An outline description of the model has been given elsewhere<sup>10,11</sup>. The burn model considers the growth of an explosive burn as a series of coupled Arrhenius chemical kinetic steps. The rate of reaction is a function of the constituents, the temperature and the pressure. If sufficient energy is released then the explosive may burn to detonation. Alternatively, if the energy losses outweigh the energy released, the reactions may die out. Important features of the model are that it is temperature driven and that the chemistry is active throughout a simulation. That is, there are no arbitrary switches to control when the material should burn or detonate.

The model can be broadly divided into two separate processes that when working together mimic the behaviour of a heterogeneous explosive subjected to shock initiation. The basic model assumes that the explosive is bulk heated when shocked. This basic model reflects homogeneous behaviour as is observed in liquid explosives such as nitromethane. Heterogeneous effects are

incorporated by a ‘hotspot’ routine based on the notion of adiabatic pore collapse. Whilst it is recognised that this is not the only ‘hotspot’ mechanism there is extensive experimental evidence that it is one of the more important ones<sup>10</sup>. The effect of the pore collapse routine is to provide concentration of energy and subsequently, addition of localised heating to the underlying bulk heating mechanism. The effect is that if heat is released from the pores at the same instance as the bulk heating, an increase in sensitivity is observed. If the two heating processes are out of phase, the pore collapse mechanism has little effect and the underlying bulk heating mechanism controls the response. Both the underlying homogeneous model and the pore collapse routine are described in the following sections.

## MODEL ASSUMPTIONS

Before describing the model in some detail, it is appropriate to describe some of the important assumptions that have been made. Firstly, the model assumes that, for a homogeneous material, shock compression leads to bulk heating. The temperature rise drives up to three consecutive Arrhenius chemistry steps. The temperature is calculated by means of the internal energy through the heat capacity at constant volume, which is assumed to be temperature, but not pressure, dependant. The chemistry is controlled by its own timestep. The initial energetic material is modelled using a Murnaghan equation of state (EOS). Gaseous products are assumed to be produced as a result of the last Arrhenius step, and are described by a JWL EOS. The pressure in an element is found by equalisation between that in the reactants and that in the gaseous products.

The pore collapse model, which can be explicitly activated, assumes spherical pores. These collapse symmetrically in sympathy with the element resulting in an increase in the pore gas pressure and associated rise in temperature. All elements are assumed to be identical at the beginning of a DYNA2D run, and there are no random factors such as a distribution of pore sizes across elements or within an element. It should be noted that the concept of heterogeneity applies at the mesoscale within each element.

Within an element it is assumed that the condensed phase is an ideal viscoplastic material (this is controlled by the material model used). In order to model the effects of heat flow, and subsequent burn out from the pores, the bulk unreacted material is modelled as two regions. These are the bulk material and a thin spherical shell of constant mass surrounding a pore. There is explicit conductive heat flow from the pore gas into the shell, and from the shell into the bulk. A heat flow time step is used to increase the accuracy of the amount of heat transferred.

If reaction occurs in the shell material to produce gaseous products material from the bulk is transferred to the shell to maintain its mass. The product gases are described by the JWL EOS along with those produced as a result of reaction in the bulk. Once pressure equalisation has been calculated across the element, the product gases are transferred to the pores.

The use of the equations of state (EOS) employed in this model assumes that they can adequately describe the behaviour of the various regions over the range of temperatures and pressures experienced. The use of the heat transfer mechanism assumes that the steady state approximation is valid through the use of small timesteps. It should be noted that the notion of the different regions is a pure modelling mechanism which enables the heating of the pore to simulate a non-uniform temperature distribution in the reactive material. The transfer of detonation products to the internal pore regions assumes a complete separation of solid and gaseous parts of the material and instantaneous diffusion of products in the bulk region, through the shell, into the pore. Another assumption is that the internal energy can be weighted by the mass fraction of material. This seems to be quite reasonable.

## MODEL FORMULATION

The burn model has been implemented as a separate equation of state within the DYNA2D hydrocode. At the start of a DYNA2D simulation all the appropriate parameters are read in, stored, and initialised. After performing the initial DYNA functionality, the sound speed of the energetic material is calculated for every element. In general, the square of the sound speed for a material is given by the partial derivative of pressure with respect to density, at constant entropy. In this case, it needs to be determined for a mixture of solid and gas. An expression can be derived for a mixture of solid reactants (pressure determined by Murnaghan equation of state), final detonation products (JWL) and initial pore gas material (Ideal Gas).

$$c^2 = \frac{\left( \frac{\partial P_s}{\partial \rho} \right)_{V_g} \left[ \left( \frac{\partial P_j}{\partial V_g} \right)_E - P_j \left( \frac{\partial P_j}{\partial E} \right)_{V_g} - \frac{P_\phi \gamma}{V_g} \right]}{\left[ \left( \frac{\partial P_j}{\partial V_g} \right)_E - P_j \left( \frac{\partial P_j}{\partial E} \right)_{V_g} - \frac{P_\phi \gamma}{V_g} - \left( \frac{\partial P_s}{\partial V_g} \right)_\rho \right]} \quad (1)$$

Where  $P$  refers to pressure,  $V$  refers to volume,  $E$  is the internal energy,  $\rho$  is the density, and  $\gamma$  the ratio of  $C_p/C_v$ . The subscripts refer to the following:  $s$  is all species in the solid,  $g$  is all species in the gas,  $j$  is the partial component of the gaseous detonation products (JWL), and  $\phi$  is the partial component of the pore gas within an element (Ideal Gas).

If the material is homogeneous the  $P_\phi$  terms are explicitly set to zero. For heterogeneous materials that have yet to begin reacting (ie the mass fraction of final product is less than  $\varepsilon = 10^{-2}$ ) the JWL terms are explicitly set to zero. To avoid problems with singularities at  $V_g$  equal to 0 and  $V$ , a test is carried out to determine whether the mixture can be treated as either approximately 100% solid or 100% gas, using the volume fraction ( $f_{gv}$ ) of the gas:

$$f_{gv} < \varepsilon \Rightarrow 100\% \text{ Solid} \text{ or } f_{gv} > (1 - \varepsilon) \Rightarrow 100\% \text{ Gas}$$

It should be noted that the situation of 100% solid can not exist for a heterogeneous material and that 100% gas is only achieved when all the material has reacted within an element.

Once the sound speed for the element has been calculated the stress tensor is then linearly scaled (by multiplying by the mass fraction) to account for the partial gaseous composition of an element. The stress tensor is also updated at the end of each burn routine cycle in order to update the equilibrium pressure in the main DYNA2D code. Control is then passed to the main burn routine.

Within the main burn routine, all values for variables are initialised at the start of a DYNA2D time-step. The values are then determined for the burn model time-step. Once this has been done, the number of active regions is resolved by considering the material type and composition. In particular, the number of active regions determines where chemical reactions and heat transfer calculations need to be considered. There is always one active region, or bulk material, which becomes inert only after all reactions are complete and 100% products have been produced. For homogeneous explosives there is only one active region whilst for heterogeneous materials there are typically two, the shell and the bulk, where reactions can occur and where heat transfer between them is required. Once reaction is complete, and inert gaseous products remain within in a given element, the whole element is reassigned as the bulk with the shell explicitly set to zero.

To maintain accuracy of the model, and to be able to apply many of the steady-state assumptions, such as the pore collapse and heat flow, these processes must be strictly time controlled. Control of the burn model is therefore determined as a function of the DYNA2D timestep. Each DYNA2D timestep is resolved into several smaller burn model timesteps such that the total number of internal burn model loops matches the DYNA2D timestep. The aim is to use as large a timestep as possible, and only reduce it if either the heat transfer rate or the chemical reaction rates are high. If the energetic

material is heterogeneous, and therefore contains pores, the rates of heat transfer need to be calculated. Heat transfer between the regions of the pore collapse model is determined as a function of the temperature in the regions and the pore geometry, assuming steady-state simplifications. In the pore collapse model an individual element comprises bulk material, spherical gas filled pores surrounded by a thin shell of explosive of constant mass, as shown in figure 1 below.

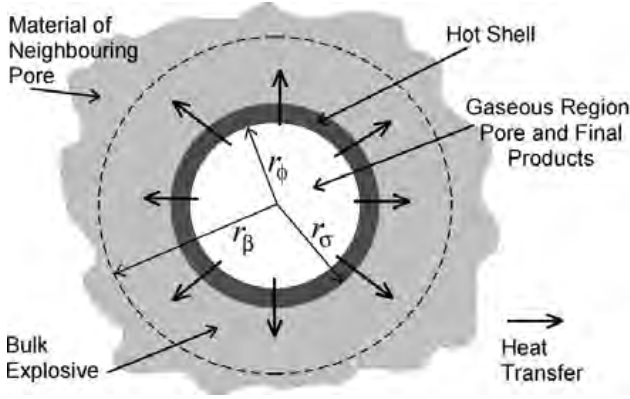


**FIGURE 1. CLOSE-UP PICTURE OF A GAS FILLED PORE SURROUNDED BY A THIN SHELL OF EXPLOSIVE OF CONSTANT MASS.  $R_\phi$  IS THE RADIUS OF THE PORE,  $R_\sigma$  IS THE RADIUS OF THE OUTER EDGE OF THE SHELL AND  $R_\beta$  IS THE OUTER RIM OF THE BULK AS MEASURED FROM THE CENTRE OF THE PORE.**

The temperature in each region of the energetic material is maintained independently. An explicit heat transfer mechanism is then applied between regions. Assuming steady-state heat transfer through a spherical shell allows explicit heat transfer expressions to be obtained. For the two thermal interfaces in the model, these are as follows:

$$\text{a) Pore to Shell } Q_{I1} = \frac{4\pi k_{gs} (T_\phi - T_\sigma)}{(1/r_{m\phi} - 1/r_{m\sigma})} \text{ at } r_\phi \quad (2)$$

$$\text{b) Shell to Bulk } Q_{I2} = \frac{4\pi k_{ss} (T_\sigma - T_\beta)}{(1/r_{m\sigma} - 1/r_{m\beta})} \text{ at } r_\sigma \quad (3)$$

Where  $k_{gs}$  is the gas to solid thermal conductivity,  $k_{ss}$  is the solid to solid thermal conductivity,  $Q_{I1}$  and  $Q_{I2}$  are the rates of heat transfer across the interfaces, and the subscripts  $m$  refer to mass,  $\phi$  the pore,  $\sigma$  is the shell and  $\beta$  is the bulk.

The rate of heat transfer *into* each region is thus as follows:

$$Q_{T\phi} = -Q_{I1} \quad (4)$$

$$Q_{T\sigma} = Q_{I1} - Q_{I2} \quad (5)$$

$$Q_{T\beta} = Q_{I2} \quad (6)$$

Assuming a first order approximation, the actual heating of a region over time  $\delta t_T$  is:

$$\delta Q_{T\Omega} = Q_{T\Omega} \delta t_T \quad (7)$$

Initially, the value of  $\delta t_T$  is set to the burn model timestep,  $\delta t$ . This itself, is determined by considering the expected rate of heat transfer. The method only provides an estimate of the heat transfer timing, so a formal check of the temperature changes must be carried out.

Using the temperatures at the start of the burn model timestep, an indicator,  $I_i$ , is set at both thermal interfaces, to record the current configuration:

$$\text{If } \left| \frac{T_x - T_y}{(T_x + T_y)/2} \right| \leq \varepsilon_I \Rightarrow I_i = 0 \quad (8)$$

$$\text{If } T_x > T_y \Rightarrow I_i = 1$$

$$\text{If } T_x < T_y \Rightarrow I_i = -1$$

where  $\varepsilon_I$  is set to 0.01, and  $x$  and  $y$  represent pore ( $\phi$ ) and shell ( $\sigma$ ) for  $I_1$ , and shell ( $\sigma$ ) and bulk ( $\beta$ ) for  $I_2$  respectively. If the first condition applies then it is assumed that the temperature difference is small and heat transfer is not necessary and the heat transfer term is explicitly set to zero. Further, once the bulk has been consumed, the second interface will cease to exist, so again the rate of heat transfer at the second region will be set to zero.

Using the value found for  $\delta t_T$ , heat transfer is carried out, the temperatures updated and a new set of  $I'_i$  are determined. These are then compared to the original set of values to test whether the temperature gradient across the interface has changed direction ( $I'_i = -I_i$ , and  $I_i \neq 0$ ), which is clearly unrealistic. This can be addressed using a smaller timestep. The value of  $\delta t_T$  is then halved, the temperatures reset, and the heat transfer process repeated. The timestep is successively halved until the above condition ceases to occur. If a reduction of the heat transfer timestep is required then the heat transfer process is repeated until the whole of the burn model timestep has been completed.

Once the rate of heat transfer has been calculated, the heat capacity in each region is determined  $C_\Omega(T_\Omega)$  at the current temperature. Bearing in mind that the heating rates defined are for a single pore, and neglecting temperature variations in the heat capacity, a rate of change of temperature can be defined in each region:

$$T_\Omega = \frac{Q_{T\Omega} N_{\phi E}}{C_\Omega(T_\Omega)} \quad (9)$$

where  $N_{\phi E}$  is the number of pores in an element.

This can then be normalised by the temperature to provide a measure of the fractional rate of change of temperature. This provides a better measure of the temperature change depending on the local temperature. In order to apply the heat transfer mechanism a pseudo steady-state condition is imposed. This can be achieved by constraining the temperature change within a given timestep to be less than some upper limit. By defining the maximum fractional change of temperature the maximum allowable heat transfer timestep can be obtained.

Once the heat transfer timestep has been set, the chemical reactions rates are determined by means of the Arrhenius equation. The rate of reaction  $r$  in region  $\omega$  is expressed as the rate of change of mass fraction:

$$\{R_r\}_\omega = \langle C \rangle_{r\omega} e^{\left(z_r - \frac{E_r}{RT_\omega}\right)} \left(\frac{P}{P_r}\right)^{N_r} \quad (10)$$

where,  $\langle C \rangle_{r\omega}$  is the product of the species concentrations,  $Z_r$  is the natural log of the frequency factor for the reaction,  $E_r$  the activation energy, and  $R$  is the universal gas constant. The pressure term has been added to allow each chemistry step to have a  $P^N$  dependence. This is generally not used. There are typically three coupled Arrhenius steps which can be linked by a variety of schemes. The most simple and widely used is that in which reactants decompose and the products form the reactants of the next step. Other reaction schemes, which are included in the model, involve the incorporation of autocatalytic steps.

From a knowledge of the reaction rate, the burn model timestep can be calculated. The total mass fraction of the reactive region across the whole element and the total rate of change of concentration are multiplied. The magnitude of the product describes the maximum current reaction rate, and will increase if any of the reaction rates are high. A constraint is then imposed on the maximum allowable concentration change which is specified relative to the initial reactive explosive. This, in turn, allows the maximum chemical timestep to be determined.

The overall burn model timestep is determined by choosing the smallest of the maximum allowable timesteps as determined by the current chemical reaction rate, the heat transfer rate, and the remaining allowable timestep for the current burn model time cycle (which is always less than or equal to the DYNA2D timestep).

Once the burn model timestep has been determined, the concentration change associated with each reaction is calculated simply from the product of the rate of change of concentration due to reaction in a given region, and the burn model timestep. The concentrations of all the chemical species are then updated to account for the reactions that have occurred over the burn model timestep. Constraints are applied to ensure no over or under flow of the concentrations can occur. The heat released (or taken up) by the chemistry is then determined through a knowledge of the concentration changes of the reactants and intermediates and therefore the mass reacted. The heat released is then calculated from the product of the mass fraction reacted and the heat per unit mass generated by that reaction. This can be both positive (representing exothermic reaction) and negative (representing endothermic reaction). The mass burned is calculated from the change of mass fraction associated with reaction and the mass within the region. The total heat release within a region over a burn model timestep is simply the sum over all reactions of all explosive components.

It is an assumption in the model that only the last step in the chemistry produces the gaseous detonation products. The current mass fraction of final products relative to the whole element is given by:

$$X_f = \sum_\omega (\Sigma_x \eta_\omega \{c_f\}_\omega) \quad (11)$$

where  $\omega$  indicates a reactive region of the material,  $x$  indicates the unreacted explosive component only,  $\eta_\omega$  is the mass fraction of the shell and bulk regions, and  $\{c_f\}_\omega$  is the concentration of the final products in a reactive region.

Binder vaporisation is assumed to occur at the same rate as the generation of final product. Hence, normalisation by  $X_0$  is required to obtain the overall gaseous mass fraction. Further, any mass already transferred to the pore region is, by definition, gas and thus the total mass fraction in the pore needs to be included. Thus:

$$X_g = \frac{X_f}{X_0} + \eta_\phi \quad (12)$$

This ensures that once reaction in an element is complete, the mass fraction for the gas will be 1, independent

of the initial fraction of energetic material. For homogeneous materials,  $\eta_\phi$  (mass fraction of pore and product gas) is explicitly set to zero. Additional constraints are applied to ensure that numerical instabilities do not produce a value less than 0 or greater than 1. If either is true,  $X_g$  is reset to the appropriate limiting value.

Next, the element volume is updated for the current burn model timestep. The volume of the element is updated by the change of volume term obtained from the main DYNA2D code. The value is adjusted to account for the burn model timestep as a fraction of the full DYNA2D timestep, over which the change of volume term applies:

$$V' = V + \Delta V \left( \frac{\delta t}{\Delta t} \right) \quad (13)$$

Having updated the volume the equilibrium pressure is determined. The equilibrium pressure is found by considering the current material composition of the element along with the appropriate equations of state for each material comprising the explosive. Unreacted and partially reacted solid explosive is described by the Murnaghan EOS, the detonation products by the JWL EOS, and the pore gas by the Ideal Gas EOS. It is then assumed that the pressure in an element is in equilibrium between the solid and gaseous components. It is further assumed that the gaseous components represent a non-reacting mixture which allows the use of Dalton's law of partial pressures. The pressure in the gas phase is then the sum of the partial pressures of the gaseous reaction products and the pore gas. If the explosive is homogeneous, the pressure in the gas phase is simply the pressure of the gaseous products. By the use of appropriate substitutions (e.g. to eliminate  $V_s$  in favour of  $V_g$ ) and with all the other parameters determined, it is possible to express each component as a function of the gas volume,  $V_g$ , as the only unknown. Thus, a solution to the following equation is sought:

$$P_j(V_g) + P_\phi(V_g) - P_s(V_g) = 0 \quad (14)$$

where  $P_j$  is the pressure of the product gases,  $P_\phi$  the pressure of the pore gas, and  $P_s$  the pressure of the solid phase. By definition, the volume of gas ( $V_g$ ) must lie between 0 and the element volume ( $V$ ). Unfortunately, this cannot be solved analytically, therefore a series of numerical techniques are applied in an iterative process. The primary solution method is a bisection, although much of the algorithm is used to improve the estimates of the initial bounds. Special cases are included for elements that are close to 100% gas or 100% solid. Once a value of  $V_g$  is found that satisfies the above equation (to within the specified tolerance), the equilibrium pressure is determined easily.

Having determined the equilibrium pressure, the internal energy of the element is then updated. The internal energy comprises of three components. These are energy changes from the main DYNA2D calculations, the energy changes due to chemical reaction, and the work done in expansion of the element volume. In the homogeneous model this is quite straightforward. However, in the heterogeneous model it is convenient to maintain the energy update to the three regions separately, so that the temperature of the individual regions can be followed. The DYNA2D energy changes are proportioned in relation to the mass fraction of each region. The energy released by the chemistry is found directly from the heat change, as a result of the chemistry, in that region. The work done is determined from a knowledge of the change in volume of each region such that the sum of these equals the total volume change of the element.

Since the DYNA2D hydrocode does not model thermal effects, the temperatures of the various regions are maintained in the burn routine. Temperatures are calculated using the standard thermodynamic relationship between the heat capacity the internal energy:

$$\int_{E_\Omega}^{E_\Omega + \delta E_\Omega} dE_\Omega = \int_{T_\Omega}^{T_\Omega + \delta T_\Omega} C_\Omega(T_\Omega) dT_\Omega \quad (15)$$

Where the subscript  $\Omega$  refers to a general region of an element. In using this relationship it is assumed that the internal energy is not a function of volume, and there is no consideration of thermal expansion. It should be noted that the heat capacity is assumed to be dependent on temperature. Two different methods have been employed to describe this. The first of these uses a linear dependence of the heat capacity with temperature up to 1000K when the heat capacity is held constant. The other, more recent addition, assumes a more complex relationship which is the solution to a fifth order polynomial. This is essentially a curve fit and allows experimental or theoretical data to be fit. The curve fit is input into the routine by means of the constants of the polynomial.

If pores are active, and hence the material is heterogeneous, mass transfer must be performed. Mass transfer enables the gaseous detonation products to accumulate in the pore region and, at the same time, allows the shell to burn out into the bulk material. The mass transfer mechanism operates by first assessing the need for mass transfer. If sufficient reaction has occurred in either the bulk or the shell region and mass transfer is necessary, the gaseous detonation products are transferred into the pore region. This produces a shortfall in the shell region which must be maintained to have constant mass. This situation is rectified by transferring material from the bulk to the shell. This effectively increases the radii of

the shell region to maintain the mass fraction of the shell. The overall result is to cause a burn out of the shell into the bulk.

Following the transfer of mass from one region to another, the internal energy of the two regions is reallocated to determine the updated temperature in each region. The temperature of each region can be specified knowing the mass, associated internal energy and heat capacity. The transfer of mass will therefore affect the temperature of a region through a change in internal energy. There are two specific cases to be considered: where mass is removed from a region and where mass is added to a region. Removal of mass from a region leaves the temperature of that region unchanged so long as a uniform temperature across the region is assumed, as in this model. This is because both mass and energy are lost in the same proportion. On-the-other-hand, the calculation of the new temperature on addition of mass to a region is not so straightforward. It is assumed that when the new mass is added to the region mixing occurs instantaneously and the region has a uniform temperature. The internal energy of mass to be added and that of the region to which the mass is to be added are calculated using equation 15, taking into account the variation of the heat capacity with temperature. The internal energy and heat capacity of the region plus the added mass is then simply the sum of the components of the original masses. Using these values, the new temperature can be calculated using equation 15 once again.

Once the regional mass fractions have been updated after mass transfer, the equilibrium pressure is again calculated and the new volume of gaseous components found. If the burn model timestep matches the DYNA2D timestep the stress tensor is again updated before passing control back to the main DYNA2D program. If the burn model timestep is less than the DYNA2D timestep the burn routine is looped over until the sum of the burn model timesteps matches the DYNA2D timestep.

## TESTING THE MODEL

Whilst the model is still under development, the current version is also undergoing extensive testing to examine its capabilities. Previous studies<sup>10,11</sup> have shown that the model can be successfully parameterised for a homogeneous explosive such as nitromethane, using standard physical constants available in the open literature, the main unknown being the global chemistry parameters. Thus, the data for the Murnaghan and JWL equations of state along with the density and viscosity were obtained from the literature, whilst the global chemistry parameters were found by fitting the model to experiment. The model obtained for this explosive was shown to be able to match experimental impact data for flat-nosed projectiles

of two diameters as well as results for pointed and round-nosed projectiles. The basic detonics properties for this model, such as detonation velocity and pressure, were also found to be in accordance with the experimentally determined values. It should be noted that features such as the curvature of the detonation front arise naturally from the parameterisation of the model and are not artificially prescribed. Moreover, the model displays initiation and growth of reaction behaviour much as expected for a homogeneous system. That is, after the initial shock is observed to pass into the explosive, reaction occurs at or very near to the interface where the shock entered the explosive. For very strong shocks, which greatly exceed the threshold for detonation, reaction can occur almost immediately as the shock enters the explosive. When the shock is near the threshold for initiation, reaction can often be observed to occur a short while after the initial shock has passed into the material, a short distance from the interface.

Including the pore collapse mechanism increases the sensitivity of the model as expected. For projectile impact experiments it was found that the model could qualitatively reproduce the experimentally determined shock threshold curves for heterogeneous explosives for a range of projectile diameters and geometries. That is, the model could reproduce the 'S' shaped response curves observed when flat-nosed rods cause shock initiation in heterogeneous explosives<sup>10,12</sup>. Furthermore, the same model parameterisation can successfully reproduce the smooth response of pointed projectiles impacting the same material. However, routine parameterisation of such models to be within say 10% of experimental values can be a lengthy process. Work is currently underway to develop a more methodical and expeditious method of parameterisation.

The phenomenon of shock desensitisation has been attributed to the occurrence of voids (or pores), which become closed and hence deactivated by precursor shocks. Since the burn model we describe in this paper explicitly models the physics of gas pore collapse we decided to investigate whether or not the model could reproduce shock desensitisation behaviour. The experiments employed a heterogeneous model with 20% porosity and pores of diameter  $1 \times 10^{-7}$  m. A rectangular mesh containing 0.5mm sided square elements of explosive was impacted by a 1mm thick aluminium plate and the threshold velocity for this system was found to be 500–510m/s. For the same system, but with pores explicitly switched off (homogeneous) a threshold velocity of 770–780m/s was found. When a 1mm aluminium plate covered the explosive the threshold velocities for both the heterogeneous and homogeneous systems were 590–600m/s and 1150–1170m/s respectively. Shock desensitisation was

simulated by impacting the bare explosive with two 1mm aluminium plates. The first plate was given a velocity of 300m/s and the velocity for initiation by the second flyer plate was determined. A velocity of 680–700m/s was obtained, (when the delay between impacts was  $2.0\mu\text{s}$ ) which is well above the threshold for the heterogeneous explosive covered by 1mm aluminium, and demonstrates the ability of the burn routine to model shock desensitisation effects. It is interesting to note that in the experiments described here the model showed a sensitivity in-between that of the heterogeneous and homogeneous systems, and it can therefore be concluded that the pores still had some reduced effect.

The method of desensitisation described by the model can be attributed to the pore size since, when the material is pre-shocked the pores will collapse, but not give up sufficient heat to the surrounding energetic material to cause growth to detonation. Since the pores are much smaller by the time the second shock arrives they will need a much stronger stimulus to heat them to the required temperature to cause runaway reaction.

A study of the pore collapse mechanism has shown that the pores can reach very high temperatures, but that the energy associated with the pores is quite low. It is the rapid heat transfer from the hot pores to a thin layer of surrounding energetic material and subsequent build-up of reaction and burn-out into the surrounding material which is responsible for the effectiveness of the pores. A study of the behaviour of the pores when the energetic material is shocked just above the threshold for initiation, and also when overdriven, has been made. The results show that for a  $1 \times 10^{-7}$  mm diameter pore, in a simulation where the shock is just above the threshold, the pores are compressed almost instantaneously (within  $2 \times 10^{-7}$  s to  $8 \times 10^{-9}$  m) and obtain a temperature of ca 17,000K. A delay of ca.  $7 \times 10^{-7}$  s was observed before full reaction of both the shell and the bulk. When the same explosive was overdriven, the pores collapsed to about the same dimensions, but a much higher pore temperature was observed (43,000K) and the delay before full reaction of the bulk and shell was approximately halved.

## CONCLUSIONS

In this paper we have given details on a new ignition and growth model for shock initiation of both homogeneous and heterogeneous explosives. The model has been developed on fundamental principles of physics and chemistry which when combined can describe mesoscopic processes such as adiabatic gas pore collapse. It is quite clear that if we are to be able to predict the complex behaviour of energetic materials in different environments, and under a variety of stimuli, it will be necessary to develop a range of mesoscale models

capable of describing the processes which are known to be important in these materials. It is, for example, widely accepted that shear and friction play key roles in determining the response of these materials. The development of models to describe mesoscopic shear processes leading to hotspot formation is a priority since it is likely that shear plays an important role at lower strain rates. This is especially important in determining the response to accidental stimuli. The development of suitable mesoscopic models for implementation in hydrocodes is currently under consideration.

Another development which needs to be addressed is the development of particle burn routines which can describe the effect of particle size. Although not described in this paper, a metal particle burn routine has been developed and incorporated into the burn model described here. This model is based on spherical particles of metal which need to be heated to their melting point before reaction with the product gases produced as a result of reaction of the base energetic material. The metal is assumed to react with available oxygen in the product gases by a single Arrhenius kinetic step. The heat produced by this reaction is fed back into the bulk energetic material to fuel further reaction.

The metal particle burn routine has been developed as the initial step in the development of a general particle burn model to describe the behaviour of single reactive particles (e.g. RDX crystals) as well as separate fuel-oxidiser particles (non-ideal systems). The development of the latter system will certainly need to address the problem of friction between particles leading to hotspots.

The ignition and growth model described here has been shown to be able to describe both homogeneous and heterogeneous behaviour in energetic materials. It is normal practice to treat these two types of material separately since they exhibit different initiation and growth of reaction characteristics. However, homogeneous and heterogeneous behaviour merely represent the two ends of a continuous spectrum. All energetic materials have homogeneous properties, but under certain circumstances heterogeneous effects can dominate. The degree to which an individual energetic material displays either properties really depends on the energetics and physical properties of the individual explosive.

## ACKNOWLEDGEMENTS

The authors would like to acknowledge the contribution made by Mr. R. Chambers (formerly of EDS Defence Ltd), Dr. J. Curtis (DERA, Fort Halstead), Mr. S. Crumpton, Mr. S. Brinton and Mr. G. Nixon (all of EDS Defence Ltd).



## REFERENCES

1. Khasainov, B. A., Borisov, A. A., Ermolaev, B. S., and Korotkov, A. I., "The two Phase Visco-Plastic Model of Shock Initiation of Detonation in High Density Pressed Explosives," 7th Symposium (International) on Detonation, Annapolis, MD, 1981, pp. 435–447.
2. Frey, R. B., "The Initiation of Explosive Charges by Rapid Shear," 7th Symposium (International) on Detonation, Annapolis, MD, 1981, pp. 36–49.
3. Taylor, P. A., "The Effects of Material Microstructure on the Shock Sensitivity of Porous Granular Explosives," 8th Symposium (International) on Detonation, Albuquerque, NM, 1985, pp. 26–34.
4. Coffey, C. S., "Hot Spot Production by Moving Dislocations in a Rapidly Deforming Crystalline Explosive," 8th Symposium (International) on Detonation, Albuquerque, NM, 1985, pp. 62–67.
5. Kim, K., and Sohn, C. H., "Modelling of Reaction Buildup Processes in Shocked Porous Explosives," 8th Symposium (International) on Detonation, Albuquerque, NM, 1985, pp. 926–933.
6. Carroll, M. M., and Holt, A. C., "Static and Dynamic Pore Collapse Relations for Ductile Porous Materials", *Journal of Applied Physics*, Vol. 59, No. 6, 1986, 1962–1967.
7. Bonnett, D., and Butler, B. P., "A Thermochemical Model for Analysis of Hotspot Formation in Energetic Materials," Univ Iowa, UIIME PBB95-003, Iowa City, IA 1995.
8. Field, J., "Hot Spot Ignition Mechanisms for Explosives", *Acc. Chem. Res.*, Vol. 25, No. 11, 1992, pp. 489–496.
9. DYNA2D, a nonlinear, explicit, two-dimensional finite element code for solid mechanics., R. G. Whirley, B. E. Englemann and J. O. Hallquist, LLNL, UCRL-MA-110630, 1992.
10. Cook, M. D., and Haskins, P. J., "Projectile Impact Initiation of a Homogeneous Explosive", American Physical Society Topical Group on Shock Compression of Condensed Matter Conference, held at Seattle, Washington, 14–18 August 1995, pp. 823.
11. Cook, M. D., and Haskins, P. J., "The Development of a new Arrhenius based burn model for both homogeneous and heterogeneous explosives", American Physical Society Topical Group on Shock Compression of Condensed Matter Conference, held at University of Mass, Amherst, MA, USA., 28 July–1 August 1997.
12. Cook, M. D., and Haskins, P. J., and James, H. R., "An Investigation of Projectile and Barrier Geometry Effects on Impact Initiation of a Secondary Explosive", *Proceedings of the American Physical Society Topical Conference on Shock Compression of Condensed Matter*, held in Williamsburg, VA, June 1991, p. 675.

© British Crown Copyright 1998 / DERA. Published with the permission of the Controller of Her Britannic Majesty's Stationery Office.

## QUESTION BY YEHUDA PARTON

First a comment: some 15 years ago I developed a reaction model with a similar physical picture. It has been described in 3 LANL reports and elsewhere. My question has two parts:

1. What are the parameters in your model that you need to calibrate from tests, and how do you perform that calibration.
2. Your hot spot ignition model depends on pore collapse and heating up of the pore gas, but it has been shown experimentally in the early sixties that hot spot ignition does not necessarily depend on the existence of gas in the pores.

## REPLY BY MALCOLM COOK

### Answer to Question 1

Apart from EOS data for both the Murgnahan and JWL EOS, which is accessible from experimental data, the homogeneous model requires  $C_v$  as a function of temperature, and both frequency factors and activation energies for each chemical step. In addition, the pore collapse model requires the pore radius, porosity, gas to solid conductivity and solid to solid conductivity. These parameters can be estimated from a knowledge of the material. The parameters are then adjusted by comparison with experimental data from impact and shock initiation experiments.

### Answer to Question 2

The pore collapse hot spot model, which we have implemented in the DYNA2D hydrocode, represents only one type of hot spot mechanism. The fact is that there are a number of mechanisms that can lead to hot spot formation and this has been well documented in the literature. Further important mechanisms include shear heating and friction. It should be recognised however,

that pore collapse is an important hot spot mechanism which can have a significant contribution under SDT conditions. The effects of hot spots (by which ever mechanisms they are formed) are additive. In the future,

we intend to add a shear heating model to act alongside the pore collapse mechanism. This will most likely have a greater effect at low strain rates where the pore collapse model is not applicable.



## A.7 Cumulative Damage Hotspot Model...

---

Authors:	Cook, M D; Haskins, P J; Stennett, C; Wood, A D		
Title:	Cumulative Damage Hotspot Model for use with Arrhenius-Based Ignition and Growth Model		
Publication Type:	International Conference	Venue:	12 <sup>th</sup> International Detonation Symposium
Date:	2002		

---

# CUMULATIVE DAMAGE HOTSPOT MODEL FOR USE WITH ARRHENIUS BASED IGNITION AND GROWTH MODEL

M. D. Cook, P. J. Haskins, C. Stennett and A. D. Wood  
QinetiQ Ltd, Fort Halstead,  
Sevenoaks, Kent TN14 7BP, England

The hot spot model described in this paper is based on the idea of cumulative damage that can be estimated from knowledge of the hysteresis of the material. This gives the energy deposited in the energetic material as a result of the work done in terms of a temperature rise. The additional temperature created by the work done is then added to a thin shell of energetic material surrounding the outer edge of the existing gas-filled pore that has already been heated by bulk effects. Although the model is really applicable to low strain rates, it can be used as a generic hot spot model even at high strain rates. In this case, the parameterisation can be obtained by matching to specific calibration data such as flyer, bullet impact, wedge test and run distance data and tested and validated against real weapon system results.

## INTRODUCTION

We have previously reported details of our Arrhenius, temperature dependent homogeneous ignition and growth of reaction model, which includes heterogeneous effects modelled through a gas pore collapse mechanism<sup>1</sup>. The pore collapse mechanism implemented in the model only accounts for the contribution from compression of gas bubbles in the explosive matrix. The gas collapse is assumed to be adiabatic within the smallest time step in the model, which is typically that for heat conduction, but otherwise is non-adiabatic in terms of a hydrocode time step.

Shock compression of the gas has been shown experimentally to be an important hot spot mechanism<sup>2,3</sup>, and in many ways resembles the phenomenon of sonoluminescence<sup>4</sup>. There is, however, experimental evidence that other mechanisms can be important when bubbles are shocked. For example, jetting of material across the cavity has been observed<sup>5,6</sup>. Additionally, it has been proposed that visco-plastic heating of the material around a cavity is more important for shock initiation<sup>7</sup> and this has been used as the basis for a number of hot spot models<sup>8</sup>.

The existing pore collapse hot spot functionality is only expected to be relevant in the shock regime where the pore collapse time is very short and hence the pore temperature very high. At lower shock amplitudes, such as lower velocity impacts, or where low velocity projectiles penetrate an explosive store, other hot spot mechanisms would be expected to play a role in controlling the response of the underlying homogeneous model. In these regimes, mechanisms such as shear or friction are likely to be more important than adiabatic compression of gas-filled pores.

In developing shear or frictional heating models consideration must be given to the fact the model is to be implemented into a hydrocode, and that it is necessary to link the model (as a sub-model) with the existing burn model. A one-dimensional solution would be preferred, but this needs to be reconciled against the fact that shear, or friction, are three-dimensional problems.

There are a number of papers in the literature that use the idea of cumulative damage models to describe the damage caused when energetic materials, such as propellants, are stressed. Moreover the method has been shown to be applicable to high-strain rates ( $10^3$ – $10^4$  s<sup>-1</sup>)<sup>9</sup>. The

method allows relatively simple experimental techniques to be used to characterise the test material. Hopkinson bar experiments can give dynamic stress-strain data, and constant stress experiments can be performed using a dynamic mechanical thermal analyser, using either a parallel plate or shear sandwich fixture. From such measurements the overall mechanical response of the energetic material can be determined and the hysteresis energy losses in the material measured.

A knowledge of the hysteresis energy when an energetic material is deformed can be used as a measure of the damage (which is probably a mixture of shearing, plastic deformation, dewetting of crystals and binder and microvoid / cracking formation). Furthermore, it can be used as an additional heating term calibrated from experiment.

This paper describes the background and implementation of a new hot spot model. It has been designed to operate either with the existing pore collapse hot spot model or with a particle burn model. Only the pore collapse implementation will be considered in this work. The hot spot model is based on the idea of cumulative damage that can be estimated from knowledge of the hysteresis of the material. This gives the energy deposited in the energetic material as a result of the work done in terms of a temperature rise. The additional temperature created by the work done is then added to a thin shell of energetic material surrounding the outer edge of the pore that has already been heated by bulk effects. Although the model is really applicable to low strain rates, it can be used as a generic hot spot model even at high strain rates. In this case, the parameterisation can be obtained by matching to specific calibration data such as flyer, bullet impact, wedge test and run distance data and tested and validated against real weapon system results.

## BACKGROUND

The hot spot model described in this paper is designed to simulate the contribution of hot spots formed in the energetic material as a shock wave passes through it. These hot spots may occur due to shear heating, visco plastic heating and the like. It is assumed that such processes occur around dislocations in the material's structure, so a perfectly uniform (idealised) material will not exhibit this behaviour. For the Arrhenius burn model, the only irregularities currently capable of being modelled are the gas pores. However, it should be noted that it is our intention to introduce a grain burning model for the explosive crystals which will use the same methodology developed for the gaseous pores, at later date.

In the current pore collapse model, the gas filled pores are assumed to be spherical, and are surrounded by a thin shell of energetic material of constant mass. The purpose of the shell is to allow heat transfer from the pore gas to

the bulk material (which is a mixture of energetic material and binder) through a simple conduction process. As shell material is consumed by reaction, mass is transferred from the bulk to the shell (to maintain constant mass) and from shell to gaseous products. It is therefore convenient to use the degree of distortion of the shell material for the shear model. It should be noted that homogeneous explosives cannot use the shear model because of their uniform structure (they have no pores present).

The shear model monitors the change in shape (i.e. strain) of the shell of energetic material surrounding each pore as a shock wave propagates through it. A look-up table of energy vs. strain rate is then used to calculate the heating in the shell.

The leading edge of a pressure wave acts to compress the pore and shell, therefore the shell will be subjected to compressive strain. During this phase, the pressure wave will be losing energy to the shell, but it is assumed that:

- the shell does not heat up (by any more than the bulk heating effect);
- the reduction in energy of the pressure wave is negligible compared to its total energy.

After the peak of the pressure wave has passed, the pore and shell expand out. The resulting tensile strain causes energy gained from the shock wave to be liberated in the material, manifesting itself as a temperature rise. The strain rate of the shell material, once calculated, leads directly to a quantity of energy being dispersed in the material as heat. This quantity of energy is read from a table of energy vs. strain rate supplied by the user.

## MODEL SPECIFICATION

The specification detailed here can be regarded as the initial stage in an iterative process of analysing the shear model's performance and changing its functionality to improve results. The specification has been kept deliberately straightforward so as not to introduce unnecessary complexities at the first iteration.

### Strain Calculation

Strain is the change in length of a material along a single dimension. The strain is thus resolved into 3 Cartesian components. One component addresses the increase in shell thickness, and is therefore perpendicular to the tangential plane of the shell material's surface. The other two components are within (or at least parallel to) the tangential plane of the shell's surface, thus measuring the stretching of the shell's 'skin'. Due to the shell being spherically symmetrical, the last two components are equal. The total strain is assumed to be the sum of the 3 components, and this total strain is converted to an energy value using the look-up table.

**TABLE 1. Parameters Required to Calculate Shell Dimensions.**

Parameter symbol	Meaning
$\eta_\sigma$	mass fraction of pore shell
$\eta_\beta$	mass fraction of bulk
$r_\phi$	current pore radius
$\phi$	current porosity

The shell's dimensions are deduced both before and after straining. Due to the spherical symmetry of the shell, its shape is completely described by its inner and outer radius. Information required to deduce these radii is given in Table 1.

### Pore Shell Radii

The radius of the bulk region,  $r_\beta$ , is given by:

$$r_\beta = \frac{r_\phi}{\sqrt[3]{\phi}} \quad (1)$$

It is assumed that the shell and bulk have the same density. This volume ratio then follows, where  $V$  denotes the volume of a region specified by its subscript:

$$\frac{V_\sigma}{V_\sigma + V_\beta} = \frac{\eta_\sigma}{\eta_\sigma + \eta_\beta}$$

For each region  $\Omega$ , substituting  $V_\Omega$  for  $4/3\pi r_\Omega^3$  and re-arranging gives the radius (outer) of the shell,  $r_\sigma$ :

$$r_\sigma = \sqrt[3]{\frac{\eta_\sigma}{\eta_\sigma + \eta_\beta} (r_\beta^3 - r_\phi^3) + r_\phi^3}$$

The inner radius of the shell is equal to the radius of the pore,  $r_\phi$ , which is already known.

### Strain Calculation from Radii

The strain that the shell undergoes is calculated as 3 mutually perpendicular Cartesian components. The x and y components deal with stretching within the plane parallel to the shell's tangential surface. If the plane in which stretching is measured is actually on the shell's outer surface, then the strain will be overestimated as the inner surface will not be stretched by as much. Similarly, considering the inner surface will underestimate the strain. Therefore, the stretching will be measured in the spherical surface that is midway between the inner and outer radii. The radius of the surface in question is therefore given by  $r_s$ :

$$r_s = \frac{r_o + r_i}{2}$$

where  $r_o$  and  $r_i$  are the outer and inner radii of the shell respectively. The area of this surface is  $A_s$ :

$$A_s = 4\pi r_s^2$$

Hence given an updated value of  $r_s$ , an updated  $A_s$  can be deduced. The two perpendicular dimensions within the surface area, being equal, will each change by the same factor. The standard equation for strain along a length  $l$  is:

$$\varepsilon_l = \left| \frac{l'' - l'}{l'} \right|$$

where  $l''$  and  $l'$  are the latest and previous values of the length respectively. The modulus ensures that the equation is valid for compression as well as expansion. However, the model will use the following modified equation for strain:

$$\varepsilon_l = f_l \left| \frac{l'' - l'}{l_0} \right| \quad (2)$$

where  $l_0$  is the original value of  $l$ , and  $f_l$  is a multiplication factor for the strain. Making the change in length relative to  $l_0$  rather than  $l'$  means that the strain value will be independent of the number of time-steps that the strain is split into. A side effect of using  $l_0$  rather than  $l'$  for the denominator means that the latest length is compared against a value that is several iterations old. Using a long timespan introduces the possibility of mass transfer and other non-pressure effects altering the length. The multiplication factor is present to compensate for these effects. If material is transferred out of the shell so that its length along a certain axis is halved, all subsequent length measurements will be half of what they would otherwise have been. Therefore all future measurements will need to be doubled.

The multiplication factor is simply deduced by dividing the previous length by the latest length:

$$f_l = \frac{l'}{l''}$$

where the change in length is due to mass transfer etc. If such a factor already exists for a given dimension of the shell, the new factor that replaces it will be derived using the formula for  $f$  above, and by multiplying this by the existing factor:

$$f_l'' = f_l' \frac{l'}{l''} \quad (3)$$

The factor will continue to be used to calculate strain until the dimension starts to compress due to pressure,

in which case the material is deemed to have finished undergoing strain for the present time, and  $f$  will be reset to unity.

The latest value of  $x$  will be given by:

$$x'' = \sqrt{A_s''} \quad (4)$$

The strain along each of the components in the surface will be:

$$\varepsilon_x = \varepsilon_y = f_x \left| \frac{x'' - x'}{x_0} \right|$$

where  $x_0$  is the value since the expansion along the  $x$  direction began. The strain along the third component (relating to changes in the shell's thickness) is given by:

$$\varepsilon_z = f_z \left| \frac{z'' - z'}{z_0} \right|$$

The 'z length' is defined as difference between the outer and inner radii of the shell. The latest value of  $z$  will simply be the outer shell radius minus the inner shell radius.

The total strain is arrived at by adding together the individual components:

$$\varepsilon_T = \varepsilon_x + \varepsilon_y + \varepsilon_z \quad (5)$$

The total strain rate is calculated by dividing this by the current burn model time-step:

$$\dot{\varepsilon}_T = \frac{\varepsilon_T}{\Delta t} \quad (6)$$

Note that there will be a separate value of  $\dot{\varepsilon}_T$  for the explosive and metal shells.

### Heating Term

The total strain value  $\varepsilon_T$  is divided by the current burn model time-step to get a strain rate for the shell. This rate is then looked up in a table of strain rate vs. energy. The strain rate value will generally lie between two entries in the table, so the energy value will need to be interpolated (linearly, for simplicity) between the two entries. Once an energy value has been derived from the table, it is multiplied by the number of pores or metal particles (as appropriate) to arrive at the total energy contribution of shells of that type in that element. To illustrate, the energy supplied by shearing of all explosive shells in a given element,  $E_s$ , is given by:

$$E_s = n_\phi E_L \quad (7)$$

where  $n_\phi$  is the number of pores in the element and  $E_L$  is the energy corresponding to  $\dot{\varepsilon}_T$  in the lookup table.

The resulting energy term is added to the energy in the shell, which will filter through as a temperature rise in the shell.

### TESTING THE MODEL

Although the model has been developed based on the notion of cumulative damage, and it was intended to parameterise the model from hysteresis data, this has not been possible to date due to lack of experimental data. The testing has therefore been concentrated on checking the mathematical flow of data through the equations and the ability of the model to add control to the sensitivity of impact simulations of explosive charges covered with aluminium.

We have previously parameterised our Arrhenius ignition and growth model for RDX/TNT 60:40 against fragment impact data<sup>10</sup>. This parameterisation has included gas filled pores, the propensity of which has been estimated from the density, and the size was assumed to be 1mm in diameter. The preliminary fit obtained along with the experimental data is shown in figure 1. The axisymmetric mesh used for these calculations is shown in figure 2. The flat-nosed fragment is shown at the bottom of the figure impacting a 3mm aluminium barrier plate behind which is a block of explosive. Using this as a baseline, a test was performed to examine how the additional shear hot spot model can affect the outcome of

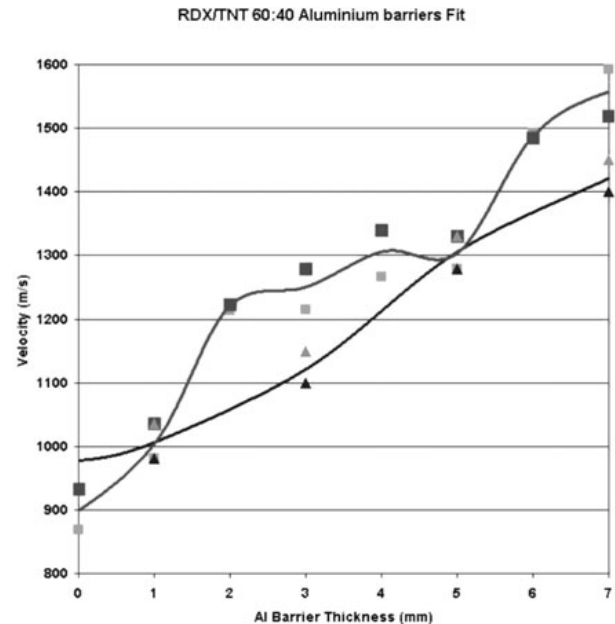


**FIGURE 1. Fragment impact of 13.15mm diameter steel projectiles against RDX/TNT charges covered by aluminium barriers. The experimental results are shown in the upper line and the calculated values in smooth lower line.**



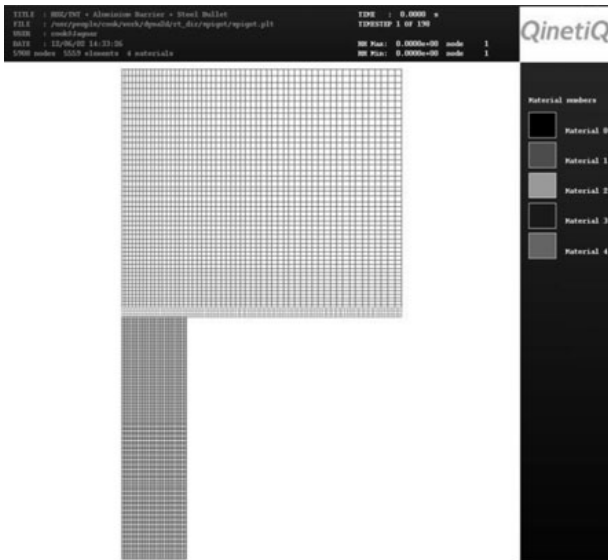


**FIGURE 2. DYN2D mesh of a fragment impact simulation.**

a run. The input deck was adapted so that it was compatible with the latest burn model. A velocity was chosen such that it does not detonate under normal conditions (i.e. without shear heating).

With the shear model disabled from the input deck, the run behaves as previously, with no detonation occurring. However, when the shear model is turned on, the extra heat being dumped into the explosive shell causes the energetic material to detonate.

Analysis of the run has shown that without shear heating (energy terms of zero in the look-up table), there is a spike in the strain rate which reaches about  $4.5 \times 10^8 \text{ s}^{-1}$  at its maximum. The energy contributions into the shell from existing sources peak at around  $3.5 \times 10^{-6}$  in any given timestep. The number of pores in each element is  $2 \times 10^9$ . Knowing this information, the data in the look-up table was chosen so that the shear heating made a significant contribution at the maximum strain rate that the material would reach. An energy of  $2 \times 10^{-14} \text{ J}$  at a strain rate of  $1 \times 10^8 \text{ s}^{-1}$  was necessary to just initiate SDT in these runs.

A further series of simulations were carried out to investigate the effect of the model at lower strain rates. The same parameterised model was used in these calculations with the shear table look-up adjusted so that an energy of  $2 \times 10^{-14} \text{ J}$  was produced at a strain rate of  $1 \times 10^4 \text{ s}^{-1}$ . In these simulations the fragment velocity was reduced to 25m/s (a velocity typical of free fall conditions). The results of these calculations showed that reaction occurred where the cover plate began to buckle in a ring to the periphery of the fragment (see figure 3). This is similar to experimental observation. Moreover, this modified model did not appear to affect the fragment

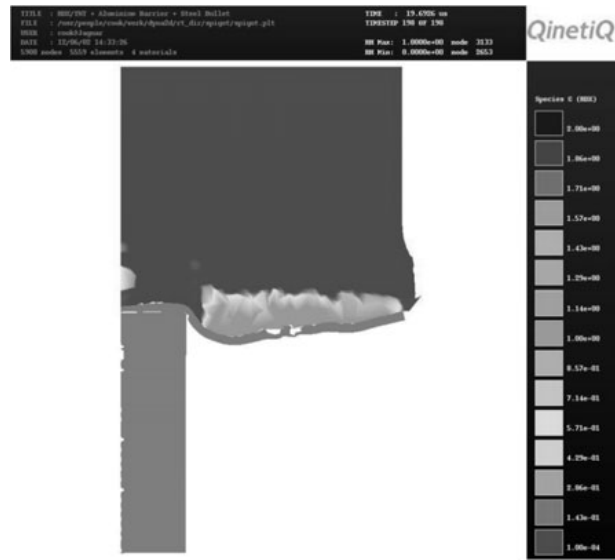


**FIGURE 3. Low velocity impact simulation of an RDX/TNT 60:40 charge protected with an aluminium barrier. The scale represents the amount of product gas produced.**

impact predictions at the higher velocities. This demonstrates that this new hot spot model can act successful in parallel to the pore collapse hot spot model to extend the predictive capability.

## CONCLUSIONS

The hot spot model specified in this report has been designed to operate either with the existing pore collapse hot spot model or with a particle burn model. Only the pore collapse implementation has been considered in this work. The hot spot model is based on the idea of cumulative damage that can be estimated from knowledge of the hysteresis of the material. This gives the energy deposited in the energetic material as a result of the work done in terms of a temperature rise. The additional internal energy created by the work done is then added to a thin shell of energetic material surrounding the outer edge of the pore or particle that has already been heated by bulk effects. Although the model is strictly applicable only to low strain rates, it appears capable of being used as a generic hot spot model even at high strain rates. In this case, the parameterisation can be obtained by matching to specific calibration data such as flyer or bullet impact, wedge test, and run distance data. The model can then be tested and/or validated against real weapon system results.

## ACKNOWLEDGEMENTS

The authors would like to acknowledge the contribution made by Mr. R. Chambers (formerly of EDS Defence

Ltd), Dr. J. Curtis (QinetiQ, Fort Halstead), Mr. S. Crumpton, Mr. S. Brinton and Mr. G. Nixon (all of EDS Defence Ltd). The authors would also like to acknowledge Dr. S. Y. Ho of DSTO for useful discussions on cumulative damage.

## REFERENCES

1. Cook, M. D., Haskins, P. J., and Stennett, C., Eleventh International Detonation Symposium. ONR 33300-5, Arlington Virginia, pp. 589–598, (1998).
2. Dear, J. P., Field, J. E., and Watson, A. J., *Nature*, **332**, 505–508 (1988).
3. Dear, J. P., and Field, J. E., *J. Fluid Mech.*, **190**, 409–425 (1988).
4. Putterman, S. J., *Scientific American*, 46–51, February 1995.
5. Bourne, N. K., and Field, J. E., *Proc. SPIE* 1358, 1046–1056 (1990).
6. Bourne, N. K., and J. E. Field, *Proc.R. Soc. Lond. A*, 435, 423–435 (1991).
7. Chou, P. C., Liang, D., and Ritman, Z., in *Proc. 10th Symposium (International) on Detonation*, edited by J. M. Short and D. G. Tasker, ONR, Arlington Virginia, pp. 979–986, (1995).
8. Kasainov, B. A., Attetkov, A. V., and Borisov, A. A., *Chem. Phys. Rep.* 15, 987–1062, (1996).
9. Ho, S. Y., Eleventh International Detonation Symposium. ONR 33300-5, Arlington Virginia, pp. 119–126, (1998).
10. Cook, M. D., Haskins, P. J., Briggs, R. I., Stennett, C., Fellows, J., and Cheese, P., “Fragment Impact Characterisation of Melt-Cast and PBX Explosives,” *Proc. APS meeting on Shock Compression of Condensed Matter*, *Bulletin of the American Physical Society*, Vol. 46, No. 4, K2.003, in print.



## A.8 Live Imaging and Heating of Confined RDX and HMX ...

---

Authors:	Stennett C; Cook M D; Cheese, P J; Wood, A; White, N; Reeves, T		
Title:	Live Imaging and Heating of Confined RDX and HMX Crystals Until Reaction Using the Dual-Windowed Test Vehicle		
Publication Type:	Journal	Venue:	APS SCCM 2017
Date:	Jul 2017		

---

# Live Imaging and Heating of Confined RDX and HMX Crystals Until Reaction Using the Dual Windowed Test Vehicle

Chris Stennett<sup>1, a)</sup> Malcolm Cook<sup>2)</sup>, Philip Cheese<sup>3)</sup>, Andrew Wood<sup>2)</sup>, Nathan White<sup>3)</sup> and Tom Reeves<sup>3)</sup>

<sup>1</sup>*Centre for Defence Chemistry, Cranfield University, Defence Academy of the United Kingdom, Shrivenham, SN6 8LA, UK*

<sup>2</sup>*Syanco Ltd, PO Box 411, West Malling, ME6 9EZ, UK*

<sup>3</sup>*Defence Equipment and Support, Fir 3a #4303, MOD Abbey Wood, BS34 8JH, UK*

<sup>a)</sup>Corresponding author: c.stennett@cranfield.ac.uk

**Abstract.** A high fidelity live camera feed recording RDX and HMX crystals, measuring 1 mm thick and 15 mm in diameter, decomposing while heavily confined and subjected to various heating rates until a reaction occurs has been analysed. Video records reveal unexpected behaviour in both RDX and HMX crystals prior to ignition. Three distinct stages can be observed: phase changes and melting; slow, flameless decomposition with production of gaseous intermediates; and finally burning with a luminous flame of the gaseous intermediates. Tests with pure RDX and HMX crystals reveal pockets of gaseous materials forming above the molten and bubbling nitramine, before a flame appears at one side then burns inwards in an apparent conductive manner at a few metres per second. This causes the remaining bubbling nitramine to be compressed. Violent reaction appears to occur via a bubble collapse mechanism. The violence of this event is dependent on the loss of confinement; if it fails in the first or second phase the reaction is less violent than if the third phase is reached. The third phase burning reaction has associated pressure waves, which is presumed oscillation of the flame front, leading to wave interactions, pressure spikes and ultimately a violent reaction.

## INTRODUCTION

The measurement and understanding of the conditions inside a heated confinement containing an explosive pellet at the point of ignition presents a significant challenge. The well-known pressure dependence on burning rate demands that the confinement be strong and gas-tight, but this presents significant difficulty in making connections from within the confinement to recording instruments outside. Most often, experimental studies of cook-off attempt to infer interior conditions from a combination of external measurement and computer modelling. In early pipe-bomb type experiments, such as the UK EMTAP Tube Test [1], the violence of reaction was assessed by simple counting of post-test casing fragments; other types of external instrumentation have included dynamic measurement of case motion [2,3,4] and measurement of internal pressure [5]. Internal observations have been made using proton radiography [6], and direct visual observation using transparent pressure windows [7].

The work presented in this paper extends the development of an early glass-windowed test vehicle [8,9] which has been used to observe solid explosive pellets during the onset of ignition with visual observations at standard video frame rates and relatively weak pressure-sealing. In this more recent work we introduce a developed experimental arrangement, in which small, low-density ( $\sim 1.0 \text{ g cc}^{-1}$ ) specimens of pure HMX and RDX crystals have been heated to ignition, and directly observed using a high-speed digital camera at time resolutions on  $\sim 30 \mu\text{s}$  and spatial resolution of  $\sim 32 \mu\text{m}$ .

## EXPERIMENTAL

The general arrangement for these experiments is shown in the diagram in Figure 1, and is discussed in detail in ref [10]. The powdered test specimens were placed onto the glass window (c) in the space inside the 'C' seal, and the glass windows clamped on either side, forming a cavity of approximately 100 bar sealing capacity. In these experiments no particular care was taken to obtain a specific loading mass or density; the specimen powder was intentionally left at tap density of approximately  $1.0 \text{ g cc}^{-1}$  to provide ullage. However, all experiments contained  $0.6 \pm 0.1 \text{ g}$  of material. The specimen thickness was controlled by a steel supporting ring of 52 mm outer diameter and 17.5 mm internal diameter to match the 'C' seal dimensions, and of 1.0 mm thickness to define the 'C' seal preload. Three heater cartridges (d) of 400 W capacity were inserted into the main confinement (a) to provide a heat source, and these were controlled by a closed-loop temperature controller.

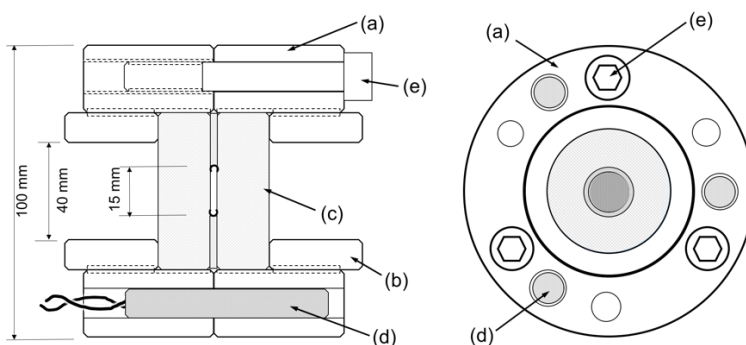


**FIGURE 1.** Test vehicle schematic, showing confining rings (a) clamped axially by bolts (e), and containing heater cartridges (d). Glass windows (c) were clamped axially on the specimen by threaded collars (b). A copper 'C' seal (Sealco CI-001550-1.57M-1/1-3-S30), clamped between the windows formed the specimen cavity, of diameter 15 mm and thickness 1 mm. The vehicle was fired in the orientation shown, i.e. the cylindrical axis of the test vehicle horizontal

Additional thermocouples were added to the experiment to monitor the temperature at 1 sample per second, but it was not possible to embed a physical thermocouple within the specimen without breaking the 'C' seal and removing confinement. However, in one experiment the 'C' seal was deliberately cut and a thin thermocouple embedded in a TNT specimen, with a second thermocouple of the same type placed to record the temperature at the outer circumference, as described above. This experiment showed that the temperature of the specimen could be estimated from the circumferential temperature recording, with an offset of approximately  $10^\circ\text{C}$ .

A Phantom 12.10 camera was used to observe the specimens during heating and through the process of ignition. This camera used a 300 mm fixed focal length lens at  $f4.5$ , and recorded between 20,000 and 40,000 pictures per second at exposures from  $5 \mu\text{s}$  to  $30 \mu\text{s}$ . Lighting was provided by high-intensity focusable LED lamps, and in most experiments a single lamp was used to illuminate the side of the specimen opposite the camera. HMX specimens were found to be generally more opaque to transmitted light at room temperature, and this opacity tended to persist up until ignition, whereas the transparency of RDX allowed the outline of larger crystals to be resolved. All images were captured at a resolution of  $32 \mu\text{m}$  per pixel. The camera memory was sufficient to capture 2.7 s of images at full resolution, but the low-speed video output from the camera was also recorded for the full length of the experiment.

## OBSERVATIONS

In RDX specimens heated at  $10^\circ\text{C}$  per minute, the specimen began melting at a temperature of  $204 \pm 5^\circ\text{C}$ , and the melted material remained until ignition at a temperature of  $214 \pm 5^\circ\text{C}$ , approximately 75 s after the onset of melting. Melting began with a brightening of the specimen at the circumference, progressing to complete melting approximately 15 s after onset. The specimen sank to the bottom of the test vehicle, forming a large transparent region occupying the entire upper portion of the specimen cavity, sometimes separated into smaller regions by thin 'webs' of liquid, and with smaller bubbles 1.0 to 1.5 mm in diameter at the liquid/gas interface.

Bubbles were noted to form within the melted material, beginning at the onset of melting and continuing until ignition. These were small, with diameters from 200 to 400  $\mu\text{m}$ , and formed at the bottom of the specimen, rising towards the top. This action produced a mass motion within the specimen similar to convection.

With continued increasing temperature the rate of formation of the smaller bubbles within the liquid region increased, with a corresponding increase in the size of the gas space above the liquid region. As bubbles emerged from the liquid surface into the gas space they tended to burst, and this set up small ripples in the liquid material clinging to the window. These ripples were measured to propagate at a speed of 1.0 to 2.0  $\text{ms}^{-1}$ , and are attributed to surface waves in the liquid clinging to the window.

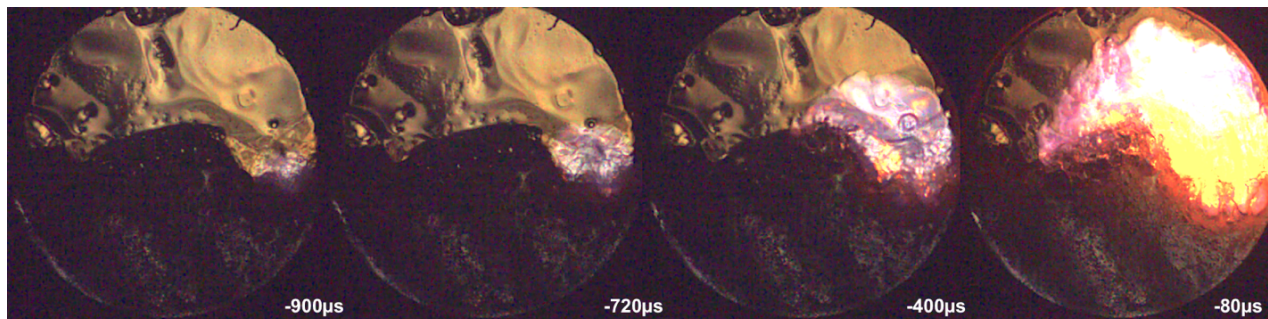


**FIGURE 2.** Onset and development of flame in RDX, pictures at 5  $\mu\text{s}$  exposure, annotated with time prior to shattering of the windows. The paler material at the top is the gas space, and this short exposure time reveals the liquid clinging to the glass windows.

In all experiments a luminous flame emerged at the interface between the liquid and gas, close to the circumference of the confinement, and the photographs shown in Fig. 2 are typical of this. The first evidence of luminous flame occurred 2–3 ms before violent de-confinement of the glass windows and the end of the experiment. In all experiments, these flames spread at a speed of 10–15  $\text{ms}^{-1}$  through the gas space, apparently accelerating. There was little evidence of burning into the liquid/solid region in the images, although the brightness of the flame eventually overwhelmed the camera, and detail was lost in the later stages of burning. However, as the flame developed, compression was clearly seen in the liquid region, as shown in Fig. 3.

In HMX specimens heated under the same conditions, the material around the circumference brightened in the same way as for the RDX specimen, and this was clearly due to the rear light beginning to shine through more transparent material. For 2 to 3 s, this bright region showed vigorous bubbling and the development of large gas bubbles, as shown in Fig. 4. The bulk of the specimen moved towards the bottom of the confinement. A dark region (labelled ‘B’) in Fig. 4, became apparent, spreading inwards toward the centre of the specimen. Prior to the onset of melting, the entire specimen was of a similar colour and texture to that seen in the region labelled ‘C’. Within region ‘B’, slight bubbling and motion could be seen towards the upper surface, suggesting its liquid or semi-liquid nature. This continued for approximately 10 s with increasingly vigorous bubbling, at which point the glass windows were shattered by the explosion.

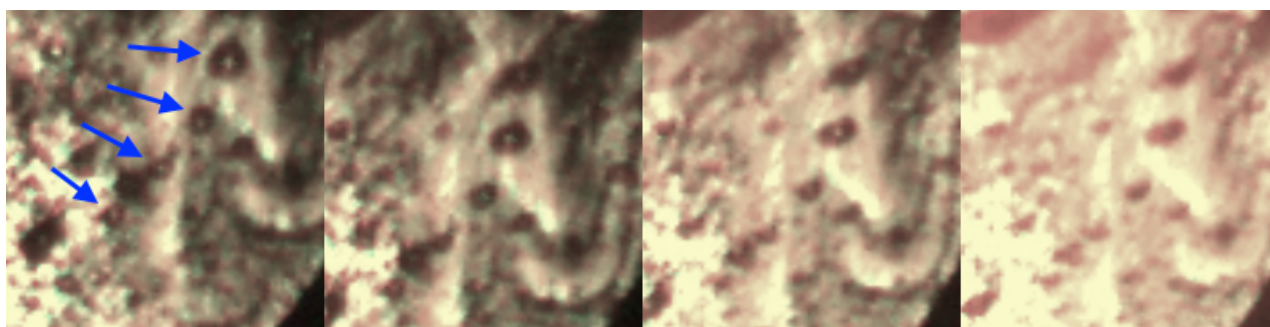


**FIGURE 3.** Compression of bubbles in RDX, at times as indicated prior to de-confinement. The luminous flame began at a point diametrically opposite the region shown. The field width of each image is 3.0 mm

The development of the explosion was observed until  $\sim 150 \mu\text{s}$  prior to final de-confinement, when the brightness of the flame obscured detail within the specimen. This process is shown in Fig. 4. A luminous flame began to grow

within one of the large bubbles at the top of the specimen, beginning at approximately 700  $\mu\text{s}$  prior to explosion. However, a thin web of liquid material was seen to be pushed away from the ignition site, beginning around 800  $\mu\text{s}$  prior to the emergence of the visible flame.

The visible flame propagated through the upper bubbled region, as shown in the later images in Fig. 4, but the material in regions 'B' and 'C' did not appear to flow or compress as was noted with RDX; compression and motion was only observed in the bubbled circumferential region. In the last 100  $\mu\text{s}$  prior to explosion, further luminosity was noted around the circumference developing ahead of the main flame front.

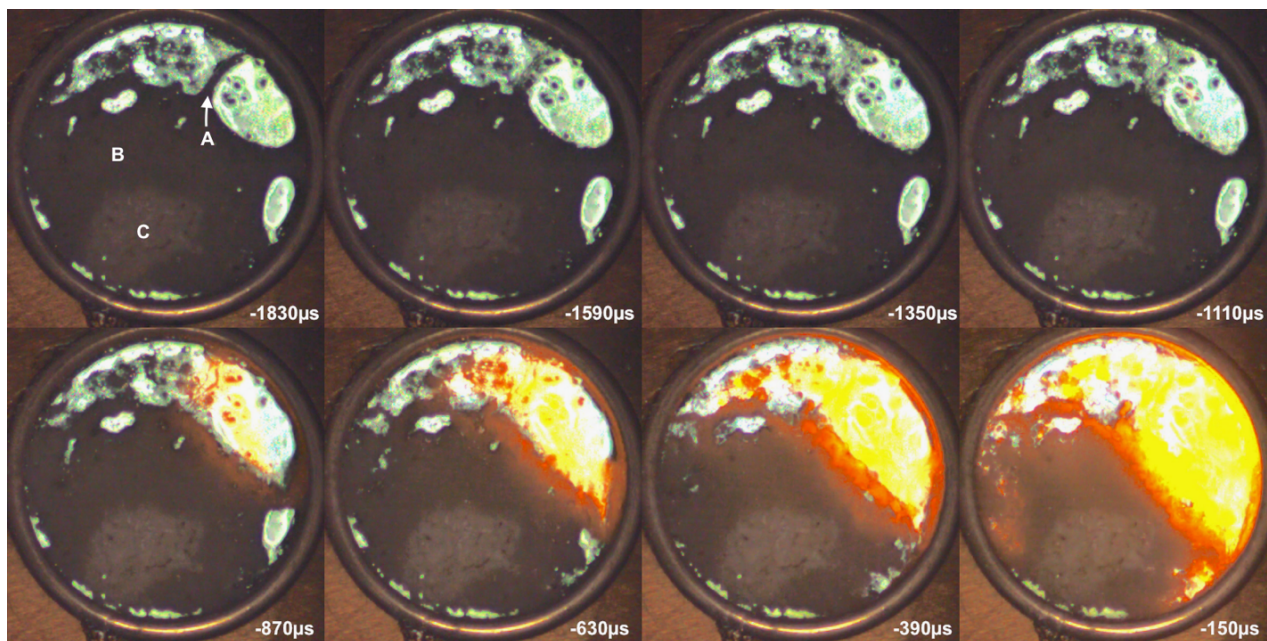


**FIGURE 4.** HMX from 1.8 ms prior to ignition. The disruption of the liquid web (arrowed 'A') moves towards the top left, prior to the onset of luminous flame  $\sim 700$   $\mu\text{s}$  later. The flame spreads through the gas bubble region, compressing material around the circumference, but not compressing the material in regions 'B' and 'C'

## DISCUSSION

In both HMX and RDX there is evidence of melting and formation of gas bubbles in the short time prior to the development of a luminous flame. At low heating rates in RDX it is possible for a complete melt pool to develop before deconfinement occurs, but melting is nevertheless quite extensive even at moderate to high heating rates. HMX, by contrast, does not undergo complete melting even at low heating rates. Differential scanning calorimetry (DSC) tests were performed on these specimens. In RDX the onset of exotherm occurred at 219.5  $^{\circ}\text{C}$  (immediately preceded by an endothermic phase indicating the onset of melting) and a peak exotherm at 241.8  $^{\circ}\text{C}$ ; in HMX the onset temperature was 280.5  $^{\circ}\text{C}$  and the peak at 285  $^{\circ}\text{C}$ .

RDX melts in a smooth and gradual way, beginning at the circumference of the specimen and moving inwards. This motion appears to be almost purely melting, with little evidence of gas production at the melt front. This melting results in the coalescence of entrapped air in the low-density specimen, to form a large gas-filled region above the porous liquid bulk. This region is therefore likely to be composed mostly of atmospheric air. The gas region can be separated into several regions by thin webs of liquid material. Bubbles begin to form within the bulk liquid zone, beginning just after the onset of melting and continuing until ignition. It might be speculated that these bubbles might begin to include nitramine in the vapour state, and possibly intermediate decomposition products, though further work would be necessary to verify or refute this.

Later, after melting, RDX bubbles are produced throughout the liquid material, resulting in a porous liquid with bubble diameters generally below 100  $\mu\text{m}$  (though a few are noted with diameters of 400 to 800  $\mu\text{m}$ ). These bubbles move quite slowly (0.05 to 0.1  $\text{ms}^{-1}$ ) so that convection-like mass motion in the melt pool is observed.



Although not directly measured, this mass motion is suggested to result in a relatively uniform temperature throughout the liquid component of the specimen.

The onset of melting in HMX is immediately accompanied by evidence of vigorous gas production at the periphery of the specimen (as with RDX) but the gas spaces are irregularly shaped and contain liquid material in rapid motion. The structure of the specimen is locally quite irregular but nonetheless has an overall arrangement of four roughly circular regions: around the circumference there is a mostly gaseous zone; inside this is a zone composed mostly of liquid material in less vigorous motion; next there is a zone in which virtually no motion is apparent, and which seems to consist of particles wetted by surface melting; at the centre is a zone which appears to be un-melted solid particles and which undergoes no motion at all. Filling density variations appear to persist through the melting phase and into ignition and flame propagation.

In RDX a luminous flame begins to develop from  $\sim 1,000 \mu\text{s}$  prior to final de-confinement, originating at the gas/liquid interface and spreading with an accelerating speed throughout the gas spaces. This is preceded by increasingly vigorous rippling in a small region  $\sim 0.5 \text{ mm}$  across. In experiments where two or more such zones of rippling were apparent, the flame originated at only one of these and it was interesting to note that the other regions did not seem to be affected by the flame as it overtook them, nor did the presence of the other regions seem to affect the propagation of the flame.

Digital image correlation (DIC) was used to measure the extent of compression noted in the RDX specimens after the onset of the luminous flame and until the developing flame obscured image details  $100 \mu\text{s}$  before final deconfinement. Fig. 5 (a) shows the maximum strain rate for two experiments, which show a broadly similar overall structure.

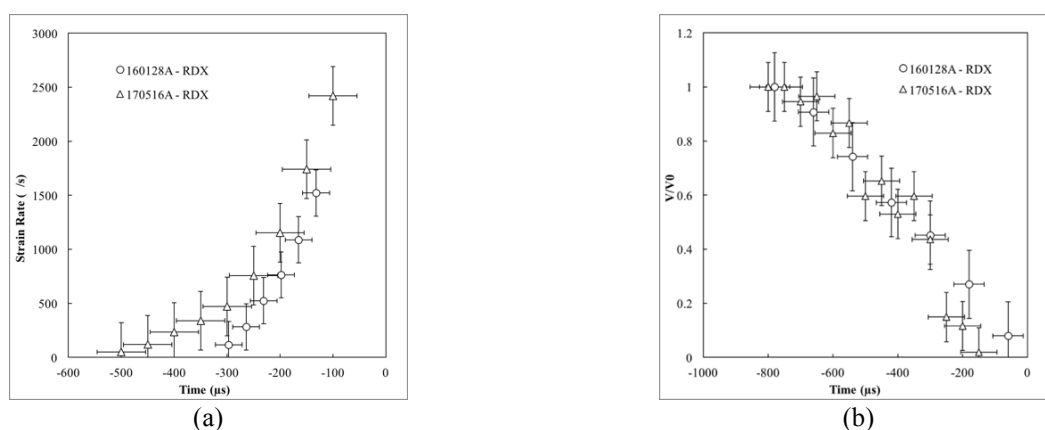


**FIGURE 5.** Compression in the liquid region in RDX specimens. Bulk strain rate (a) derived from digital image correlation; bubble compression ratio (b) derived from measurements of bubble diameter

For a small population of bubbles with diameters in the range  $150$  to  $450 \mu\text{m}$  in diameter, diameters were measured and, assuming a spherical geometry, the change in volume as a function of time were calculated. Bubbles larger than this size were not included in the compression analysis because the small specimen thickness ( $1000 \mu\text{m}$ ) would mean that the compression of the largest bubbles would be influenced by the confinement windows. The measured compression ratio as a function of time is shown in Fig. 5 (b).

Burning into the porous liquid region occurs more slowly than the flame spread, and instead, the increasing pressure due to the developing flame compresses the porous liquid at increasing strain rates up to  $2,000$  to  $5,000 \text{ s}^{-1}$  at the time of final de-confinement of the test vehicle. In HMX, a luminous visible flame develops in the gas spaces, again compacting the porous material nearby, but not compressing the solid or solid/liquid regions. The compression then appears to provoke further visible flame ahead of the initial flame front, and voids are seen to expand within this compressed region, and later to begin glow and develop new burning sites.

## CONCLUSIONS

It is clear that melting is an important physical mechanism for RDX and HMX that influences the location and initial propagation of the burning phase of the cook-off process. For materials which undergo complete melting, the microstructure of the crystalline solid placed into the confinement at the start of the experiment is completely

destroyed by the melting and is therefore irrelevant to the subsequent behaviour. Conversely, in materials where melting is only partial, it is possible that some features of the original microstructure may be preserved through the ignition and burning phase.

The extent of melting appears to be predictable from the difference between the melting and peak exotherm temperatures noted on DSC. Materials with a small temperature difference (such as HMX) are less likely to undergo complete melting, whereas those with a large temperature difference (e.g. RDX) can form complete melt pools. Melting is also likely to be influenced by the degree of ullage in the test cell. In these experiments the powdered, tap-density specimens only filled approximately 60% of the test cell, and this would have allowed relatively free motion during melting, leading to the observed arrangement where the solid and liquid components settled towards the bottom. For pressed specimens containing a binder, flow of the melted material would be expected to be more restricted and the overall structure at ignition would be quite different to that observed here.

In these few experiments at fast heating rates, the location of ignition may depend mainly upon the temperature distribution across the specimen, influenced locally by the microstructure set up as melting proceeds. The observed ignitions at liquid/gas interfaces close to the circumference of the specimen may therefore be peculiar to the heating rates and geometry chosen. For more uniform temperature gradients at slow heating rates, ignition may arise within the bulk of the specimen in either the solid or semi-liquid regions. The speed and nature of the spread of the burn front away from the first ignition site will depend strongly on whether the burn moves from a porous, melted region into a more solid region, or vice versa.

These observations suggest a possible mechanism of ignition, in which the visible flame begins at a point, grows, compresses the porous material, and provokes further mass ignition at multiple sites throughout the compressing region. This was observed in the HMX specimens, where breakout of visible flames ahead of the initial burn front were noted. However, these experiments were not sufficient to directly observe a possible mass ignition resulting from the compression of the entrapped gas bubbles in RDX. The compressive strain rates measured and presented could, however, be used to support or refute this hypothesis from a theoretical standpoint.

## REFERENCES

1. "Energetic Materials Test and Assessment Policy Committee Manual of Tests", UK Defence Ordnance Safety Group, 2007
2. M. R. Williams, M. V. Matei, "The Decomposition of Some RDX and HMX Based Materials in the One-Dimensional Time to Explosion Apparatus. Part 2. Estimation of the Violence of the Cook-off Event", *Propellants, Explosives, Pyrotechnics*, Vol. 32, 7 (2007)
3. C. L. Bauer, P. J. Rae, C. Stennett, H. M. Flower, "Small-Scale Thermal Violence Experiments for Combined Insensitive Explosive and Booster Materials", *Proc. 14<sup>th</sup> International Detonation Symposium*, ONR 351-10-185, 2014
4. J. F. Wardell, J. L. Maienschein, "The Scaled Thermal Explosion Experiment", *Proc. 12<sup>th</sup> International Detonation Symposium*, 2002
5. S. Y. Ho, "Thermochemical Properties of Rocket Propellants and Correlation with Cookoff Behaviour", *Propellants, Explosives, Pyrotechnics*, Vol. 20, 206 (1995)
6. L. Smilowitz, B. F. Henson, J. J. Romero, B. W. Asay, C. L. Schwartz, A. Saunders, F. E. Merrill, C. L. Morris, K. Kwiatkowski, G. Hogan, P. Nedrow, M. M. Murray, T. N. Thompson, W. McNeil, P. Rightley, and M. Marr-Lyon, "Direct Observation of the Phenomenology of a Solid Thermal Explosion Using Time-Resolved Proton Radiography", *Phys. Rev. Lett.*, **100**, 228301 (2008)
7. S. F. Son, H. L. Berghout, C. A. Bolme, D. E. Chavez, D. Naud, M. A. Hiskey, "Burn Rate Measurements of HMX, TATB, DHT, DAAF and BTATz", *Proceedings of the combustion Institute*, Vol. 28 (2000), p919
8. C. Stennett, M. D. Cook, R. I. Briggs, P. J. Haskins, J. Fellows, "Direct Observation of Cook-off Events Using a Novel Glass-Windowed Vehicle and Pipe Bombs", *Proc. 12<sup>th</sup> International Detonation Symposium*, 2002
9. M. D. Cook, C. Stennett, P. J. Haskins, R. I. Briggs, A. D. Wood and P. J. Cheese, "The Role of Binders in Controlling the Cook-Off Violence of HMX/HTPB Compositions" in *Shock Compression of Condensed Matter-2005*, Conference Proceedings 620, edited by M.D.Furnish et al. (American Institute of Physics, Melville, NY)
10. P. J. Cheese, T. Reeves, N. White, C. Stennett, A. Wood, M. D. Cook, "Development of a Dual-Windowed Test Vehicle for Live Streaming of Cook-off in Energetic Materials", *ibid*



## A.9 One Dimensional Thermal Violence ...

---

Authors:	Cook, M.D.; Stennett C		
Title:	One-Dimensional Thermal Violence Cook-off Test		
Publication Type:	Journal	Venue:	APS SCCM 2017
Date:	Jul 2017		

---

# One-Dimensional Thermal Violence Cook-Off Test

Malcolm D. Cook<sup>1a</sup>, and Christopher Stennett<sup>2</sup>

<sup>1</sup>*AWE plc, Aldermaston, Reading, Berkshire RG7 4PR, UK.*

<sup>2</sup>*Centre for Defence Chemistry, Cranfield University, Defence Academy of the United Kingdom, Shrivenham, SN6 8LA, UK*

<sup>a</sup>Corresponding author: malcolm.cook@awe.co.uk

**Abstract.** The One-Dimensional Thermal Violence (ODTV) test is designed to quantify and rank the violence of HE charges when heated to elevated temperatures. The test design consists of a central spherical explosive pellet encased in two aluminium barrel shaped halves, fitted with a copper sealing ring, encased by two aluminium locking rings placed over them from either end. The outer surface of the capsule is heated uniformly by placing in a pre-heated molten melt alloy bath. This allows the time-to-explosion to be recorded for different initial bath temperatures. The ODTV capsule can hold samples up to 30mm in diameter. Diagnostics include both thermocouples and Photon Doppler Velocimetry (PDV). A series of live firings have been carried out on a range of bespoke HMX/HTPB explosives. These include HMX/HTPB mix ratios of 95/5, 92/8, 90/10, 88/12 and 85/15. These tests showed that the ODTV capsule had sufficient confinement and size that it could capture the spectrum of events expected from these formulations. It has been demonstrated that PDV wall velocities of the aluminium ODTV capsule can be used as an additional violence metric along with the capsule fragmentation.

## INTRODUCTION

The One-Dimensional-Thermal-Violence (ODTV) experiment, described in this paper, was primarily devised to determine Cook-Off violence while providing data for models. The ODTV capsule was design to hold spherical samples up to 30mm in diameter which were deemed large enough to capture the violence of the test material. The design employs a double shell arrangement such that the two halves of the inner vehicle are orthogonal to the outer casing, which improves confinement. This arrangement means that the hoop strength of the outer rings controls the confinement rather than the strength of the bolts. Heating is by immersion of the ODTV capsule in a hot molten melt alloy bath preheated to a set temperature. By repeating over a range of initial temperatures until thermal explosion is observed, this test can replicate the smaller ODTX test [1], [2]. Furthermore, unlike the ODTX test, it does not require a dedicated machine and can be deployed in a standard firing facility. Particular features of the test are that: it offers high confinement (ca. 300MPa); the capsule can be heated from a set temperature or using a ramp; it has a range of instrumentation including thermocouples and Photon Doppler Velocimetry (PDV) [3]. PDV laser interferometry allows highly time-resolved measurements of the expansion of the confinement at the instant of ignition and beyond, which together with case fragmentation provides an additional metric for event violence.

## EXPERIMENTAL

The One-Dimensional Thermal Violence (ODTV) test capsule (Figure 1) was designed around a 30 mm diameter spherical central charge. The central spherical explosive pellet was encased in two aluminium barrel shaped halves fitted with a copper sealing ring. The aluminium barrel was further encased by two outer aluminium rings deployed from either end which force the inner barrel halves together. These outer rings were held together by two groups of four opposing bolts. The arrangement is shown in Figure 1 where the central 30 mm diameter

spherical test pellet can be seen coloured yellow, the copper sealing ring is shown in red and the outer cylindrical locking rings that bolt together using eight bolts (four from opposite ends) to form the completed capsule.

The barrel shape ensures that the inner and outer metal shells of the confinement capsule are easily aligned. This provides enhanced confinement, provided by the hoop strength of the outer rings. This can be compared to designs that house the explosive sample in the hollow between two metal blocks held together with bolts. In this instance the confinement is controlled by the strength of the bolts.

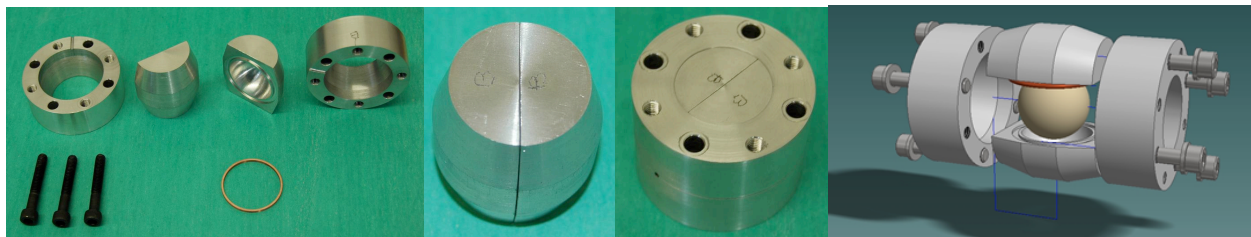


**FIGURE 1.** Photographs of ODTV capsule parts (left image), inner barrel housing the explosive sphere (centre left image) and completed capsule (centre right image). An exploded cartoon of the ODTV confinement capsule showing how the major components join together is shown in the right-hand image.

The capsule was heated in a cup formed from a steel plate welded to a 75 mm square-section steel tube with 6 mm thick walls, wrapped in a heating coil, overwrapped with additional glass-tape insulation and held in place with wire. The depth of the container was 150 mm, and the internal cross section was 68 mm square, which was sufficient to allow 4mm clearance around the capsule. Standard solder, which melts at approximately 180°C and could be heated in excess of 300°C was utilised as the heat transfer medium. The heater bath was typically heated to a set temperature before immersing the ODTV capsule. The whole process was tested and rehearsed using an empty ODTV capsule before live testing.

Thermocouples were deployed in the heater bath, to monitor and control the solder temperature, and in a hole machined between the outer rings. In Figure 1 (left image) this appears as the groove in the outer rings and allowed monitoring of the temperature of the capsule at the interface between the barrel wall and the outer locking rings.

Some experiments have been performed with a modified specimen cavity that includes a machined probe pocket. This probe pocket was designed to accommodate three fine-gauge thermocouples to measure the temperature at points along the radius of the sample, while retaining the capsules high pressure-sealing capacity. Unfortunately, this design does not allow direct reading of the local specimen temperature and heat flow in the walls of the pocket influences the thermocouples readings.

The ODTV capsule was arranged with its cylindrical axis horizontal. This allowed the internal thermocouple package to be deployed vertically along with the fibre-coupled collimator lens for the PDV, and a piezo-electric trigger probe to provide a signal at the instant of explosion. This vertical arrangement of the instrumentation helped prevent direct contact with the molten solder and avoid spurious readings. The external instrumentation was mounted within a metal support frame attached to the capsule. In the experiments where an internal probe pocket was not used, an external K-type thermocouple was placed in the hole between the two locking rings.

A remote deployment method was used to deliver the filled ODTV capsule to the pre-heated solder bath. The relative densities of the capsule and the heating medium required that the capsule be positively immersed into the heater bath, rather than simply allowing the capsule to sink into the hot metal under its own weight. When immersed, the use of the PDV required that the top surface of the capsule be above the level of the molten metal in the heater bath.

The PDV output was recorded on two oscilloscopes. The interferometer data were reduced using the well-known FFT technique [4] to obtain a time-resolved Spectrogram image representing the velocity of the surface, using a piece of purpose-developed software. The software included the ability to capture velocity data points from the image with an accuracy of 1% in the velocity domain and 2% in the time domain with minimum effort.

The test specimens consisted of compositions of HMX and cured, cross-linked HTPB. These compositions are detailed in Table 1. In all compositions, the HMX was Type B (RDX < 2%) with a particle size Class 2, passing a 45  $\mu\text{m}$  ASTM sieve. The HTPB was R45M grade, fast cured and cross-linked with IPDI and MDI. These compositions have been used in other experimental work reported by the authors at this conference.

**TABLE 1.** HMX/HTPB test compositions.

HMX weight %	HTPB weight %	Density g cm <sup>-3</sup>	% T.M.D
95 ±0.25	05 ±0.25	1.32 ±0.1	72
92 ±0.25	08 ±0.25	1.48 ±0.1	82
90 ±0.25	10 ±0.25	1.55 ±0.1	87
88 ±0.25	12 ±0.25	1.60 ±0.1	91
85 ±0.25	15 ±0.25	1.61 ±0.1	93

The specimens were hand filled into the test vehicles in an uncured state, after which the vehicles were assembled and allowed to oven-cure at 60°C for 7 days. The resulting materials had a lower than typical density, and a greater range of defects and inhomogeneity's than would be expected in production-grade materials.

## RESULTS

In total, fifteen live firings were carried out. Three experiments were run for each composition type, at bath temperatures in the range 190 to 250°C. The aim was to produce plots of time to explosion versus set temperature analogous to those obtained in ODTX experiments as well as violence metrics.

The efficiency of heating the sample was dependent on the position of the capsule in the bath and the capacity of the heating element. The former is due to heat losses to the surrounding air and the latter due to the low heat capacities of the steel heater cup, molten metal alloy and aluminium ODTV capsule. This latter effect is manifest in the cooling of the heating medium after insertion of the (cool) capsule such that once temperature equilibrates the heating rate is governed by the capacity of the heating element. Despite these drawbacks it can be shown that the heater bath technique is more efficient at rapidly heating the capsule than applying an electrical heater tape to the capsule surface and heating from cold. Furthermore, the deployment of thermocouples in the capsule and PDV on the surface allows the exact bath / sample temperatures to be monitored and the surface velocity history to be recorded.

**TABLE 2.** Metrics of violence: ODTV capsule fragments and change in heater bath volume as a function of composition.

Composition (HMX/HTPB)	Set Temperature (°C)	Capsule Surface Temperature at explosion (°C)	Time to Explosion (s)	Wall velocity at 1.5mm displacement (ms <sup>-1</sup> )	Number of fragments	Change in heater bath volume (cm <sup>3</sup> )
95/05	215	215	1455	101.4	16	Broken
95/05	220	200	1107	105.4	18	Broken
95/05	230	195	1355	92.8	22	Broken
92/08	190	214	9600	89.0	14	111
92/08	220	190	1572	70.6	14	83
92/08	240	195	973	56.2	11	129
90/10	205	205	2879	52.8	9	82
90/10	210	210	2097	30.8	8	89
90/10	230	200	1031	22.1	4	28
88/12	215	230	762	46.6	4	N/A
88/12	230	180	712	65.0	4	<20
88/12	230	230	650	16.0	4	<20
85/15	200	210	1555	101.4	7	39
85/15	230	190	684	105.4	8	66
85/15	250	190	447	92.8	4	22

The explosions provoked in the experiments destroyed the capsule in every case, resulting in complete loss of confinement. Two features of the resulting damage have been recorded: the number of capsule fragments and the change in volume of the heater bath structure (see Table 2). The 95/5 composition completely shattered the heater bath as well as causing considerable damage to the capsule. Despite this the results show a correlation between the

number of fragments and the average change in heater bath volume across the compositions. The relationship between the set temperature and the change in heater bath volume is less clear, although the average heater bath volume does match the trend of violence: 95/5 completely broken and therefore more violent than 92/10 (108 cm<sup>3</sup>); is more violent than 90/10 (66 cm<sup>3</sup>); is more violent than the 85/15 HMX/HTPB composition (42 cm<sup>3</sup>).

The plots in Figure 2 show the time to ignition plotted against the set-point temperature and also as the natural logarithm of time-to-explosion versus reciprocal temperature for each composition. It can be seen that the results from this work largely span ODTX data for a high density pressed HMX/HTPB 95/5 formulation. From the firings carried out here, it appears that the higher the binder content the lower the time to explosion implying that the binder decomposition contributes significantly.

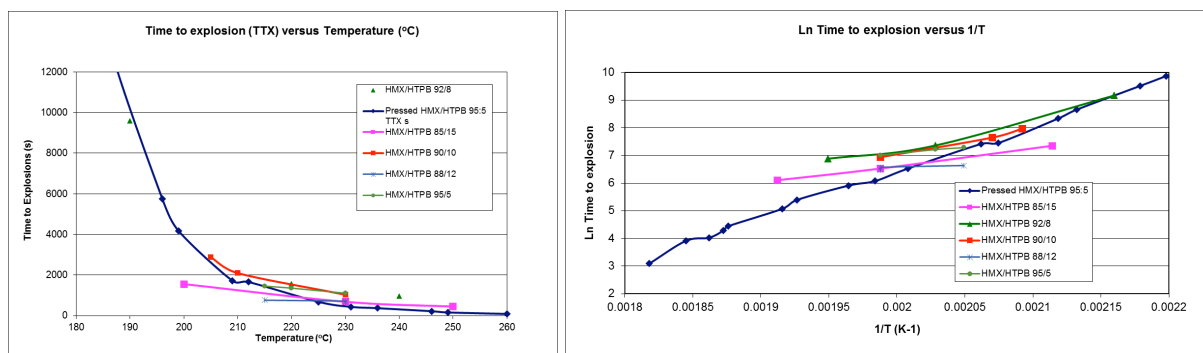


**Figure 2:** Time to explosion versus temperature (°C) and Ln time-to-explosion versus reciprocal temperature for the five HMX/HTPB compositions tested here and a high density pressed HMX 95/5 formulation.

The PDV data covering the initial motion of the outer surface of the aluminium capsule after explosion are summarised in Figure 3. In this plot, the surface velocity of the capsule is plotted as a function of displacement.

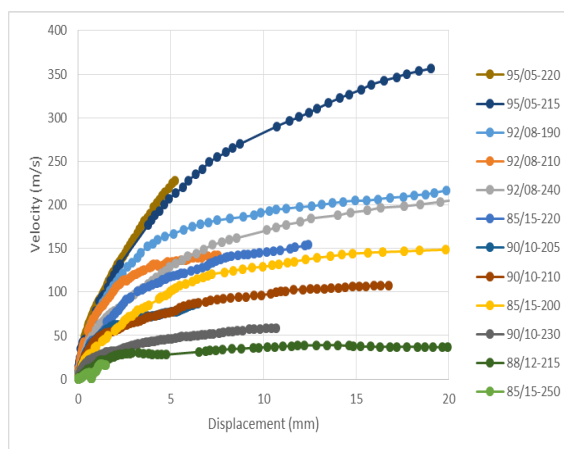


**Figure 3:** Heterodyne velocimetry data showing velocity as a function of displacement.

It can be seen, from the experiments performed in this study that the wall velocity for the 95% composition are all higher than those for the 92% composition and these are all greater than those for all the other compositions. Note, however, that there is also a broad trend of increasing velocity with decreasing temperature so that care should be taken when comparing different compositions that experiments are at the same temperature.



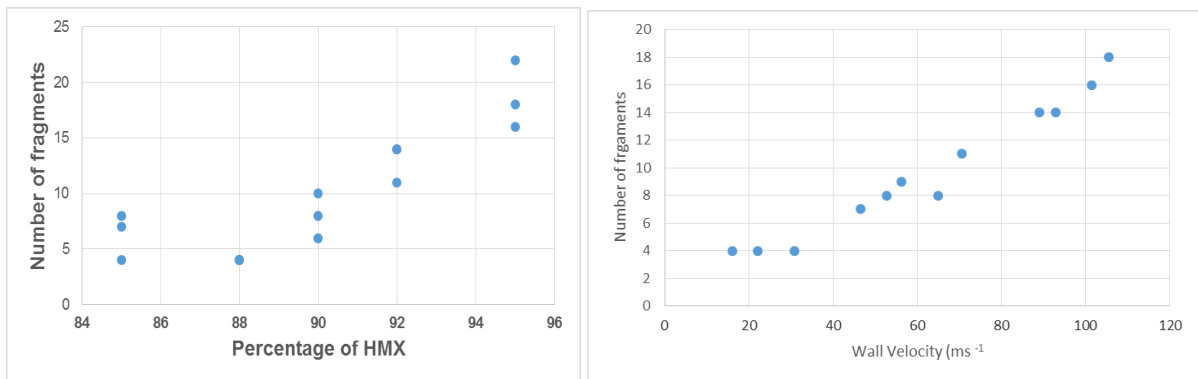


**Figure 4:** Percentage of HMX plotted as a function of degree of fragmentation of the capsule and wall velocity

The data shows the general trend of decreasing violence with increasing temperature with the 95/5 HMX/HTPB formulation producing generally more violent reactions than the 92/8, 90/10, 88/12 and 85/15 formulations.

Figure 4 shows a plot of wall velocity against number of fragments and there appears to be a good correlation between the two. This demonstrates that, in this test configuration, the PDV records correlate well with the number of fragments obtained and therefore PDV can be used as a metric of violence. A similar trend is observed between percentage of HMX in the formulation and the degree of fragmentation of the capsule. One feature that stands out is that the 85/15 composition appears to produce a wider variety of responses and appears to produce more violent reactions than the 88/12 mix. The results also suggest that there may be a ‘sweet spot’ of binder content (in these tests 88/12 HMX/HTPB) above which the violence increases slightly. It would be beneficial to carry out more firings to confirm this behaviour.

## CONCLUSIONS

The One-Dimensional Thermal Violence (ODTV) test capsule has been successfully designed around two inner aluminium barrel shaped shell halves that hold a spherical sample and two outer cylindrical aluminium casing halves. The outer casing split is orthogonal to the inner shell halves such that failure is determined by the hoop strength of the outer rings. The outer cylindrical casing halves are bolted together to form the complete capsule.

The current ODTV capsule can hold samples up to 30 mm in diameter. A heating method based on a pre-heated molten solder bath has been developed and tested using a range of bespoke cast cured HMX/HTPB based formulations. These include HMX/HTPB mix ratios of 95/5, 92/8, 90/10, 88/12 and 85/15 that are known to give a spectrum of reaction violence levels the 95/5 being the most violent. A series of tests were carried out at three set temperatures per explosive formulation and these showed that the vehicle had sufficient confinement and size that it can capture violent events. A hollow finger machined into one ODTV barrel half has been demonstrated to allow the thermal profile across a sample to be captured without compromising confinement. In addition PDV has been deployed and demonstrated to provide a viable metric of violence in the geometry employed.

The results obtained for the time-to-explosion for the HMX/HTPB formulations employed in this work largely span those for a 95/5 HMX/HTPB formulation, pressed to high density, tested in the ODTX apparatus. This provides strong evidence that the ODTV test produces similar data in terms of time-to-explosion as the ODTX test.

Analysis of the PDV records can be made in terms of the capsule wall velocity and this correlates well with the number of fragments. This suggests that PDV can be used as a metric for violence in this test configuration.

The results show that the higher the HTPB binder content the lower the time to explosion implying that the binder decomposition contributes significantly to the reaction. The 85/15 HMX/HTPB composition showed a tendency to be more violent than the 88/12 formulation which also adds weight to this finding. There is a possibility that the 88/12 formulation represents a ‘sweet spot’ in the formulation space.

## REFERENCES

1. E. Catalano, R. McGuire, E. Lee, E. Wren, D. Ornellas, and J. Walton, "Thermal Decomposition and Reaction of Confined Explosives", *6<sup>th</sup> Symposium (International) on Detonation*, Coronado, CA, August 24-27, 1976, Office of Naval Research ACR-221, pp. 214.
2. R. R. McGuire and C.M. Tarver, "Chemical Decomposition Models for the Thermal Explosion of Confined HMX, TATB, RDX, and TNT Explosives", *7th International Detonation Symposium 1989*.
3. D. H. Dolan, "Accuracy and precision in photonic Doppler velocimetry", *Review of Scientific Instruments*, 81:053905, 2010.
4. D. N. Rockmore, "The FFT: an algorithm the whole family can use", *Computing in Science Engineering*, 2(1): 60-64, January 2000.
5. R. C. Drake and I Belcher, "Effect of HMX Particle size on the Times to Explosion of HMX Charges", *Fifteenth International Detonation Symposium*, ONR-43-280-15, 2015, pp1496-1505.

©British Crown Owned Copyright 2017/AWE



## A.10 Development of a Dual-Windowed ...

---

Authors:	Cheese, P., Reeves, T., White, N., Stennett, C., Wood, A., Cook, M.D.		
Title:	Development of a Dual Windowed Test Vehicle for Live Streaming of Cook-off in Energetic Materials		
Publication Type:	Journal	Venue:	APS SCCM 2017
Date:	Jul 2017		

---

# Development of a Dual Windowed Test Vehicle for Live Streaming of Cook-Off in Energetic Materials

Phil Cheese<sup>1</sup>, Tom Reeves<sup>1</sup>, Nathan White<sup>1</sup>, Christopher Stennett<sup>2</sup>, Andrew Wood<sup>3</sup>  
and Malcolm D. Cook<sup>3,a)</sup>

<sup>1</sup>*Defence Equipment & Support, MOD Abbey Wood, Bristol, BS34 8JH, UK*

<sup>2</sup>*Centre for Defence Chemistry, Cranfield University, Defence Academy of the United Kingdom, Shrivenham, SN6 8LA, UK*

<sup>3</sup>*Syanco Ltd, PO Box Box 411, West Malling, Kent, ME6 9EZ, UK*

<sup>3a</sup>Corresponding author: malcolm.cook@syanco.co.uk

**Abstract.** A modular, axially connected test vehicle for researching the influence of various heating rates (cook-off) on energetic materials and how they fundamentally decompose, leading to a violent reaction has been developed and tested. The vehicle can accommodate samples measuring up to 50 mm in diameter, with thicknesses variable from 0.5 mm up to 50 mm long. A unique feature of this vehicle is the ability to have a live high speed camera view, without compromising confinement during the cook-off process. This is achieved via two special windows that allow artificial backlighting to be provided at one end for clear observation of the test sample; this has allowed unprecedented views of how explosives decompose and runaway to violent reactions, and has given insight into the reaction mechanisms operating, and challenges current theories. Using glass windows, a burst pressure of 20 MPa has been measured. The heating rate is fully adjustable from slow to fast rates, and its design allows for confinement to be varied to study the influence on the violence of reaction during cook-off. In addition to being able to view the test sample during cook-off, embedded thermocouples provide detailed temperature records and the ability to use Photon Doppler Velocimetry (PDV) instrumentation is also incorporated.

## INTRODUCTION

Cook-Off test vehicles typically comprise a metal (steel or aluminium) cylinder sealed either end with the energetic material placed inside. The level of confinement depends on both the wall thickness and the quality of the seal. If the dimensions of the vehicle are adjusted to accommodate a right regular cylindrical charge it approaches a more symmetric geometry. A spherical charge represents the simplest 1D geometry. While it is possible to deploy internal thermocouples and sample the pressure of the product gases this can compromise confinement. More challenging is to attempt to directly observe the various changes and processes as the charge is heated until thermal explosion is achieved. Researchers at LANL have developed the Lab-scale Asynchronous Radiographic System (LARS), a small-scale radiography device for continuous high-speed x-ray imaging of spontaneous dynamic events, such as thermal explosions, reaction-front propagation, and material failure. This system can provide an x-ray movie revealing density changes within the energetic material contained in a metallic Cook-Off bomb [1]. Such systems are costly to build and deploy and do not necessarily provide a complete picture of the physical and chemical changes occurring when a confined energetic material is heated to elevated temperatures.

Modern high-speed video cameras combined with transparent windows offer a more cost-effective solution to observe the Cook-Off process. Only one other research group has reported the use of glass or sapphire windows combined with high-speed photography to observe the Cook Off process [2]. However, their work was hampered by the need to trigger the event so that it could be captured by the camera. This was achieved by heating a wire placed

at the centre of the charge. Hobbs et. al. [3], have used a borescope to visually observe the decomposing PBX during Cook-Off in their SITI test and obtained information about the onset of phase changes, expansion and foaming.

The test vehicle described in this paper was designed to allow the decomposition of energetic materials (when heated to elevated temperatures) to be directly observed using a modern high speed video camera with the aim of developing an understanding of the processes controlling cook-off. The test vehicle differs from other designs in that it is flexible accommodating sample sizes from 1mm thick layers 15mm in diameter up to a 50mm right regular cylinder. The windows can be replaced with metal end plates to represent a more conventional all metal Cook-Off test vehicle. As well as development of the test vehicle the Advanced Cook-Off Experimental (ACE) approach encompassed Cook-Off testing of a range of energetic systems, including: pressed/cured formulations; melt-cast formulations; and pure materials. In this manner, an improved understanding of the mechanisms leading to Cook-Off violence has been achieved. This work is aimed at developing a quantitative predictive modelling capability.

## TEST VEHICLE DESIGN REQUIREMENTS

There are a number of significant challenges when attempting to study the Cook-Off of energetic materials. Firstly, the process occurs over a range of time-scales spanning the initial heating, which can take place over many hours and includes physical as well as chemical changes such as phase changes, through to the final violent response which occurs sub-microsecond. In between, the initial decomposition which is followed by burning occurs in the millisecond regime. In addition, the Cook-Off process is confinement and sample size dependent. An experimental design is required to follow the evolving processes over the entire duration of the event.

Methods to directly observe Cook-Off of energetic materials using glass-windowed Cook-Off vehicles have been reported previously [1]-[5]. In the work of Dickson et. al., discs of PBX 9501 were heated with a confining glass or sapphire window through which the early stages of the combustion process could be observed directly by high-speed photography. The Cook-Off event was triggered using a hot wire at the centre of the charge in order to capture the event. Cook et. al., used a similar single glass windowed vehicle combined with real time video photography to attempt to capture images of events when the test material was heated until Cook-Off.

These early experiments were hampered by lack of suitable lighting and high-speed imagery covering the entire duration. A further complication is the fact that it is not possible to predict the exact occurrence particularly of the final event. With the introduction of light sensitive high-speed video cameras using post trigger technology it is now possible to capture Cook-Off events routinely using glass windowed test vehicles. Modern high-speed video cameras also have the advantage of being able to stream live real-time video records before the camera is triggered. This allows both the long-time heating, and associated physical changes, to be recorded as well as the sub-millisecond final events.

The design features of the dual glass-windowed Cook-Off test vehicle used in this work include: flexible sample size up to a maximum of a 50 x 50mm right regular cylinder; the ability to back light through thin layers of test material; the ability to replace the glass windows with steel end plates; and the ability to deploy both high-speed video and PDV instrumentation. The final design was achieved by means of modelling both the heat transfer and mechanical failure of the vehicle. Heat flow modelling was carried out to ensure that the heat transfer into the sample was adequate and occurred primarily from the circumference of the sample. Structural failure was determined from the computer aided design package and hydrocode simulations. The burst pressure was estimated to be in excess of 20MPa.

## TEST VEHICLE DESCRIPTION

The test vehicle has been designed around a three part system made from steel. An image of the constituent parts is shown alongside a cartoon of the assembled vehicle in Fig. 1. The parts are shown labelled in Fig. 1 as follows: (1) the outer ring (with inner thread); (2) inner locking ring (with outer thread); (3) glass window cylinder or steel end plates; (4) central steel sample locating ring; (5) explosive sample; (6) containment ring.

The three outer rings bolt together. The two end rings are threaded to take inner threaded locking rings. The middle ring houses the sample. An inner middle ring can be machined to take a variety of thicknesses and diameters of explosive pellets. The sample is confined by means of cylindrical glass blocks placed either end, or steel plates or,

indeed a combination of both. Gaskets play onto the inner central steel sample ring to form a gas-tight seal. The whole structure is bolted together by means of two sets of three bolts applied from both ends. Final adjustment of the confinement is made by means of the locking rings which bear down on gaskets placed next to the glass blocks. Heating of the vessel is achieved by means of three heater rods held within dedicated holes within the cylinder walls.

Thin explosive samples are held in within the inner middle metal ring in order to make the whole sample within the observation of the window, and to provide a bearing surface against which gaskets will provide a gas-tight seal around the explosive specimen. The central section ensures adequate confinement for the explosive samples. It also allows a variety of sample sizes.

Borosilicate glass has a very low coefficient of thermal expansion, and a high (820°C) softening point. The window dimensions selected for this study are nominally 19mm thick, and 50mm diameter. This is identical to that deployed previously [4],[5].

Thermocouple wires can be deployed horizontally in the gap between two sections. A suitable gasket material prevents escape of product gases before thermal explosion. For thicker samples, where thermocouples are deployed, the explosive may need to bridge between two end sections. Thermocouples can also be deployed vertically through steel end plates that replace one of the outer locking rings.

The maximum explosive sample size that can be accommodated is a 50 x 50mm cylindrical pellet. This size was chosen in order to ensure that the vehicle was capable of capturing the true violence of the test materials.

PDV can be used in tests where one or both glass windows are replaced with metal plates or where a suitable reflecting surface can be effected at the explosive surface through the glass window(s). This technique allows for the capture of plate velocity history and therefore distinguish pressure waves within the system and can be used, alongside the deformation in the base plate (if deployed), as a measure of explosion violence.

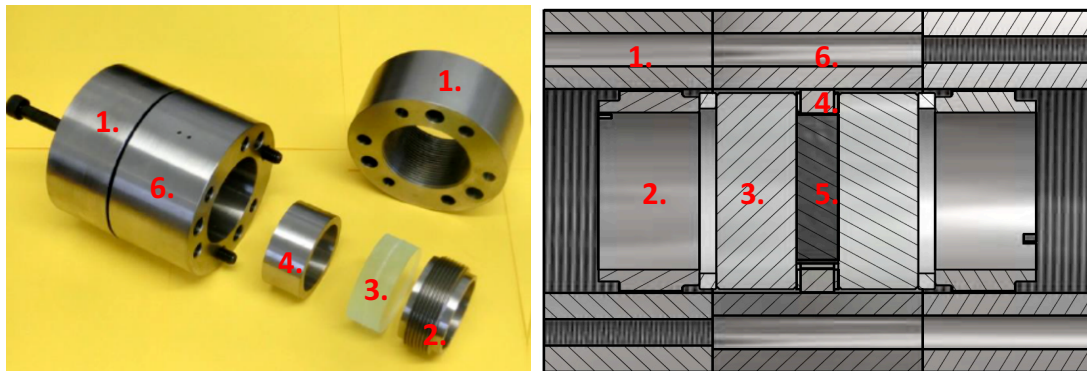


**FIGURE 1.** Photographs of ACE test vehicle parts (left image) and cartoon of the assembled vehicle (right image).

## TEST VEHICLE CONFIGURATIONS

The test vehicle has been deployed in three configurations [6]-[8]. The principle configuration used dual glass windows with thermocouples radially positioned at various depths in the test sample. Sealing was achieved by means of fibre gaskets. This configuration was used with samples up to the maximum size of the test vehicle.

A modification of the dual glass-windowed setup was required when small samples were deployed. A high precision commercially available 'C' seal was used for samples 15mm in diameter and 1mm thick. This arrangement was used for the majority of the tests performed and allowed details of the Cook-Off process to be followed by back lighting through the thin sample. Multiple tests have shown that the small sample size can produce violent events in a range of energetic materials. The operation of the 'C' seal is shown in the cartoon in Fig. 2. Also shown in Fig. 2 are photographs of a partially built test with a sample housed in a 'C' seal and the completed vehicle ready for testing.

The final configuration replaces the glass windows with steel end plates. This configuration is more in line with conventional steel cased Cook-Off pipe bombs. This arrangement offers increased confinement and sample size up to the full capacity of the vehicle. The metal plate thickness can be adjusted to suit the required confinement conditions. It also allows the deployment of thermocouples axially through one or both of the plates. PDV can be

deployed along the axis of either plate. PDV gives a detailed record of the steel plate velocity which can be used as an indication of reaction violence. Complimentary information about the reaction violence can be obtained by post examination of the recovered end plate pieces. To illustrate this effect Fig. 3 shows end plates recovered from tests that showed increasing violence.

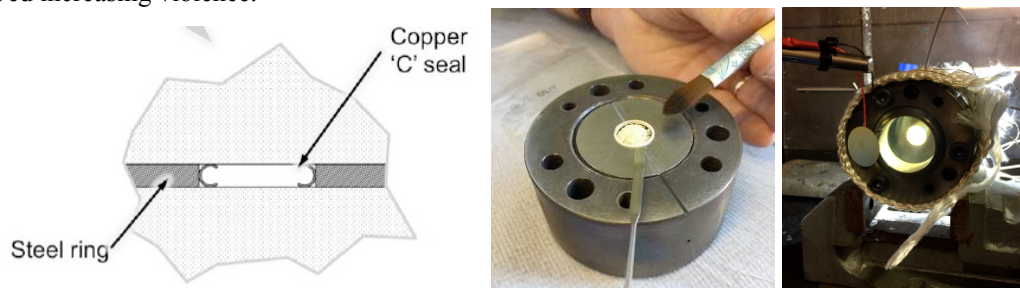


FIGURE 2. A cartoon and photographs showing a 'C' seal deployed in a test vehicle.



FIGURE 3. Photographs of steel end plates recovered from separate tests showing increased violence from left to right.

## OVERVIEW OF TESTS PERFORMED

Over 112 tests have been performed utilising the three configurations described above. A range of heating rates have been applied although the typical heating rates of 1°C and 10°C per minute have been used for the majority of the tests to date.

A range of materials have been tested. Neat crystalline energetic materials including: RDX, HMX, TNT, PETN, TETRYL, TATB, FOX-7, DNAN, NTO, PZO having been examined in the 'C' seal configuration. In addition, sample mixes such as RDX/TNT, DNAN/NTO, RDX/TATB have been examined. These tests have revealed a lot of information about the mechanisms and behaviour of these materials when heated to elevated temperatures. These materials generally undergo: phase changes (some with associated volume changes); melting; decomposition; variable amounts of bubbling; burning of the gas phase (intermediates) and final accelerated burning.

We have also examined a range of HMX/HTPB PBX formulation ranging in 85-95% HMX solid loading as well as HMX based PBX formulations with either HyTemp/DOA or Viton binder systems and an aluminium content of between 10 and 20%. Neat RDX and HMX and HMX/HTPB compositions have been used in other experimental work reported at this conference [6]-[8].

This short paper cannot give detailed information regarding the experimental results of all the samples tested. Here we summarise some general observations. On heating a given composition polymorph phase changes, such as the renowned HMX  $\beta$ - $\delta$  can be observed through expansion of the sample to fill more of the space and in the thermocouple data. At some point colour changes and, or, darkening of the sample can be seen which is an indication of flameless decomposition. Such observation are often made in formulations with binder whereby the binder decomposes prior to the energetic filler. Melting of energetic filler and subsequent bubbling is typically observed before any luminous flame. A few materials, such as TATB, do not appear to exhibit significant melting of the body of the material before the luminous flame is observed. However, most of the common ones do and some show gradual colour changes from clear through yellow, red and eventually turn very dark (e.g. TNT and Tetryl). When ignition of the gas phase finally occurs it is typically observed at the gas/liquid interface. The subsequent burn



of the gas phase rapidly increases the pressure experienced by the bubbling molten energetic filler causing local mass movement of both molten and any remaining solid material. If confinement is lost before luminous flame is seen then any event is typically mild. Once the luminous flame is observed the reaction rapidly runs away even if the confinement is subsequently lost.

Figure 4 shows a few frames from the high-speed video record of heated neat RDX. Molten bubbling RDX liquid can be seen to bottom of the image and two pockets of gaseous intermediate to the top. The luminous flame is seen to originate at the gas-liquid interface where it is hottest and progress at about 10m/s across the gas phase. This compresses the liquid layer and the bubbles. It is thought that escalating collapse of the bubbles which contain reactive intermediate gases in a domino effect, is what is responsible for the very violent reaction.

It seems that a good binder appears to compartmentalise the process leading to a milder controlled burn and less violent events assuming that there is sufficient of it. Binders with high melting temperatures can entrap molten energetic filler and can therefore produce more violent reactions than might be expected. Binder systems are rarely inert and there will always be an optimum formulation that provides the best response in Cook-Off.

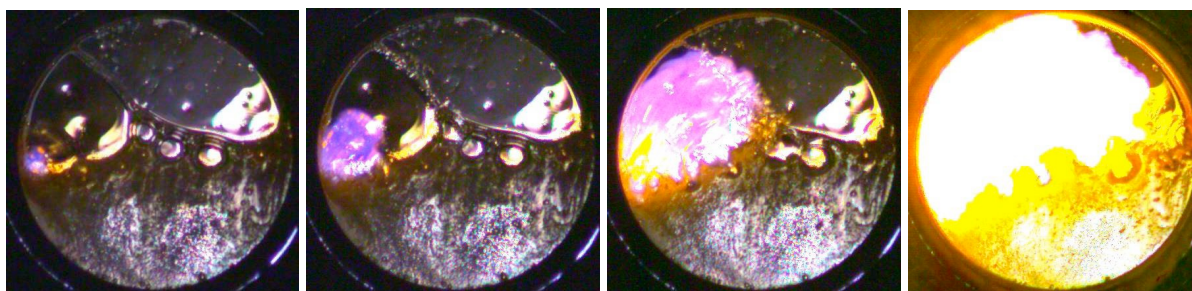


**FIGURE 4.** Images from the high-speed video record of RDX crystals heated in a ‘C’ seal until reaction at 1°C /min.

## CONCLUSIONS

This paper has described a new Cook-Off test vehicle that is flexible in terms of sample size and instrumentation and easy to deploy. Confinement levels can be altered by appropriate choice of end-plate material. The test vehicle has been tested on neat energetic crystals and formulations. The results obtained have given valuable insight into the thermal and physical cook-off processes leading to violent reaction. Tests have shown the early flameless decomposition of some materials and demonstrated the importance of the luminous flame to the outcome of the reaction. It has been shown that small masses of material can give reproducible violent responses. The new test vehicle is a convenient tool that can be used to de-risk new formulations using small amounts of material.

## REFERENCES

1. L. Smilowitz, B. F. Henson, D. Oswald and D. Remelius, “Internal sub-sonic burning during an explosion viewed via dynamic X-ray radiography”, *Applied Physics Letters* 111(18):184103, October 2017.
2. Dickson, P. M., et al. "Thermal cook-off response of confined PBX 9501." *Proceedings of the Royal Society of London A: Mathematical, Physical and Engineering Sciences*. Vol. 460. No. 2052. The Royal Society, 2004.
3. M. L. Hobbs, M. J. Kaneshige, and W. W. Erikson, “Modeling the measured effect of a nitroplasticizer (BDNPA/F) on cookoff of a plastic bonded explosive (PBX 9501”.
4. Cook, M. D., Briggs, R. I., Stennett, C., Haskins, P. J., & Fellows, J. (2002). Direct Observation of Cook-off Events Using a Novel Glass-Windowed Vehicle and Pipe Bombs. In *12th International Detonation Symposium*, August 2002 (pp. 11-16).
5. Cook, M. D., et al. "The Role of Binders in Controlling the Cook- Off Violence of HMX/HTPB Compositions." *AIP Conference Proceedings*. Vol. 845. No. 1. AIP, 2006.
6. C. Stennett, N. White, T. Reeves, P. J. Cheese, A. D. Wood and M. D. Cook, “Live Imaging and Heating of Confined RDX and HMX Crystals Until Reaction Using the Dual Windowed Test Vehicle”, these proceedings.
7. N. White, T. Reeves, P. J. Cheese, C. Stennett, A. D. Wood and M. D. Cook, “Live Decomposition Imaging of HMX/HTPB Based Formulations During Cook-Off in the Dual Window Test Vehicle”, these proceedings
8. M. D. Cook and C. Stennett, “One-Dimensional Thermal Violence Cook-Off Test”, these proceedings.



## **A.11 Live Decomposition Imaging of HMX/HTPB ...**

Authors: White, N., Reeves, T., Cheese, P., Stennett, C., Wood, A.D.,  
Cook, M.D.

Title: Live Decomposition Imaging of HMX/HTPB Based  
Formulations During Cook-Off in the Dual Windowed Test  
Vehicle

Publication Type: Journal                      Venue:                      APS SCCM 2017

Date: Jul 2017

# Live Decomposition Imaging of HMX/HTPB Based Formulations During Cook-Off in the Dual Window Test Vehicle

Nathan White<sup>1</sup>, Tom Reeves<sup>1</sup>, Phil Cheese<sup>1</sup>, Christopher Stennett<sup>2</sup>, Andrew Wood<sup>3</sup> and Malcolm Cook<sup>3,a)</sup>

<sup>1</sup>*DE&S, Ministry of Defence, Abbey Wood, Bristol BS34 8JH, UK.*

<sup>2</sup>*Centre for Defence Chemistry, Cranfield University, Defence Academy of the United Kingdom, Shrivenham, SN6 8LA, UK*

<sup>3</sup>*Syanco Ltd, PO Box 411, West Malling, Kent, ME6 9EZ, UK*

<sup>3a</sup>Corresponding author: malcolm.cook@syanco.co.uk

**Abstract.** Thin, cylindrical samples of HMX/HTPB formulations with solids loadings from 85-95% by mass have been heated at 1°C and 10°C minute until a reaction occurred in the new dual window cook-off test vehicle. The test vehicle has captured the response of these formulations, and shown the influence of variables such as confinement, heating rate and sample size. Live imaging of the heated samples revealed that, as with pure nitramine samples, three distinct stages of change take place during heating: phase changes, melting and slow, flameless decomposition with production of gaseous intermediates and finally burning with a luminous flame of the gaseous intermediates. In addition, the binder appears to undergo decomposition before the HMX, darkening along the edge closest to the thermal input before the HMX melts. No apparent volume change has been detected during the beta-delta phase change in HMX, however this could be due to the low-density hand pressed samples, allowing possible occlusions to be present. Prior to violent reaction, flame speeds were measured at approximately 30m/s for high confinement, which reduces by 2-3 orders of magnitude when confinement is lowered.

## INTRODUCTION

The Advanced Cook-off Experimental (ACE) programme has developed a dual window test vehicle that allows live real-time imaging and high-speed video records to be captured of the decomposition process of energetic material samples heated until reaction. A Phantom v711 high-speed video camera combined with high intensity front and, or, backlighting was used capture the various stages of decomposition including ignition before the final thermal explosion.

This paper describes the test vehicle, its modularity and experiments to observe the decomposition of a number of HMX/HTPB formulations with varying solids loadings at two heating rates. While this work has focused on experimental HMX/HTPB formulations to prove the dual window test vehicle a number of other formulations as well as neat energetic fillers have been tested used the technique. Currently any type of solid phase energetic sample can be tested using very small sample sizes.

The dual window test vehicle can be configured to provide three gradients of confinement: high, high-intermediate and intermediate. The HMX/HTPB samples were prepared specially for this series of experiments and contained 85 - 95% HMX by mass. They were hand mixed and pressed and this resulted in low densities and high porosities especially for the high percentage HMX compositions. All three levels of confinement have been tested on these formulations. In addition to high-speed video photography 'K-Type' thermocouples and Photon Doppler Velocimetry (PDV) instrumentation was deployed to record the vehicle / sample temperature and velocity data. The

initial test results for all formulations tested, show good correlation to the One-Dimensional-Thermal-Violence (ODTV) experiment which employed the same formulations. The ODTV experiment is described in a separate paper at this conference [1].

## EXPERIMENTAL

The ACE dual windowed test vehicle is designed to use modern high-speed photography to capture the processes and events that govern, and lead up to a cook-off event. These processes occur over a range of times scales spanning hours to sub-microsecond. The dual windowed vehicle can be configured to provide front and, or, back lighting to a thin energetic material sample, which allows live imaging and high-speed photography to capture the stages of decomposition as they take place as the sample is heated to elevated temperatures. A brief account of the test vehicle is given below. A more detailed description can be found in a separate paper at this conference [2].

The test vehicle itself consists of a cylindrical three-section body, made from steel. These three sections are held together by six bolts (three at either end). An inner, middle ring houses the energetic material sample and can be machined to accommodate different sample diameters and thicknesses up to a maximum of a 50x50mm cylindrical pellet. The upper and lower outer rings house glass windows or can be replaced by flat metal backing plates. The sample is confined by means of cylindrical glass blocks placed either end, or steel plates or, indeed a combination of both. Gaskets fit onto the inner central steel sample ring to form a gas-tight seal. Final adjustment of the confinement is made by means of the locking rings which bear down on gaskets placed next to the glass blocks. Heating of the vessel is achieved by means of three heater rods held within dedicated holes within the cylinder walls.

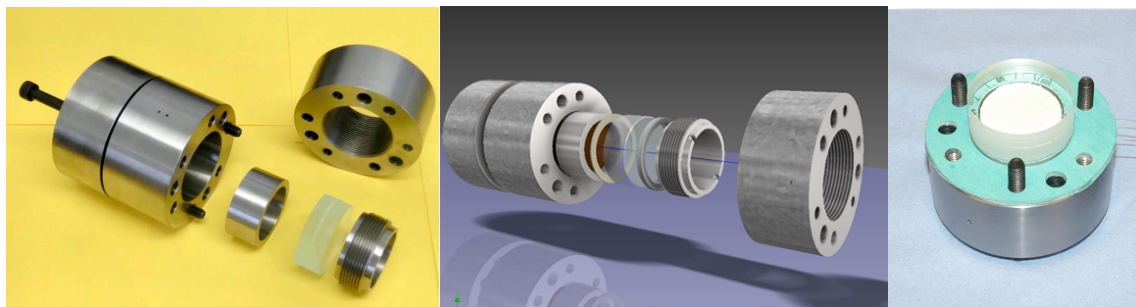


**FIGURE 1.** Images of the ACE dual window test vehicle main sections (left image), CAD 3D drawing (centre) and partially built vehicle with test sample between glass windows, shown in right image.

The window dimensions selected for this study are nominally 19mm thick, and 50mm in diameter. Thermocouple wires can be deployed horizontally in the gap between two sections. A suitable gasket material prevents escape of product gases before thermal explosion. Thermocouples can also be deployed vertically through steel end plates that replace one of the outer locking rings.

PDV can be used in tests where one or both glass windows are replaced with metal plates or where a suitable reflecting surface can be effected at the explosive surface through the glass window(s). This technique allows for the capture of pressure waves within the system and can be used, alongside the deformation in the base plate (if deployed), as a measure of explosion violence.

A total of five HMX/HTPB PBX compositions were produced by Cranfield University for the project. A polyurethane binder system, produced from the reaction between hydroxyl-terminated polybutadiene (HTPB, with Low-Molecular-Weight Liquiflex P-Grade) and isophorone diisocyanate (IPDI, supplied by Sigma Aldrich) was used. Four drops of dibutyltin dilaurate (DBTL) catalyst were used to increase the cure rate. The HTPB was dried overnight in a desiccator to remove water, which would otherwise react with the IPDI to produce undesirable gas bubbles within the binder. The IPDI was added to the HTPB and mixed by hand for 5 minutes to produce a homogeneous blend. After mixing, five containers were taken, and the appropriate mass of binder weighed into the containers to an accuracy of 10mg. HMX (Type C, fine grade, 30 $\mu$ m) was dried overnight at 70°C to remove water, and the appropriate mass was added to each of the five specimen containers, again to an accuracy of 10mg. The total mass of each mix was approximately 90g.

In view of the small specimen sizes required for the 3mm thick sheets, it was necessary to perform the mixing of the formulations by hand. Ordinarily, formulations of this type would be produced in larger quantities, using a mechanical mixer and under vacuum. However, for quantities less than 300g it is impractical to use even the smallest high-shear mixer. Moulds were made from PTFE, in which the formulations could be oven-cured. These moulds consisted of a square base plate 250x250mm in size and 12mm thick, onto which the specimen was placed. Four PTFE spacer strips, 3mm thick, were placed around the specimen, and a second square PTFE plate was placed upon the specimen. Manual pressure was used to press the specimen into a flat sheet of the required thickness.

The formulations of 85%, 88% and 90% solids loading were found to flow relatively well into a flat sheet shape. However, above this loading it was found to be increasingly difficult to manually press the specimens by this method. The 95% HMX formulation was spread with a PTFE spatula and hand moulded into an approximately flat sheet, with pressing to final thickness using the upper plate.

Specimen sheets were manufactured in each of the mix ratios in the range 85/15wt% to 95/5wt% HMX/HTPB. Small specimens taken from each sheet have had their density measured using the Archimedes method as shown in Table 1.

**TABLE 1.** Solids loadings versus density and Theoretical Maximum Density

<b>% Solids Loading</b>	<b>Theoretical Maximum Density (T.M.D)</b>	<b>Measured Density (g cm<sup>-1</sup>)</b>	<b>% T.M.D</b>
85	1.67	1.61	96.4
88	1.70	1.62	95.1
90	1.74	1.61	92.7
92	1.77	1.63	91.9
95	1.81	1.68	92.8

## RESULTS

The HMX/HTPB formulations were chosen to span a range of reaction levels, thereby testing the ability of the ACE Cook-Off vehicle to reproduce all levels of events up to the most violent. As expected the 85/15 HMX/HTPB produced relatively benign reactions and the 95/5 HMX/HTPB composition the most violent reactions, with the other compositions producing intermediate levels of violence.

A total of 42 tests were performed in three configurations with 1°C/minute and 10°C/minute heating rates. Fourteen experiments used a 'C' seal (a copper ring) sandwiched between glass windows. The specimen size for these experiments was 15mm diameter and 1mm thick. The 'C' seals are designed to provide high quality sealing of metallic surfaces, but were demonstrated to be also suitable with glass. Because the 'C' seal provided superior confinement, experiments that utilised them showed typically more violent reactions and more detail of the processes leading up to the final event. One drawback was that it was not possible to deploy thermocouples internally. However, a thermocouple was placed touching the outer edge of the seal.

In another series of seventeen tests fibre gaskets were used with glass windows. This configuration allowed the deployment of thermocouples. Typically, three thermocouples were deployed: one near the middle; another near the outer rim; and one in between. The sample size was 3mm thick and 39mm in diameter. This gave temperature - time profiles, but sealing was poorer than the 'C' seal experiments and generally gave lower violence for a given composition.

The final configuration utilised 5mm thick steel plates front and back of the sample instead of the glass windows. The purpose of these experiments was to use larger pellets of explosive and higher confinement in order to ensure capture of the true violence of reaction to compare with the 'C' seal experiments. The slower heating rate (1°C/minute) experiment for each composition was found to be generally more violent, generating greater deformation of the steel plates with higher velocities recorded by PDV, than the corresponding faster heating rate (10°C/minute) experiment.

A few representative frames from the high-speed video for the 85/15, 92/8 and 95/5 HMX/HTPB compositions are given in Fig. 2, Fig. 3 and Fig. 4. The high-speed camera records typically revealed significant changes in the appearance of the specimen for several tens of milliseconds prior to 'ignition' (appearance of a visible flame). Often distinct areas of blackening at tens of milliseconds prior to ignition were observed (see Fig. 2, Fig. 3 and Fig. 4). The precise nature of this blackening is unclear, but the regions are observed to spread gradually. Additionally, molten

HMX can normally be seen near the edge. In experiments where the confinement was sufficient, flames are seen to appear at a later time. It is suggested that the blackened dark regions represent flameless decomposition of the HTPB binder, possibly prompted by decomposition of the entrapped HMX within. Blackening is also noted along the paths of cracks that appear to develop during heating. Cracks often become very distinct, again prior to the first onset of flame. It is also notable that the first onset of flame usually does not occur within these cracks, and examination of the records shows that the flames appear in the cracked region a considerable time after their appearance elsewhere. We have not observed new cracks being generated in the compositions tested, rather we have observed existing cracks open and sometimes close as heating progressed.

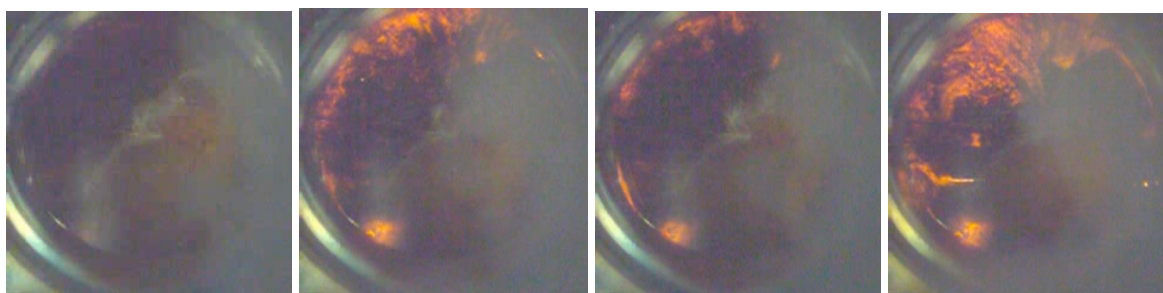


**FIGURE 2.** Selected images from the high-speed video record of a 85/15 HMX/HTPB sample heated at 1°C/minute.

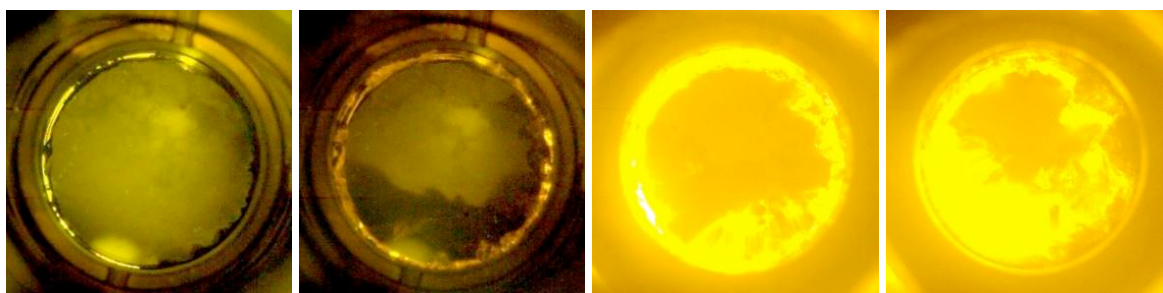


**FIGURE 3.** Selected images from the high-speed video record of a 92/8 HMX/HTPB sample heated at 10°C/minute.

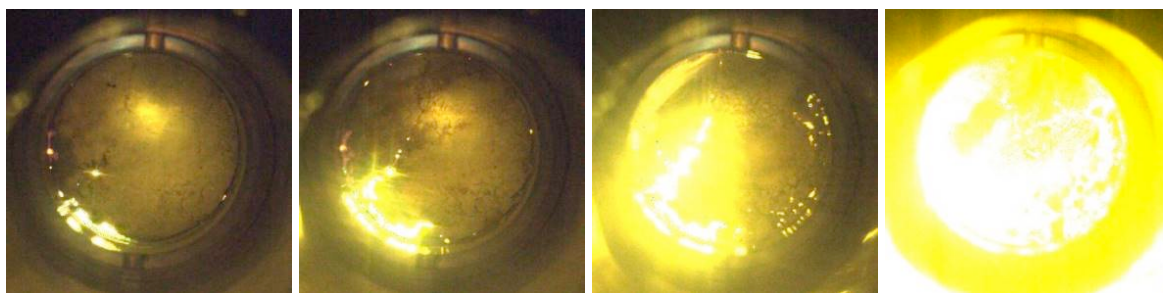


**FIGURE 4.** Selected images from the high-speed video record of a 95/5 HMX/HTPB sample heated at 10°C/minute.

In tests with the 95/5 HMX/HTPB formulation the appearance of the visible flame is associated with increasingly bright regions which may originate from a single or several positions. The flame is often seen to spread rapidly from its origin at an increasing rate, in a uniform manner, until the sample is totally engulfed (Fig. 4). This is in contrast to samples with a high binder content (e.g. 85/15 HMX/HTPB) which show similar blackening of the binder and melting of the nitramine, but a slow, controlled, laminar, although ragged, luminous burn front that spreads more slowly across the sample (Fig. 2). Intermediate reaction is exhibited by the 92/8 HMX/HTPB formulation which showed a more vigorous burn reaction (Fig. 3).

## CONCLUSIONS

In a companion paper, we described the behaviour of both neat RDX and HMX when heated in the ACE Cook-Off test vehicle until reaction [3]. These experiments on both crystal RDX and HMX gave good background information that allowed the Cook-Off behaviour of HMX/HTPB formulations to be understood. For example, where thermocouples were deployed the beta to delta phase change was observed at around 160°C (most of the formulations were not at T.M.D. and therefore had inherent porosity). At higher temperatures, the blackening was observed which has been attributed to decomposition of the binder to form a carbon honeycomb structure which was typically recovered in low violence tests. Melting around the edge of the sample was also seen above 220°C. Finally, the luminous flame was observed at higher temperatures and generally emanated from the edge.

The binder rich HMX formulations gave mild reactions while the binder poor ones gave violent reactions, as might be expected. The difference between the two types is probably how the molten HMX is partitioned.

In the case of the binder rich material it is speculated that the molten HMX can be compartmentalised within pockets in the carbonised binder backbone. The intermediate product gases produced are also held in these pockets and the flame spread is cell to cell in a controlled fashion.

In the binder poor HMX formulations molten HMX as well as the intermediate gases can more readily flow through the carbonised binder backbone structure and collect at the top of the charge. When the gaseous intermediates finally ignite and the luminous flame appears, the burning gas pocket will give rise to compression of the bed and subsequent collapse of the bubbles in the molten HMX. These bubbles contain HMX vapour and intermediate gaseous decomposition products. Since the molten HMX is more likely to be connected via porosity this can lead to the domino bubble collapse mechanism thought to be responsible for violent reaction in pure crystalline HMX.

## REFERENCES

1. M. D. Cook and C. Stennett, "One-Dimensional Thermal Violence Cook-Off Test", these proceedings.
2. P. J. Cheese, T. Reeves, N. White, C. Stennett, A. D. Wood and M. D. Cook, "Development of a Dual Windowed Test Vehicle for Live Streaming of Cook-Off in Energetic Materials", these proceedings.
3. C. Stennett, N. White, T. Reeves, P. J. Cheese, A. D. Wood and M. D. Cook, "Live Imaging and Heating of Confined RDX and HMX Crystals Until Reaction Using the Dual Windowed Test Vehicle", these proceedings.



# **Annex B: Presentations**

## **B.1 Direct Observation of the Onset of Ignition ...**

---

Authors:	Stennett C; Cook M D		
Title:	Direct observations of the onset of ignition in explosives when heated to elevated temperatures		
Publication Type:	International Workshop	Venue:	NATO Science of Workshop, GA, USA MSIAC Cook-off Atlanta, GA, USA
Date:	Apr 2016		

---

# Direct Observations of the Onset of Ignition in Explosives When Heated to Elevated Temperatures

Cranfield  
UNIVERSITY  
**Syanco**



Mr Chris Stennett ([c.stennett@cranfield.ac.uk](mailto:c.stennett@cranfield.ac.uk))

Prof Malcolm Cook ([malcolm.cook@syanco.co.uk](mailto:malcolm.cook@syanco.co.uk))

[www.cranfield.ac.uk](http://www.cranfield.ac.uk)

## Contents

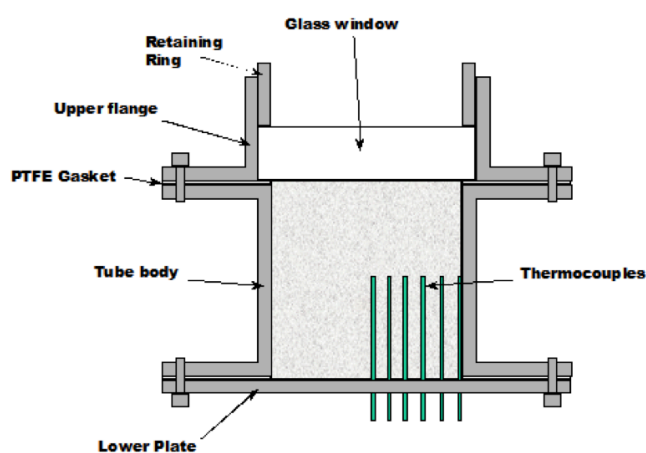
Cranfield  
UNIVERSITY

- Background
- Experimental Design
- Preliminary Observations – HMX/HTPB
- Preliminary Observations – RDX
- Discussion and Conclusions
- Future themes

## Test Vehicle Design Objectives

- MoD-funded project to develop this topic further
- Direct observation of the surface of the test specimen during heating and up to the point of ignition, potentially with back-lighting
- Accommodate a variety of specimen sizes and types
- Ability to replicate the witness plate method to assess violence of response
- Instrumentation:
  - Thermocouples
  - High speed video
  - Heterodyne velocimetry
- High burst pressure to provoke strong responses

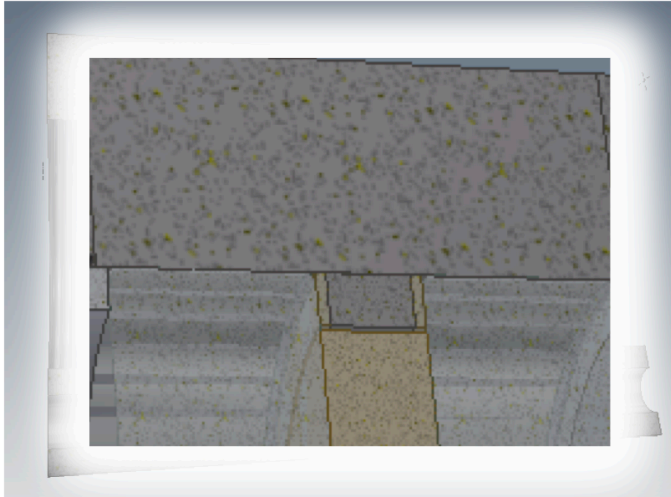
## Prior Work



- Single glass window to observe specimen
- 50x50mm pellet size
- Range of explosive compositions from ~88% to 95% solids loading
- Internal thermocouple instrumentation
- Extent of deformation of lower plate correlated with solids loading

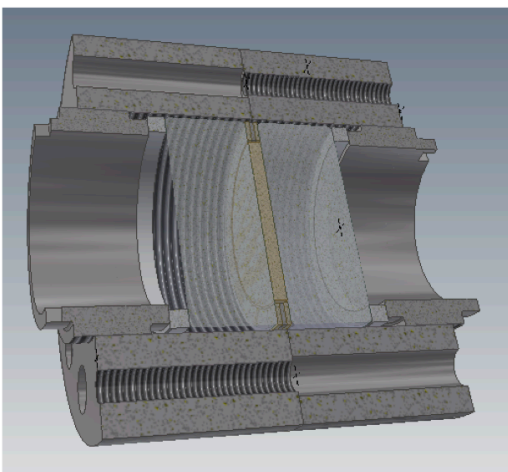
M. D. Cook, C. Stennett, P. J. Haskins, R. I. Briggs, A. D. Wood and P. J. Cheese, "The Role of Binders in Controlling the Cook-Off Violence of HMX/HTPB Compositions", APS Shock Compression of Condensed Matter, 2005.

## ACE Test Vehicle Design Thick Disk Version



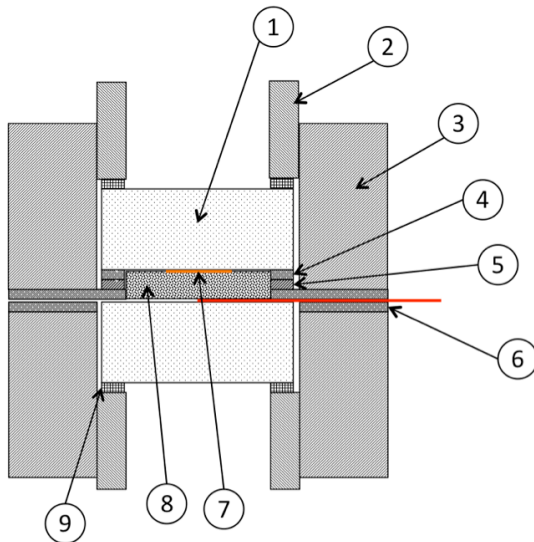
- Rigid outer tube, axially bolted, and containing heating elements
- Thick glass windows to allow view of the specimen, and giving back lighting
- Inner confining ring, together with gaskets, forms a gas-tight cavity to enclose the test specimen
- Specimens up to 40mm diameter and 50mm long

## ACE Test Vehicle Design Thin Disk Version



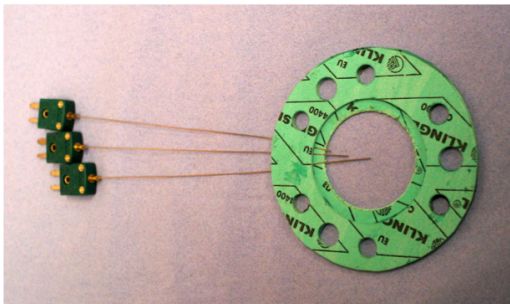
- Centre section omitted to accommodate thinner disks, down to ~1mm
- Placement of the specimen at the joining plane, allowing probes (e.g. thermocouples) to measure the specimen directly
- Flexible design allows experiments with different details, but use the same basic hardware set

## Preliminary Instrumented Experiments – HMX/HTPB

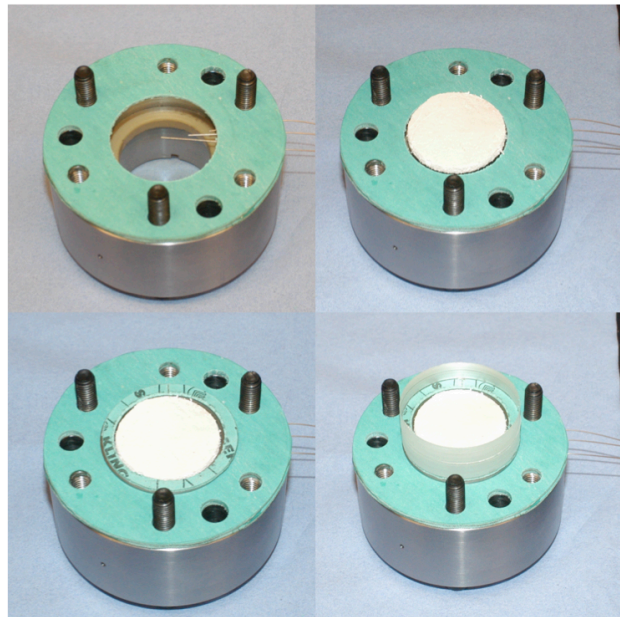


1. Glass window  $\varnothing 50 \times 19\text{mm}$
2. Adjustable retaining collar
3. Confining body
4. Fibre gasket
5. Steel ring
6. Thermocouple/gasket assembly
7.  $50\mu\text{m}$  reflective foil
8. Test specimen,  $\varnothing 39 \times 3\text{mm}$
9. Levelling spacer

## $\varnothing 39 \times 3\text{mm}$ Instrumented Experiments

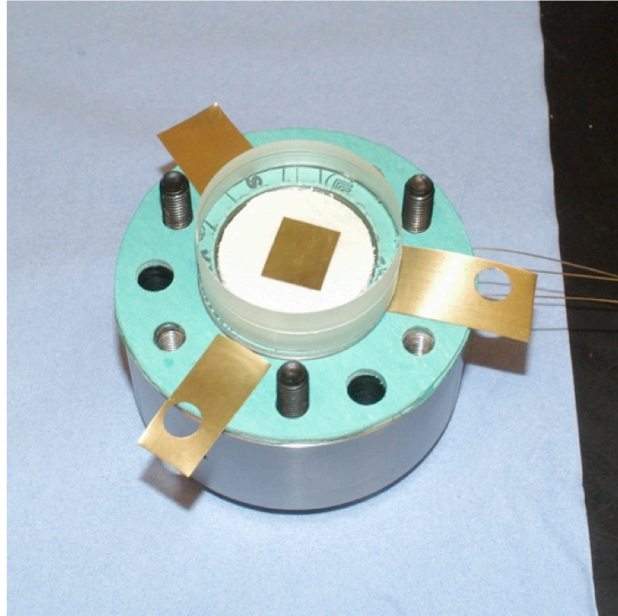


- Thermocouple array (3x stainless steel sheathed, 0.6mm probes)
- Foil reflector for interferometry experiments
- Direct observation with HSV and back-lighting



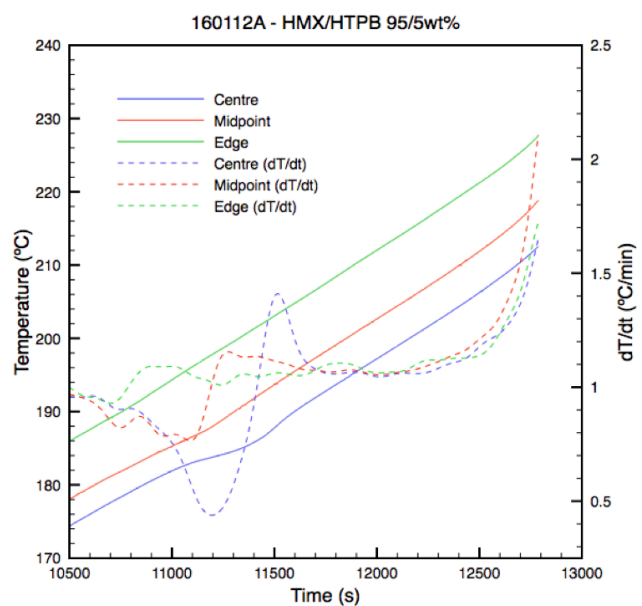
## Ø39 x 3mm Instrumented Experiments - Confinement

- During assembly, three shims are placed around the circumference between the two confinement halves
- The final assembly is made
- The shims are removed, and the retaining bolts tightened to final torque
- Selection of different shim thicknesses allows the pre-load on the glass windows to be controlled, giving variable confinement



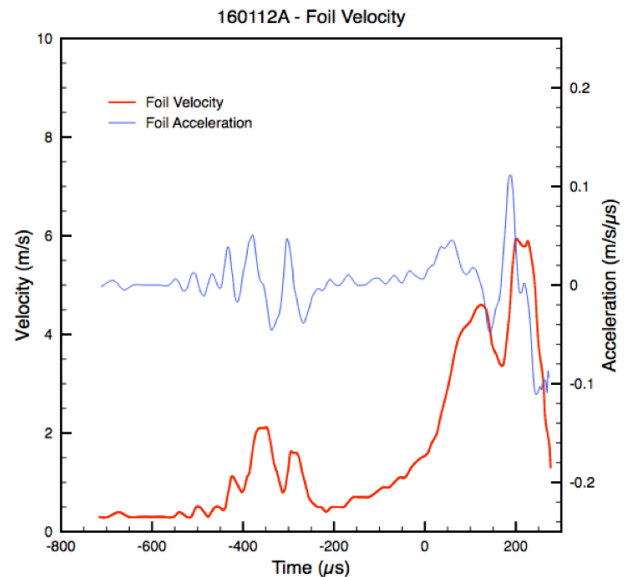
## Thermocouple observations

- 95/5 HMX/HTPB, slow heating
- 3x 0.6mm diameter stainless steel thermocouples
  - ‘Centre’ 0mm from the axis
  - ‘Midpoint’ 8mm from the axis
  - ‘Edge’ 14.5mm from the axis
- Endotherm at 168-180°C
- Thermal runaway begins >700s before deconfinement
- Thermal runaway seems to be away from the specimen axis



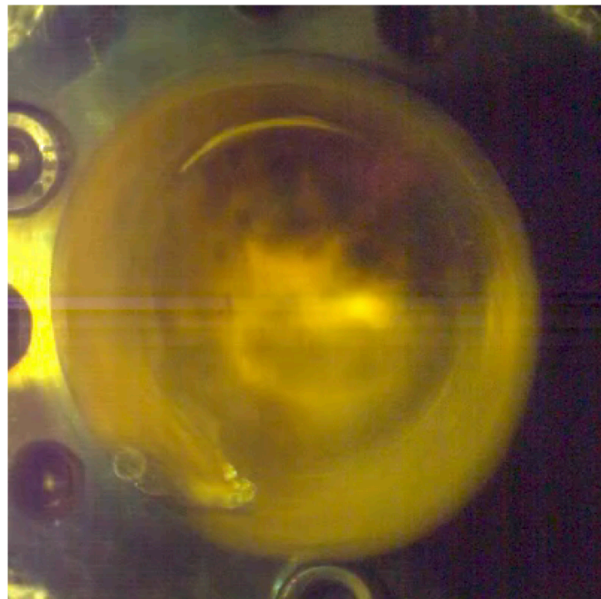
## Velocimeter observations

- 95/5 HMX/HTPB, slow heating
- Motion of a 50 $\mu$ m foil located between the specimen and the glass window
  - Glass window is stiff and massive, so velocity is low
- Motion is not steady or smooth
- Confinement failure was observed at 0 $\mu$ s (on this plot) but peak velocity reached at  $\sim$ 200 $\mu$ s
- Common time-base for instrumentation
  - can associate HSV observations with the velocity trace



## Video observations

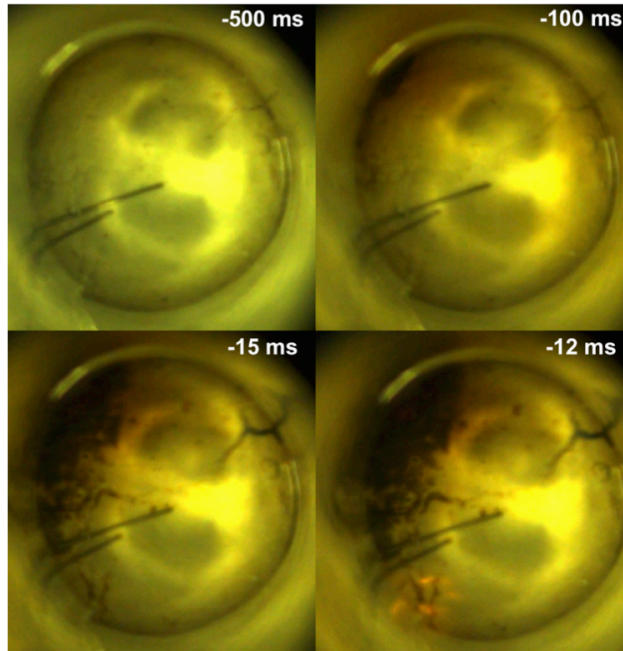
- 95/5 HMX/HTPB, slow heating
- 50 $\mu$ s inter-frame time
- Image resolution  $\sim$  200 $\mu$ m per pixel
- Onset of flames at top of specimen, with propagation of flame possibly along pre-existing defects
- Relatively weak confinement, resulting in pressure relief early in the burn process





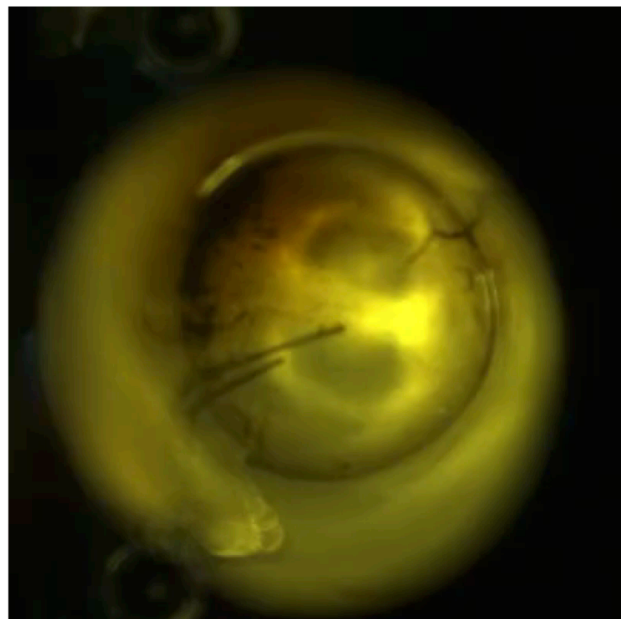
## Changes in Binder Prior to Ignition

- 95/5 HMX/HTPB
- Still images showing the change in appearance of the specimen prior to ignition
- Darkening is attributed to decomposition of HTPB
  - DSC indicates HTPB decomposition at  $\sim 400$  °C
  - Possibly decomposition products from HMX are either sufficiently hot to decompose HTPB, or chemical species in the decomposition products cause a chemical change



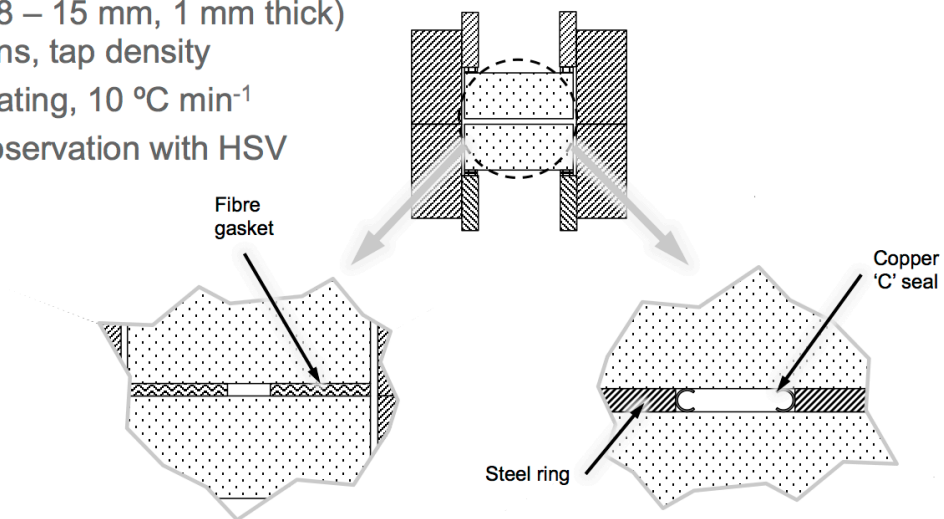
## Ignition and development of flame

- 95/5 HMX/HTPB
- Sequence from  $\sim 20$  ms prior to explosion
- Image resolution  $\sim 200$   $\mu\text{m}$  per pixel
- Flame seen to originate at lower left edge
- Further flames appear throughout sample
- Cracks seem to play little part in flame propagation

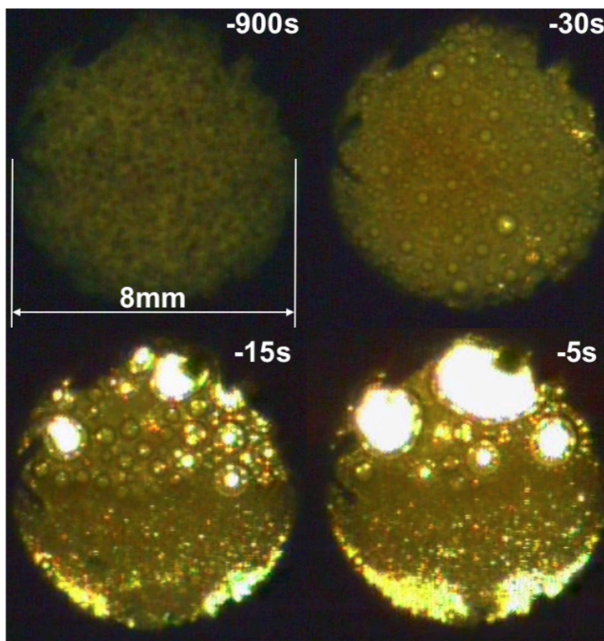


## Small-scale pure RDX experiments

- Two sealing arrangements
- Small ( $\varnothing 8 - 15$  mm, 1 mm thick) specimens, tap density
- 'Fast' heating,  $10\text{ }^{\circ}\text{C min}^{-1}$
- Direct observation with HSV

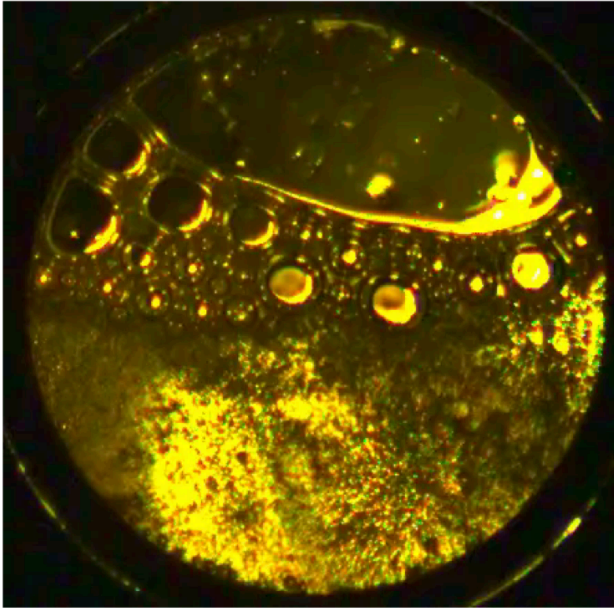


## Pure RDX - Melting



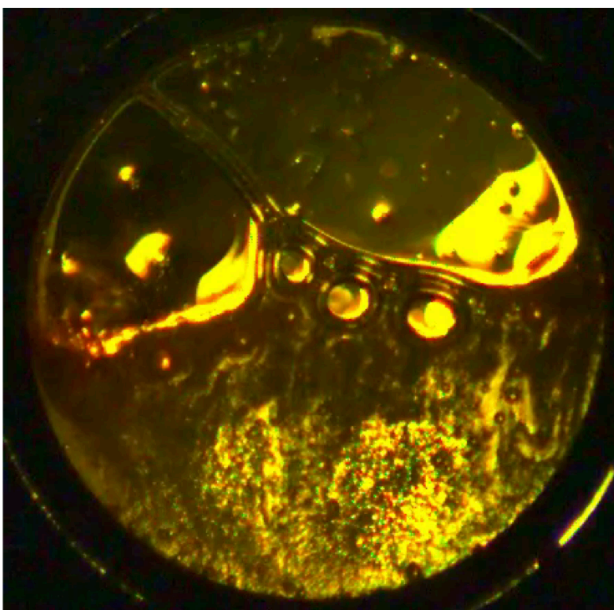
- Pure RDX powder, loose-filled at  $\sim 1.0\text{g/cc}$
- $10^{\circ}\text{C/min}$  heating rate
- Melting seems to begin at around 60s prior to ignition
- Initial phase of melting shows mass motion of the powder bed and the development of gas-filled bubbles
  - Brightness due to decrease in opacity and transmission of back-light

## Pure RDX - Melting



- From ~5s prior to ignition, bubbles have formed and risen to the top of the specimen
- Lower area shows texture, which could be either many tiny bubbles, or a 'slurry' of semi-molten RDX
- Convection and circulation seen to the left and right, with trails of bubbles rising and merging
- Liquid around bubbles towards the top of the specimen appears much lower viscosity than that in the bottom 'slurry' area

## Pure RDX – Flame, Bulk Compression and Explosion



- Flame seen to originate at the liquid/bubble interface. Onset of flame is quite gradual
- Flame spreads at  $10 - 15 \text{ ms}^{-1}$
- Disruption in the liquid interface between the two largest bubbles suggests a pressure wave, min speed  $150 \text{ ms}^{-1}$
- Bulk compression of the slurry region immediately prior to mass explosion, increasing flame area
- Large bubbles ( $> 1 \text{ mm}$ ) do not seem to be compressed uniformly; small bubbles ( $\sim 200 \mu\text{m}$ ) are compressed reasonably uniformly

## Observations of the final phases of cook-off – HMX/HTPB Systems

- Onset of self heating occurs a long time prior to 'ignition' even for a small specimen at moderate heating rate
- Discolouration of the HTPB binder in HMX/HTPB systems prior to the onset of visible flames
  - Some evidence of flame spread along pre-existing cracks, though not in every experiment
  - Some evidence that hot gases permeate through pre-existing spaces without visible flame
- 85/15 composition seems to de-confine, vent, and stall the increase in reaction rate
- Reaction rate (after ignition) in 95/5 composition seems to be capable of continued increase after confinement is overcome

## Observations of the final phases of cook-off – Pure RDX

- Melting of RDX and formation of bubbles and convection cells for ~45 sec prior to 'ignition'
- First sight of visible flame in melted RDX occurs at solid/liquid interface, accompanied by a pressure wave of at least  $150 \text{ ms}^{-1}$
- Initial pressure wave does not seem to provoke further ignition away from the ignition site
- Prolonged development of flame in the gas bubble leads to bulk compression of the liquid material. Mass explosion after ~1500  $\mu\text{s}$  of compression
- Large (~ 25% area decrease) compression of the melted RDX suggests it is composed of a relatively large proportion of entrapped gas

## Phases of cook-off

- Phase I
  - Ongoing chemical reaction, Arrhenius kinetics driven. Primarily temperature dominated/controlled
- Phase II
  - Decomposition and/or melting leading to gas production and significant microstructure changes. The contents at this point no longer resemble the material at room temperature
- Phase III
  - Onset of flame and 'ignition', rapid pressurisation, bulk compression of solid/liquid material and potential mass explosion. Primarily mechanically and confinement controlled

## Questions ?

- Work carried out under funding from UK MoD Weapons Science and Technology Centre (WSTC) funding
- Thanks to:
  - Andrew Wood – photography & instrumentation
  - Sally Gaulter – test specimen formulation
  - Jim Clements – experimental support

# **Annex C: Co-Author Statements**

**Research Contribution Statement**

**Research publication:** "Live Imaging and Heating of Confined RDX and HMX Crystals Until Reaction Using the Dual-Windowed Test Vehicle", APS SCCM 2017 - AIP Conference Proceedings **1979**, 150037 (2018); <https://doi.org/10.1063/1.5044993>

**Lead Author:** C Stennett  
**Co-authors:** M D Cook, P J Cheese, A D Wood, N White, T Reeves

As co-author on the above publication, I confirm that Mr Stennett:

Made a significant contribution to the research that produced the publication particularly in the design of the experimental vehicle and then the analysis of the results obtained.

**Name:** Andrew David Wood

**Signature:** 

**Date:** 21<sup>st</sup> January 2019

**Research Contribution Statement**

**Research publication:** "Live Imaging and Heating of Confined RDX and HMX Crystals Until Reaction Using the Dual-Windowed Test Vehicle", APS SCCM 2017 - AIP Conference Proceedings **1979**, 150037 (2018); <https://doi.org/10.1063/1.5044993>

**Lead Author:** C Stennett

**Co-authors:** M D Cook, P J Cheese, A D Wood, N White, T Reeves

As co-author on the above publication, I confirm that Mr Stennett:

- Led the research that ultimately produced the publication
- Performed the majority of the research that produced the publication
- Made a significant contribution to the research that produced the publication
- Made a contribution to the research that produced the publication
- Is someone not known to me! Who the hell is Chris Stennett anyway?

**Name:** Prof Malcolm Cook \_\_\_\_\_

**Signature:** Malcolm Cook

**Date:** 24 January 2019 \_\_\_\_\_



### **Research Contribution Statement**

**Research publication:** “Live Imaging and Heating of Confined RDX and HMX Crystals Until Reaction Using the Dual-Windowed Test Vehicle”, APS SCCM 2017 - AIP Conference Proceedings **1979**, 150037 (2018); <https://doi.org/10.1063/1.5044993>

**Lead Author:** C Stennett

**Co-authors:** M D Cook, P J Cheese, A D Wood, N White, T Reeves

As co-author on the above publication, I confirm that Mr Stennett:

- Led the research that ultimately produced the publication; and
- Performed the majority of the research that produced the publication

Name: **PJ Cheese** \_\_\_\_\_

Signature: *Philip J Cheese* \_\_\_\_\_

Date: 29 January 2019 \_\_\_\_\_

**Research Contribution Statement**

**Research publication:** "Direct Observation of Cook-off Events Using A Novel Glass-Windowed Vehicle and Pipe Bombs" - 11<sup>th</sup> International Detonation Symposium, 1998

**Lead Author:** C Stennett

**Co-authors:** M D Cook, R I Briggs, P J Haskins, J Fellows

As co-author on the above publication, I confirm that Mr Stennett:

- Led the research that ultimately produced the publication
- Performed the majority of the research that produced the publication
- Made a significant contribution to the research that produced the publication
- Made a contribution to the research that produced the publication
- Is someone not known to me. Who the hell is Chris Stennett anyway ?

**Name:** Prof Malcolm Cook \_\_\_\_\_

**Signature:** *Malcolm Cook*

**Date:** 24 January 2019 \_\_\_\_\_

**Research Contribution Statement**

**Research publication:** "Direct Observation of Cook-off Events Using A Novel Glass-Windowed Vehicle and Pipe Bombs" - 11<sup>th</sup> International Detonation Symposium, 1998

**Lead Author:** C Stennett

**Co-authors:** M D Cook, R I Briggs, P J Haskins, J Fellows

As co-author on the above publication, I confirm that Mr Stennett:

- Led the research that ultimately produced the publication
- Performed the majority of the research that produced the publication
- Made a significant contribution to the research that produced the publication
- Designed, assembled and operated key elements of instrumentation utilised in practical experiments /trials

Name: Richard I. Briggs



Signature:

Date: 21/01/2019

### **Research Contribution Statement**

**Research publication:** “Direct Observation of Cook-off Events Using A Novel Glass-Windowed Vehicle and Pipe Bombs” - 11<sup>th</sup> International Detonation Symposium, 1998

**Lead Author:** C Stennett

**Co-authors:** M D Cook, R I Briggs, P J Haskins, J Fellows

As co-author on the above publication, I confirm that Mr Stennett:

- Led the research that ultimately produced the above publication

X

---

Dr Peter J Haskins

### **Research Contribution Statement**

**Research publication:** "Direct Observation of Cook-off Events Using A Novel Glass-Windowed Vehicle and Pipe Bombs" - 11<sup>th</sup> International Detonation Symposium, 1998

**Lead Author:** C Stennett

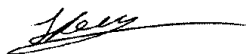
**Co-authors:** M D Cook, R I Briggs, P J Haskins, J Fellows

As co-author on the above publication, I can confirm that Mr Stennett:

- Was the lead author on the research that resulted in the publication.
- Undertook the role of research leader on the subject of Cook-Off in energetic materials and subsequently published this in the Detonation Symposium proceedings.
- Was the key contributor to the research, especially on the design of the novel charge vessel and in the conduct of the experiments, which was the core subject of the publication.

**Name:** Justin Fellows OBE BSc CChem FRSC MIEExpE

**Signature:**



**Date:** 21<sup>st</sup> January 2019

**Research Contribution Statement**

**Research publication:** "Development and Implementation of an Ignition and Growth Model for Homogeneous and Heterogeneous Explosives", 11<sup>th</sup> International Detonation Symposium, 1998

**Lead Author:** M D Cook  
**Co-authors:** P J Haskins, C Stennett

As lead author on the above publication, I confirm that Mr Stennett:

- Led the research that ultimately produced the publication
- Performed the majority of the research that produced the publication
- Made a significant contribution to the research that produced the publication
- Made a contribution to the research that produced the publication
- Is someone not known to me. Who the hell is Chris Stennett anyway ?

**Name:** Prof Malcolm Cook \_\_\_\_\_

**Signature:** Malcolm Cook

**Date:** 24 January 2019 \_\_\_\_\_

**Research Contribution Statement**

**Research publication:** "Small-scale Thermal Violence Experiments for Combined Insensitive High Explosive and Booster Materials - 14<sup>th</sup> International Detonation Symposium, 2010

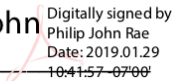
**Lead Author:** C L Bauer

**Co-authors:** P J Rae, C Stennett, H Flower

As lead author on the above publication, I confirm that Mr Stennett:

Made a significant contribution to the research that produced the publication. Specifically he assisted with test article assembly, application of diagnostics, experimental execution procedures, data collection and data analysis.

Name: Philip Rae, LANL

Signature: Philip John Rae  Digitally signed by Philip John Rae  
Date: 2019.01.29 10:41:57 -0700

Date: 1/29/19

**Research Contribution Statement**

**Research publication:** "The Role of Binders in Controlling the Cook-off Violence of HMX/HTPB Compositions" – APS SCCM 2005 - AIP Conf. Proc. 845, 952 (2006); <http://doi.org/10.1063/1.2263479>

**Lead Author:** M D Cook  
**Co-authors:** C Stennett, P J Haskins, R I Briggs, A D Wood, P J Cheese

As lead author on the above publication, I confirm that Mr Stennett:

- Led the research that ultimately produced the publication
- Performed the majority of the research that produced the publication
- Made a significant contribution to the research that produced the publication
- Made a contribution to the research that produced the publication
- Is someone not known to me. Who the hell is Chris Stennett anyway?

**Name:** Prof Malcolm Cook \_\_\_\_\_

**Signature:** Malcolm Cook

**Date:** 24 January 2019 \_\_\_\_\_



**Research Contribution Statement**

**Research publication:** "One-Dimensional Thermal Violence Cook-off Test", APS SCCM  
2017 - AIP Conference Proceedings **1979**, 150010 (2018);  
<https://doi.org/10.1063/1.5044966>

**Lead Author:** M D Cook  
**Co-authors:** C Stennett

As lead author on the above publication, I confirm that Mr Stennett:

- Led the research that ultimately produced the publication
- Performed the majority of the research that produced the publication
- Made a significant contribution to the research that produced the publication
- Made a contribution to the research that produced the publication
- Is someone not known to me. Who the hell is Chris Stennett anyway?

**Name:** Prof Malcolm Cook \_\_\_\_\_

**Signature:**  \_\_\_\_\_

**Date:** 24 January 2019 \_\_\_\_\_

**Research Contribution Statement**

**Research publication:** "Cumulative Damage Hotspot Model for use with Arrhenius-Based Ignition and Growth Model" - 12<sup>th</sup> International Detonation Symposium, 2002

**Lead Author:** M D Cook  
**Co-authors:** P J Haskins, C Stennett

As lead author on the above publication, I confirm that Mr Stennett:

- Led the research that ultimately produced the publication
- Performed the majority of the research that produced the publication
- Made a significant contribution to the research that produced the publication
- Made a contribution to the research that produced the publication
- Is someone not known to me. Who the hell is Chris Stennett anyway ?

**Name:** Prof Malcolm Cook \_\_\_\_\_

**Signature:** Malcolm Cook

**Date:** 24 January 2019 \_\_\_\_\_

### **Research Contribution Statement**

**Research publication:** “Developments in a Small-Scale Test of Violence” – APS SCCM  
- AIP Conf Proc. **1426**, 563-566 (2012);  
<http://doi.org/10.1063/1.3686341>

**Lead Author:** S Sorber  
**Co-authors:** C Stennett, M Goldsmith

As lead author on the above publication, I confirm that Mr Stennett:

- Led the Cranfield University partnership of the research that was a fundamental element to the whole success of the project without which the publication would not have been possible
- Provided continuity throughout a long project that I joined as the second AWE lead scientist
- Made a significant contribution to the research that produced the publication, including;
  - Providing significant insight into the physics of the data interpretation
  - Coordinating the research and development that ultimately produced the publication
  - Engaging with multiple partners to enable progression of the research that produced the publication

Name: Susan Wright (née Sorber)

Signature: *S Wright*

Date: 28/01/2019

**Research Contribution Statement**

**Research publication:** "Development of a dual windowed test vehicle for live streaming of cook-off in energetic materials", APS SCCM 2017 - AIP Conference Proceedings **1979**, 150009 (2018); <https://doi.org/10.1063/1.5044965>

**Lead Author:** P J Cheese

**Co-authors:** T Reeves, N White, C Stennett, A Wood, M D Cook

As lead author on the above publication, I confirm that Mr Stennett:

- Performed the majority of the research that produced the publication

Name: PJ Cheese

Signature: *Philip J Cheese*

Date: 29 January 2019

**Research Contribution Statement**

**Research publication:** "Direct observations of the onset of ignition in explosives when heated to elevated temperatures" – MSIAC Science of Cook-off Workshop, 2015

**Lead Author:** C Stennett  
**Co-authors:** M D Cook

As co-author on the above publication, I confirm that Mr Stennett:

- Led the research that ultimately produced the publication
- Performed the majority of the research that produced the publication
- Made a significant contribution to the research that produced the publication
- Made a contribution to the research that produced the publication
- Is someone not known to me. Who the hell is Chris Stennett anyway ?

**Name:** Prof Malcolm Cook \_\_\_\_\_

**Signature:**  \_\_\_\_\_

**Date:** 24 January 2019 \_\_\_\_\_